Variabilité chimique et isotopique créée par les processus sédimentaires dans les sédiments de rivière Himalayennes

Marion Garçon

UNIVERSITÉ DE GRENOBLE

THÈSE

Pour obtenir le grade de

DOCTEUR DE L'UNIVERSITÉ DE GRENOBLE

Spécialité : **Sciences de la Terre, de l'Univers, et de l'Environnement**

Arrêté ministériel : 7 août 2006

Présentée par

Marion GARÇON

Thèse dirigée par **Catherine CHAUVEL**

préparée au sein de **l'Institut des Sciences de la Terre de Grenoble**
dans **l'École Doctorale Terre Univers Environnement**

Variabilité chimique et isotopique créée par les processus sédimentaires dans les sédiments de rivières Himalayennes

Thèse soutenue publiquement le **23 Novembre 2012**
devant le jury composé de :

Mme Dominique WEIS
Rapporteur
M. Jérôme GAILLARDET
Rapporteur
M. Stéphane GUILLOT
Président du jury
Mme Janne BLICHERT-TOFT
Examinateur
M. Steven GOLDSTEIN
Examinateur
Mme Catherine CHAUVEL
Directrice de thèse
M. Francis ALBAREDE
Invité

Université Joseph Fourier / Université Pierre Mendès France /
Université Stendhal / Université de Savoie / Grenoble INP

UNIVERSITÉ DE GRENOBLE

Université Joseph Fourier / Université Pierre Mendès France /
Université Stendhal / Université de Savoie / Grenoble INP

Remerciements

Je tiens tout d'abord à préciser que cette section est provisoire... et qu'elle sera plus amplement développée lorsque l'effervescence des derniers jours de rédaction sera un peu retombée.

Je tenais tout de même à remercier mes rapporteurs (Dominique Weis et Jérôme Gaillardet) et examinateurs (Janne Blichert-Toft, Steven Goldstein et Stéphane Guillot) d'avoir accepté de relire et juger mon travail de thèse. J'espère que vous prendrez plaisir à lire ce manuscrit...

Je remercie évidemment ma chef préférée ... sans qui toutes ces années n'auraient jamais été si agréables. Merci de m'avoir guidée et soutenue depuis ma première année de Master... dire que ça fait plus de 5 ans que je te supporte ;) !! Merci aussi pour tout le reste : les pauses café interminables du samedi matin dans un labo désert, les innombrables restos du midi ou du soir, les BBQ chez toi, toutes nos sessions sushis quand Nick était à l'autre bout du monde, les dizaines de bouteilles de chartreuse VEP descendues entre minuit et 3h du matin (oui oui, je suis sure que si on les compte, on arrive bien à 10 bouteilles !! D'ailleurs, je tiens à te faire remarquer que celle que tu m'as offerte pour mon anniversaire n'est toujours pas terminée !! Il faudrait peut-être s'en occuper !), bref, j'en passe et des meilleurs...

Merci à Christian pour m'avoir donnée accès à sa collection de sédiments Himalayens et m'avoir conseillée sur le choix des échantillons à analyser. Merci aussi de m'avoir emmenée sur le terrain avec Marteen, Valier et Britta. Ta tentative de mesure de vitesse de courant dans la Narayani sur une pirogue accrochée à un câble que nous avons mis trois jours à faire passer au dessus de la rivière en pleine mousson, restera à jamais gravée dans ma mémoire, j'ai bien cru qu'on allait tous passer à l'eau !
Merci aussi à Eduardo, Mara et Sergio à Milan, sans qui je n'aurais jamais pu séparer tous ces petits minéraux.
Merci à Nick pour toutes les discussions scientifiques et autres, que nous avons pu avoir ! Merci aussi pour toutes les sorties ski-snowboard du samedi ! Tu resteras toujours mon chef BBQ préféré !

Je remercie aussi toutes les personnes qui ont contribuées, de près ou de loin, à l'acquisition des données que je présente aujourd'hui dans ce manuscrit: Sarah, qui m'a appris à maniper en salle blanche lors de ma première année de Master, et qui était toujours dispo quand il le fallait ; Christèle, qui venait à mon secours quand l'ICP avait décidé de faire des caprices ; Philippe Télouk à Lyon et Philippe Nonnotte à Brest, sans qui je n'aurais jamais pu mesurer aucun rapport isotopique !! Et François Sennebier qui m'a bien aidé pour la séparation des minéraux à Grenoble.

Merci à toutes les personnes du labo ISTerre (et ex LGCA) pour avoir rendu ces 5 années aussi géniales ! Je pense notamment à mes co-bureaux : Shaz, Kiwi et Carole. Shaz, je te dédicace les quelques figures « couleurs flashy » de mon manuscrit ! Kiwi, merci de m'avoir tant emmer*** pendant toutes ces années, j'avoue que ça aurait été beaucoup moins drôle sans toi... Merci à toi aussi Carole, j'espère que tu n'as pas trop eu peur, au début, quand on t'a débarquée dans mon bureau !
Merci à ma Chacha qui a égayé toutes ces pauses clops au labo, toutes ces réunions LaiTUE, ces restos, sorties, week-ends et vacances.
Merci aussi à ma Lulu, qui m'a soutenue pendant toute cette dernière année et sans qui j'aurais surement fini les deux derniers mois de ma thèse sans manger, ni dormir...
Je remercie aussi mes camarades de master et de thèse : Mog et Pierre mais aussi les anciens et les ptis nouveaux.
Merci à tous les autres : Pifou, Vivi, Nomadus, Alex-fille, Alex-gars, Peter, Jean, Carcaillou, ma ptite Clo-clo, Roro, France, Eric, Matthias, Emilie, Marie, ...

Merci à tous les membres de l'expédition 333 sur le Chikyu japonais avec qui j'ai passé un très bon noël et nouvel an 2011.

Enfin, je remercie toute ma famille, plus particulièrement mon papa et ma maman (oui oui), ... et mes sœurs aussi, qui m'ont toujours soutenus dans mes choix universitaires et qui ont accepté de me voir qu'une fois tous les trois mois (peut-être même moins !) au cours de ces trois dernières années. Merci d'avoir été là.

Résumé

Les compositions isotopiques en Nd, Hf, Pb et Sr des sédiments de rivière sont souvent considérées comme étant représentatives de celles de leurs roches sources. Elles sont donc largement utilisées pour tracer la provenance des sédiments ou pour moyenner les compositions isotopiques des lithologies drainées. L'influence des processus sédimentaires sur les compositions isotopiques de ces sédiments est cependant mal connue. L'objectif de l'étude présentée ici est de caractériser l'ampleur de la variabilité isotopique pouvant être générée par les processus de tri minéralogique au cours du transport des sédiments dans le milieu fluviatile. Pour ce faire, nous avons analysé les concentrations en éléments traces et les compositions isotopiques en Nd, Hf, Pb et Sr dans différents types de sédiments de rivière (bedload, suspended load, bank) échantillonnés à plusieurs endroits dans le système fluviatile du Ganges qui draine une partie de l'orogène Himalayenne. Nous avons également mesuré les compositions chimiques et isotopiques de nombreuses fractions minérales et granulométriques séparées de ces sédiments afin de mieux comprendre l'influence de chaque espèce minérale dans le budget isotopique total d'un sédiment de rivière.

Dans le cas où les lithologies drainées sont essentiellement cristallines et sédimentaires, nous montrons que les isotopes du Nd dans les sédiments de rivière sont très peu affectés par les processus de tri minéralogique puisqu'ils sont toujours contrôlés par les mêmes minéraux, à savoir la monazite et l'allanite. Au contraire, les systèmes isotopiques de l'Hf, du Pb et du Sr s'avèrent particulièrement touchés par les processus de tri minéralogique. Les isotopes de l'Hf et du Pb sont tous deux affectés par un effet zircon qui génère de larges variations isotopiques entre les sédiments de fond de rivières et ceux transportés en suspension. Pour le Sr, les variations observées entre les différents types de sédiments résultent des proportions variables de micas et feldspath-K qu'ils contiennent.

Dans le cas où les principales lithologies drainées présentent de forts contrastes d'érodabilité i.e. basaltes versus roches cristallines, nous montrons que les effets combinés de l'érosion différentielle dans le bassin de drainage et du tri sédimentaire dans la colonne d'eau sont responsables d'importantes variations isotopiques en Nd, Hf et Pb entre les sédiments de fond de rivière et ceux transportés en suspension. Nos calculs suggèrent que les produits d'érosion basaltique, relativement fins, sont préférentiellement transportés en suspension, proche de la surface de l'eau, alors que les produits d'érosion des roches plus cristallines sont préférentiellement concentrés dans les sédiments de fond de rivière.

Enfin, nous suggérons que les variations isotopiques observées entre les différents types de sédiments transportés par les rivières sur les continents pourraient avoir d'importantes implications pour les systématiques isotopiques des sédiments océaniques terrigènes et sur l'évolution à long terme du réservoir mantellique si ces derniers sont recyclés au niveau des zones de subduction.

Abstract

The Nd, Hf, Pb and Sr isotopic compositions of river sediments are often considered to be representative of those of their source rocks. Thus, they are widely used to trace sediment provenance or to average the isotopic compositions of the drained lithologies. The influence of sedimentary processes on the isotopic composition of these sediments is however poorly known. The aim of the present study is to characterize the extent of the isotopic variability that can be generated by mineral sorting process during sediment transport in fluvial system. To do this, we analyzed trace element concentrations and Nd, Hf, Pb and Sr isotopic compositions in river bank, bedload and suspended load sampled at several locations in the Ganga fluvial system draining part of the Himalayan orogen. We also measured the chemical and isotopic compositions of numerous mineral and granulometric fractions separated from these sediments to better understand the contribution of each mineral species to the bulk isotopic budget of river sediments.

When the drained lithologies are mainly crystalline and sedimentary, we show that Nd isotopes are very little affected by mineral sorting processes because, whatever the sediment type, those isotopes are always controlled by the same minerals i.e. monazite and allanite. In contrast, Hf, Pb and Sr isotopic systems are significantly affected by mineral sorting processes. Both Hf and Pb isotopes are affected by a zircon effect that generates large isotopic variations between bedload and suspended load. For Sr, variations between the different sediment types more likely result from variable proportions of K-feldspar and mica.

When the main drained lithologies are characterized by strong differences in erodibility i.e. basalts versus crystalline rocks, we show that the combined effects of differential erosion in the drainage basin and sediment sorting in the water column are responsible for significant Nd, Pb and Hf isotopic variations between bedload and suspended load. Our calculations suggest that basaltic erosion products are preferentially transported in suspension, near the water surface, whereas the erosion products of more crystalline rocks are preferentially concentrated in bottom sediments.

Finally, we suggest that the isotopic variations observed between bedload and suspended load on continents may have important implications for the isotopic systematics of oceanic terrigenous sediments and the long-term evolution of the mantle if these latters are recycled in subduction zones.

Table des Matières

INTRODUCTION 1

CHAPITRE 1 : LE SYSTÈME HIMALAYEN 11

I.1. MORPHOLOGIE DU SYSTEME HIMALAYEN 15

I.2. LA CHAINE HIMALAYENNE 17

I.2.1. DE LA DERIVE DE L'INDE A LA NAISSANCE DE L'HIMALAYA 17

I.2.2. PRINCIPALES UNITES STRUCTURALES 18

I.3. LE SYSTEME FLUVIATILE DU GANGE 22

I.3.1. RESEAU HYDROGRAPHIQUE ET BASSIN DE DRAINAGE 22

I.3.2. HYDROLOGIE 22

I.3.3. DYNAMIQUE SEDIMENTAIRE 23

CHAPITRE 2 : MÉTHODES 25

II.1. STRATEGIES D'ECHANTILLONNAGE 29

II.1.1. LOCALISATION DES ECHANTILLONS 29

II.1.2. METHODES D'ECHANTILLONNAGE 30

II.2. SEPARATION ET PREPARATION DES ECHANTILLONS 32

II.2.1. SEPARATION DES FRACTIONS MINERALES ET GRANULOMETRIQUES 32

II.2.2. PREPARATION DES ECHANTILLONS 34

II.2.2.A. BROYAGE ET REPRESENTATIVITE 34

II.2.2.B. DISSOLUTION 35

II.3. ANALYSES CHIMIQUES 38

II.3.1. ELEMENTS TRACES 38

II.3.1.A. DILUTION ET PREPARATION DES SOLUTIONS POUR ICP-MS 38

II.3.1.B. MESURE ET CALCUL DES CONCENTRATIONS EN ELEMENTS TRACES 40
II.3.1.C. EVALUATION DE LA QUALITE DES DONNEES ACQUISES 42
II.3.2. COMPOSITIONS ISOTOPIQUES EN ND, HF, PB ET SR 42
II.3.2.A. ISOLATION DU ND, HF, PB ET SR PAR CHROMATOGRAPHIE IONIQUE 42
II.3.2.B. CALCUL DES QUANTITES DE ND, HF, SR ET PB ISOLES 47
II.3.3.C. MESURE DES RAPPORTS ISOTOPIQUES EN ND, HF, PB ET SR 48
II.3.3.D. EVALUATION DE LA QUALITE DES DONNEES 49

CHAPITRE 3 : INFLUENCE DU TRI MINÉRALOGIQUE SUR LES COMPOSITIONS ISOTOPIQUES DES SÉDIMENTS **53**

III.1. SYSTEMATIQUES ISOTOPIQUES DU ND ET DE L'HF 57

Almost half of worldwide sedimentary Nd - Hf isotopic decoupling done on continents
(To be submitted to G-cubed)

***ABSTRACT* 59**
***1. INTRODUCTION* 60**
***2. THE GANGA FLUVIAL SYSTEM* 61**
***3. SEDIMENT SAMPLING AND ANALYTICAL PROCEDURE* 63**
3.1. SEDIMENT SAMPLING 63
3.2. CHEMICAL ANALYSES 64
***4. RESULTS* 65**
4.1. MAJOR AND TRACE ELEMENT CONCENTRATIONS 65
4.2. ND-HF ISOTOPIC COMPOSITIONS 69
***5. DISCUSSION* 73**
5.1. SOURCE ISOTOPIC VARIABILITY 73
5.2. EFFECTS OF MINERALOGICAL SORTING 77
5.3. WHERE DOES DECOUPLING OF ND AND HF ISOTOPES OCCUR ON CONTINENTS? 81
5.4. IMPACT OF CONTINENTAL FRACTIONATION ON OCEANIC SEDIMENTS 84
***6. SUMMARY AND CONCLUSIONS* 87**
***ACKNOWLEDGMENTS* 87**
***REFERENCES* 88**
***SUPPLEMENTARY MATERIAL* 92**

New approach to the average upper continental crust Pb isotopic value
(To be submitted to Nature Geoscience)

MAIN TEXT ***101***
METHODS ***109***
ACKNOLEDGEMENTS ***110***
REFERENCES ***110***
SUPPLEMENTARY MATERIALS ***112***

CHAPITRE 4 : QUELS MINÉRAUX CONTRÔLENT LES COMPOSITIONS ISOTOPIQUES DES SÉDIMENTS ? **117**

Which minerals control the Nd-Hf-Sr-Pb isotopic compositions of river sediments?
(To be submitted to Chemical Geology)

ABSTRACT ***123***
1. INTRODUCTION ***124***
2. STUDIED AREA AND SAMPLES ***125***
3. METHODS ***127***
3.1. MINERAL SEPARATION 127
3.2. CHEMISTRY 127
4. RESULTS ***129***
4.1. TRACE ELEMENT CONCENTRATIONS 129
4.2. ISOTOPIC COMPOSITIONS 129
5. DISCUSSION ***133***
5.1. WHICH MINERALS CONTROL ND ISOTOPES OF RIVER SEDIMENTS? 135
5.2. WHICH MINERALS CONTROL HF ISOTOPES OF RIVER SEDIMENTS? 137
5.3. WHICH MINERALS CONTROL SR ISOTOPES OF RIVER SEDIMENTS? 140
5.4. WHICH MINERALS CONTROL PB ISOTOPES OF RIVER SEDIMENTS? 143
5.5. GEOLOGICAL IMPLICATIONS 144
6. SUMMARY AND CONCLUSIONS ***147***
ACKNOWLEDGMENTS ***148***
REFERENCES ***149***
SUPPLEMENTARY MATERIAL ***154***

CHAPITRE 5 : EFFET DE L'ÉROSION DIFFÉRENTIELLE SUR LES COMPOSITIONS ISOTOPIQUES DES SÉDIMENTS ? **157**

Isotopic data suggest strong bias towards basalts in river surface sediments
(To be submitted to Geology)

ABSTRACT ***163***
INTRODUCTION ***164***
GEOLOGICAL SETTING ***164***
RESULTS AND DISCUSSION ***166***
ACKNOWLEDGMENTS ***171***
REFERENCES ***171***
SUPPLEMENTARY MATERIAL ***175***

CONCLUSION **181**

BIBLIOGRAPHIE **189**

ANNEXES **205**

Introduction

Les processus sédimentaires occupent un rôle prépondérant dans la redistribution des masses à la surface de la Terre et participent activement au recyclage de la croûte continentale à grande échelle. L'altération et l'érosion de cette dernière conduit à la formation de produits détritiques, en partie exportés vers l'océan puis recyclés dans les zones de subduction avant d'être réutilisés pour la production de magma dans le réservoir mantellique et être finalement de nouveau exposés à la surface de la Terre (Armstrong, 1981; McLennan, 1988) (Figure i.1).

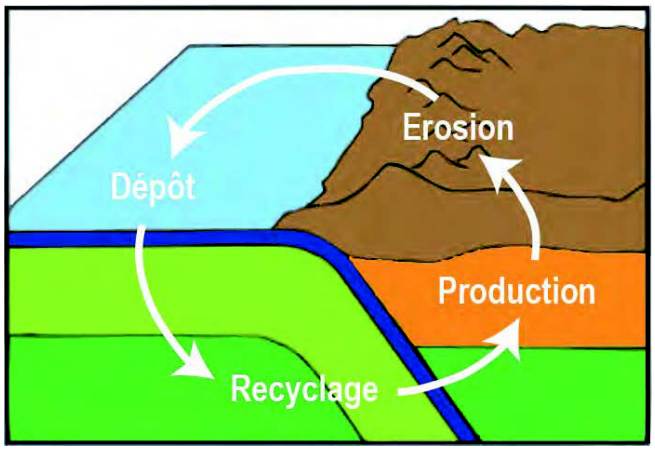

Figure i.1 : Schéma simplifié illustrant le recyclage de la croûte continentale

Sur les continents, les roches sont soumises à des processus d'altération chimique ou physique qui préparent les matériaux au mouvement en les réduisant en fines particules solides ou ioniques. L'altération chimique, qui s'effectue généralement en présence d'eau, modifie la chimie des roches, facilite leur dissolution sous forme d'ions et conduit à la formation de minéraux secondaires tels que les argiles. L'altération physique ou mécanique provoque la fragmentation des roches en particules solides plus fines. L'importance des processus d'altération dépend essentiellement de la lithologie et du climat au sens large (température, précipitations, type de végétation,…) (Friedman and Sanders, 1978; Chamley, 1989; Berner and Berner, 2012).

Les rivières constituent le moyen le plus efficace pour transporter les produits d'altération de la croûte continentale sous forme dissoute ou particulaire vers l'océan. Elles sont à l'origine de l'exportation de plus de 15 milliards de tonnes de sédiments chaque année dans l'océan mondial (Hay, 1998; Walling, 2006). La quantité et la nature des sédiments transportés par les rivières dépendent de plusieurs facteurs dont les principaux sont la taille du bassin versant, la nature des roches soumises à l'altération, le relief local, le relief à grande échelle, le climat (température, précipitations,…) et les activités anthropiques

(Hay, 1998). Ces sédiments sont principalement constitués de minéraux primaires plus ou moins résistants (quartz, feldspath, zircon,…), de minéraux secondaires (argiles, oxydes,…) et de matériaux biogéniques qui sont transportés en suspension ou dans le fond de la rivière en fonction de leurs propriétés hydrodynamiques. Plusieurs études ont, en effet, montré que les minéraux étaient ségrégués, dans la colonne d'eau, au cours du transport fluviatile, en fonction de leur taille, de leur densité et de leur forme (Komar, 2007; Garzanti et al., 2008). De manière générale, les grains les plus denses et grossiers, caractérisés par des vitesses de sédimentation rapides, auront tendance à être déplacés dans le fond de la rivière par des mécanismes de roulement, glissement et saltation (Figure i.2). Les grains plus fins et légers seront, quant à eux, mobilisés en suspension, à différentes profondeurs dans la colonne d'eau, en fonction de leur vitesse de sédimentation. Les particules les plus fines ayant des vitesses de sédimentation très faibles seront préférentiellement transportées proche de la surface de l'eau.

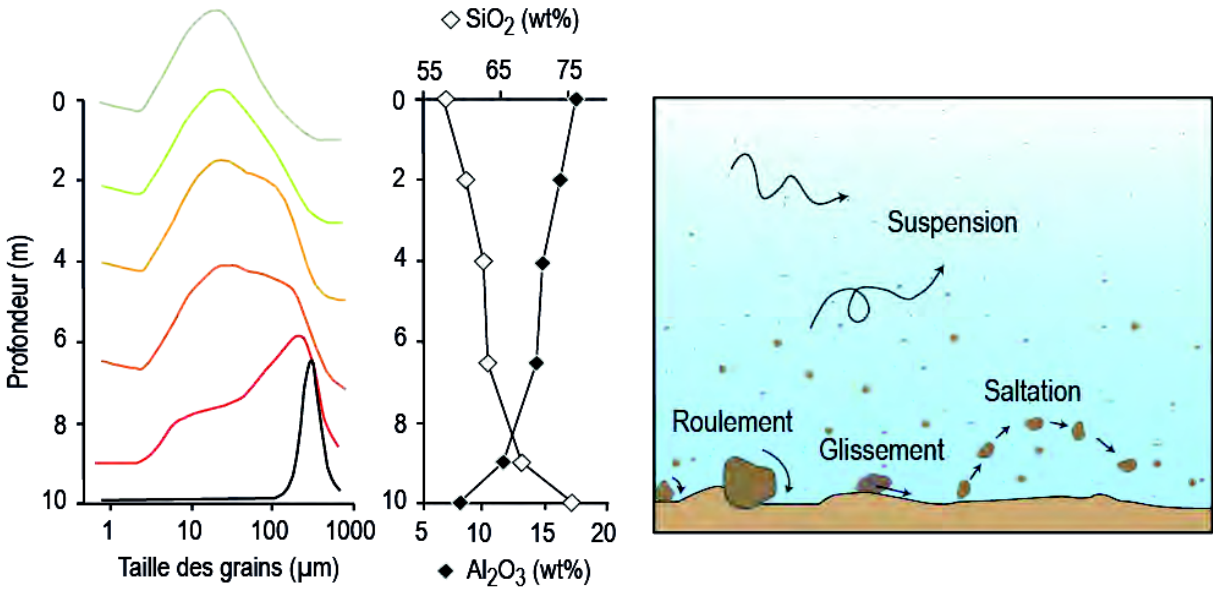

Figure i.2 : *A gauche :* Distribution de la taille des grains et variations des concentrations en SiO_2 et Al_2O_3 dans les sédiments en fonction de la profondeur d'échantillonnage dans le Ganges (d'après Lupker et al. (2011)). *A droite :* Schéma illustrant les différents modes de transport des sédiments dans une rivière.

Plusieurs travaux montrent que la ségrégation des minéraux, dans la colonne d'eau, par les processus hydrodynamiques, conduit à de larges variations de composition chimique (éléments majeurs et éléments traces) entre les sédiments de fond de rivières et ceux transportés en suspension (e.g. Dupré et al., 1996; Garzanti et al., 2010; Bouchez et al.,

2011; Garzanti et al., 2011; Lupker et al., 2011). Par exemple, les concentrations en SiO_2 mesurées dans les sédiments de fond de rivière sont généralement plus importantes que celles mesurées dans les sédiments de surface puisque que le quartz, minéral très riche en SiO_2, est préférentiellement transporté dans le lit des rivières (Figure i.2). A l'inverse, les concentrations en Al_2O_3 sont généralement plus élevées dans les sédiments de surface puisque cet oxyde est principalement porté par les phyllosilicates qui se trouvent préférentiellement dans le haut de la colonne d'eau. Les concentrations en éléments traces des sédiments sont, quant à elles, largement affectées par les effets de dilution du quartz (pauvre en éléments traces) et par les proportions relatives de minéraux lourds (riches en éléments traces) qu'ils contiennent.

De la même manière, les processus de tri minéralogique dans la colonne d'eau pourraient conduire à d'importantes variations isotopiques puisque chaque espèce minérale est caractérisée par une signature isotopique particulière qui dépend principalement de son âge de cristallisation et de la quantité d'éléments pères et fils initialement piégés. Cependant, l'influence du tri minéralogique sur les compositions isotopiques des sédiments de rivière n'a jamais été profondément étudiée et reste donc encore mal connue. Plusieurs travaux ont pourtant souligné leur importance dans la sédimentation océanique terrigène. Patchett et al. (1984) suggèrent, pour la première fois, l'existence d'importantes variabilités isotopiques en Hf entre les sédiments grossiers de type sable, stockés près des marges continentales, et les argiles de grands fonds océaniques. Cette variabilité est attribuée à l'effet zircon, c'est à dire à la concentration préférentielle de ces minéraux très riches en Hf et très peu radiogéniques, dans les sédiments grossiers. Cette idée est, par la suite, reprise et confirmée par de nombreux auteurs (Vervoort et al., 1999; Chauvel et al., 2008; Bayon et al., 2009; Carpentier et al., 2009; Vervoort et al., 2011). Quelques études rapportent également des variabilités de compositions isotopiques en Nd et Sr entre les sédiments océaniques sableux et argileux (McLennan et al., 1989; Revel et al., 1996; Eisenhauer et al., 1999).

L'existence de ces variabilités montre que les compositions isotopiques des sédiments océaniques détritiques peuvent être biaisées par les processus de tri sédimentaire. En est-il de même pour les sédiments transportés par les rivières sur les continents ? Observe t-on des différences isotopiques significatives entre les sédiments de fond de rivière et ceux transportés en suspension ?

Ces questions ont des enjeux capitaux puisque les isotopes du Nd, de l'Hf, du Pb et du Sr dans les sédiments de rivière sont, d'ores et déjà, couramment utilisées pour leur capacité à fournir des informations naturellement moyennées sur l'ensemble de leur bassin de drainage. Ils ont fait l'objet de nombreuses études visant à estimer la composition isotopique moyenne de la portion de croûte continentale drainée et contraindre son histoire au cours des temps géologiques (Goldstein et al., 1984; Goldstein and Jacobsen, 1988; Asmerom and Jacobsen, 1993; Allègre et al., 1996; Millot et al., 2004; Dhuime et al., 2011) ou encore tracer les changements de provenance des sédiments pour étudier l'influence des variations climatiques passées ou celles de la tectonique sur un bassin de drainage donné (Chen et al., 2000; Clift et al., 2002; Singh and France-Lanord, 2002; Richards et al., 2005; Roddaz et al., 2005; Gingele et al., 2007; Singh et al., 2008; Cina et al., 2009; Wu et al., 2010; Padoan et al., 2011; Hu et al., 2012). La plupart de ces études se base sur le concept que les signatures isotopiques des sédiments de rivières reflètent celles de leurs roches sources dans le bassin versant. Que se passerait-il si le message isotopique porté par les sédiments de rivière était, en fait, fractionné par le tri sédimentaire ? Peut-on considérer que les systèmes isotopiques Sm-Nd, Lu-Hf, U-Th-Pb et Rb-Sr sont de bon traceurs de provenance sur le continent ?

A l'échelle du système sédimentaire global, l'analyse approfondie des systématiques isotopiques dans les sédiments de rivière pourrait permettre de mieux comprendre certains processus, tels que le recyclage des sédiments sur le continent ou dans les zones de subduction. Pourquoi observe t-on un décalage significatif entre les âges modèles Nd des sédiments et leur âge stratigraphique systématiquement plus jeunes (Goldstein et al., 1984; Dia et al., 1990)? Quelle est l'origine des fractionnements isotopiques observés dans les sédiments océaniques ? Ces derniers sont, en partie, recyclés dans les zones de subduction et ont donc potentiellement un effet sur l'évolution à long terme du réservoir mantellique (Chauvel et al., 2008). De nombreuses études ont fourni l'évidence de l'implication des sédiments subduits dans la genèse de certains magmas, par exemple dans les magmas d'arc (White and Dupré, 1986; Elliott et al., 1997; Shimoda et al., 1998; Marini et al., 2005; Carpentier et al., 2008; Labanieh et al., 2010). Ceux-ci sont souvent caractérisés par des compositions isotopiques en Hf légèrement plus radiogéniques que les laves générées au niveau des dorsales océaniques (MORB) ou des points chauds (OIB) (Figure i.3). Cette signature isotopique particulière pourrait-elle refléter la contribution des sédiments océaniques, plus radiogéniques en Hf que leur source continentale, comme le suggère déjà Chauvel et al (2009) ?

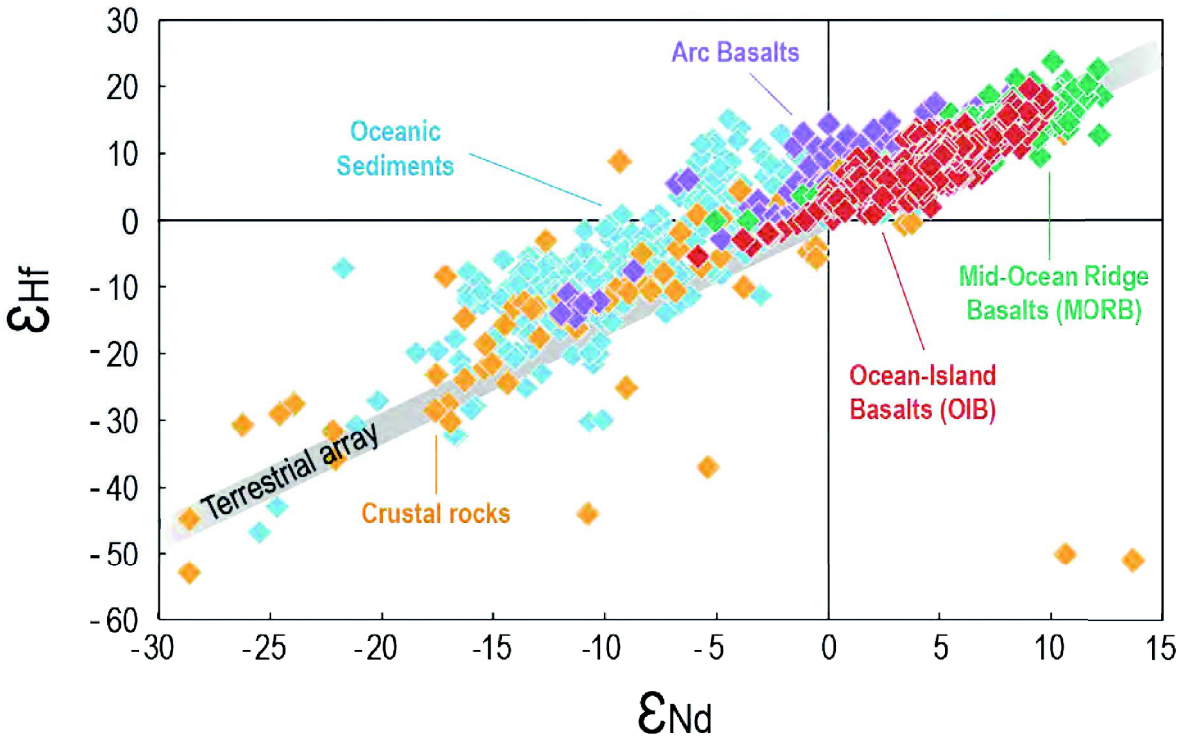

Figure i.3 : Compositions isotopiques en Nd et Hf connus pour les basaltes d'Arc, ceux de type MORB et OIB (GEOROC et PetDB databases ; Chauvel et al., 2009) ainsi que pour les roches d'affinité continentale (Bennett et al., 1993; Vervoort and Patchett, 1996; Blichert-Toft et al., 1999; Vervoort and Blichert-Toft, 1999; Vervoort et al., 2000) et les sédiments océaniques de type argile, silt, sable et boue biogénique (White et al., 1986; Ben Othman et al., 1989; McLennan et al., 1990; Pearce et al., 1999; Vervoort et al., 1999; Woodhead et al., 2001; Vlastélic, 2005; Prytulak et al., 2006; Carpentier et al., 2008; Bayon et al., 2009; Carpentier et al., 2009; Chauvel et al., 2009). Le "Terrestrial array" est celui de Vervoort et al. (2011). Tous les ε_{Nd} et ε_{Hf} présentés dans cette figure ont été recalculés en utilisant les compositions du CHUR publiées par Bouvier et al. (2008).

Le but de cette étude est de caractériser l'ampleur des variabilités chimiques et isotopiques pouvant être générées par les processus sédimentaires au cours du transport des sédiments sur le continent. Il s'agit également de s'intéresser aux implications que cela pourrait avoir pour les études de provenance et, à plus grande échelle, pour le système sédimentaire global incluant la sédimentation océanique. Pour ce faire, j'ai réalisé une étude géochimique approfondie des sédiments de rivière dans le système fluviatile du Ganges qui draine une partie de l'orogène Himalayenne. L'ampleur et l'importance de ce système fluviatile dans la sédimentation mondiale (Milliman and Meade, 1983) en font un lieu idéal pour étudier les systématiques géochimiques des sédiments à échelle continentale.

J'ai donc analysé les concentrations en éléments traces et les compositions isotopiques en Nd, Hf et Pb d'une centaine de sédiments (sédiments de fond de rivière, sédiments en suspension et sédiments de bord de berge) échantillonnés dans la chaîne orogénique, en sortie de chaîne, dans la plaine alluviale et, plus en aval, dans le delta. Quelques compositions isotopiques en Sr ont été analysées dans les sédiments de rivière mais nous avons choisi de ne pas centrer notre étude sur ce système isotopique puisque cet élément chimique, relativement soluble, est en grande partie transporté sous forme dissoute par les rivières (Gaillardet et al., 2003). L'Hf, le Nd et le Pb sont, quant à eux, beaucoup moins solubles (Gaillardet et al., 2003). Ils sont essentiellement transportés sous forme particulaire dans les rivières. L'analyse de leurs isotopes dans les sédiments est donc plus représentative pour étudier les systématiques isotopiques du système sédimentaire à l'échelle globale.

J'ai également mesuré les concentrations en éléments traces et les compositions isotopiques en Nd, Hf, Pb et Sr dans de nombreuses fractions de minéraux purs (feldspath-K, plagioclase, muscovite, biotite, magnétite, zircon, titanite, apatite, monazite/allanite, amphibole, épidote, grenat, carbonate et fraction argileuse) et dans des fractions de granulométries différentes, qui ont été séparées à partir de différents sédiments échantillonnés dans le système fluviatile du Ganges. Le but étant de mieux comprendre l'influence des différentes espèces minérales et celle de la granulométrie sur la signature isotopique globale d'un sédiment de rivière.

Le premier chapitre de cette thèse est consacré à la présentation du système Himalayen. La géographie et la géologie de la chaîne Himalayenne, ainsi que l'hydrologie et la dynamique sédimentaire du système fluviatile du Ganges y sont présentées dans le but de fournir au lecteur les quelques éléments nécessaires à la bonne compréhension de cette étude.

Le deuxième chapitre présente l'ensemble des méthodes utilisées pour mener à bien ce projet. La stratégie et les méthodes d'échantillonnage des sédiments de rivière étudiés sont décrites dans une première section. Les méthodes de séparation des différentes fractions granulométriques et minérales ainsi que la préparation des échantillons (broyage, dissolution) sont exposées dans une deuxième section. Enfin, les procédures analytiques utilisées pour mesurer les concentrations en éléments traces et les compositions isotopiques en Nd, Hf, Pb et Sr sont détaillées dans une troisième section.

Le troisième chapitre de cette thèse s'intéresse à la variabilité isotopique causée par le tri minéralogique au cours du transport des sédiments sur le continent. Il s'articule autour de deux manuscrits qui seront très prochainement soumis à G-cubed (Geochemistry, Geophysics, Geosystems) et Nature Geoscience. Le premier manuscrit est consacré au comportement des systèmes isotopiques du Nd et de l'Hf dans les sédiments du Ganges et de ses principaux affluents drainant la chaîne Himalayenne. Nous montrons que les isotopes du Nd sont très peu affectés par le tri minéralogique alors que ceux de l'Hf sont significativement fractionnés entre les sédiments de fond de rivière et ceux transportés en suspension. Les implications de nos résultats sont discutées dans un contexte plus global incluant les sédiments océaniques terrigènes et leur recyclage dans le réservoir mantellique.

Le second manuscrit s'intéresse aux compositions isotopiques en Pb de ces mêmes sédiments et à celles des fractions granulométriques et minérales. Nous montrons que les isotopes du Pb dans les sédiments de fond de rivière et dans ceux transportés en suspension sont significativement biaisés vers des valeurs très radiogéniques à cause d'un "effet zircon". A partir de ces données, nous proposons une nouvelle méthode pour estimer la composition isotopique moyenne de la croûte continentale supérieure.

Le quatrième chapitre vise à comprendre l'influence de chaque espèce minérale sur les compositions isotopiques en Nd, Hf, Pb et Sr des sédiments de rivière. Il est présenté sous la forme d'un manuscrit qui sera prochainement soumis à Chemical Geology. La contribution de chaque espèce minérale dans les budgets isotopiques des sédiments est quantifiée en utilisant des simulations Monte-Carlo. Nous montrons que les compositions isotopiques des sédiments de rivière ne sont contrôlées que par un petit nombre de minéraux et que ces derniers peuvent expliquer la variabilité isotopique observée entre les sédiments de fond de rivière et ceux transportés en suspension. Les conséquences de ces résultats pour les études de provenance utilisant des traceurs isotopiques sont discutées à la fin du manuscrit.

Le cinquième chapitre de cette thèse s'intéresse aux systématiques isotopiques du Nd, de l'Hf et du Pb dans des sédiments de rivière drainant d'importantes proportions de basaltes appartenant au Traps du Deccan, au sud de la plaine Indo-Gangétique. Il est présenté sous la forme d'un manuscrit que nous souhaiterions soumettre à Geology. Dans ce chapitre, nous montrons que les produits d'érosion basaltique sont préférentiellement transportés en suspension à la surface de l'eau alors que les produits d'érosion de roches plus cristallines sont préférentiellement concentrés dans les sédiments de fond de rivière.

Nous discutons le fait que ce phénomène pourrait conduire à une sur-représentation de la contribution des basaltes dans les argiles de grands fonds océaniques.

Enfin, cette étude s'achève par une conclusion dans laquelle nous résumerons l'ensemble des résultats et interprétations faites dans les différents chapitres. En annexe, se trouvent les informations complémentaires mentionnées au Chapitre II ainsi que deux articles publiés au cours de ma thèse sur mes travaux de Master 1 et de Master 2, mais qui n'ont pas de rapport direct avec les sédiments analysés au cours de cette thèse.

Chapitre I

Le Système Himalayen

L'objectif de ce chapitre est de situer le cadre géographique et géologique de cette étude en présentant brièvement le système Himalayen constitué de la chaîne Himalayenne à proprement parler mais aussi de la large plaine alluviale du Gange qui draine une partie de ses produits d'érosion jusqu'à l'océan Indien. Ce chapitre s'articule autour de trois grandes parties dans lesquelles nous commencerons par décrire la morphologie globale du système pour se concentrer ensuite sur la formation et la géologie de la chaîne Himalayenne puis sur l'impressionnant système fluviatile du Gange.

I.1. MORPHOLOGIE DU SYSTEME HIMALAYEN 15

I.2. LA CHAINE HIMALAYENNE 17

I.2.1. DE LA DERIVE DE L'INDE A LA NAISSANCE DE L'HIMALAYA 17

I.2.2. PRINCIPALES UNITES STRUCTURALES 18

I.3. LE SYSTEME FLUVIATILE DU GANGE 22

I.3.1. RESEAU HYDROGRAPHIQUE ET BASSIN DE DRAINAGE 22

I.3.2. HYDROLOGIE 22

I.3.3. DYNAMIQUE SEDIMENTAIRE 23

I.1. Morphologie du Système Himalayen

Le système Himalayen se situe au sud du continent asiatique (Figure I.1). Il se développe, d'est en ouest, sur plus de 2500 km entre la Birmanie et le Pakistan en passant par l'Inde, la Chine, le Bangladesh, le Bhoutan et le Népal. Il comprend plusieurs unités morphologiques au cœur desquelles se trouve la chaîne Himalayenne à proprement parler (Mascle et al., 2010).

L'ensemble le plus au nord est constitué par le plateau du Tibet qui se développe sur plus de 1000 km au nord de l'Indus-Tsangpo (Figure I.1) et qui s'élève à une altitude moyenne de 5000 m.

Au Sud de l'Indus-Tsangpo, se trouve la chaîne Himalayenne arquée, d'orientation globale WNW-ESE et d'une largeur moyenne de 250 km. Celle-ci se décompose en quatre unités topographiques. Au nord, la zone du Trans-Himalaya forme une chaine d'altitude un peu plus élevée que le plateau du Tibet (Figure I.2). Viens ensuite la haute chaîne Himalayenne avec son relief très marqué et ses fameux sommets culminants à plus de 8000 m d'altitude. Cette dernière domine le Moyen-Pays Himalayen avec ses vallées perchées à 1500 m d'altitude et son paysage incisé par les rivières Himalayennes. Enfin, les premiers reliefs de la chaîne sont constitués par le domaine des Siwaliks (Figure I.2). Il s'agit d'une série de collines parallèles à l'axe de la chaîne, d'extension nord-sud relativement variable (2 à 60 km) et d'altitude comprise entre 250 et 800 m.

Au pied de la chaîne Himalayenne, la plaine Indo-Gangétique s'étend, au sud, jusqu'aux premiers reliefs du craton Indien (Figure I.1). Elle est parcourue par de nombreux fleuves, dont le Gange, et est caractérisée par de très faibles reliefs, en moyenne de l'ordre de 100 m. Au sud-ouest du système Himalayen, se trouve le delta du Bangladesh qui canalise les eaux du Gange et du Brahmapoutre. Ces deux fleuves se déversent dans l'océan Indien au niveau de la Baie du Bengale.

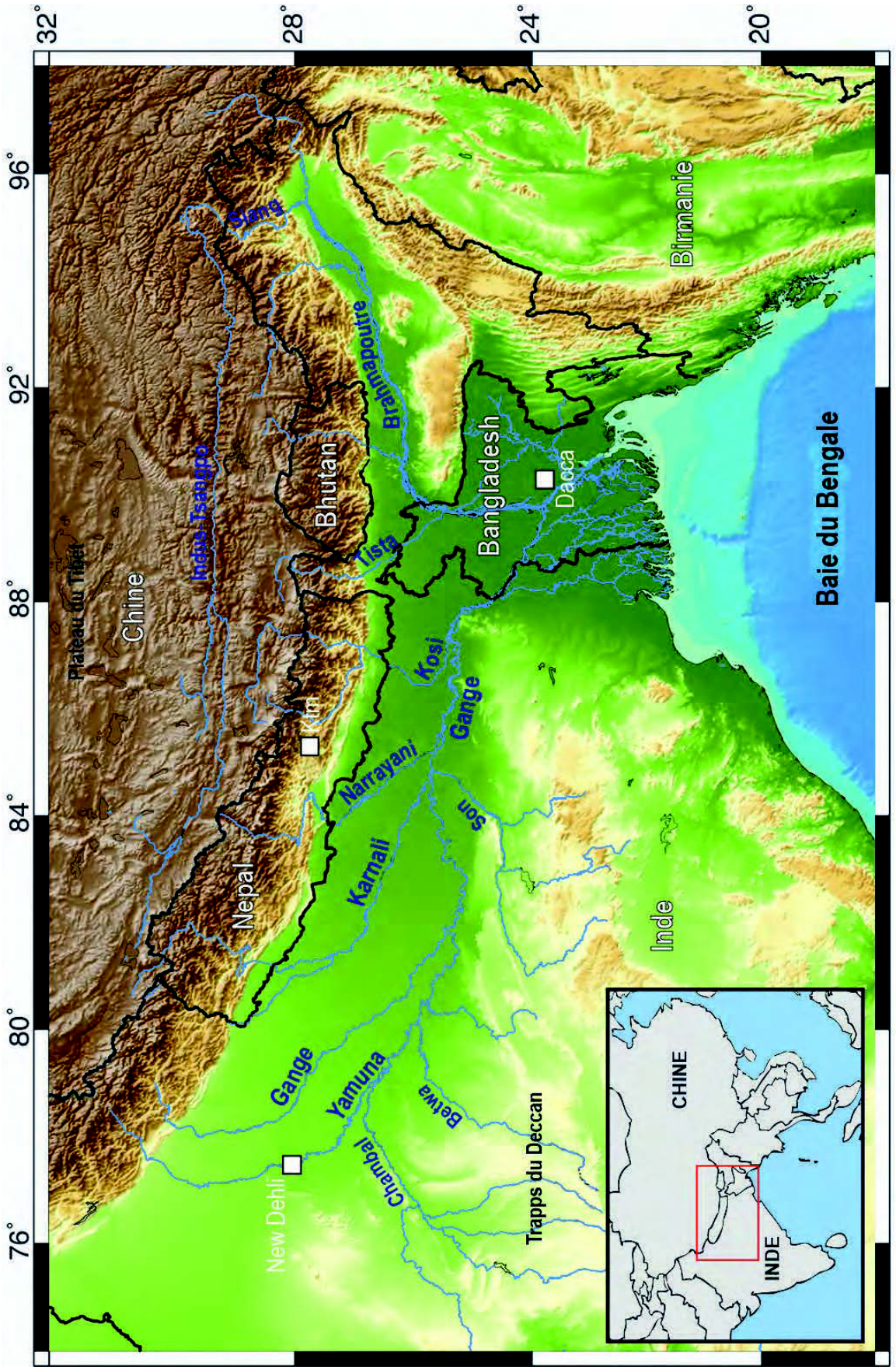

Figure I.1 : Géographie du système Himalayen modifié d'après Lupker (2011)

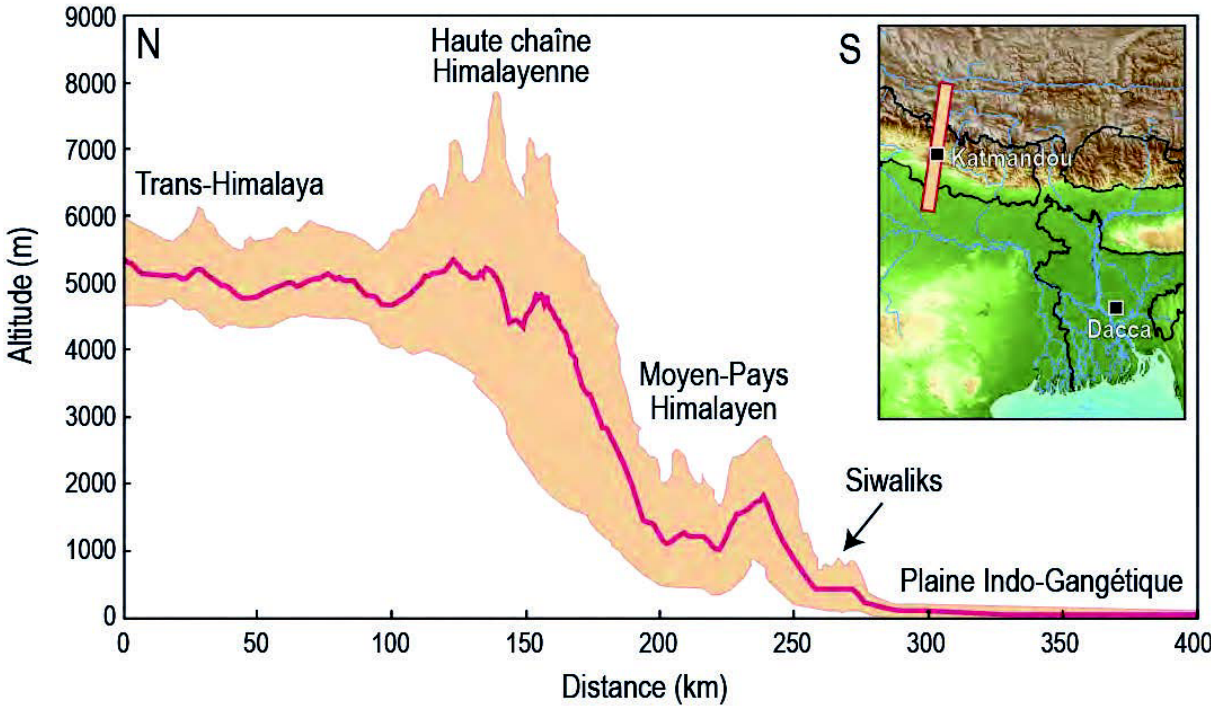

Figure I.2 : Profil d'altitude perpendiculaire à l'axe de la chaîne sur une largeur de 50 km de part et d'autre de Katmandou au Népal. La ligne rouge correspond au profil d'altitude moyen. Modifié d'après Takada and Matsu'ura (2007).

I.2. La Chaîne Himalayenne

I.2.1. De la dérive de l'Inde à la naissance de l'Himalaya

Il y a plus de 100 millions d'années, l'Inde se sépare de l'Afrique, l'Antarctique et l'Australie pour entamer sa remontée vers le Nord en direction de l'Eurasie à une vitesse relativement rapide atteignant les 18 cm.an^{-1} (Klootwijk et al., 1992). Ce rapprochement entraîne la fermeture progressive de l'océan Téthysien qui disparait en subduction sous la marge Eurasienne. L'Inde et l'Eurasie entre en contact vers 55 Ma (Patriat and Achache, 1984; Guillot, 2003). Vers 50-45 Ma, l'arrivée de l'épaisse croûte Indienne dans la zone de convergence marque le début de la subduction continentale et la topographie commence à s'élever : c'est la naissance de la chaîne Himalayenne. A partir de 20-25 Ma, le prisme orogénique Himalayen s'épaissit considérablement, les chevauchements se propagent au sud et le bassin d'avant-pays, cré' à l'avant de la chaîne Himalayenne par le bombement flexural de la plaque Indienne, commence à se remplir avec les produits d'érosion de la chaîne. Aujourd'hui encore l'Inde se déplace vers le Nord à la vitesse d'environ 5 cm.an^{-1} (Guillot, 2003). Cette convergence est accommodée par de grands accidents tectoniques subparallèles à la chaine qui délimitent les principales unités structurales Himalayennes (Le Fort, 1975).

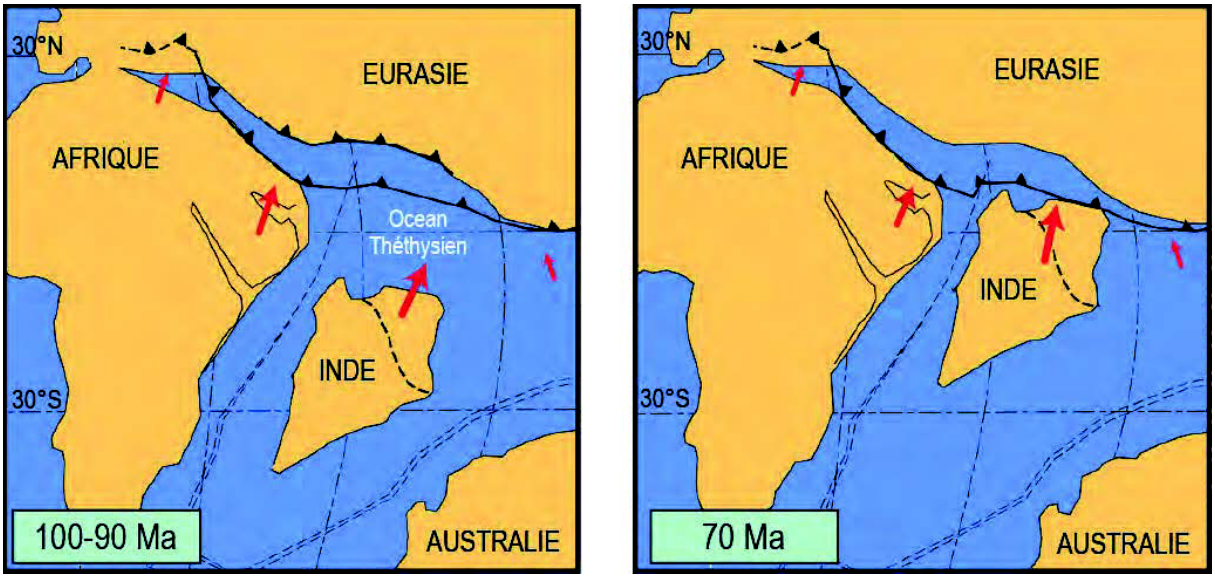

Figure I.3 : Schéma illustrant la dérive de l'Inde vers l'Eurasie au Crétacé

I.2.2. Principales unités structurales

Dans la chaîne actuelle, l'unité structurale la plus au sud est formée par les Siwaliks ("Cenozoic foreland basins" in Figure I.4). Elle est séparée de la plaine Indo-Gangétique par le "Main Frontal Thrust" (MFT) et limitée au nord par le "Main Boundary Thrust" (MBT). L'unité est constituée de dépôts fluviatiles Néogène à Quaternaire, plus ou moins consolidés, et issus de l'érosion de la chaîne Himalayenne (Mascle and Herail, 1982; Mugnier et al., 1999). Elle est subdivisée en trois séries sédimentaires granoclassées vers le haut, constituée d'argilites, de grès et de conglomérats.

Au dessus des Siwaliks, se trouve la formation du Bas-Himalaya ("Lesser Himalaya", Figure I.4.), qui est limitée au nord par le "Main Central Thrust" (MCT). Elle est constituée de roches sédimentaires faiblement métamorphisées (quartzites, grès, pélites carbonates, schistes) et de quelques affleurements de gneiss (Le Fort, 1975). Les âges U-Pb des zircons détritiques de cette formation sont majoritairement Paléo-Protérozoïques (>1.5 Ga, Figure I.5), indiquant que les protolithes du Bas-Himalaya pourraient être des produits d'érosion du vieux craton Indien qui se seraient déposés au nord de la marge Indienne bien avant la collision Inde-Eurasie (Parrish and Hodges, 1996; DeCelles et al., 2000). Les compositions isotopiques en Nd mesurées dans cette unité sont, pour la plupart, très peu radiogéniques (Figure I.6).

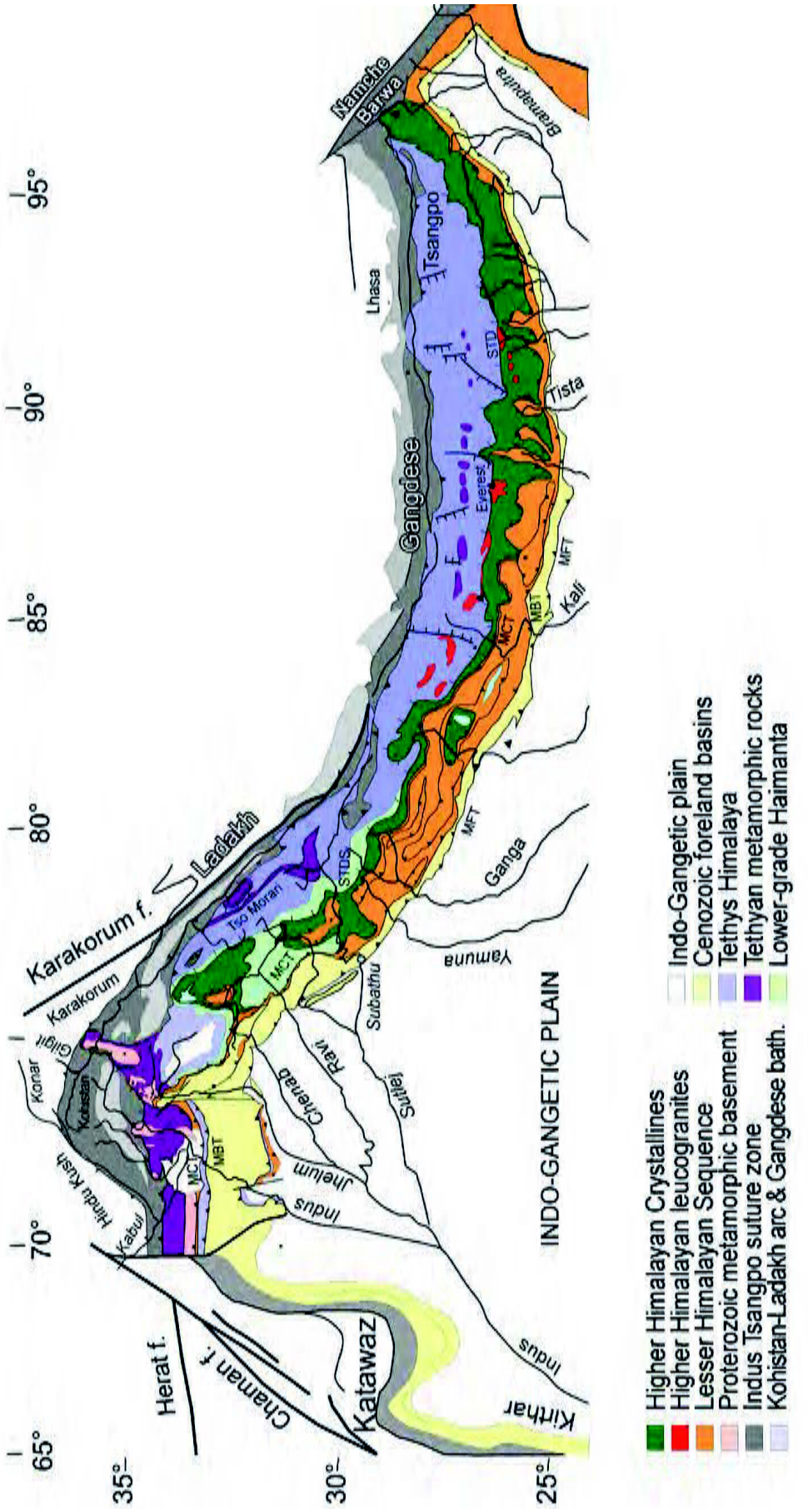

Figure I.4 : Géologie de la chaîne Himalayenne d'après Guillot et Replumaz (2012)

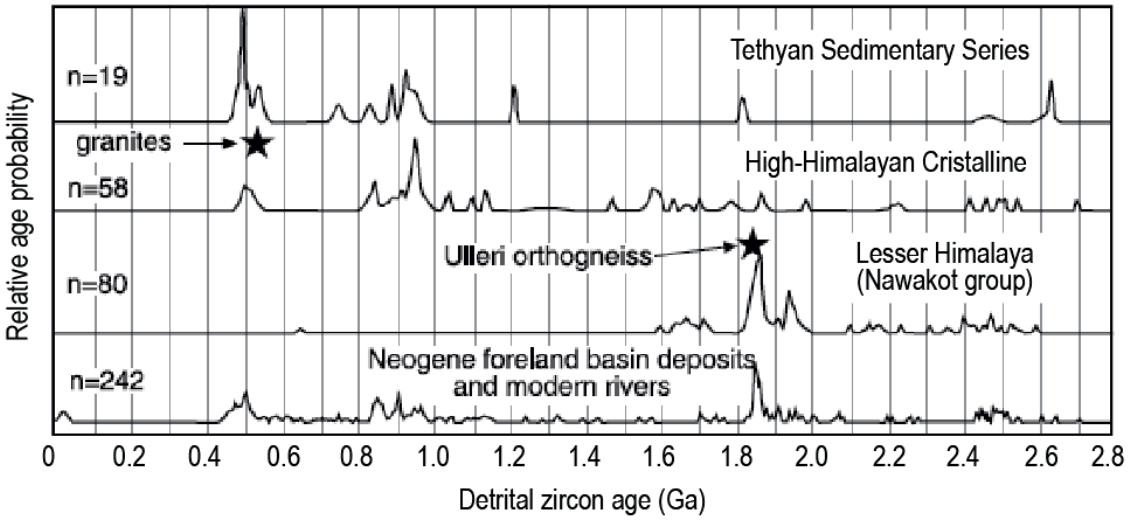

Figure I.5 : Distribution des âges U-Pb sur zircons détritiques dans les principales entités géologiques de la chaîne Himalayenne (Tethyan Sedimentary Series, High-Himalayan Cristalline, Lesser Himalaya) et dans ses produits d'érosion (Neogene foreland basin deposits i.e. Siwaliks et modern rivers). Modifié d'après DeCelles et al. (2000).

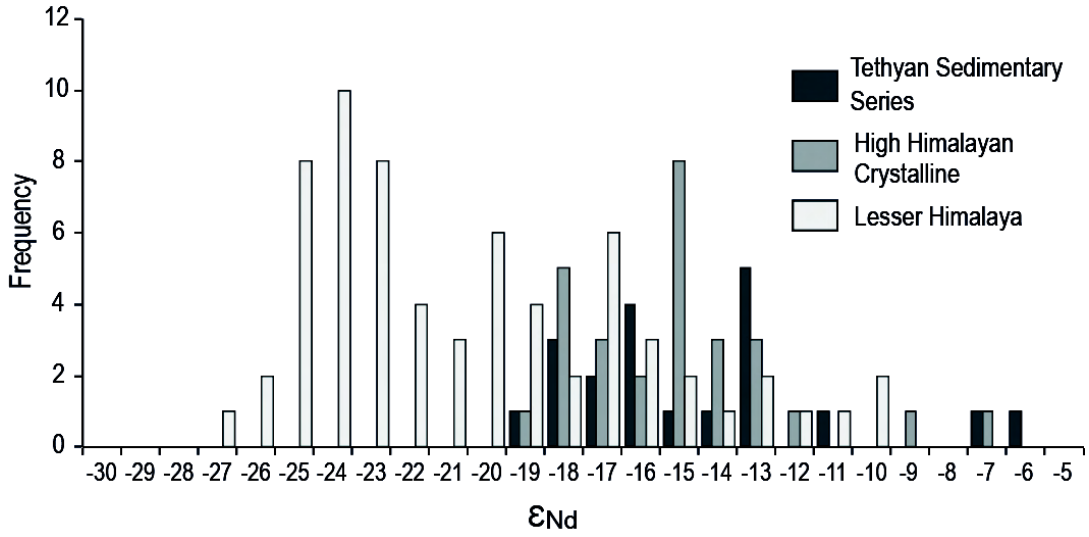

Figure I.6 : Répartition des compositions isotopiques en Nd dans les principales entités géologiques de la chaîne Himalayenne (Tethyan Sedimentary Series, High-Himalayan Cristalline, Lesser Himalaya) compilée à partir des données de Parrish et Hodges (1996), Ahmad et al. (2000), Robinson et al. 2001) et Richards et al. (2005). Les εNd sont recalculés en utilisant la valeur actuelle du CHUR déterminée par Bouvier et al. (2008).

L'unité du Haut-Himalaya Cristallin ("High Himalayan Cristalline" ou "Greater Himalaya") se situe entre le chevauchement central du MCT et le "South Tibetan Detachment" (STD) ayant fonctionné en faille normale (Figure I.4). Elle est constituée de méta-sédiments fortement métamorphisés (faciès amphibolite à granulite) dans lesquels se

trouvent quelques intrusions de leucogranites (Le Fort, 1975; Upreti, 1999). L'unité est classiquement divisée en trois formations constituées de différents types de gneiss (gneiss quartzeux et micacés, gneiss calciques et gneiss oeillés). Elle contient des zircons d'âge U-Pb Protérozoïque à Cambrien, globalement plus jeunes que ceux du "Lesser Himalaya" (Figure I.5), et est donc caractérisée par des compositions isotopiques en Nd plus radiogéniques (Figure I.6). L'origine des précurseurs sédimentaires du Haut-Himalaya Cristallin est encore débattue. Parrish et Hodges (Parrish and Hodges, 1996) suggèrent qu'ils se seraient déposés, à partir du Néoprotérozoïque, au nord de la marge Indienne, en discordance sur les protolithes du Bas-Himalaya alors que DeCelles et al. (2000) et Robinson et al. (2001) proposent une origine plus exotique (orogène Panafricaine) suivie d'une une accrétion tardive à la marge Indienne.

Viennent ensuite les Séries Sédimentaires Téthysiennes ("Tethyan Sedimentary Series"), délimitée au nord par la zone de suture de l'Indus-Tsangpo (ITSZ) qui sépare la plaque Indienne de la plaque Eurasiatique (Figure I.4). Cette unité est constituée d'une succession quasi-complète de roches sédimentaires marines d'âge Cambrien à Crétacé Supérieur (ca. 500-100 ma), plissée, faiblement métamorphisée et riche en fossiles (Garzanti, 1999; Upreti, 1999). Pratiquement tous les stades de la sédimentation marine Téthysienne y sont enregistrés: dépôts épicontinentaux siliciclastique-carbonate du stade pré-rift ; sédiments de rampe carbonatée, grès et mudrock syn-rift ; unité transgressive sableuse à marneuse et carbonates pélagiques ; plate-forme carbonatée de marge passive mature ; et enfin, dépôt d'arénites, calcaires marneux pélagiques et argiles profondes (Garzanti, 1999). Les compositions isotopiques en Nd et la répartition des âges U-Pb sur zircons détritiques des Séries Sédimentaires Téthysiennes sont quasi indissociables de celles du Haut-Himalaya Cristallin (Figures I.5 et I.6).

Enfin, la zone de suture de l'Indus-Tsangpo est relativement complexe. Elle est principalement constituée d'un mélange de flysch à blocs et d'ophiolites. Plus au nord, sur la marge Eurasiatique, se trouvent les batholithes du Trans-Himalaya ("Trans-Himalayan Batholits" ou "Gangdese Batholits" dans l'Himalaya central ; Figure I.4) datés du Crétacé Supérieur à l'Eocène (100-50 Ma). Il s'agit d'intrusions de roches magmatiques et volcaniques (diorites, granodiorites, andésites) interprétés comme la trace d'un volcanisme d'arc ou d'avant arc associée à la subduction de l'océan Téthysien (Wen et al., 2008 ; Schärer et al., 1984).

I.3. Le système fluviatile du Gange

I.3.1. Réseau hydrographique et bassin de drainage

Le système fluviatile du Gange draine une superficie d'environ 1 million de km^2 dont la moitié est constituée par la plaine Indo-Gangétique (Singh et al., 2007) (Figure I.1). Le Gange trouve sa source dans la haute chaîne Himalayenne, à 3800 m d'altitude, à la base du glacier de Gangotri dans la région du Garhwal. Après avoir parcouru plus de 500 km dans la chaîne Himalayenne, il émerge dans la plaine Indo-Gangétique à Haridwar à 300 m d'altitude (Singh et al., 2007).

Dans la plaine Indo-Gangétique, le Gange s'écoule sub-parallèlement à la chaîne Himalayenne. Il est rejoint par de nombreux tributaires dont la Yamuna, la Karnali (appelée Ghaghara en Hindi), la Narrayani (appelé Gandak en Hindi) et la Kosi (Figure I.1) qui drainent la partie centrale du flanc sud de la chaine Himalayenne i.e. les Séries Sédimentaires Téthysiennes, le Haut-Himalaya Cristallin, le Bas-Himalaya et les Siwaliks. Au sud, certains de ses tributaires, notamment la Chambal et la Betwa, drainent une partie du craton nord Indien et les basaltes des Traps du Deccan (Figure I.1). Après son parcours de plus de 2000 km au travers de la plaine Indo-Gangétique, le Gange rejoint le Brahmapoutre dans le delta du Bangladesh pour se jeter dans la Baie du Bengale et rejoindre l'océan Indien.

I.3.2. Hydrologie

Le débit moyen du Gange au Bangladesh est colossal. Il est estimé à environ 12 000 $m^3.s^{-1}$ (Islam et al., 1999), soit 380 km^3 d'eau par an, ce qui équivaut à environ 10 fois la consommation annuelle d'eau en France. Il est marqué par de fortes variations saisonnières largement influencées par le système de mousson Indienne qui affecte l'ensemble du système Himalayen de Juin à Septembre (Figure I.7a).

La mousson est provoquée par le déplacement d'une zone dépressionnaire contenant des masses d'air chaudes et humides (i.e. la zone de convergence intertropical) en direction de la Baie du Bengale pendant la période estivale (Gadgil, 2003). Ce système dépressionnaire favorise le déplacement des systèmes convectifs formés au dessus de la Baie du Bengale vers le N-NW (Figure I.7b) et donne naissance à d'intenses précipitations

(70 à 80% des précipitations annuelles) (Singh et al., 2007) qui se concentrent essentiellement sur les reliefs Himalayens à cause de l'effet orographique. Pendant cette période, le débit fluviatile du Gange au Bangladesh peut atteindre jusqu'à 40 000 $m^3.s^{-1}$ alors qu'il est généralement inférieur à 10 000 $m^3.s^{-1}$ en hiver (Figure I.7a).

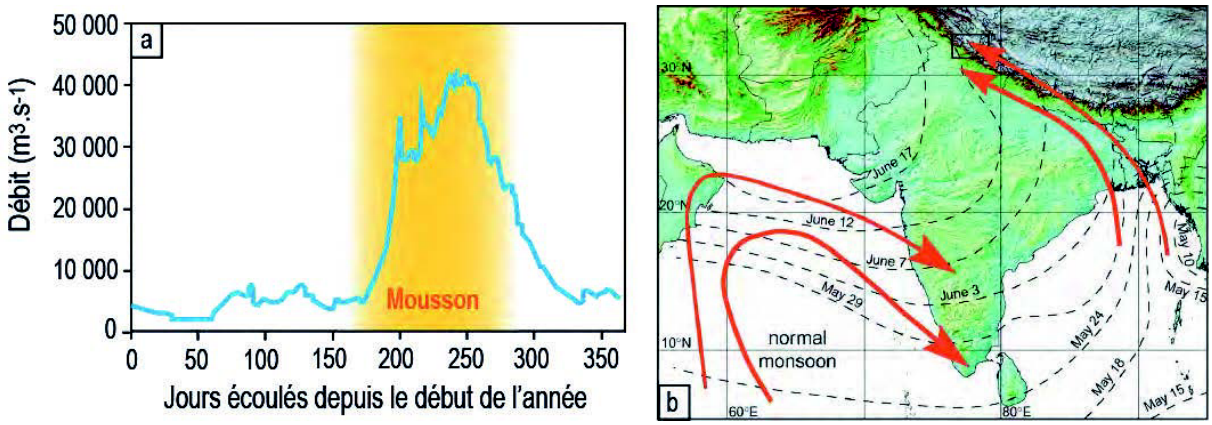

Figure I.7 : **a.** Hydrogramme du Gange au Bangladesh pour la période 1997-2005, modifié d'après Lupker et al. (2011). **b.** Direction des vents pendant la mousson Indienne (flèches oranges). Les lignes pointillées indiquent l'avancée temporelle de la mousson et sa propagation vers le nord-ouest. Modifié d'après Bookhagen et al. (2005a).

I.3.3. Dynamique sédimentaire

Malgré l'étendue de la plaine Indo-Gangétique, la plus grande partie du matériel érodé en amont est exporté vers la Baie du Bengale. Lupker et al. (2011) estiment que moins de 10% des produits d'érosion de la chaîne Himalayenne sont séquestrés dans la plaine Indo-Gangétique. Le temps de résidence des sédiments dans le bassin de drainage est peu connu et sujet à de nombreuses controverses. L'étude du déséquilibre des séries de l'uranium dans les sédiments Himalayens (Granet et al., 2007; 2010) suggère un temps de transfert relativement long entre le front de chaine et la plaine alluviale (i.e. la confluence avec le Gange) pour les sédiments grossiers transportés en fond de rivière (environ 100 000 ans) et un transfert beaucoup plus rapide pour les particules en suspension (<25 000 ans).

Au Bangladesh, le flux sédimentaire du Gange est estimé à environ 400 millions de tonnes par an (Lupker et al., 2011). Tout comme le débit fluviatile, la quantité de sédiment transportée par le Gange et ses principaux tributaires est fortement controlée par le système de mousson Indienne (Bookhagen et al., 2005b; Chakrapani and Saini, 2009; Wulf et al., 2010). Plus de 95% des particules en suspension sont exportées pendant la saison estivale,

de Juin à Septembre (Islam et al., 1999). La mousson et ses intenses précipitations jouent donc un rôle essentiel dans la dynamique sédimentaire du Gange. Elles favorisent, entre autres, les processus d'altération et d'érosion dans le basin de drainage et le transport des sédiments par le réseau fluviatile (Bookhagen et al., 2005b).

Avec le flux sédimentaire du Brahmapoutre, la quantité totale de sédiments délivrée dans la Baie du Bengale atteint plus d'un milliard de tonnes par an, ce qui fait du système Gange-Brahmapoutre le 3ème plus grand exportateur de sédiments au monde après l'Amazone et la "Yellow river" (Milliman and Meade, 1983; Milliman, 2001). Cette énorme quantité de sédiments, d'origine Himalayenne (France-Lanord et al., 1993), vient alimenter le Cône du Bengale qui s'étend sur plus de 3000 km au Sud du continent asiatique (Curray, 1994; Curray et al., 2003) (Figure I.8). L'épaisseur de sédiments est estimée à plus de 20 km juste au sud des côtes du Bangladesh et le volume total du cône avoisine les dix millions de km^3 (Curray, 1994; Radhakrishna et al., 2010). Les sédiments sont transportés dans les parties les plus distales du cône par le biais de systèmes turbiditiques (Curray, 1994; Curray et al., 2003).

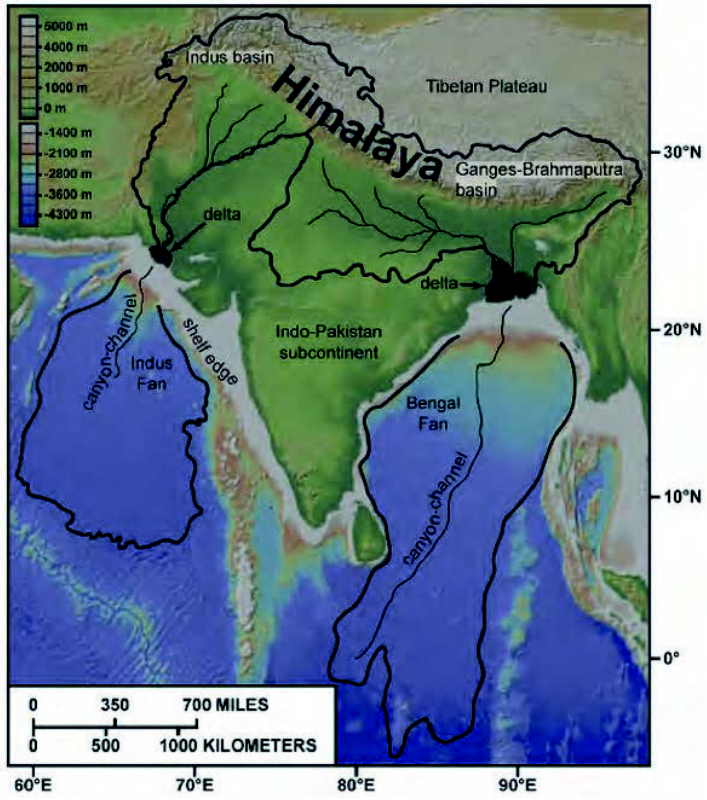

Figure I.8 : Situation et étendue du Cône du Bengal alimenté par les produits d'érosion de la chaine Himalayenne. D'après Covault (Mascle and Herail, 1982; Mugnier et al., 1999; Covault, 2011).

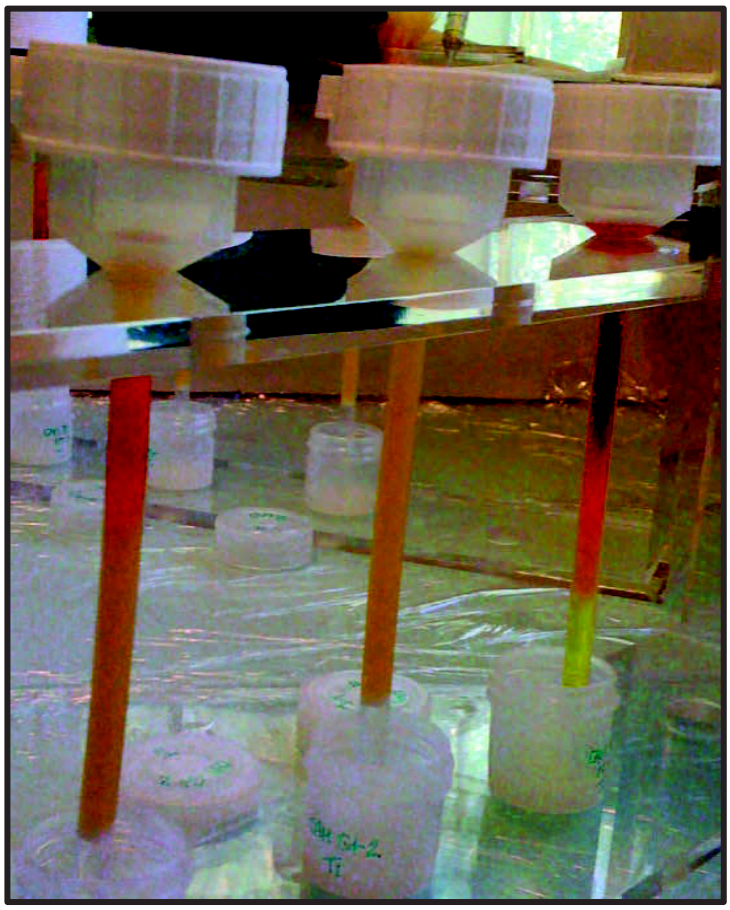

Chapitre 2

Méthodes

Ce chapitre a pour but de décrire les différentes méthodes et techniques analytiques utilisées au cours de ma thèse. Sont donc développés ici, l'échantillonnage et les méthodes de prélèvement sur le terrain, la séparation des fractions minérales et granulométriques, la préparation des sédiments de rivière à analyser et, enfin, l'ensemble des procédures analytiques utilisées pour mesurer les concentrations en éléments traces et les compositions isotopiques en Nd, Hf, Pb et Sr.

II.1. STRATEGIES D'ECHANTILLONNAGE 29

II.1.1. LOCALISATION DES ECHANTILLONS 29

II.1.2. METHODES D'ECHANTILLONNAGE 30

II.2. SEPARATION ET PREPARATION DES ECHANTILLONS 32

II.2.1. SEPARATION DES FRACTIONS MINERALES ET GRANULOMETRIQUES 32

II.2.2. PREPARATION DES ECHANTILLONS 34

II.2.2.A. BROYAGE ET REPRESENTATIVITE 34

II.2.2.B. DISSOLUTION 35

II.3. ANALYSES CHIMIQUES 38

II.3.1. ELEMENTS TRACES 38

II.3.1.A. DILUTION ET PREPARATION DES SOLUTIONS POUR ICP-MS 38

II.3.1.B. MESURE ET CALCUL DES CONCENTRATIONS EN ELEMENTS TRACES 40

II.3.1.C. EVALUATION DE LA QUALITE DES DONNEES ACQUISES 42

II.3.2. COMPOSITIONS ISOTOPIQUES EN ND, HF, PB ET SR 42

II.3.2.A. ISOLATION DU ND, HF, PB ET SR PAR CHROMATOGRAPHIE IONIQUE 42

II.3.2.B. CALCUL DES QUANTITES DE ND, HF, SR ET PB ISOLES 47

II.3.3.C. MESURE DES RAPPORTS ISOTOPIQUES EN ND, HF, PB ET SR 48

II.3.3.D. EVALUATION DE LA QUALITE DES DONNEES 49

II.1. Stratégies d'échantillonnage

II.1.1. Localisation des échantillons

Les sédiments de rivières analysés dans cette étude ont été échantillonnés dans le système fluviatile du Gange, en Inde, au Népal et au Bangladesh, en amont de la confluence avec le Brahmapoutre (Figure II.1). Dans la chaîne Himalayenne, des sédiments de petites rivières drainant des bassins monolithologiques ont été analysées pour documenter la variabilité chimique et isotopique des différentes formations géologiques. Nous avons également étudié une dizaine d'échantillons prélevés dans la Marsyandi au Népal, le long d'un profil traversant les Séries Sédimentaires Téthysiennes, le Haut Himalaya Cristallin et le Bas Himalaya. Le reste des échantillons a été prélevé dans le Gange et ses principaux tributaires, en sortie de chaîne et dans la plaine Indo-Gangétique, dans le but d'étudier les fractionnements chimiques et isotopiques liés au transport des sédiments, de leur source jusqu'à l'océan. Quand cela était possible, plusieurs types de sédiments ont été analysés à un même lieu d'échantillonnage : la charge de fond de rivière ("bedload") ou les sédiments déposés sur les berges ("bank sediment"), et les sédiments en suspension prélevés à différentes profondeurs dans la colonne d'eau ("suspended load").

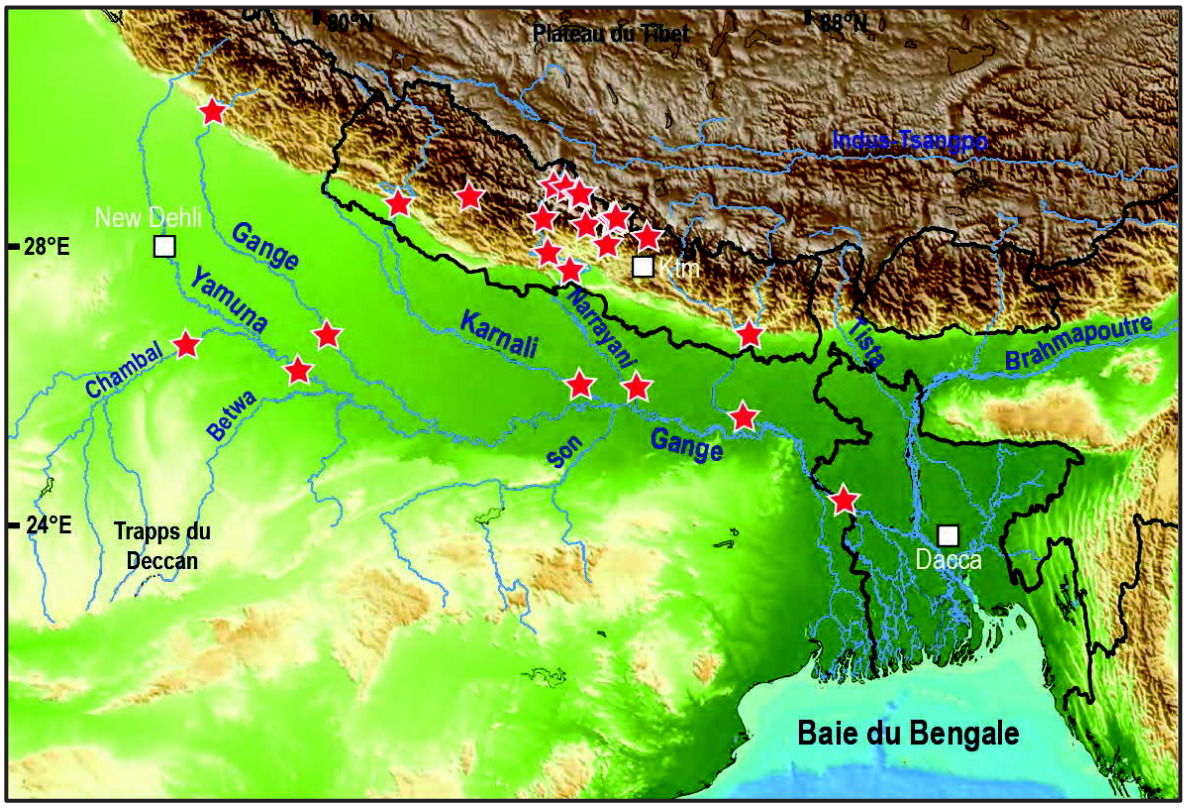

Figure II.1 : Lieux d'échantillonnage des sédiments de rivière analysés dans cette étude

La grande majorité des échantillons analysés dans cette étude provient des campagnes d'échantillonnage réalisées entre 1993 et 2009 par Christian France-Lanord, Albert Galy, Valier Galy, Jérôme Lavé et Marteen Lupker. La mission de terrain effectuée pendant ma première année de thèse (3 semaines en juillet 2010) au Bangladesh et au Népal avec Christian France-Lanord, Valier Galy, Marteen Lupker et Britta Voss, a permis de compléter cette collection d'échantillons et de ré-échantillonnés à certains endroits afin d'appréhender la variabilité temporelle des sédiments transportés par le Gange.

II.1.2. Méthodes d'échantillonnage

A l'exception des échantillons de la Marsyandi, pratiquement tous les sédiments analysés dans cette étude ont été collectés pendant la période de mousson Indienne i.e. entre Juin et Septembre.

Les sédiments en suspension sont échantillonnés depuis un bateau dans le chenal d'écoulement principal de la rivière, là ou la vitesse de l'eau est la plus importante. Les échantillons prélevés avant l'année 2007 ont été collectés dans des bouteilles lestées, descendues à la profondeur souhaitée, depuis le bateau. Depuis 2007, les sédiments en suspension sont prélevés à l'aide d'un échantillonneur conçu au Centre de Recherches Pétrographiques et Géochimiques (CRPG) de Nancy (Figure II.2a). Celui ci est constitué d'un tube en plastique d'une contenance de 5 litres, munis de 2 clapets latéraux qui peuvent être fermés depuis la surface par un système de vérin pneumatique. Des ailerons assurent la stabilité horizontale du tube dans l'eau (Figure II.2a). L'échantillonneur est lesté d'un poids de 20 kg et doter d'une sonde de profondeur. Il est attaché au bateau et plongé dans l'eau, clapets ouverts pour permettre à l'eau de circuler à l'intérieur du tube. Lorsque la profondeur d'échantillonnage souhaitée est atteinte, les clapets sont fermés pneumatiquement depuis la surface et l'échantillonneur est remonté à bord du bateau. Le contenu du tube est soigneusement vidé et transféré dans des poches plastiques (Figure II.2b). Quelques heures plus tard, les 5 litres d'eau prélevés par l'échantillonneur sont filtrés sous 2 à 4 bars de pression dans des unités en inox gainées par du téflon dans lesquelles se trouvent des filtres Micropore® 0.22 µm qui permettent de récupérer les particules en suspension (Figure II.2c). Les échantillons sont séchés à l'air libre avant d'être expédiés en France où ils seront lyophilisés.

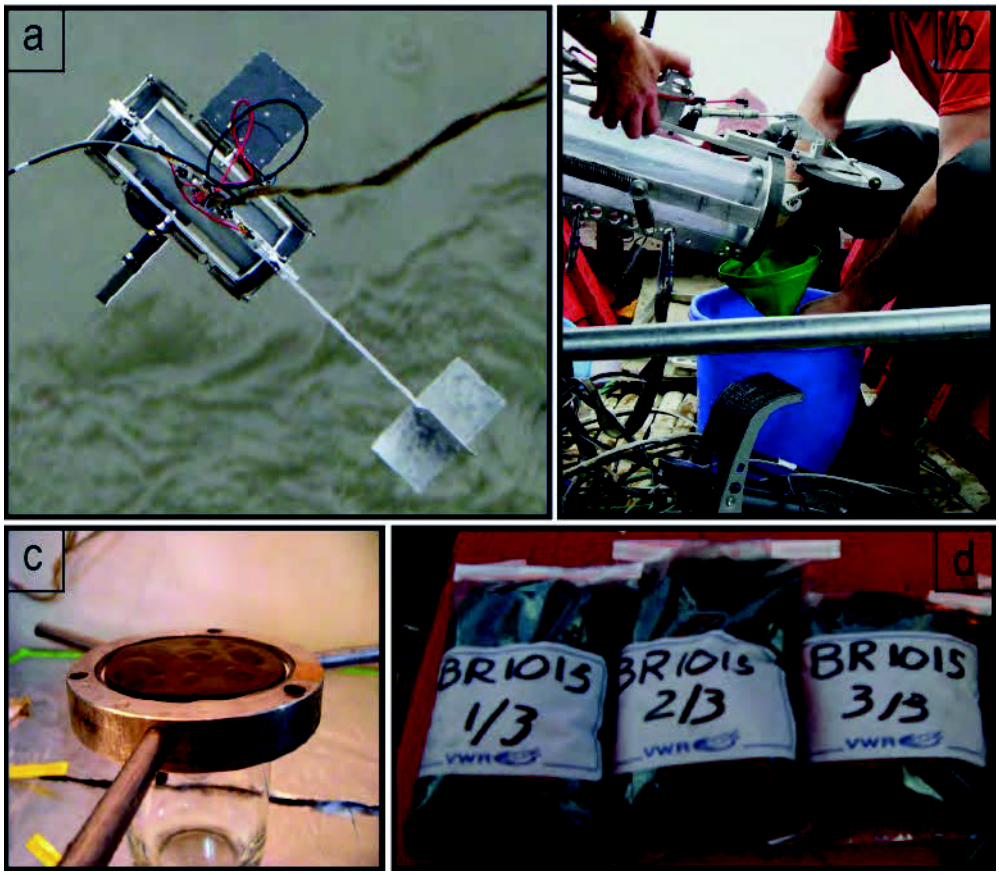

Figure II.2 : a. Echantillonneur de particules en suspension. **b.** Transvasage du contenu de l'échantillonneur dans une poche en plastique. **c.** Particules en suspension récupérées sur le filtre après filtration sous pression. **d.** Echantillons de "bedload".

Les sédiments de fond de rivière ("bedload") sont également échantillonnés depuis un bateau, si possible au même endroit que les sédiments en suspension. L'échantillonnage s'effectue par dragage en utilisant les moyens du bord c'est à dire à l'aide d'un tube en acier inoxydable munie d'une poche de récupération pouvant contenir plusieurs kilos de sédiments. Le tube est lancé au fond de la rivière et remonté une dizaine de minutes plus tard. Le contenu de la poche est directement transféré dans des sacs à échantillons hermétiques (Figure II.2d).

Lorsqu'il n'est pas possible d'échantillonner la charge de fond à cause des forts courants ou parce qu'il n'y a pas d'embarcation disponible, les sédiments sont prélevés sur la berge de la rivière ("bank sediment").

II.2. Séparation et préparation des échantillons

II.2.1. Séparation des fractions minérales et granulométriques

Les fractions granulométriques analysées dans cette étude ont été séparées au CRPG de Nancy, par tamisage sous flux d'eau distillée, à partir d'un "bedload" échantillonné à l'embouchure du Gange dans le delta du Bangladesh (échantillon BGP 6) et d'un "suspended load" échantillonné en front de chaîne dans la Narrayani (échantillon PB 60).

Les fractions minérales (biotite, muscovite, plagioclase, quartz, feldspath potassique, carbonate, magnétite, amphibole, apatite, grenat, épidote, titanite, monazite, allanite et zircon) ont toutes été séparées à partir d'un "bedload" échantillonné en 2007 dans le delta du Bangladesh (échantillon BR 717). Cet échantillon a été choisi pour sa position stratégique (i.e. à l'embouchure du Gange) et parce qu'il présentait des teneurs élevés en éléments traces qui présageaient d'une forte concentration en minéraux lourds et donc d'une séparation plus aisée des différentes fractions minérales. Les fractions minérales ont été séparées à partir de différentes fractions granulométriques (63-100 µm, 125-250 µm et >250 µm) à Grenoble et au "Laboratorio di Petrografia del Sedimentario" à Milan en collaboration avec Eduardo Garzanti et son étudiante, Mara Limonta.

Le protocole de séparation est illustré sous forme d'organigramme en Annexe 1. Les séparations sont effectuées en fonction de la densité grâce à plusieurs passages en liqueurs denses (iodure de méthylène et metatungstate de sodium) préalablement calibrées à la densité souhaitée. Chaque passage nécessite plusieurs centrifugations et au moins une journée de décantation afin de bien séparer les minéraux lourds des minéraux légers. Les minéraux lourds tombés au fond des tubes remplis de liqueur dense sont ensuite congelés à l'azote liquide afin de faciliter la récupération des minéraux légers flottant à la surface. Les fractions récupérées sont abondamment rincées à l'eau distillée pendant une journée et re-séparées en fonction de leur susceptibilité magnétique à l'aide d'un aimant et d'un séparateur magnétique isodynamique Frantz. L'ensemble de ces étapes permet d'obtenir des fractions enrichies en certains types de minéraux mais qui contiennent de très nombreuses impuretés. Celles-ci doivent donc être méticuleusement triées, purifiées et vérifiées plusieurs fois sous la loupe binoculaire et le microscope polarisant afin d'obtenir des fractions minérales pures (Figure II.3).

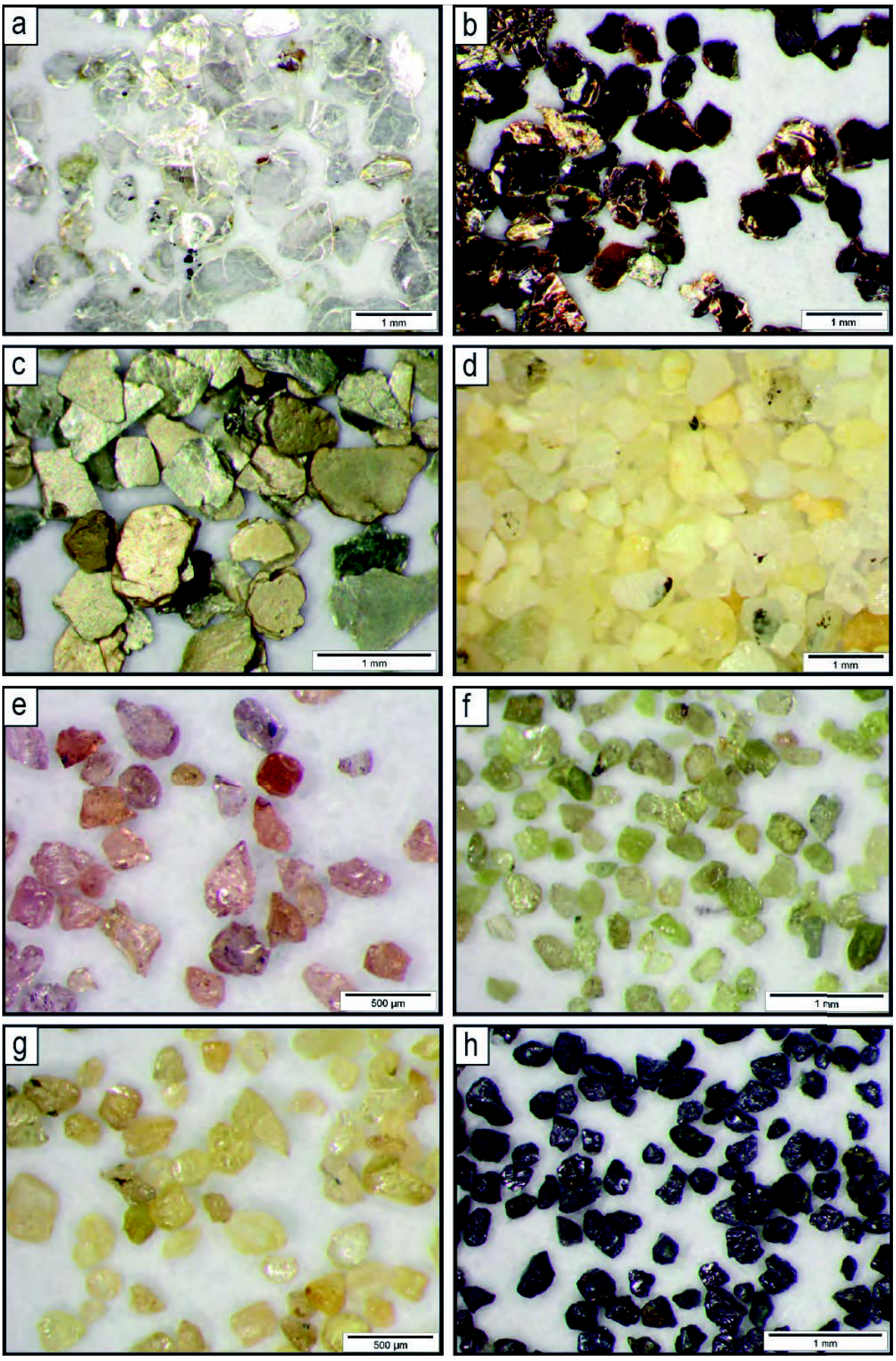

Figure II.3 : Exemples de fractions minérales séparées du “bedload” BR 717. **a.** Muscovite **b.** Biotite **c.** Vermiculite **d.** Feldspath-K **e.** Grenats **f.** Epidote **g.** Titanite **h.** Amphibole

Malgré toutes ces techniques, certaines fractions n'ont pas pu être totalement purifiées du fait de la petite taille des minéraux ou de leur très faible abondance dans l'échantillon de départ, c'est notamment le cas des fractions de monazites, allanites et apatites. Ce problème est abordé dans le Chapitre IV consacré aux compositions chimiques et isotopiques des minéraux, il conviendra donc de s'y reporter pour de plus amples détails.

Il est à noter que la fraction de carbonate n'a pas été séparée selon le protocole décrit ci-dessus. Elle a été obtenue par leaching à l'acide acétique 1M d'une fraction déjà enrichie en carbonates mais contenant de grandes quantités de quartz, feldspaths et micas (fraction non magnétique 125-250 µm d'une densité < 2.90 $g.cm^{-3}$). Ce leaching e été réalisé à température ambiante selon le protocole décrit par Galy et al. (Figure I.4; Le Fort, 1975; Galy et al., 1999).

II.2.2. Préparation des échantillons

II.2.2.a. Broyage et représentativité

Tous les échantillons sont broyés dans des bols en agate à l'aide d'un broyeur à rotation planétaire afin d'obtenir une poudre fine qui soit la plus homogène possible. La qualité de la poudre est systématiquement vérifiée sous la loupe binoculaire. Elle est re-broyée si l'on distingue encore des minéraux résiduels au grossissement maximum. Malgré ces précautions, les premières mesures d'éléments traces réalisées sur des sédiments de rivière dupliqués présentaient des variations importantes, vraisemblablement liées à une trop faible quantité de matériel initialement dissous et donc à une mauvaise représentativité des analyses effectuées. Nous avons donc réalisés des tests de représentativité à partir d'un échantillon prélevé dans la chaîne Himalayenne ("bank sediment" MO 59). Ces tests consistaient à mesurer les teneurs en éléments traces dans différentes quantités de poudre finement broyée et dissoute (25 mg, 50 mg, 75 mg, 100 mg, 125 mg et 150 mg) afin de déterminer la quantité minimale d'échantillon nécessaire à une bonne représentativité des analyses de sédiments de rivières Himalayennes.

Si l'on considère que les analyses réalisées sur 150 mg de poudre sont représentatives de la composition du sédiment de départ, les résultats montrent que la représentativité des analyses est d'autant moins bonne que la quantité d'échantillon initialement dissoute est faible (Figure II.4). Les différences relatives de concentrations en éléments traces mesurées dans 25 mg d'échantillon, par rapport à celles mesurées dans

150 mg d'échantillon, varient entre -35 et +15%. Ces différences, qui diminuent lorsque la quantité d'échantillon augmente (Figure II.4), sont probablement liées à des "effets pépites" (i.e. à l'hétérogénéité du matériel de départ). Dans la suite de notre étude, les analyses chimiques de sédiments de rivières sont donc systématiquement effectuées sur plus de 50 mg de poudre d'échantillon afin de garantir une bonne représentativité des mesures.

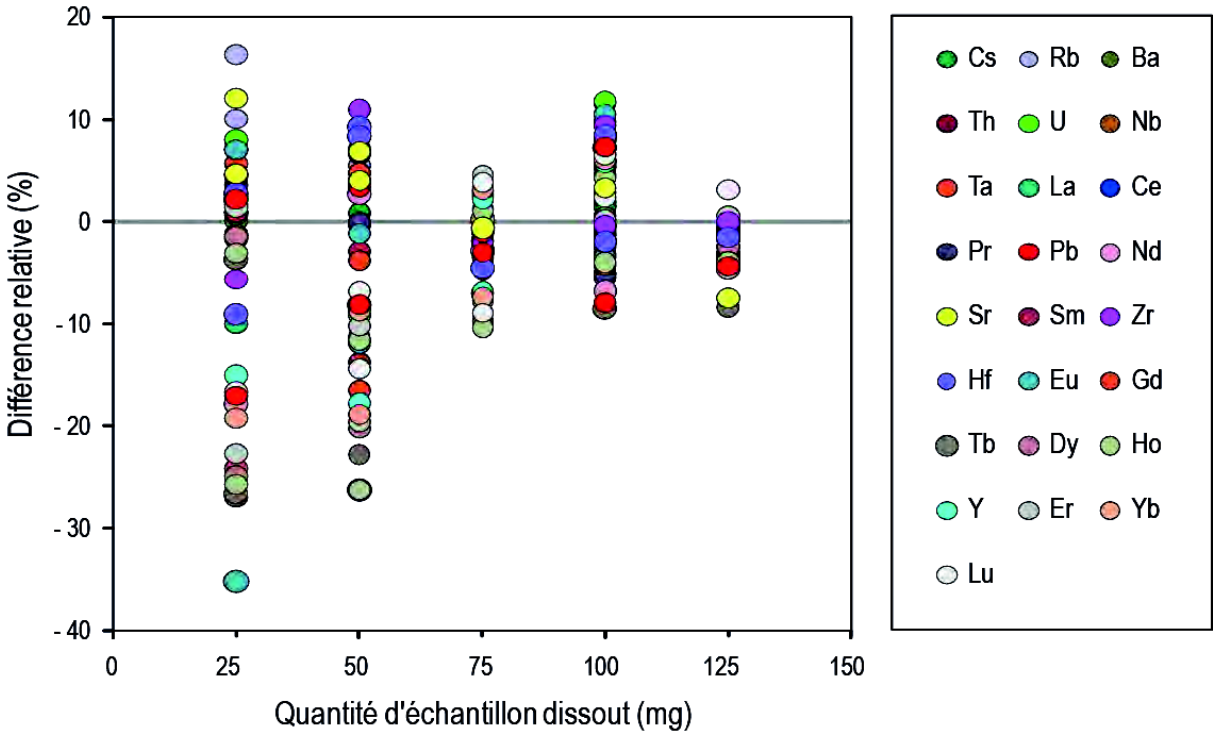

Figure II.4 : Différences relatives entre les concentrations en éléments traces mesurées dans différentes quantités de poudre d'échantillon MO 59 (25 mg, 50 mg, 75mg, 100mg et 125 mg) par rapport à la moyenne des concentrations mesurées dans 150 mg de poudre de ce même échantillon.

II.2.2.b. Dissolution

La dissolution des échantillons par attaque acide est une étape critique, notamment lorsqu'il s'agit de sédiments de rivières contenant de nombreux minéraux réfractaires tels que les zircons. La non-dissolution totale de ces minéraux peut, en effet, significativement biaisé certaines analyses chimiques, notamment les concentrations en éléments traces et les compositions isotopiques en Hf. Nous l'avons malheureusement appris à nos dépens puisque nous avons du ré-analyser plus d'une soixantaine d'échantillons (éléments traces et

compositions isotopiques en Hf) pour des problèmes liés à la dissolution de ces minéraux réfractaires. Plusieurs tests ont donc été effectuées sur différents types de sédiments (bank, bedload et suspended load) afin d'élaborer un protocole de dissolution efficace qui permettrait la mise en solution totale et systématique des zircons présents dans les sédiments de rivières.

Les tests de dissolution sont réalisés sur 100 mg de poudre d'échantillon finement broyée. Ces dernières sont attaquées dans un mélange constitué de 5 mL d'acide fluorhydrique (HF) 24N et 40 gouttes d'acide perchlorique ($HClO_4$) 14N, en bombes pressurisées (bombes PARR®) à différentes températures (140°C, 150°C ou 200°C) pendant des durées variables (1, 3 ou 6 semaines). L'effet d'une pré-attaque dans 3mL d'acide nitrique (HNO_3) 14N ou dans 2mL d'acide fluorhydrique 24N, en bécher Savillex® sur plaque à 130°C pendant 48h suivi d'une évaporation avant la mise en bombes des échantillons, est également testé. Précisons que le laboratoire de Géochimie a dû se doter de nouveau matériel pour pouvoir réaliser ces tests et attaquer les échantillons à plus de 150°C (achat de 6 nouvelles bombes PARR® résistantes à des températures supérieures à 150°C et nouvelle étuve pouvant monter à plus de 150°C). Les concentrations en éléments traces de ces différentes attaques sont ensuite mesurées et comparées à celles mesurées sur des résidus de fusion au métaborate de lithium (analyses réalisées par le Service d'Analyse des Roches et des Minéraux du CRPG de Nancy sur les mêmes échantillons, données publiées par Lupker et al. (2011)). La technique de mesure des concentrations en éléments traces par fusion au métaborate de lithium garantit une destruction totale des minéraux réfractaires, y compris des zircons, mais elle est souvent plus polluante que les techniques de dissolution par attaque acide, qui sont donc plus appropriées pour les mesures de compositions isotopiques réalisées dans cette étude.

Les résultats de nos tests de dissolution sont présentés dans la Figure II.5. Elle montre les différences relatives de concentrations en Zr mesurées dans nos différentes attaques par rapport à celles mesurées sur les résidus de fusion dans lesquels nous estimerons que tous les zircons ont été détruits. Un protocole de dissolution efficace dans lequel tous les zircons ont été dissous se traduit donc par une différence relative de concentration en Zr proche de zéro. Au contraire, plus le protocole de dissolution est inefficace, plus la différence relative de concentration en Zr est négative.

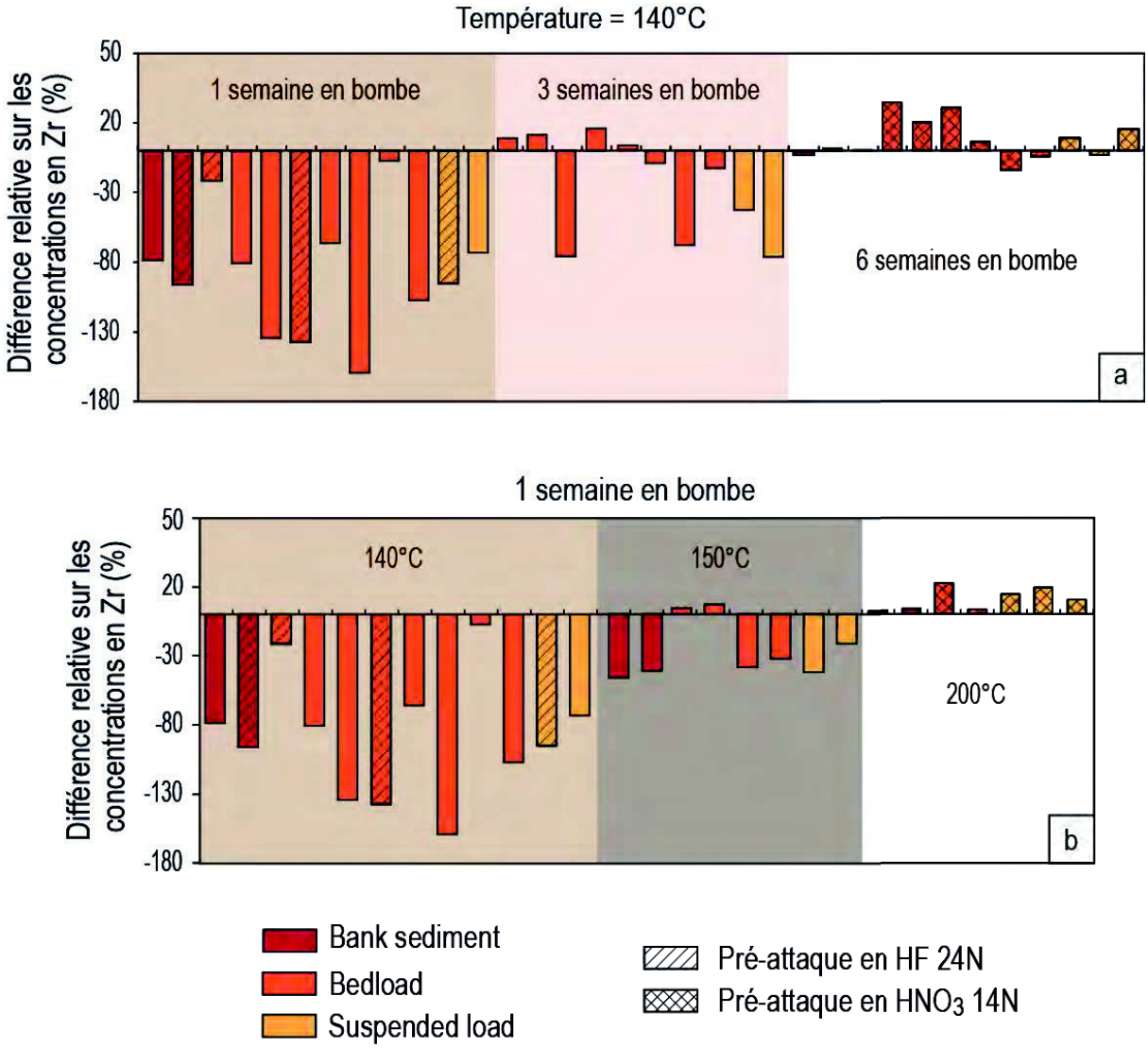

Figure II.5 : Histogrammes présentant les différences relatives entre les concentrations en Zr mesurées dans les sédiments de rivières Himalayennes sur des résidus de fusion au métaborate de Lithium et celles mesurées sur les mêmes sédiments ayant subi des protocoles d'attaque chimique différents. Chaque barre représente un échantillon. **a.** Attaques en bombes pressurisées à 140°C pendant 1, 3 ou 6 semaines. **b.** Attaques en bombes pressurisées pendant 1 semaine à différentes températures i.e. 140°C, 150°C ou 200°C.

Nos résultats démontrent que la dissolution est d'autant plus efficace que la durée d'attaque est longue ou que la température est élevée (Figure II.5). Quelque soit le type de sédiments, l'attaque en bombe à 140°C doit durer plus de 6 semaines et être précédée d'une pré-attaque en HNO_3 14N pour garantir une dissolution totale des zircons présents dans les sédiments de rivière (Figure II.5.a). Notons que la pré-attaque en HF 24N avant la mise en bombe des échantillons n'a aucun effet remarquable sur l'efficacité de la dissolution

à 140°C pendant 1 semaine. La durée d'attaque peut être considérablement réduite à condition d'augmenter la température (Figure II.5.b). Ainsi, après une pré-attaque en HNO_3 14N, une semaine d'attaque à 200°C donne des résultats aussi satisfaisants que 6 semaines d'attaque à 140°C. Les concentrations en éléments traces et les compositions isotopiques de tous nos échantillons ont donc été analysées après 1 semaine d'attaque à 200°C ou 6 semaines à 140°C, en fonction du matériel disponible.

II.3. Analyses chimiques

Pour chaque échantillon, l'ensemble des analyses chimiques est généralement réalisé sur la même attaque. Une fois dissous, l'échantillon est séparé en deux fractions : la première est utilisée pour mesurer les concentrations en éléments traces et la deuxième est utilisée pour mesurer les compositions isotopiques en Nd, Hf, Pb et Sr. La Figure II.6 résume les différentes étapes de la procédure analytique.

J'ai mesuré les concentrations en éléments traces et les compositions isotopiques en Nd, Hf et Pb sur plus d'une centaine d'échantillons (sédiments de rivière, fractions minérales et fractions granulométriques) et les compositions isotopiques en Sr sur une trentaine d'échantillons (quelques sédiments de rivières et les fractions minérales et granulométriques).

II.3.1. Eléments traces

La préparation des échantillons et les mesures de concentrations en éléments traces sur spectromètre de masse à plasma couplé par induction (ICP-MS) sont réalisées à Grenoble, au laboratoire de Géochimie d'ISTerre.

II.3.1.a. Dilution et préparation des solutions pour ICP-MS

Une fois dissous, les échantillons sont transvasés dans des savillex® et les solutions d'attaque sont évaporées sur plaque chauffante à 130-150°C. Pour éliminer tous les complexes fluorés formés pendant l'attaque, les échantillons sont repris dans 2 fois 3 mL d'HNO_3 14N sur plaque chauffante à 120°C puis évaporés à sec.

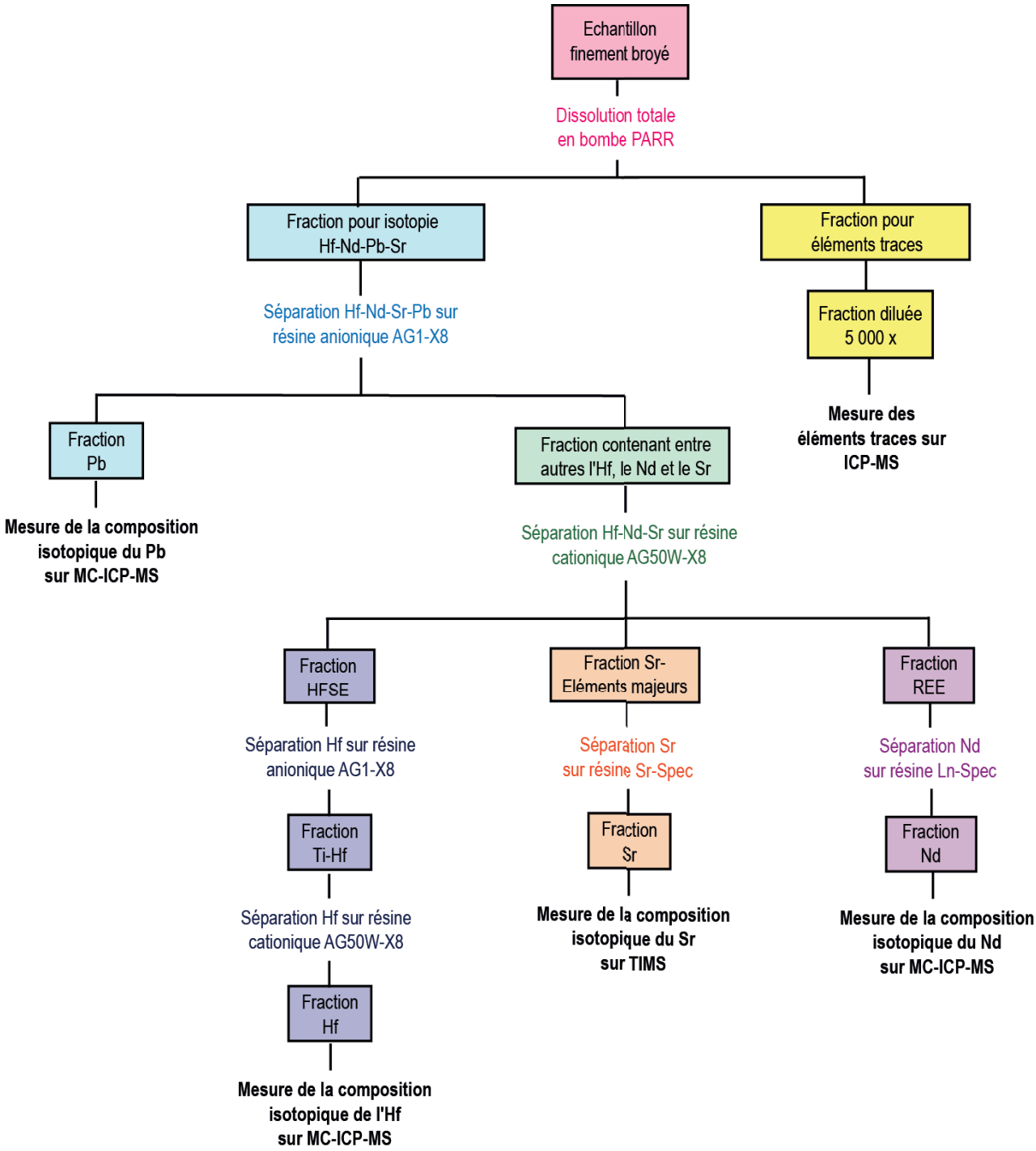

Figure II.6 : Organigramme présentant les différentes étapes de la procédure analytique permettant de mesurer les concentrations en éléments traces et les compositions isotopiques en Nd, Hf, Pb et Sr à partir d'une même attaque.

Préparation des solutions mères

Les résidus d'évaporation à sec sont repris dans 20 à 40 mL d'HNO_3 7N + quelques gouttes d'HF sur plaque chauffante à 120°C. Une aliquote correspondant à 2 ou 4 mg d'échantillon est prélevée et transvasée dans un autre savillex® : elle sera utilisée pour mesurer les concentrations en éléments traces dans l'échantillon. Le reste de la solution servira à mesurer les compositions isotopiques en Hf, Nd, Sr et Pb.

Une solution d'HNO_3 7N + quelques gouttes d'HF est ajoutée dans les savillex® contenant l'aliquote pour les éléments traces afin d'obtenir environ 4g de solution. Cette dernière solution est appelée "solution mère". Elle est pesée précisément et peut être conservée plusieurs jours au réfrigérateur du fait de la forte normalité de l'acide utilisée.

Préparation des solutions filles pour l'ICP-MS

Les solutions filles sont les solutions très diluées (environ 5000 fois) qui seront réellement analysées par l'ICP-MS. Pour préparer ces solutions, des aliquotes des solutions mères sont prélevées dans les savillex® et transvasés dans des petits béchers en PTFE en téflon préalablement pesés. La quantité d'aliquote prélevée est pesée précisément, elle varie entre 1 et 2mL en fonction de la quantité exacte d'échantillon réellement présente dans la solution mère. Une solution dopée en Be, Ge, In, Tm et Bi (multispike de concentrations connues) est ajoutée dans chacun des échantillons. L'ajout de ces éléments permet de contrôler et corriger la dérive instrumentale liée aux fluctuations de sensibilité de l'ICP-MS lors de la séquence de mesures (cf partie suivante). La quantité de multispike ajoutée dans les échantillons est calculée de manière à ce que sa concentration soit d'environ 15 ppb dans la solution fille finale. Le contenu des béchers en PTFE est évaporé à sec sur plaque chauffante à 110°C afin de bien mélanger le multispike et l'échantillon.

Dans les béchers en PTFE, les résidus secs sont repris dans quelques mL d'HNO_3 2% + traces d'HF (solution de reprise pour l'ICP-MS) puis transvasés dans des piluliers préalablement pesés. Les solutions filles finales sont obtenues en ajoutant la quantité d'HNO_3 2% + traces d'HF nécessaire pour obtenir le facteur de dilution souhaité (i.e. 5 à 30 mL dans notre cas). La faible concentration d'acide dans la solution de reprise rend les solutions filles finales particulièrement instables, elles sont donc préparées quelques heures avant d'être analysées sur l'ICP-MS.

II.3.1.b. Mesure et calcul des concentrations en éléments traces

Les mesures sont réalisées sur ICP-MS (Agilent 7500ce) en mode plasma robuste. Une séquence de mesure permet de mesurer les concentrations en éléments traces d'une vingtaine d'échantillons. La procédure type consiste à analyser :

(1) les solutions de reprise,

(2) le (ou les) blanc(s) de chimie, généralement 1 blanc par série de 10 échantillons,

(3) des solutions d'interférences de concentrations connues (solutions pures de Ba, Ce et Pr+Nd) qui serviront à corriger les interférences isobariques liées à la formation d'oxydes et d'hydroxydes pendant la séquence de mesure,

(4) des standards de roches qui serviront à évaluer la validité des concentrations mesurées,

(5) les échantillons (solutions filles) et les standards de calibration externe (BR ou BR 24) que l'on passera tous les quatre ou cinq échantillons,

(6) des échantillons dupliqués issus d'attaques différentes, généralement un par série de 10 échantillons,

(7) des échantillons répliqués (solutions filles préparées à partir de la même solution mère), généralement un par série de 10 échantillons,

(8) des solutions filles analysées en début de séquence et repassées à la fin (échantillons "bis").

Pour chaque échantillon et pour chaque élément mesuré, l'ICP-MS renvoie un nombre de coups (donnée brute) sur lequel il est nécessaire d'effectuer quelques corrections avant de calculer les concentrations en éléments traces. Pour chaque élément, le nombre de coups mesurés dans le blanc de chimie est soustrait aux nombres de coups mesurés dans les échantillons et les standards. Les interférences isobariques liées à la formation d'oxydes et d'hydroxydes dans la torche à plasma du spectromètre sont corrigées sur les éléments interférés grâce aux nombres de coups mesurés dans les solutions d'interférences (correction basée sur la valeur du rapport métal sur hydroxyde ou oxyde dans la solution d'interférence). La dérive instrumentale pendant la séquence d'analyse est corrigée grâce aux nombres de coups mesurés sur les éléments constitutifs du multispike qui a été ajouté dans chacun des échantillons lors de la préparation des solutions filles (Be, Ge, In, Tm et Bi). En considérant les teneurs naturelles en Be, Ge, In, Tm et Bi négligeables par rapport à la quantité apportée par le multispike, les nombres de coups mesurés sur ces cinq éléments dans tous les échantillons correspondent aux concentrations connues du multispike ajouté. La dérive instrumentale au cours de la séquence de mesures peut donc être évaluée à partir des nombres de coups mesurés sur ces éléments. Elle est supposée dépendante de la masse autrement dit deux éléments de masse similaire sont supposés être affectés par des dérives instrumentales similaires.

Les concentrations en éléments traces dans tous les échantillons sont finalement calculées en tenant compte des facteurs de dilution exactes des solutions filles et en utilisant la relation linéaire qui relie les nombres de coups corrigés et les concentrations connues des standards de calibration externes BR et BR 24 (valeurs publiées par Chauvel et al., 2011).

II.3.1.c. Evaluation de la qualité des données acquises

Pendant une séquence d'analyse sur ICP-MS, plusieurs échantillons sont analysés deux fois ("échantillons bis") pour évaluer la reproductibilité des mesures. Pour tous les échantillons analysés dans cette étude, les différences relatives de concentration entre deux "échantillons bis" sont généralement inférieures à 2%. La dérive instrumentale est donc bien corrigée et l'on peut considérer que les mesures sont reproductibles.

Les concentrations mesurées dans les échantillons répliqués (solutions filles préparées à partir de la même solution mère) permettent d'évaluer la reproductibilité de la procédure analytique de préparation des solutions filles. Les différences relatives de concentration entre les solutions répliquées sont généralement inférieures à 5% pour la plupart des éléments traces.

La reproductibilité de la procédure analytique complète (dissolution, préparation des solutions mères et filles) est estimée grâce aux concentrations mesurées dans les échantillons dupliqués. Les différences relatives de concentration entre les échantillons dupliqués sont inférieures à 5% pour la grande majorité des éléments traces mesurés. Des différences plus importantes (jusqu'à 10%) sont quelquefois remarquées sur certains éléments (Pb, Cs, Rb, Th, U) probablement dues à l'hétérogénéité du matériel de départ.

Enfin, la validité des concentrations mesurées est évaluée par comparaison entre les résultats obtenus pour les standards de roche analysés en tant qu'échantillons inconnus (BEN, AGV-1, JSd-2) et les valeurs de référence publiées pour ces mêmes standards (2000; Chauvel et al., 2011). Les différences entre les valeurs de référence et celles mesurées sont généralement inférieures à 5%. Ces résultats satisfaisants assurent la fiabilité des concentrations en éléments traces mesurées dans cette étude.

Les valeurs obtenues pour les échantillons dupliqués et les standards de roche analysés en tant qu'échantillons sont présentées et discutés dans les parties "Méthodes" des différents manuscrits.

II.3.2. Compositions isotopiques en Nd, Hf, Pb et Sr

II.3.2.a. Isolation du Nd, Hf, Pb et Sr par chromatographie ionique

La mesure précise des isotopes du Nd, de l'Hf, du Pb et du Sr nécessite une séparation chimique de ces 4 éléments afin de limiter les interférences isobariques et les effets de matrice lors de la mesure des rapports isotopiques sur MC-ICP-MS (Multi-Collector - Inductively Coupled Plasma - Mass Spectrometer) et TIMS (Thermal Ionization Mass Spectrometer). La procédure analytique utilisée pour isoler le Nd, l'Hf, le Pb, et le Sr à partir

d'une même attaque (Figure II.6) est basée sur les techniques décrites par Chauvel et al. (2011), Carpentier (2007), Blichert-Toft et al. (1997), Mahnès et al. (1984). Toute la procédure de séparation chimique est réalisée à Grenoble, au laboratoire de Géochimie d'ISTerre. Les mesures de compositions isotopiques sont effectuées à l'Ecole Nationale Supérieure (ENS) de Lyon et au Laboratoire Domaines Océaniques de Brest.

Isolation du Pb

La première étape consiste à isoler le Pb des autres éléments chimiques (Figure II.6), notamment du ^{204}Hg et du ^{205}Tl qui peuvent interférer lors de la mesure des rapports isotopiques du Pb sur MC-ICP-MS. Les fractions non utilisées pour les mesures de concentration en éléments traces sont évaporées à sec et reprises deux fois dans 5 mL d'HCl 6N + 5 gouttes d'HBr concentré sur plaque chauffante à 120°C. L'ajout d'acide bromhydrique (HBr) permet de complexer le plomb présent dans l'échantillon sous la forme $PbBr_2$, $PbBr^+$, $PbBr_3^-$ et $PbBr_4^{2-}$. Ce sont ces complexes qui seront retenus sur la résine échangeuses d'ions. Les échantillons sont ensuite évaporés à sec et repris dans de l'HBr 0.7N sur plaque à 120°C. Ils sont passés aux ultra-sons pour dissocier les précipités résiduels puis centrifugés à 6000 tours/minute pendant 5 minutes. A ce stade, certains échantillons présentent des résidus importants au fond des tubes à centrifuger (précipités insolubles en HBr 0.7N). Seul le surnageant sera chargé sur les résines car les particules solides pourraient empêcher le liquide de s'écouler correctement et nuire à la bonne séparation du Pb.

L'extraction du Pb s'effectue dans des colonnes en téflon rétractable contenant environ 0.1 mL de résine anionique AG1-X8, 100-200 mesh à usage unique. Les résines sont lavées et conditionnées avec de l'HCl 6N, de l'eau dé-ionisée puis de l'HBr 0.7N. Les échantillons sont chargés en HBr 0.7N (uniquement le surnageant) et les résines sont rincées par élution de 0.5 mL d'HBr 0.7N puis 0.2 mL d'HCl 2N. Toutes les fractions éluées à partir du chargement de l'échantillon sont récupérées : elles contiennent le Sr, le Nd et l'Hf qui seront utilisées dans la suite de la procédure analytique (Figure II.6). Le Pb, qui était jusqu'à présent retenu sur les résines, est désorbé et collecté par élution de 2mL d'HCl 6N. La fraction contenant le Pb est évaporée à sec, reprise dans 0.2 mL d'HBr 0.7 N et repassée sur la résine anionique en suivant exactement la même procédure que celle décrite ci-dessus. Le deuxième passage sur résine anionique est systématiquement réalisé afin d'améliorer la séparation du Pb. Les fractions Pb sont évaporées à sec sur plaques chauffantes à 120°C.

Séparation des Terres Rares (REE), des "High Field Strength Elements" (HFSE) et du Sr

Cette étape permet (1) d'isoler l'Hf, le Sr et le Nd dans trois fractions différentes (Figure II.6) et (2) de séparer l'Hf de l'Yb et du Lu (Terre Rare lourde) qui interfèrent sur la masse 176 lors de la mesure des rapports isotopiques $^{176}Hf/^{177}Hf$ au spectromètre de masse. Les fractions récupérées après la séparation du Pb sont évaporées et repris plusieurs fois dans de l'HCl 2N sur plaque chauffante à 130°C puis dans 2 mL d'HCl 2N + 1 goutte d'HF 24N.

La chromatographie est effectuée dans des colonnes en plastique remplies d'environ 2 mL de résine cationique AG50W-X8, 200-400 Mesh. Les résines sont conditionnées avec de l'HCl 2N. Les échantillons sont chargés et les résines sont rincées par élution d'HCl 2N. Les HFSE, dont l'Hf, sont collectés lors de ces deux dernières étapes. A la différence des Terres Rares et du Sr, ces éléments ne sont pas retenus par la résine cationique en milieu HCl peu concentré et migrent donc très rapidement le long de la colonne. Les éléments majeurs et le Sr sont élués avec de l'HCl 3.5N. Enfin les Terres Rares sont collectées par élution d'HCl 6N.

Les savillex® contenant les HFSE, le Sr et les Terres Rares sont mis à évaporer sur plaque chauffante à 120°C.

Isolation de l'Hf

L'isolation de l'Hf dans la fraction HFSE est habituellement réalisée en deux étapes : (1) un passage sur résine échangeuse d'anions AG1-X8 pour séparer l'Hf des éléments majeurs et (2) un passage sur résine échangeuse de cations AG50W-X8 pour séparer l'Hf du Zr et du Ti résiduels qui peuvent altérer la qualité de l'émission de l'Hf sur MC-ICP-MS (Blichert-Toft et al., 1997) (Figure II.6).

Pour la première séparation sur résine anionique AG1-X8, les fractions contenant les HFSE sont reprises dans 1 mL d'un mélange HF 0,5N / HCl 0,5N. Ce mélange d'acides permet la formation de complexes fluorés d'HFSE (complexes chargés négativement) qui seront préférentiellement retenus par les résines anioniques. Les colonnes, remplies avec 2 mL de résine anionique AG1-X8, 100-200 Mesh, sont conditionnées avec le mélange d'acides HF/HCl. Les échantillons sont chargés sur les colonnes et les résines sont rincées avec 3 fois 0,5 mL d'HF/HCl. Alors que les complexes d'HFSE restent fixés sur la résine, les éléments majeurs sont désorbés par élution de 18,5 mL d'HF/HCl. L'Hf, le Zr et le Ti sont finalement collectés dans des petits béchers en téflon PTFE par élution de 10 mL d'HCl 6N.

40 gouttes d'$HClO_4$ 14N sont ajoutées dans les fractions contenant l'Hf, le Zr et le Ti. Elles sont ensuite réduites à quelques µL par évaporation sur plaque chauffante à 170°C. 20 gouttes d'$HClO_4$ 14N sont de nouveau ajoutées et les fractions sont de nouveau réduites sur plaque chauffante à 170°C. Cette opération (ajout d'$HClO_4$ 14N + réduction par évaporation)

est répétée trois fois afin d'éliminer toute trace d'acide fluorhydrique (condition sine qua non pour l'étape de séparation suivante). Les fractions ne sont jamais évaporées à sec pour éviter la formation de précipité.

La chromatographie visant à séparer l'Hf du Zr et du Ti sur résine échangeuse de cations (Figure II.7) est réalisée dans une salle ne contenant pas de vapeur d'acide fluorhydrique. Les colonnes, remplies avec 2 mL de résine cationique AG50W-X8, sont conditionnées par élution d'HCl 2,5N. Avant le chargement sur colonnes, 300 µL d'HCl 2,5N et 2 gouttes d'H_2O_2 sont ajoutés dans chacun des échantillons. L'H_2O_2 permet de complexer le Ti (complexe de couleur rouge) pour qu'il ne soit pas retenu par les résines cationiques. Une fois les échantillons chargés, les résines sont rincées avec 0,4 mL d'HCl 2,5N + traces d' H_2O_2 et les complexes de Ti sont élués avec 6,5 mL du même mélange HCl / H_2O_2. L'Hf reste fixé sur les résines à condition qu'il n'y ait pas d'HF dans le milieu. Les cycles d'ajout d'$HClO_4$ 14N + réduction par évaporation doivent donc avoir été soigneusement effectués afin qu'il ne reste aucune trace d'acide fluorhydrique dans les échantillons. Dans le cas contraire, l'Hf est désorbé des résines en même temps que le Ti et la chromatographie visant à séparer ces deux éléments échoue. Quand tous les complexes de Ti sont élués, l'Hf sont collectés par élution de 5 mL d'un mélange HCl 2,5N / HF 0,3N. Les fractions Hf sont évaporées à sec sur plaques chauffantes à 120°C.

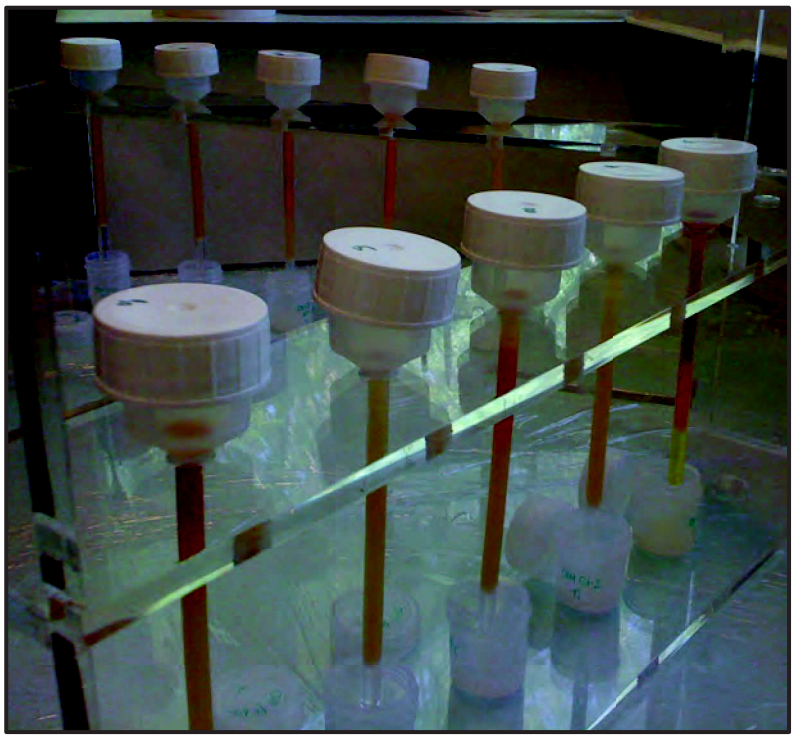

Figure II.7 : Photo des colonnes cationiques utilisées pour séparer l'Hf du Ti et du Zr

Isolation du Sr

Cette séparation a pour but d'isoler le Sr de la matrice de l'échantillon, notamment du Rb qui possède un isotope de masse 87 pouvant interférer sur la mesure des rapports isotopiques $^{87}Sr/^{86}Sr$. La fraction Sr issue de la séparation sur résine cationique (Figure II.6) est reprise dans de l'HNO_3 3N. Les échantillons sont chargés dans de petites colonnes en teflon rétractable contenant environ 150 µL de résine Eichrom® Sr-Spec, à usage unique, lavée et conditionnée avec de l'eau dé-ionisée et de l'HNO_3 3N. Les éléments majeurs et la matrice de l'échantillon contenant le Rb sont élués avec de l'HNO_3 3N. Le Sr est désorbé et récupéré par élution de 2 mL d'eau dé-ionisée. Les fractions Sr sont évaporées à sec sur plaques chauffantes à 120°C.

Isolation du Nd

L'isolation du Nd dans les fractions REE (fractions issues du premier passage sur résine cationique, Figure II.6) est effectuée par chromatographie sur résine Eichrom® Ln-Spec. Cette opération a pour but de séparer le Nd du Sm qui interfère sur la masse 144 lors de la mesure des rapports isotopiques $^{143}Nd/^{144}Nd$ au spectromètre de masse.

Les colonnes en quartz utilisées pour cette chromatographie sont préalablement calibrées avec un indicateur coloré (Carpentier, 2007). Sur les résines Ln-Spec en milieu HCl dilué, les Terres Rares sont désorbées les unes après les autres, dans l'ordre croissant de leur masse (Figure II.8). Le volume d'HCl nécessaire pour récupérer le maximum de Nd seul (sans les autres Terres Rares) varie sensiblement en fonction de la quantité de résine contenue dans les colonnes. La calibration consiste donc à déterminer spécifiquement ce volume idéal pour chaque colonne préalablement remplie d'une certaine quantité de résine Ln-Spec.

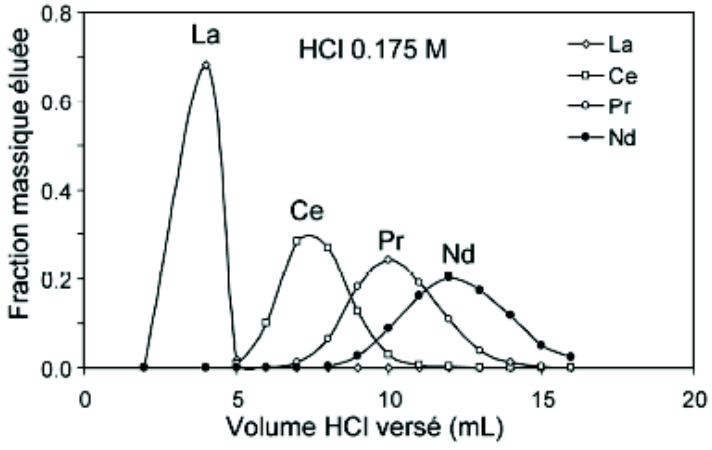

Figure II.8 : Profil d'élution des colonnes Nd contenant environ 1.5 mL de résine Ln-Spec. D'après Carpentier (2007)

Pour réaliser la chromatographie, les fractions de Terres Rares sont reprises dans 0,2 mL d'HCl 0,175N et sont passées aux ultra-sons afin de faciliter la reprise des résidus secs. Les résines Ln-Spec sont conditionnées par élution d'au moins 10 mL d'HCl 0,175N. Les échantillons sont chargés sur les résines qui sont ensuite rincées avec 2 fois 0,5 mL d'HCl 0,175N. Le Lanthane (La) et le Cérium (Ce) sont élués avec des volumes d'HCl 0,175N compris entre 9 et 11 mL (cela dépend de la colonne). Le Nd est collecté par élution de 10 mL d'HCl 0,175N. Les fractions de Nd sont évaporées à sec sur plaque chauffante à 120°C.

II.3.2.b. Calcul des quantités de Nd, Hf, Sr et Pb isolés

Les quantités de Nd, Hf, Sr et Pb isolés dans les échantillons et présents dans les blancs de chimie sont systématiquement mesurées à la fin de la procédure analytique. Ces mesures permettent (1) d'estimer les rendements de la chimie, c'est-à-dire le pourcentage d'élément isolé par rapport à la quantité d'élément initialement présente dans l'échantillon, (2) d'évaluer la qualité de la chimie et (3) de faciliter les procédures de dilution nécessaires à la mesure des rapports isotopiques sur les spectromètres de masse.

Pour mesurer les quantités de Nd, Hf, Sr et Pb isolés, les échantillons sont repris dans 1 mL d'HNO_3 14N sur plaque chauffante à 100°C. Les concentrations en Nd, Hf, Sr et Pb sont mesurées par ICP-MS (Agilent 7500ce) dans des solutions contenant 5% de la totalité du Nd, Hf, Sr et Pb isolé (aliquote de 50 µL d'échantillon dilué dans 5 mL d'HNO_3 2% + traces d'HF). Les blancs de chimie sont directement dilués dans 2mL d'HNO_3 2% + traces d'HF. La relation entre les concentrations et le nombre de coups mesuré par le spectromètre est établie grâce à l'analyse d'une gamme de standards mono-élémentaires de Nd, Hf, Sr et Pb (solutions étalons de concentrations connues). Les quantités d'éléments chimiques pouvant interférer lors des mesures de rapports isotopiques (Lu et Yb dans les fractions d'Hf, Sm dans les fractions Nd, Tl dans les fractions Pb et Rb dans les fractions Sr) sont également mesurées afin de vérifier l'efficacité des chromatographies. Si ces éléments interférents sont présents en trop grandes quantités, les échantillons sont repassés sur les différentes colonnes échangeuses d'ions.

II.3.3.c. Mesure des rapports isotopiques en Nd, Hf, Pb et Sr

Compositions isotopiques en Nd, Hf et Pb

Les rapports isotopiques $^{143}Nd/^{144}Nd$, $^{176}Hf/^{177}Hf$, $^{208}Pb/^{204}Pb$, $^{207}Pb/^{204}Pb$ et $^{206}Pb/^{204}Pb$ sont mesurés sur un spectromètre de masse multi-collecteur à source plasma (MC-ICP-MS, Nu plasma), en collaboration avec Philippe Telouk à l'Ecole Normale Supérieure (ENS) de Lyon. Pour le Nd, les échantillons sont repris dans de l'HNO_3 0,05N, pour l'Hf dans de l'HNO_3 0,05N + traces d'HF et pour le Pb dans de l'HNO_3 0.05N dopée au Thallium. Les concentrations des solutions analysées (50-150 ppb) sont définies en fonction de la sensibilité du spectromètre de masse le jour de l'analyse.

La procédure d'analyse consiste à passer un standard isotopique de référence en Nd (AMES Rennes Nd), Hf (AMES Grenoble Hf) ou Pb (NBS 981) tous les deux ou trois échantillons pour contrôler et corriger la dérive instrumentale au cours de la séquence d'analyse. Pour chaque échantillon, les rapports isotopiques sont, au minimum, mesurés quarante fois par le spectromètre de masse. Pour le Nd et l'Hf, le fractionnement de masse du spectromètre est corrigé en se basant sur la mesure de rapports isotopiques stables ($^{146}Nd/^{144}Nd$=0,7219 pour le Nd et $^{179}Hf/^{177}Hf$=0,7325 pour l'Hf). Pour le Pb, qui ne possède pas de rapport isotopique stable (seul le ^{204}Pb est stable), les corrections de fractionnement de masse s'effectuent grâce à l'ajout d'un standard interne de Thallium (spike de Thallium SRM 997). Ce dernier possède un rapport isotopique stable et connu ($^{205}Tl/^{203}Tl$) qui est mesuré et utilisé pour corriger le fractionnement sur les isotopes du Pb selon une loi exponentielle (White et al., 2000). Même si la grande partie des éléments interférents sur les masses du Nd, de l'Hf et du Pb a été retirée lors de la séparation chimique, les interférences isobariques causées par ces éléments sont corrigées grâce à la mesure des intensités sur le ^{147}Sm pour le Nd, sur l' ^{173}Yb et le ^{175}Lu pour l'Hf et sur le ^{204}Hg pour le Pb. L'ampleur de ces corrections est, par définition, toujours faible.

Pour l'Hf et le Nd, la dérive instrumentale au cours de la séquence d'analyse est supposée aléatoire. Elle est estimée en calculant la différence entre les compositions isotopiques des standards de référence publiées dans la littérature et la moyenne de celles réellement mesurées pendant la séquence d'analyse. Les rapports isotopiques en Hf et Nd de chaque échantillon sont corrigés par soustraction de cette différence. Les rapports isotopiques du Pb sont corrigés de la dérivé instrumentale par la méthode de "sample-standard bracketting" (White et al., 2000; Blichert-Toft, 2003; Weis et al., 2005; 2006). Avec cette méthode, les rapports isotopiques des échantillons sont corrigés de la différence entre la moyenne pondérée des valeurs mesurées sur les standards de référence encadrant l'échantillon et les valeurs de référence publiées dans la littérature.

Compositions isotopiques en Sr

Les rapports isotopiques $^{86}Sr/^{87}Sr$ sont mesurés sur un spectromètre de masse à thermo-ionisation (TIMS, Thermo Fisher Triton T1), en collaboration avec Philippe Nonnotte au laboratoire Domaines Océaniques de Brest. L'utilisation du TIMS permet d'éviter les interférences isobariques créées par le Krypton, qui possède un isotope de masse 86 comme le Strontium, et qui est présent dans les gaz (Argon) qui circulent dans les MC-ICP-MS.

Le principe de fonctionnement du TIMS est très différent de celui de l'ICP-MS puisque l'ionisation de l'échantillon n'est pas créée dans une torche à plasma mais par chauffage d'un filament sous vide, à très haute température. Pour les mesures de compositions isotopiques sur TIMS, l'échantillon est dilué dans de l'eau dé-ionisée de manière à obtenir une concentration d'environ 0.5 $g.L^{-1}$. 1 µL d'activateur au Tantale (régulateur d'émission) est déposé sur chaque filament simple en Tungstène, préalablement dégazé sous vide. Une fois l'activateur sec, 1 µL d'échantillon est déposé sur chaque filament. Le dépôt est séché à une intensité de 1.1 A puis flashé à plus de 4.6 A pendant 20 secondes. Les filaments sont déposés sur un barillet contenant 21 positions. Trois standards internationaux (NBS 987) sont mesurés dans chaque barillet. Pour chaque échantillon, les rapports isotopiques sont mesurés cent fois par le spectromètre de masse. Les corrections de fractionnement de masse sont effectuées en utilisant le rapport isotopique stable $^{88}Sr/^{86}Sr$ = 8.375209.

II.3.3.d. Evaluation de la qualité des données

Les possibles contaminations extérieures au cours de la procédure de séparation chimique des éléments sont évaluées par la mesure des quantités de Nd, Hf, Pb et Sr présents dans les blancs de chimie avant l'analyse des rapports isotopiques (Tableau II.1). Ces blancs ont subi exactement la même procédure analytique que les échantillons, de la première étape de dissolution jusqu'à la mesure des rapports isotopiques. Les quantités de Nd, Hf, Pb et Sr exogènes sont, en moyenne, comprises entre 50 et 280 pg, ce qui représentent généralement moins de 0.1% du Nd, de l'Hf, du Pb ou du Sr isolés. Ces quantités peuvent donc être considérées négligeables devant les quantités d'éléments isolées. Il est à noter que les quantités de Pb et Sr présents dans les blancs de chimie sont relativement élevées à cause de la reprise des échantillons dans de très grands volumes d'acide concentré (20 à 40 mL d'HNO_3 7N), reprise nécessaire pour le prélèvement des aliquotes qui servent à mesurer les concentrations en éléments traces.

Elément	Quantité d'éléments (pg)															Moyenne (pg)
Hf	36	72	6	71	47	39	25	11	32	26	150	129	47	32	33	50
Nd	128	14	50	51	39	80	100	316	117	192	331					129
Sr	277	196	23	136												158
Pb	228	330	524	287	268	149	198	266								281

Tableau II.1 : Quantité d'éléments présents dans les différents blancs de chimie analysés au cours de cette étude

Les analyses répétées des standards pendant les séquences de mesures (Figure II.9) permettent de contrôler la stabilité et la validité des compositions isotopiques mesurées. Le standard AMES Rennes Nd a été mesuré 106 fois au cours de cette thèse. La valeur moyenne des rapports $^{143}Nd/^{144}Nd$ mesurés et non corrigés de la dérive instrumentale est de 0.511959 ± 10 (2σ), ce qui est tout à fait satisfaisant au vu de la valeur recommandée par Chauvel et Blichert-Toft (2001) (0.511961 ± 13 (2σ)).

Pour l'Hf, le standard AMES Hf Grenoble, qui possède un rapport $^{176}Hf/^{177}Hf$ similaire au standard international JMC 475 plus couramment utilisé (Chauvel et al., 2011), a été mesuré 126 fois. La valeur moyenne des rapports $^{176}Hf/^{177}Hf$ mesurés est de 0.282162 ± 20 (2σ), ce qui est en accord avec la valeur recommandée par Chauvel et al. (2011) (0.282163 ± 9 (2σ)).

Le standard de Pb NBS 981 a été mesuré 66 fois. Les moyennes des trois rapports isotopiques mesurés sont : $^{208}Pb/^{204}Pb$ = 36.6876 ± 200 (2σ), $^{207}Pb/^{204}Pb$ = 15.4899 ± 56 (2σ), $^{206}Pb/^{204}Pb$ = 16.9322 ± 142 (2σ). Ces mesures sont donc très variables en fonction des séquences de mesure et systématiquement plus basses que les valeurs recommandées par Galer et Abouchami (1998) : $^{208}Pb/^{204}Pb$ = 36.7219 ± 44 (2σ), $^{207}Pb/^{204}Pb$ = 15.4963 ± 16 (2σ), $^{206}Pb/^{204}Pb$ = 16.9405 ± 15 (2σ) (Figure II.9). Le fait de corriger les rapports isotopiques des échantillons de la différence entre les valeurs mesurées sur les standards de référence et leurs valeurs certifiées permet de corriger ce biais analytique.

Enfin, les valeurs mesurées pour les rapports $^{86}Sr/^{87}Sr$ du standard NBS 987 moyennent à 0.710270 ± 10 (2σ), ce qui est tout à fait compatible avec les données compilées par GEOREM i.e. 0.710252 ± 91 (2σ) (Figure II. 9).

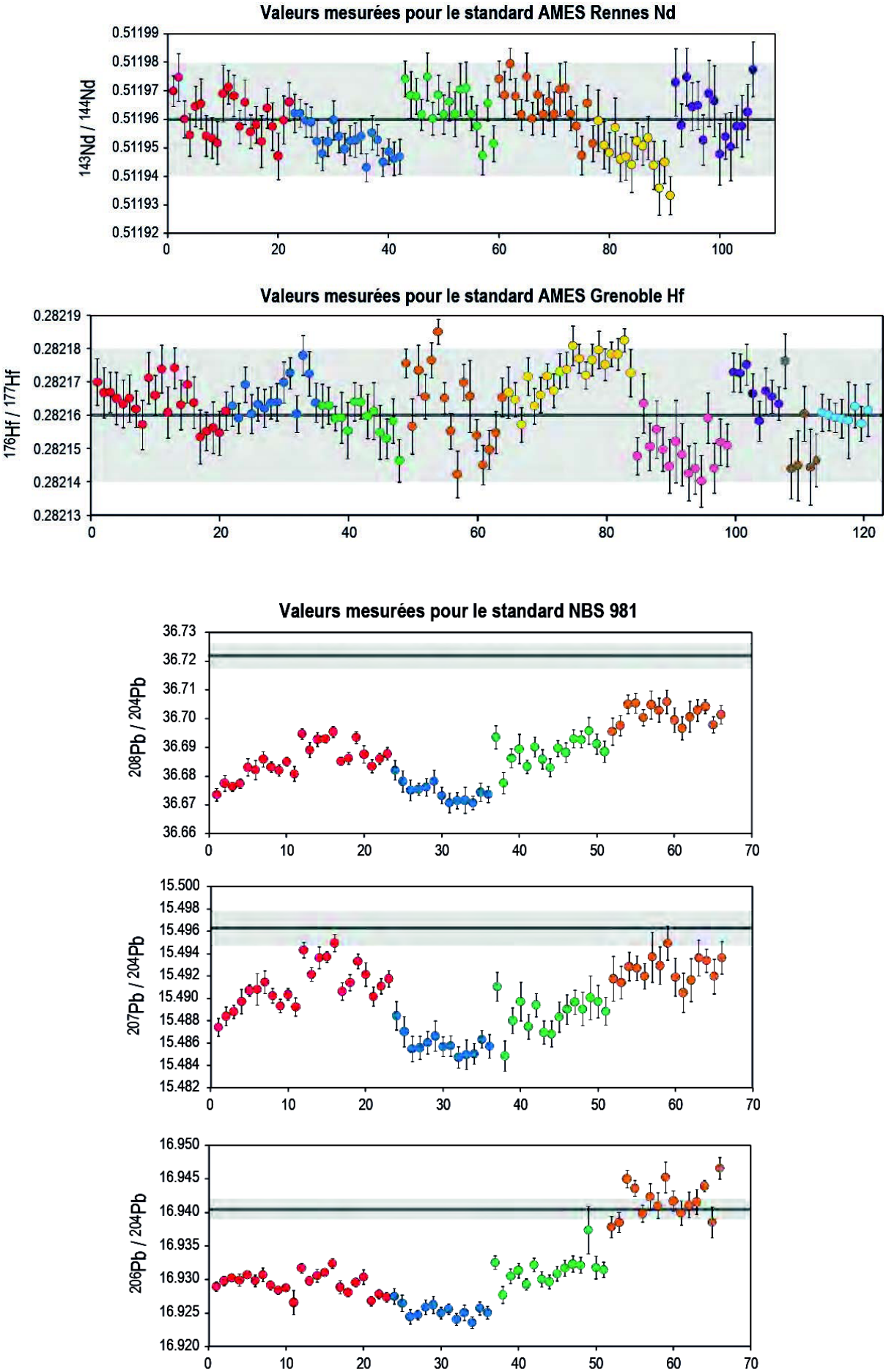
Valeurs mesurées pour le standard AMES Rennes Nd
143Nd / 144Nd
0.51199
0.51198
0.51197
0.51196
0.51195
0.51194
0.51193
0.51192
0
20
40
60
80
100
Valeurs mesurées pour le standard AMES Grenoble Hf
176Hf / 177Hf
0.28219
0.28218
0.28217
0.28216
0.28215
0.28214
0.28213
0
20
40
60
80
100
120
Valeurs mesurées pour le standard NBS 981
208Pb / 204Pb
36.73
36.72
36.71
36.70
36.69
36.68
36.67
36.66
0
10
20
30
40
50
60
70
207Pb / 204Pb
15.500
15.498
15.496
15.494
15.492
15.490
15.488
15.486
15.484
15.482
0
10
20
30
40
50
60
70
206Pb / 204Pb
16.950
16.945
16.940
16.935
16.930
16.925
16.920
0
10
20
30
40
50
60
70

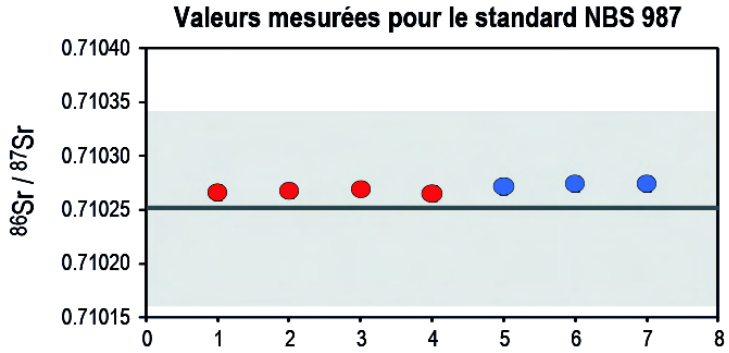

Figure II.9 : Valeurs des rapports isotopiques des standards de référence mesurés au cours de cette thèse. Chaque couleur représente une séquence de mesure i.e. un jour d'analyse sur les spectromètres. La taille des points est supérieure aux incertitudes de mesure pour les rapports $^{86}Sr/^{87}Sr$ du standard NBS 987. Les valeurs de référence des différents standards et leur incertitude à ± 2σ sont indiquées par les traits et champs gris horizontaux sur chaque figure.

Pendant les séquences d'analyse, plusieurs échantillons sont également analysés deux fois sur le spectromètre de masse ("échantillon bis" ou "re-run sample") afin d'estimer la reproductibilité des mesures. Les différences de composition isotopique en Nd, Hf, Pb et Sr entre tous les "échantillons bis" mesurés dans cette étude sont quasi-systématiquement inférieures aux erreurs analytiques (2σ) renvoyées par le spectromètre de masse (voir les différents tableaux de données présentés dans les manuscrits aux chapitres III, IV et V). Les mesures de rapports isotopiques sont donc jugées reproductibles.

Les valeurs obtenues sur les échantillons dupliqués issus d'attaques différentes sont présentées dans les différents tableaux de mesures associés aux chapitres III, IV et V. Elles permettent d'évaluer la reproductibilité et la représentativité des mesures effectuées. Pour l'Hf et le Nd, les écarts entre deux échantillons dupliqués sont, dans la grande majorité des cas, inférieurs à 0.5 ε. Pour le Pb, les moyennes des écarts entre deux échantillons dupliqués sont un peu plus importantes, elles atteignent 315 ppm pour les rapports $^{208}Pb/^{204}Pb$ et $^{206}Pb/^{204}Pb$ et 85 ppm pour les rapports $^{207}Pb/^{204}Pb$. Pour le Sr, l'unique échantillon dupliqué est une fraction minérale de feldspath-K très hétérogène et très radiogénique (cf Chapitre IV). L'écart de rapports isotopiques $^{87}Sr/^{86}Sr$ entre ces dupliqués est donc particulièrement élevé (i.e. de l'ordre de 2900 ppm) mais il ne remet pas en cause la validité des mesures effectuées.

Chapitre 3

Influence du Tri Minéralogique sur les Compositions Isotopiques des Sédiments

L'objectif de ce chapitre est d'évaluer l'influence du tri minéralogique au cours du transport fluviatile sur les compositions isotopiques en Nd, Hf et Pb des sédiments de rivière. Il est construit autour de deux manuscrits. Le premier documente les systématiques isotopiques du Nd et l'Hf dans les sédiments du Ganges et de ses affluents drainant la chaîne Himalayenne (sédiments de fond de rivière, sédiments de bord de berge et sédiments en suspension). Le second manuscrit s'intéresse aux variations de compositions isotopiques en Pb dans ces mêmes sédiments ainsi que dans les différentes fractions minérales et granulométriques que nous avons séparées et analysées.

III.1. SYSTEMATIQUES ISOTOPIQUES DU ND ET DE L'HF **57**

Almost half of worldwide sedimentary Nd - Hf isotopic decoupling done on continents
(To be submitted to G-cubed)

ABSTRACT ***59***
1. INTRODUCTION ***60***
2. THE GANGA FLUVIAL SYSTEM ***61***
3. SEDIMENT SAMPLING AND ANALYTICAL PROCEDURE ***63***
4. RESULTS ***65***
5. DISCUSSION ***73***
6. SUMMARY AND CONCLUSIONS ***87***
ACKNOWLEDGMENTS ***87***
REFERENCES ***88***

III.2. SYSTEMATIQUES ISOTOPIQUES DU PB **99**

New approach to the average upper continental crust Pb isotopic value
(To be submitted to Nature Geoscience)

MAIN TEXT ***101***
METHODS ***109***
ACKNOLEDGEMENTS ***110***
REFERENCES ***110***
SUPPLEMENTARY MATERIALS ***112***

III.1. Systématiques isotopiques du Nd et de l'Hf

Le manuscrit présenté ci-après se propose d'étudier les variations de compositions isotopiques en Nd et Hf entre les sédiments de fond de rivière, ceux de bord de berge et ceux transportés en suspension, à différents lieux d'échantillonnage i.e. dans la chaîne Himalayenne, au front de chaîne, dans la plaine alluviale et au niveau du delta. La variabilité des concentrations en éléments majeurs (données de Christian France-Lanord mesurées au SARM de Nancy) et en éléments traces (données acquises au cours de cette thèse) dans ces sédiments sont également discutées.

L'étude de l'influence des processus de tri minéralogique sur la composition isotopique des sédiments nécessite tout d'abord d'évaluer l'importance des variations isotopiques pouvant être causées par des effets de provenance sur les différents sédiments étudiés. Ce sujet est l'objet de la première partie de la discussion. L'évaluation des effets du tri minéralogique s'effectue dans une deuxième partie, en comparant les compositions isotopiques des sédiments de fond de rivière et de bord de berge avec celles des sédiments transportés en suspension. Dans la troisième partie de la discussion, nous nous intéressons à la variabilité spatiale des compositions isotopiques c'est à dire à leur evolution entre la source des sédiments, dans la chaîne Himalayenne, jusqu'au delta du Ganges au Bangladesh. Enfin, la dernière partie de ce manuscrit se propose d'étudier les potentielles implications de nos résultats à l'échelle du système sédimentaire global, notamment sur les sédiments océaniques térrigènes et leur recyclage dans le réservoir mantellique.

Almost half of worldwide sedimentary Nd - Hf isotopic decoupling done on continents

(To be submitted to G-cubed)

Marion Garçon[1], Catherine Chauvel[1], Christian France-Lanord[2], Pascale Huyghe[1]

[1] ISTerre, CNRS, Université Joseph Fourier de Grenoble, BP 53, 38041 Grenoble Cedex 09, France

[2] CRPG-CNRS, Vandoeuvre lès Nancy, France

Note : Figures were integrated into the text to facilitate the reading

Abstract

While Nd and Hf isotopic systems are coupled in most crustal and mantle rocks, it is now well established that sedimentary processes can decouple the two systems in oceanic sediments: coarse detrital sediments follow the same trend as crustal rocks but authigenic sediments such as Fe-Mn crusts have extremely radiogenic Hf isotopes relative to their Nd isotopic compositions. However, it remains uncertain whether the fractionation of the two isotopic systems only occurs in the oceanic environment or if it already starts through sedimentary processes in continental environments. Here, we focus on Hf and Nd isotopic compositions of large river sediments to constrain the behavior of the two isotopic systems during erosion and sediment transport from continent to ocean.

We report major and trace element concentrations together with Nd and Hf isotopic compositions of bedloads, banks and suspended loads from the Ganga River and its tributaries draining the Himalayan range i.e. the Karnali, the Narayani, the Kosi and the Marsyandi Rivers. Our sample set includes sediments sampled in the Himalayan range in Nepal, at the Himalayan Mountain front but also downstream in the floodplain and at the outflow of the Ganga in Bangladesh. We show that mineralogical sorting processes explains the entire Hf isotopic variability observed in the studied river sediments i.e. more than 10 ε_{Hf} units while it does not affect Nd isotopic compositions. Bedloads and bank sediments have systematically lower ε_{Hf} values than the suspended loads sampled at the same location. Coarse-grained sediments lie below or next to the Terrestrial Array in a ε_{Hf} vs. ε_{Nd} diagram. In contrast, fine-grained sediments, including most of the suspended loads, deviate from the Terrestrial Array toward higher ε_{Hf} relative to their ε_{Nd}, as it is also the case for oceanic terrigenous clays. We explain the observed Nd-Hf decoupling by mineralogical sorting processes that enrich bottom sediments in coarse and dense minerals, such as unradiogenic zircons, while surface sediments are enriched in fine material with radiogenic Hf signatures. Finally, we demonstrate that the Nd-Hf isotopic decoupling increases with sediment transport in the floodplain to reach its maximum at the river mouth. We conclude that almost half of the Nd-Hf isotopic decoupling observed in worldwide oceanic terrigenous sediments is already acquired during fluvial transport on continents.

Keywords: Nd, Hf, river sediments, decoupling of isotopic systems, mineralogical sorting

1. Introduction

Because Nd and Hf isotopes behave in the same way during most magmatic processes, Vervoort et al. (1999; 2011) demonstrated that the Nd and Hf isotopic compositions of almost all crustal and mantle-derived rocks are well correlated and define the so-called “Terrestrial Array” in a Nd-Hf isotopic space. However, it is also well recognized that some oceanic sediments, in particular oceanic Fe-Mn crusts and terrigenous clays, can significantly deviate from this Terrestrial Array towards higher ε_{Hf} values relative to their ε_{Nd} (Albarède et al., 1998; Chauvel et al., 2008; Bayon et al., 2009; Vervoort et al., 2011). The origin of the “Seawater Array” defined by Fe-Mn crusts is still highly debated (e.g. Bau and Koschinsky, 2006; Van de Flierdt et al., 2007) but the isotopic decoupling observed in terrigenous oceanic sediments is usually attributed to fractionation of rare earth elements (REE) and high-field strength elements (HFSE) by sedimentary processes (Patchett et al., 1984; Carpentier et al., 2009; Vervoort et al., 2011). More specifically, it is believed that the retention of unradiogenic Hf-rich zircons on continents leads to the delivery in the oceans of detrital material poor in zircons and having more radiogenic Hf isotopes. While several studies suggest that this fractionation may occur quite early in the sedimentary system i.e. on continents (Patchett et al., 1984; Bayon et al., 2006; Vervoort et al., 2011), Nd-Hf isotopic systematic of river sediments has never been thoroughly investigated. A proper understanding of the process is required because it has several important implications depending on whether the zircon-rich sediments remain stuck on continents or make it to the ocean. For example, what is its impact on isotopic modeling of crustal growth? And, at a more global scale, how decoupling of the two isotopic systems affects the long term evolution of the mantle if sediments recycled into the mantle through subduction zones differ from average continental crust?

The aim of this paper is to accurately document the Nd-Hf isotopic message carried by large river sediments to better understand the behavior of the two isotopic systems during erosion and sediment transport from continent to ocean. To accomplish this, we use a comprehensive sample set including bedloads, banks and suspended loads recovered at the Himalayan front and downstream in the floodplain from the Ganga River and its major tributaries. We also analyzed sediments sampled in the Himalayan range, along the Marsyandi River in Nepal and at the outflow of small rivers draining single geological units. In addition to the fact that they belong to one of the largest fluvial systems in the world, sediments from the Ganga River and its tributaries have the advantage to have been already

widely studied, in particular (a) for provenance studies (Galy and France-Lanord, 2001; Garzanti et al., 2007; Tripathi et al., 2007; Singh et al., 2008; 2009; 2010), (b) to determine the effects of chemical weathering (Lupker et al., 2012), (c) to characterize the mineralogical variations associated to hydraulic sorting (Garzanti et al., 2010; 2011), (d) to quantify organic carbon transfer (Galy et al., 2007; 2008) and (e) to estimate global sediment flux budgets (Lupker et al., 2011). Based on these studies and our new results, we investigate both the effects of sediment provenance and mineralogical sorting processes during sediment transport on the trace-element concentrations and Nd-Hf isotopic compositions of the studied river sediments. We show that Nd and Hf isotopes are progressively decoupled in the floodplain till the river mouth and we link this phenomenon to the anomalous Nd-Hf isotopic compositions observed in worldwide terrigenous oceanic sediments.

2. The Ganga fluvial system

The Ganga fluvial system is one of the main conveyors of material eroded from the Himalayan range, delivering ca. 400 million tons of sediments per year into the ocean in the Bay of Bengal (Lupker et al., 2011). This system drains a total drainage area of about 1 million km^2 and stretches to more than 2500 km from its sources in the High Himalayan range to its delta in Bangladesh. The water discharge of the Ganga is strongly controlled by the monsoon (June to September), which accounts for about 75% of its annual flow in Bangladesh (Singh et al., 2007).

The Ganga basin (Figure 1) includes several major tributaries draining the Himalayan range in the north (Yamuna, Karnali, Narayani and Kosi Rivers) and part of the Indian shield and the Deccan Traps basalts in the south (mainly the Chambal River). In the Himalayan range, the drainage area of the Ganga can be divided in four geological units after Le Fort (1975): (1) the Tethyan Sedimentary Series consisting in variably low metamorphosed carbonates and clastic sedimentary rocks that are Cambrian to Eocene in age (dark grey in Figure 1); (2) the High Himalayan Crystalline units mostly composed of Neoproterozoic to Ordivicien highly metamorphosed gneiss, migmatites, and marbles (light grey in Figure 1); (3) the Lesser Himalaya units mainly formed by weakly metamorphosed sedimentary rocks that are Proterozoic in age (white in Figure 1); and (4) the Siwalik molasses made of Neogene to Quaternary floodplain deposits i.e. recycled erosion products of the Himalayan range (orange in Figure 1). As shown by France-Lanord et al. (1993) and Galy and France-

Lanord (2001), more than two third of the sediments transported by the Ganga River most probably derived from the High Himalayan Crystalline units, the rest mainly originates from the Lesser Himalaya units.

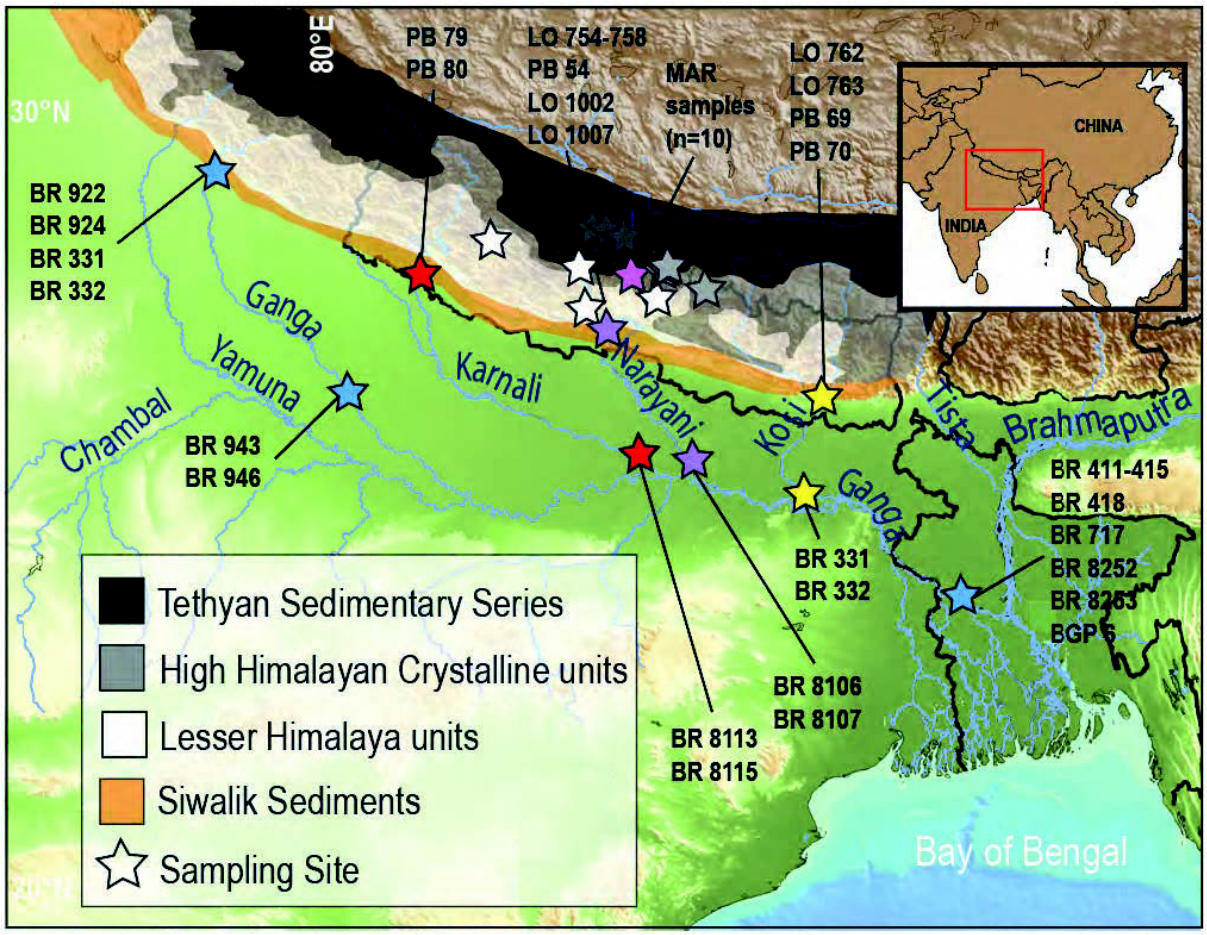

Figure 1: Map of the Ganga fluvial system showing the main sampling sites for the river sediments analyzed in this study.
Blue stars indicate the locations of samples from the Ganga River, red stars those from the Karnali River, purple stars those from the Narrayani river, yellow stars those from the Kosi River. White, light and dark grey stars indicate the locations of the samples from Nepalese rivers draining the Lesser Himalaya units, the High Himalayan Crystalline units and the Tethyan Sedimentary Series, respectively. The precise locations can be found in Pierson-Wickmann et al. (2000) and Garzanti et al. (2007). Detailed locations of the 10 samples recovered in the Marsyandi River (pink star) can be found in Garzanti et al. (2007).

The mineralogical composition of the sediments transported by the Ganga is quite variable and mainly controlled by hydrodynamic processes depending on the grain size, shape and density of the minerals (Galy et al., 2008; Garzanti et al., 2010; 2011). Bedload sediments at the bottom of the river tend to be coarser (Lupker et al., 2011) and mineralogically different from surface suspended load sediments taken at the same location. According to (Garzanti et al., 2010; 2011), bedloads sampled in Bangladesh are characterized by higher proportions in quartz (40 to 60%) and heavy minerals (up to 15%) than suspended loads (27 to 55% quartz and 3 to 6% heavy minerals). Heavy minerals include amphibole, epidote, garnet and many accessories such as titanite, zircon, monazite, allanite, apatite and tourmaline. By contrast, suspended load sediments tend to be enriched in phyllosilicates such as clays (8 to 26%) and micas (9 to 30%). Feldspar proportions are similar in both types of sediments with values ranging from about 5 to 20%.

3. Sediment Sampling and analytical procedure

3.1. Sediment Sampling

River sediments analyzed in this study were sampled over several years of field campaigns, in Nepal, India and Bangladesh. A large part of these samples were already analyzed for major element contents (Lupker et al., 2012), Re-Os isotopes (Pierson-Wickmann et al., 2000), mineralogical proportions (Garzanti et al., 2007; 2010; 2011) and C_{org} isotopes (Galy et al., 2008).

To document the Nd-Hf isotopic variability of river sediments at a large scale, i.e. during their transport and deposition in the floodplain from the mountain range to the ocean, we choose to analyze a set of samples from the Ganga and its major tributaries (Karnali, Narayani and Kosi Rivers) collected at the front of the Himalayan range and further downstream in the floodplain (see location of sampling sites in Figure 1). Because more than 95% of the suspended load is transported during the monsoon (Islam et al., 1999), most samples were collected in July, August and September. We also studied the isotopic variability of the sediments at a smaller scale using 10 samples collected in the Himalayas along the Marsyandi River, from its source to its confluence with a mainstream in Nepal (pink star in Figure 1). The precise locations of the samples together with a detailed description of the Marsyandi basin can be found in Attal and Lavé (2006) and Garzanti et al. (2007). Finally, we also analyzed sediments from small Nepalese rivers draining monolithologic basins to

characterize the chemical and isotopic compositions of three Himalayan geological units i.e. the Lesser Himalaya, the High Himalayan Crystalline and the Tethyan Sedimentary Series (white, light grey and dark grey stars in Figure 1).

To study the effects of mineralogical sorting on the eroded material transported by the Ganga, we analyzed different types of river sediment at each sampling site. When possible, it includes suspended load sediments sampled at the surface as well as at different depths in the water column, dredged bedload sediments and bank sediments. Sampling techniques for suspended load, bedload and bank sediments are provided in Galy et al. (2008) and Lupker et al. (2011).

3.2. Chemical analyses

3.2.1. Major element contents

Major element contents were measured in the sediments from the Marsyandi River and from the Nepalese rivers draining single geological units. Major element concentrations in all the other studied samples were published by Lupker et al. (2012) (See Supplementary Table 1). After being freeze-dried and powdered in an agate mortar to ensure homogeneity of powder, about 100 mg of sediments were fused using lithium metaborate to measure major element concentrations by ICP-AES at the SARM in Nancy (France) according to the technique described by Govindaraju and Mevelle (1987) and Carignan et al. (2007).

3.2.2. Trace element concentrations and Nd-Hf isotopes

Sample preparation and dissolution

To measure trace element concentrations together with Nd-Hf isotopes, the above mentioned powders were re-crushed in agate bowls using a planetary ball mill to insure fine grain size for all samples. 50 to 100 mg of powder were first attacked for 2 days in HNO_3 14N on a hot plate at 130°C, then evaporated and dissolved by acid attack (mixture of HF and $HClO_4$) in teflon containers placed in steel PARR bombs for 6 weeks at 140°C or one week at 200°C. After complete dissolution, two aliquots were taken from each sample: the equivalent of 2 mg powder to measure trace element concentrations and the rest to isolate Nd and Hf for isotopic measurements.

Trace element concentrations

Trace element concentrations were measured using an Agilent 7500ce ICP-MS in Grenoble (France) following the procedure described by Chauvel et al. (2011). Measurements were performed on samples diluted 5000 times in a solution of 2% HNO_3 with traces of HF. They are corrected for oxide interference and ICP-MS analytical drift using a multispike of Be, Ge, In, Tm and Bi. Repeated measurements of BR or BR-24 rock standards are used as an external calibration to calculate trace element concentrations in all samples. The validity and the reproducibility of our results are assessed by repeated measurements of international rock standards as unknown samples, including sedimentary materials such as JSd-2, and the measurements of several complete duplicates (see Supplementary Table 1).

Nd-Hf isotopic compositions

Hf and Nd were isolated using ion chromatography (Chauvel et al., 2011). Total procedural blanks reached on average 94 pg (n=6) for Nd and 47 pg (n=11) for Hf and are negligible compared to the amount of Nd and Hf isolated in all samples. Nd and Hf isotopic compositions were measured on a Nu Plasma HR MC-ICP-MS at the ENS Lyon (France). We used $^{146}Nd/^{144}Nd=0.7219$ and $^{179}Hf/^{177}Hf=0.7325$ to correct isotopic ratios from mass fractionation bias. The average measured values for the Ames-Rennes Nd and Ames-Grenoble Hf reference standards run every two or three samples are $^{143}Nd/^{144}Nd = 0.511959 \pm 8$ (2σ, n = 59) and $^{176}Hf/^{177}Hf = 0.282163 \pm 10$ (2σ, n = 99), respectively. MC-ICP-MS analytical drift was corrected using the recommended values published by Chauvel and Blichert-Toft (2001) and Chauvel et al. (2011) for these two standards. The reproducibility of our results estimated using complete duplicate analyses is usually better than 0.5 ε units for Nd and Hf isotopic compositions (see Table 1).

4. Results

4.1. Major and Trace element concentrations

Major element contents are presented in Supplementary Table 1. For the purpose of this study, we focus on the SiO_2 and Al_2O_3 contents of the studied bedloads, banks and suspended loads, as shown in Figure 2a. Details concerning the variations of other major elements can be found in Lupker et al. (2011; 2012). In general, SiO_2 and Al_2O_3 contents are strongly correlated with sediment grain-size (Lupker et al., 2011). Bedloads and banks tend to be concentrated in SiO_2 (ca. 70-80%) because they are enriched in coarse-grained quartz.

By contrast, suspended loads are characterized by lower SiO_2 (ca. 50-70%) and tend to have higher Al_2O_3 (ca. 10-18%), Fe_2O_3, K_2O, MgO and TiO_2 because these elements are mainly hosted by fine phyllosilicates such as clays. Because of this chemical differentiation, Al_2O_3/SiO_2 ratios can be used as a reliable grain-size proxy for crustal-derived sediments. Indeed, it can be seen in Figure 2b that bedloads and banks have lower Al_2O_3/SiO_2 ratios than suspended loads. Moreover, Lupker et al. (2011) showed that Al_2O_3/SiO_2 ratios of suspended loads are very well correlated with their sampling depth in the water column. This feature, not shown in Figure 2, accounts for the variability of Al_2O_3/SiO_2 ratios in suspended loads: surface suspended loads have higher Al_2O_3/SiO_2 ratios than those sampled at greater depths. It can also be seen in Figure 2 that some of the studied bedloads and banks have surprisingly high Al_2O_3/SiO_2 ratios. These exceptional samples were not recovered during the monsoon season, and the rather slow flow conditions favored deposition of Al_2O_3-rich phyllosilicates in bedloads and bank sediments.

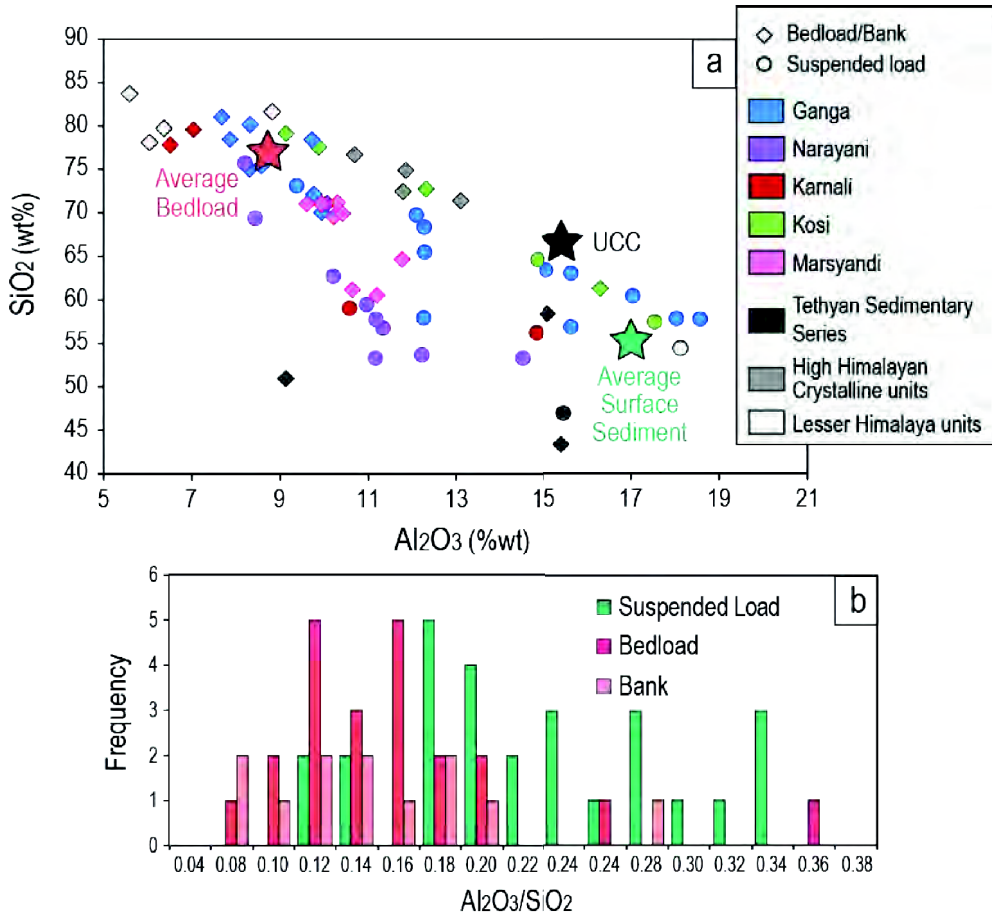

Figure 2: a) Variability of SiO_2 and Al_2O_3 contents in river sediments. **b)** Histogram showing the frequency of Al_2O_3/SiO_2 ratios for the studied bedloads, banks and suspended loads.
Red and green stars correspond to the average composition of the Ganga bedloads and surface sediments as published by Lupker et al. (2011). The composition of the average Upper Continental Crust (UCC, Rudnick and Gao, 2003) is shown as indication.

Trace element concentrations measured in all sediments are presented in the Supplementary Table 1. Spidergrams normalized to the average upper continental crust composition of (Rudnick and Gao, 2003) are shown in Figure 3 for sediments from the Nepalese rivers draining exclusively the Tethyan Sedimentary Series, the High Himalayan Crystalline and the Lesser Himalaya units (Figure 3a-c) and for the Marsyandi, Ganga, Narayani, Karnali and Kosi Rivers (Figure 3d-h).

In the Himalayan range, sediments from small Nepalese rivers draining single sources display variable trace element distributions (Figure 3a-c). They are systematically depleted in transition elements and some mobile elements such as Ba and Sr. Enrichment factors are globally higher for the Tethyan Sedimentary Series than for the High Himalayan Crystalline and the Lesser Himalaya units. Sediments derived from Tethyan Sedimentary Series show clear enrichments in Cs, Rb, Li and As, very high $(Th/U)_{UCCnorm}$ ratios (2.04 on average) and rather flat REE patterns (average $(La/Yb)_{UCCnorm}$ of 1.17). By contrast, the REE patterns of the sediments eroded from High Himalayan Crystalline units are characterized by significant enrichments in heavy REE (average $(La/Yb)_{UCCnorm}$ of 0.39). Lesser Himalaya sediments show much more variability with their $(La/Yb)_{UCCnorm}$ ratios ranging from 0.9 to 1.4.

Trace element concentrations measured in the Marsyandi bedloads are more variable than in the other rivers sampled in the floodplain (see Figure 3d-h). When compared to the average upper continental crust composition, most of them are enriched in Cs, Rb and depleted in Ba, Sr and transition elements (Sc, V, Cr, Co, Ni, Cu, Zn and As). Enrichment factors for Zr-Hf range from 0.3 to 1.5 and from 0.8 to 4.4 for Th-U. Their REE patterns display a relative enrichment in heavy REE as shown by their average $(La/Yb)_{UCCnorm}$ ratio of about 0.65.

In the floodplain, trace element patterns for sediments from the Ganga and its major tributaries draining the Himalayan range i.e. the Narayani, the Karnali and the Kosi Rivers resemble each other (Figure 3e-h). No systematic downstream variation in their composition occurs and trace element distributions are globally comparable to the composition of the average upper continental crust, except for the transition elements and some mobile elements (Ba, Sr) that are always depleted. REE patterns are generally flat with an average $(La/Yb)_{UCCnorm}$ ratio of 0.84 for the Ganga sediments, 0.93 for the Narayani sediments, 0.90 for the Karnali sediments and 0.87 for the Kosi sediments and there is no significant REE fractionation between bedload, bank and suspended load sediments (average $(La/Yb)_{UCCnorm}$ of 0.86 for all of the bedloads and banks and 0.89 for all of the suspended loads).

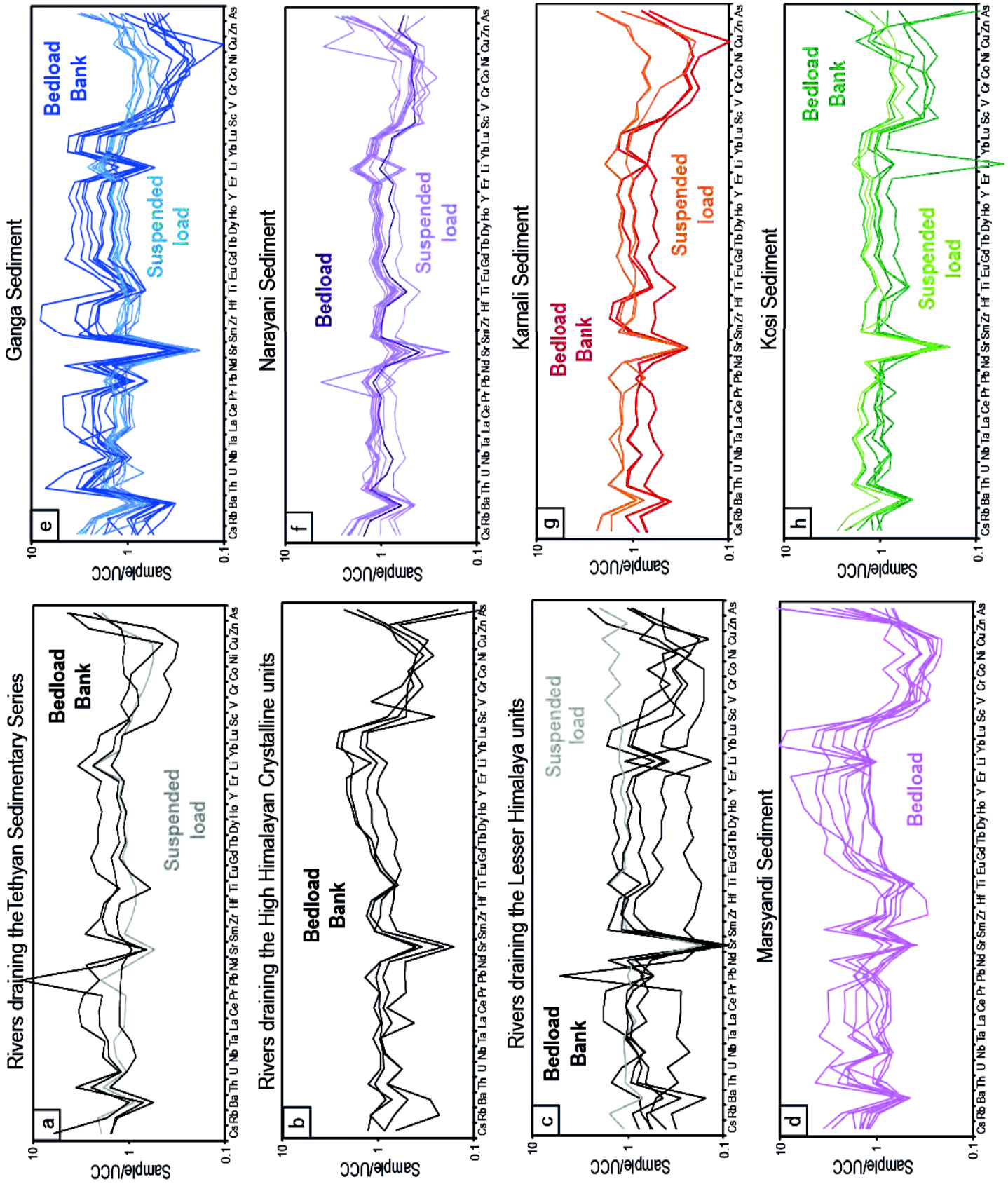

Figure 3: Trace element patterns normalized to the average composition of the upper continental crust (UCC) of Rudnick and Gao (2003) for sediments sampled in rivers draining single geological units (a-b-c) as well as in the Marsyandi (d), the Ganga (e), the Narayani (f), the Karnali (g) and the Kosi rivers (h).

In general, bedloads and banks are characterized by a positive anomaly in Zr-Hf and are more depleted in transition elements and mobile elements such as Cs, Rb and Ba than suspended loads. In the Ganga River, bedloads and banks show significant enrichments in all REE and positive anomalies in Th-U (Figure 3e). These features are not observed in the Narayani, the Karnali and the Kosi Rivers for which the chemical compositions of bedloads, banks and suspended loads resemble each other.

4.2. Nd-Hf isotopic compositions

Nd and Hf isotopic compositions measured in this study are given in Table 1. Sediments sampled in the Himalayan range from rivers draining single geological units and from the Marsyandi River are shown in a ε_{Hf} vs. ε_{Nd} diagram in Figure 4 together with worldwide isotopic compositions of oceanic sediments (orange, yellow and brown diamonds). Sediments from the Ganga and its major tributaries sampled in the floodplain are shown in Figure 5.

In the Himalayan range (Figure 4), Nd-Hf isotopes of sediments derived from the Lesser Himalaya units display significantly less radiogenic values ($-40.3 < \varepsilon_{Hf} < -28.8$ and $-25.1 < \varepsilon_{Nd} < -20.1$) than those derived from the High Himalayan Crystalline units ($-22.2 < \varepsilon_{Hf} < -12.7$ and $-17.7 < \varepsilon_{Nd} < -12.9$) and the Tethyan Sedimentary Series ($-23.7 < \varepsilon_{Hf} < -19.5$ and $-18.3 < \varepsilon_{Nd} < -16.6$). The ε_{Nd} values are comparable to the Nd isotopic compositions published for bedrocks from the Lesser Himalaya, the High Himalayan Crystalline and the Tethyan Sedimentary Series (see the histogram in Figure 4 and references therein).

Nd and Hf isotopic compositions of bedloads sampled all along the Marsyandi River (Figure 4) are much less variable ($-25.5 < \varepsilon_{Hf} < -19.9$ and $-18.0 < \varepsilon_{Nd} < -15.4$) and resemble those of the High Himalayan Crystalline and the Tethyan Sedimentary Series. There is no clear downtream variation in ε_{Hf} and ε_{Nd} values (see Figure 6; Table 1).

From rivers draining monolithologic basins in the Himalayan range

Sample Name	Locality	River	Type of sediment	$^{176}Hf/^{177}Hf$	± 2σ	εHf	$^{143}Nd/^{144}Nd$	± 2σ	εNd
Lesser Himalaya units									
R 94-12	Sarmi, Nepal	Tributary of the Bheri River	Bedload	0.281956	11	-29.3	0.511422	11	-23.6
MO 102	Darondi/Marsel Khola, Nepal	Marsel Khola	Bank	0.281798	5	-34.9	0.511436	9	-23.3
MO 112	Bhuri Gandaki/Isul Khola, Nepal	Isul Khola	Bank	0.281646	5	-40.3	0.511380	6	-24.4
MO 112 re-run							0.511379	6	-24.4
PB 33	Nepal	Ghara khola	Suspended Load	0.281972	9	-28.8	0.511577	8	-20.5
PB 37	Nepal	Beg Khola	Bank	0.281659	13	-39.8	0.511488	5	-22.3
PB 37 re-run							0.511488	5	-22.3
MO 207	Waling, Nepal	Andi Khola	Bedload	0.281672	20	-39.4	0.511343	7	-25.1
MO 207 re-run				0.281663	7	-39.7			
High Himalayan Crystalline units									
MO 73	Nepal	Tributary of the Chepe khola	Bank	0.282243	12	-19.2	0.511724	10	-17.7
MO 50	Nepal	Chepe khola	Bank	0.282427	13	-12.7	0.511968	5	-12.9
MO 59	Nepal	Chepe khola	Bank	0.282374	9	-14.5	0.511953	9	-13.2
MO 59 re-run				0.282348	5	-15.4			
KN 83	Ghyangphedi, Nepal	Tadi khola	Bedload	0.282156	10	-22.2	0.511811	6	-16.0
Tethyan Sedimentary Series									
MO 504	Tukche, Nepal	Yamkim khola	Suspended Load	0.282235	8	-19.5	0.511730	6	-17.6
NAG 22	Pedi, Nepal	Marsyandi (10 km away from the River Source)	Bedload	0.282175	9	-21.6	0.511779	5	-16.6
NAG 22 re-run					0		0.511778	6	-16.6
MAR-50	Temang, Nepal	Marsyandi (60 km away from the River Source)	Bedload	0.282138	8	-22.9	0.511760	6	-17.0
MAR-50 re-run				0.282146	11	-22.6	0.511756	5	-17.0
MAR-40	Sabche, Nepal	Sabche khola	Bedload	0.282114	8	-23.7	0.511693	6	-18.3
MAR-40 Dup							0.511695	8	-18.2

From the Marsyandi River in the Himalayan range

Sample Name	Locality	Distance from River Source (km)	Type of sediment	$^{176}Hf/^{177}Hf$	± 2σ	εHf	$^{143}Nd/^{144}Nd$	± 2σ	εNd
MAR-55	Tal, Nepal	72	Bedload	0.282202	9	-20.6	0.511798	7	-16.2
MAR-58	Chamje, Nepal	75	Bedload	0.282151	8	-22.4	0.511803	7	-16.1
MAR-70	Besi Sahar, Nepal	104	Bedload	0.282178	8	-21.5	0.511813	8	-15.9
MAR-31	Philesangu, Nepal	111	Bedload	0.282065	8	-25.5	0.511816	6	-15.9
MAR-29	Suribar, Nepal	119	Bedload	0.282207	8	-20.4	0.511715	6	-17.8
MAR-29 re-run							0.511724	8	-17.7
MAR-19	Turture, Nepal	133	Bedload	0.282222	6	-19.9	0.511841	6	-15.4
MAR-19 re-run				0.282218	9	-20.1			
MAR-12	Anpu, Nepal	161	Bedload	0.282126	9	-23.3	0.511803	5	-16.1
MAR-10	Lobrang, Nepal	166	Bedload	0.282189	6	-21.1	0.511724	7	-17.7
MAR-10 Dup	Lobrang, Nepal	166	Bedload	0.282219	11	-20.0	0.511709	7	-18.0

From the Ganga river and its major tributaries in the floodplain

Sample Name	Locality	Distance from River Source (km)	Type of sediment	$^{176}Hf/^{177}Hf$	± 2σ	εHf	$^{143}Nd/^{144}Nd$	± 2σ	εNd
Ganga River									
BR 931	Devrapayag, India	260	Suspended Load	0.282118	7	-23.6	0.511818	8	-15.8
BR 932	Devrapayag, India	260	Suspended Load	0.282070	6	-25.3	0.511724	5	-17.7
BR 922	Rishikesh, India	260	Suspended Load	0.282180	6	-21.4	0.511706	6	-18.0
BR 922 re-run							0.511715	7	-17.9
BR 924	Rishikesh, India	260	Bank	0.282053	7	-25.9	0.511737	7	-17.4

Sample Name	Locality	Distance from River Source (km)	Type of sediment	$^{176}Hf/^{177}Hf$	± 2σ	εHf	$^{143}Nd/^{144}Nd$	± 2σ	εNd
BR 943	Kanpur, India	800	Suspended Load	0.282217	8	-20.1	0.511829	6	-15.6
BR 946	Kanpur, India	800	Bedload	0.282055	5	-25.8	0.511780	8	-16.6
BR 946 Dup	Kanpur, India	800	Bedload	0.282004	8	-27.6	0.511728	5	-17.6
BGP 6	Rajshahi, India	2570	Bedload	0.282027	11	-26.8	0.511758	9	-17.0
BGP 6 re-run		2570					0.511752	6	-17.1
BGP 6 Dup	Rajshahi, India	2570	Bedload	0.282009	7	-27.5	0.511749	7	-17.2
BR 415	Harding bridge, Bangladesh	2640	Suspended Load	0.282241	9	-19.2	0.511752	6	-17.1
BR 414	Harding bridge, Bangladesh	2640	Suspended Load	0.282226	6	-19.8	0.511736	8	-17.4
BR 413	Harding bridge, Bangladesh	2640	Suspended Load	0.282205	6	-20.5	0.511748	6	-17.2
BR 413 re-run				0.282198	5	-20.8			
BR 412	Harding bridge, Bangladesh	2640	Suspended Load	0.282209	6	-20.4	0.511745	7	-17.3
BR 411	Harding bridge, Bangladesh	2640	Suspended Load	0.282133	7	-23.0	0.511755	6	-17.1
BR 411 Dup	Harding bridge, Bangladesh	2640	Suspended Load				0.511723	7	-17.7
BR 418	Harding bridge, Bangladesh	2640	Bedload	0.281992	11	-28.1	0.511719	5	-17.8
BR 8252	Harding bridge, Bangladesh	2640	Bedload				0.511788	11	-16.4
BR 8253	Harding bridge, Bangladesh	2640	Suspended Load	0.282268	7	-18.3	0.511767	8	-16.8
BR 717	Harding bridge, Bangladesh	2640	Bedload	0.281930	6	-30.2	0.511769	7	-16.8
BR 717 re-run				0.281944	8	-29.8			
Karnali River									
PB 79	Chisapani, Nepal	260	Suspended Load	0.282155	8	-22.3	0.511721	6	-17.7
PB 79 re-run							0.511717	6	-17.8
PB 80	Chisapani, Nepal	260	Bank	0.282033	8	-26.6	0.511775	8	-16.7
BR 8113	Revelganj, India	850	Suspended Load	0.282206	6	-20.5	0.511758	7	-17.0
BR 8113 re-run							0.511744	6	-17.3
BR 8113 Dup	Revelganj, India	850	Suspended Load	0.282192	6	-21.0			
BR 8115	Revelganj, India	850	Bedload	0.282027	8	-26.8	0.511684	6	-18.5
BR 8115 Dup	Revelganj, India	850	Bedload				0.511714	9	-17.9
BR 8115 Ter	Revelganj, India	850	Bedload				0.511712	5	-17.9
Kosi River									
LO 762	Chatara, Nepal	180	Suspended Load	0.282155	6	-22.3	0.511714	5	-17.9
LO 762 re-run				0.282162	9	-22.0			
LO 763	Chatara, Nepal	180	Bank	0.282049	5	-26.0	0.511689	7	-18.4
LO 763 Dup	Chatara, Nepal	180	Bank	0.282040	7	-26.3			
PB 69	Chatara, Nepal	440	Suspended Load	0.282123	5	-23.4	0.511601	8	-20.1
PB 70	Chatara, Nepal	440	Bank	0.282064	9	-25.5	0.511649	8	-19.1
BR 331	Dumarighat, India	440	Bank	0.282136	7	-23.0	0.511656	7	-19.0
BR 332	Dumarighat, India	440	Bank	0.282125	6	-23.3	0.511722	9	-17.7
BR 332 re-run				0.282122	6	-23.5			
Narayani River									
LO 757	Narayanghat, Nepal	200	Suspended Load	0.282112	7	-23.8	0.511711	7	-17.9
LO 756	Narayanghat, Nepal	200	Suspended Load	0.282114	6	-23.7	0.511686	6	-18.4
LO 754	Narayanghat, Nepal	200	Suspended Load	0.282085	5	-24.7	0.511681	6	-18.5
LO 755	Narayanghat, Nepal	200	Suspended Load	0.282092	10	-24.5	0.511662	7	-18.9
LO 755 Dup	Narayanghat, Nepal	200	Suspended Load	0.282067	10	-25.4			
LO 758 C	Narayanghat, Nepal	200	Suspended Load	0.282135	4	-23.0	0.511661	5	-18.9
PB 54	Narayanghat, Nepal	200	Suspended Load	0.282055	7	-25.8	0.511661	5	-18.9
LO 1002	Narayanghat, Nepal	200	Suspended Load	0.282129	15	-23.2	0.511712	8	-17.9
LO 1002 re-run				0.282125	12	-23.3	0.511743	11	-17.3
LO 1007	Narayanghat, Nepal	200	Suspended Load	0.282007	12	-27.5	0.511655	13	-19.0
LO 1007 Dup	Narayanghat, Nepal	200	Suspended Load	0.282001	6	-27.7	0.511632	11	-19.5
BR 8106	Hajipur, India	550	Suspended Load	0.282149	6	-22.5	0.511633	6	-19.4
BR 8107	Hajipur, India	550	Bedload	0.282100	5	-24.2	0.511734	7	-17.5

Table 1: Nd-Hf isotopes for sediments analyzed in this study

Re-run samples correspond to run duplicates and Dup samples stand for complete analytical duplicates. Uncertainties (± 2σ) indicated in the Table are in-run errors. ε_{Nd} and ε_{Hf} values were calculated using the CHUR composition published by Bouvier et al. (2008).

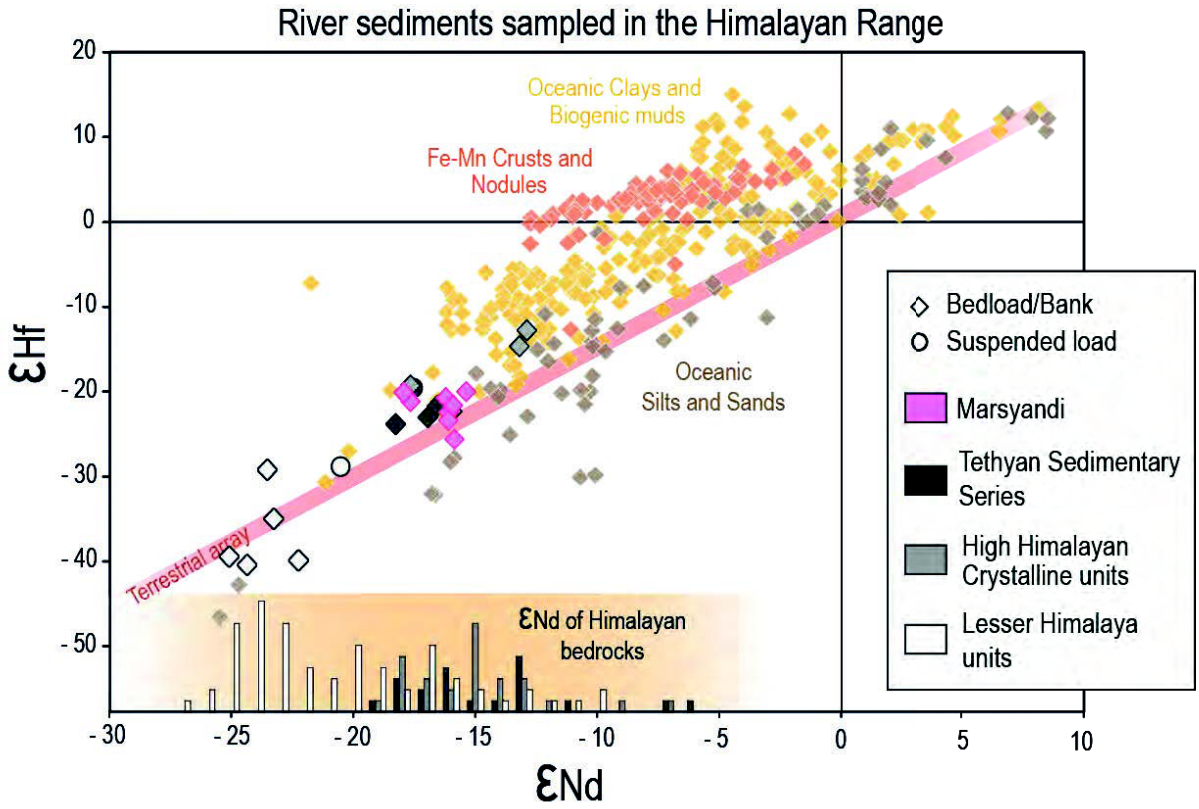

Figure 4: ε_{Hf} versus ε_{Nd} diagram showing river sediments sampled in the Himalayan range i.e. in the Marsyandi River and in small Nepalese rivers draining only the Tethyan Sedimentary Series, the High Himalayan Crystalline and the Lesser Himalaya.
Nd-Hf isotopic compositions of worldwide oceanic sediments are also shown. Data for Fe-Mn crusts and nodules are from Albarède et al. (1997); Godfrey et al. (1997); Albarède et al. (1998); David et al. (2001); Van De Flierdt et al. (2006); oceanic clays and biogenic muds are from White et al. (1986); Ben Othman et al. (1989); McLennan et al. (1990); Pearce et al. (1999); Vervoort et al. (1999); Woodhead et al. (2001); Vlastélic (2005); Prytulak et al. (2006); Carpentier et al. (2008); Bayon et al. (2009); Carpentier et al. (2009); Chauvel et al. (2009); Vervoort et al. (2011) and oceanic silts and sands are from McLennan et al. (1990); Vervoort et al. (1999); Prytulak et al. (2006); Carpentier et al. (2008); Bayon et al. (2009); Carpentier et al. (2009); Vervoort et al. (2011). The Terrestrial Array is that of Vervoort et al. (2011). The histogram along the ε_{Nd} axis shows ε_{Nd} values reported for Himalayan bedrocks from the three main geological units (Parrish and Hodges, 1996; Ahmad et al., 2000; Robinson et al., 2001; Richards et al., 2005). All ε_{Nd} and ε_{Hf} values were recalculated using the CHUR composition published by Bouvier et al. (2008).

In the floodplain (Figure 5), Nd-Hf isotopic compositions of sediments from the Ganga River and its major tributaries are remarkably similar. The Hf isotopic compositions are nevertheless more variable ($-30.2 < \varepsilon_{Hf} < -18.3$) than Nd isotopes ($-20.1 < \varepsilon_{Nd} < -15.6$). With the exception of few outliers, bedloads and banks tend to lie below or next to the Terrestrial Array while suspended loads usually plot above the Terrestrial trend, towards higher ε_{Hf} values like worldwide oceanic terrigenous clays. By contrast, suspended loads, bedloads and banks cannot be distinguished by their Nd isotopic compositions.

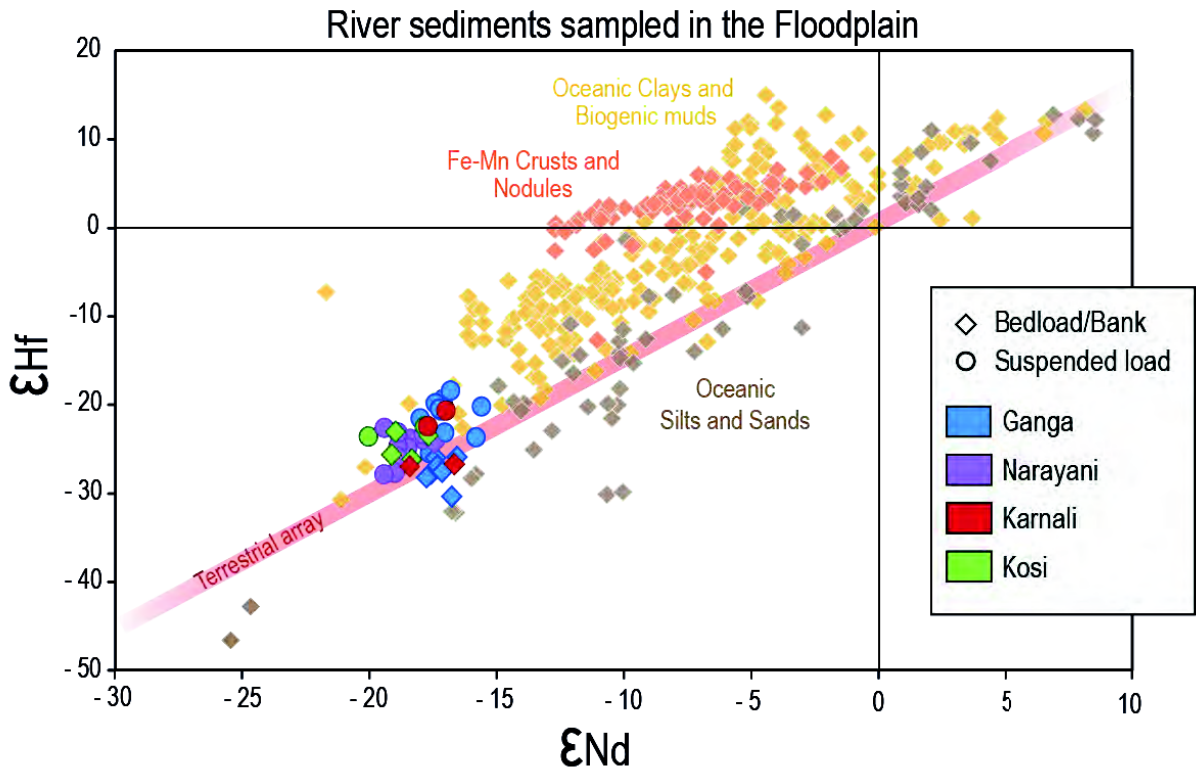

Figure 5: ε_{Hf} versus ε_{Nd} diagram showing data obtained on sediments sampled in the floodplain i.e. in the Ganga and its main tributaries.
Same sources of data as in Figure 4. ε_{Nd} and ε_{Hf} values calculated using the CHUR composition published by Bouvier et al. (2008).

5. Discussion

5.1. Source isotopic variability

Variations of the Nd and Hf isotopic compositions of sediments along a river course can be due to contributions of materials with different isotopic compositions that are supplied by tributaries. These source effects need to be first carefully considered before we can consider the effects of sedimentary processes on the geochemistry of river sediments.

Because the concentrations of immobile elements, such as the REE, are not really modified by weathering, they have been used as proxies when studying the provenance of detrital sediments (e.g. Singh et al. 2008; 2009; 2010). More specifically, ratios such as La/Yb, or Nd isotopic compositions are considered as representative of sediment sources (Goldstein and Jacobsen, 1988; Condie, 1991; Taylor and McLennan, 1995). Below we evaluate how much these proxies vary in the Himalayan river sediments.

5.1.1. The Marsyandi River in the Himalayan range

In the Himalayan range, the Marsyandi River takes its source in the Tethyan Sedimentary Series, then it flows successively through the High Himalayan Crystalline units and the Lesser Himalaya units (see the river profile in Figure 6). Samples recovered upstream, where the river drains only the Tethyan Sedimentary Series (samples NAG 22 and MAR-50), are characterized by an average $(La/Yb)_{UCCnorm}$ ratio of 1.19 and an ε_{Nd} value of -16.8 (Table 1).

Downstream, when the river passes through the High Himalayan Crystalline units (samples MAR-55 and MAR-58), the average $(La/Yb)_{UCCnorm}$ ratio drops to 0.66 while ε_{Nd} values average -16.2. The REE patterns of sediments are thus clearly affected by materials eroded from the High Himalayan Crystalline units, which have an average $(La/Yb)_{UCCnorm}$ ratio of 0.39 (see section 4.3). Because the Nd isotopic signature of the Tethyan Sedimentary Series is similar to that of the High Himalayan Crystalline units (see the histogram in Figure 4 and references therein), there is no significant change in the average ε_{Nd} values of the sediments.

Further downstream, sediments sampled where the river passes through the Lesser Himalaya units (all MAR samples downstream of MAR-58) are characterized by an average $(La/Yb)_{UCCnorm}$ ratio of 0.59 and an ε_{Nd} value of -16.7. This value is remarkably similar to what is measured upstream even though the Lesser Himalaya units have a significantly less radiogenic Nd isotopic signature (see the histogram in Figure 4 and references therein). This implies that the Lesser Himalaya units contribute little to the final sediment load of the Marsyandi River. The main contribution comes from the High Himalayan Crystalline units, as already shown by Garzanti et al. (2007). Indeed, these authors used petrographic and mineralogical data on the same samples as those analyzed here, and suggested a contribution of the Tethyan Sedimentary Series at 13±5%, one of 68±3% for the High Himalayan Crystalline units and one of 20±2% for the Lesser Himalaya units. Assuming comparable Nd concentrations for sediments coming from the three main sources, our mixing calculations show that addition of 20% Lesser Himalayan sediments with an ε_{Nd} of -23.2, to sediments derived from the other two sources ($\varepsilon_{Nd} \approx -16.5$) only lowers the final isotopic composition by 1.3 ε_{Nd} unit, a value consistent with our measurements.

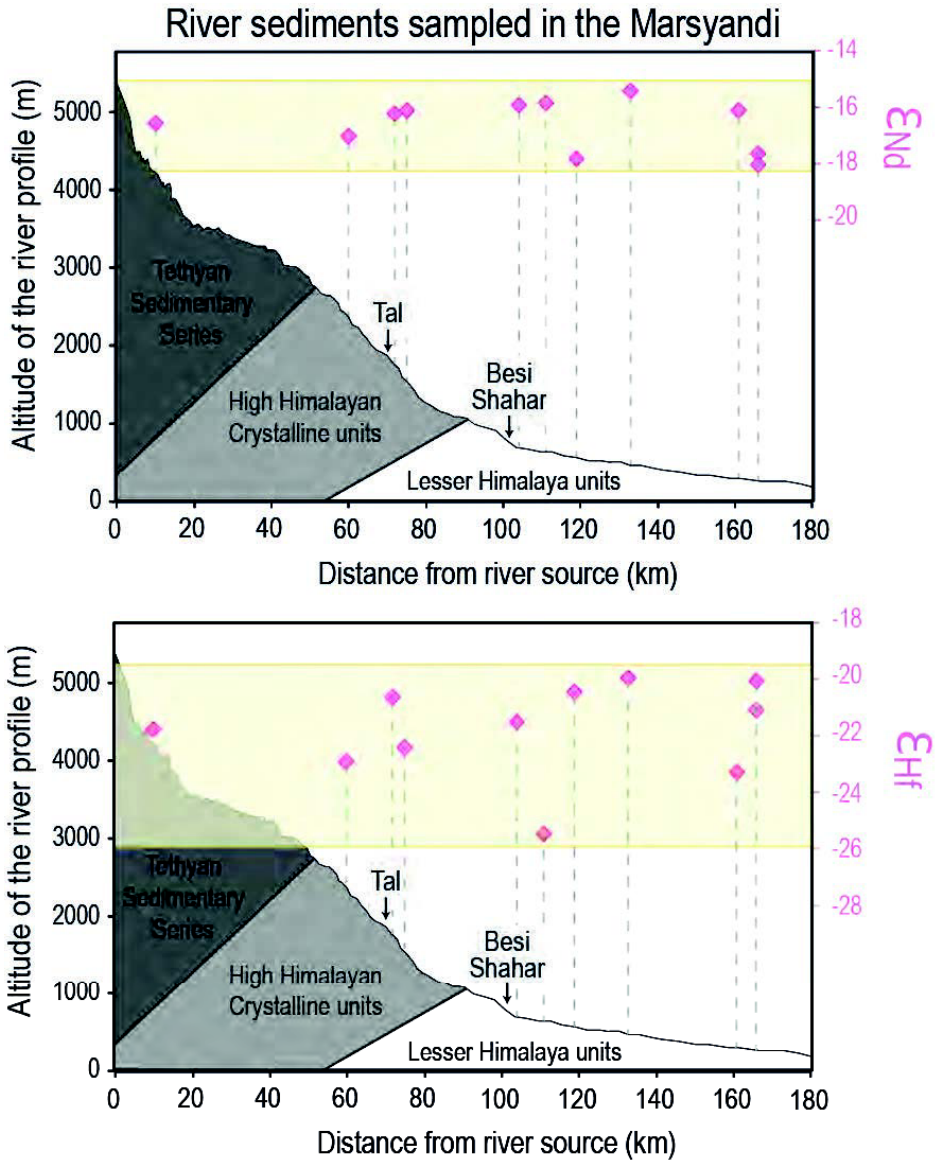

Figure 6: Downstream evolution of ε_{Nd} and ε_{Hf} in sediments along the Marsyandi River located in the Himalayan range.
The river profile and the main geological units on which the river flows are shown together with the location of two towns, Tal and Besi Shahar.

In summary, despite the fact that the Marsyandi River crosses several geological units with distinct isotopic signatures, its sediments have rather constant ε_{Nd} values at -16.6 on average. The variability of Nd isotopic compositions due to source effects is limited (i.e. about 3 ε_{Nd} units) and the sediments are quickly homogenized within the Himalayan range.

5.1.2. The Ganga and its major tributaries in the floodplain

Sediments from the Ganga and its major tributaries sampled in the floodplain have remarkably similar REE patterns with an average $(La/Yb)_{UCCnorm}$ ratio at 0.88 (see section 4.3. and Figure 3). As shown in Figure 5, their Nd isotopic compositions span a small range of values (less than 5 ε_{Nd} units) similar to values obtained for the bedrocks from the High Himalayan Crystalline units and the Tethyan Sedimentary Series (Figure 4). There is also no clear change of either REE patterns or Nd isotopic compositions as a function of sampling site in the floodplain. These constant geochemical characteristics indicate that no significant amount of new material is added along the course of the Ganga, ss already suggested by several authors (Tripathi et al., 2007; Singh et al., 2008; Singh, 2009; Lupker et al., 2012) using major and trace element concentrations. Actually, the sediments are well reworked and already homogenized before entering the floodplain.

Sediments coming from the erosion of the Indian shield and the Deccan Traps are also added to the Ganga (see Figure 1) and one could expect that these different terranes could influence the Nd isotopic composition of sediments after their confluence. However, Lupker et al. (2012) excluded significant contributions from these sources and estimated the contribution of the southern tributaries to the whole Ganga sediment load to be less than 4% in Bangladesh for our samples recovered in 2004, 2007 and 2008. Our new ε_{Nd} values support these ideas since sediments collected in Bangladesh have values similar to upstream samples.

Within the range of ε_{Nd} values obtained on the floodplain samples (-20 to -15), the most negative values are likely due to higher contributions of sediments derived from the Lesser Himalaya units depending on the sampling year and/or location. This could notably be the case for the Kosi and Narrayani sediments (green and purple dots in Figure 5). For example, the ε_{Nd} values of the Narrayani samples, that were all collected at the same location in Nepal, vary from -19.5 to -17.3 depending of the sampling year (2005, 2007 and 2010). This suggests that part of the Nd isotopic variability seen in Figure 5 could be temporal and related to local inefficient homogenization of the sediments. Such a phenomenon was already pointed out by Lupker et al. (2012) in the Ganga sediments sampled in Bangladesh but it remains very limited in our sample set.

5.2. Effects of mineralogical sorting

Sediments transported by rivers consist of various particles and minerals having different hydrodynamic properties depending on their size, shape and density (Komar, 2007). This results in a mineralogical sorting within the water column: coarser and heavier grains are preferentially transported in bedload by sliding and bouncing while finer and lighter grains are preferentially transported in suspended load and at different depth in the water column depending on their settling velocities. Because chemical elements are carried in different concentrations by minerals, mineralogical sorting accounts for significant geochemical variability in river sediments (e.g. Singh and France-Lanord, 2002; Garzanti et al., 2010; Bouchez et al., 2011; Garzanti et al., 2011; Lupker et al., 2011). In order to assess the impact of mineralogical sorting on the Nd-Hf isotopic systematics of the Himalayan river sediments, we first briefly describe its influence on major and trace element concentrations, to focus later on the Nd and Hf budgets.

5.2.1. Impact on the overall chemical compositions

The influence of mineralogical sorting during sediment transport on the major and trace element concentrations of sediments from the Himalayan rivers was studied in detail by Garzanti et al. (2010; 2011) and Lupker et al. (2011; 2012) and our new measurements are consistent with results obtained by these authors. In general, the factor controlling the chemical composition is sediment grain size (Lupker et al., 2011) and Al_2O_3/SiO_2 ratio can be used as a reliable grain-size proxy because coarse-grained sediments i.e. most of the bedloads and banks are enriched in SiO_2-rich quartz while finer-grained sediments, i.e. most of the suspended loads are enriched in Al_2O_3-rich phyllosilicates (see Figure 2).

Systematic changes of trace element concentrations between bedloads, banks and suspended loads also occur (Figure 3). Suspended loads have generally higher concentrations in transition elements and mobile elements due to their high proportion of phyllosilicates, oxyhydroxides, soil particles and organic matter (Garzanti et al., 2011). For the other trace elements, differences between bedload, bank and suspended load are more complex to explain because they result from the combined effects of several processes: (1) contribution of individual mineral phases, such as zircon, rutile or monazite that strongly control the budget of Zr-Hf, Nb-Ta and REE respectively (Garçon et al., 2011); (2) relative proportions of mineral species that occur in different quantities in bedloads, banks and

suspended loads and (3) dilution of the overall contents by minerals such as quartz that are relatively poor in trace elements. These dilution effects are particularly obvious when looking at the trace element patterns of bedloads and banks from the Ganga River (Figure 3e). These samples have similar positive and negative anomalies but variable enrichment factors relative to the composition of average upper continental crust.

The heavy minerals play a key role for the budget of some trace elements in sediments because they host these elements in extreme concentrations (e.g. Götze and Lewis, 1994; Totten, 2007; Garçon et al., 2011). The large variability observed in the trace element patterns of bedloads from the Marsyandi River (Figure 3d) can indeed be linked to variable proportions of heavy minerals, between 1 and 31 wt.% as estimated by Garzanti et al. (2007). Similarly, the positive Zr-Hf anomalies of bedloads and banks from the Ganga and its major tributaries (Figure 3e-h) are likely due to the preferential concentration of zircons. Garzanti et al. (2010; 2011) already demonstrated that zircons control almost the entire Zr-Hf budget of the Ganga bedloads while they account for about half of the Zr-Hf budget of surface suspended loads. The same authors also showed that the proportion of monazite and allanite in the Ganga bedloads controls the REE budget, including that of Nd, while phyllosilicates together with titanite and monazite are the carrier of REE in suspended loads. Our new trace element data further support this interpretation.

5.2.2. Nd-Hf isotopic decoupling

We have seen in the above section that Nd and Hf in bedloads and suspended loads are carried by different minerals due to sorting processes during transport. Since the various minerals do not all have the same Sm/Nd and Lu/Hf ratios and/or crystallization ages, the Nd and Hf isotopic compositions of bedloads and suspended loads can differ.

Figures 4 and 5, where ε_{Hf} is plotted as a function of ε_{Nd}, show that bedload and bank sediments plot next to the Terrestrial Array while suspended loads plot above. This suggests that the minerals present in bedloads carry isotopic signatures different from those constituting the suspended loads. A clue is provided by Figure 7, which shows the variations of ε_{Nd} and ε_{Hf} as a function of Al_2O_3/SiO_2 ratios i.e. the grain-size proxy. No clear change of ε_{Nd} occurs as a function of the sediment grain-size, but the ε_{Hf} of coarse-grained sediments with low Al_2O_3/SiO_2 ratios are systematically lower than those of fine-grained sediments with high Al_2O_3/SiO_2 ratios. This is particularly true for bedloads and banks sampled at the same

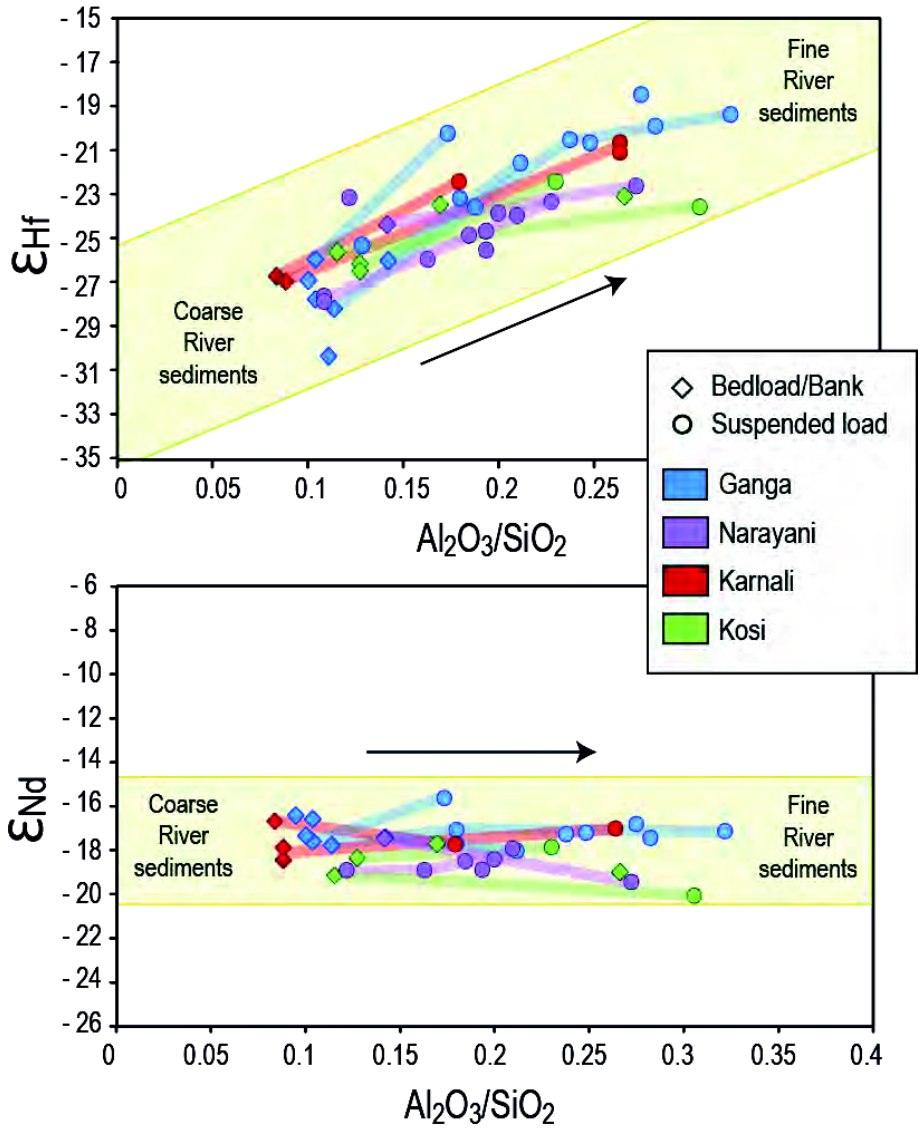

Figure 7: Variations of ε_{Hf} and ε_{Nd} as a function of Al_2O_3/SiO_2 ratio used as a grain-size proxy for the Ganga, the Narayani, the Karnali and the Kosi river sediments.
The color lines link bedloads and banks to their corresponding suspended loads sampled at the same location at different depths in the water column.

location as their corresponding suspended loads sampled at different depths in the water column (see the color bands linking related samples in Figure 7). Given that source variability is limited in the studied sediments (see section 5.1), these observations suggest that mineralogical sorting processes during transport have a significant effect on Hf isotopic compositions while they do not change the Nd isotopic signature. Nd and Hf isotopes are thus decoupled in fine-grained sediments with high Al_2O_3/SiO_2 ratios. This is confirmed by the remarkable correlation between $\Delta\varepsilon_{Hf}$, a measure of the vertical ε_{Hf} deviation from the Terrestrial Array, and Al_2O_3/SiO_2 as shown in Figure 8. With few exceptions, coarse-grained sediments lie below or on the Terrestrial Array while all other sediments have increasing $\Delta\varepsilon_{Hf}$

when their grain size diminishes. We conclude that the entire Hf isotopic variability observed in the Himalayan river sediments (more than 10 ε_{Hf} units) relates to changes in sediment grain size, and is therefore due to mineralogical sorting processes during sediment transport. Using the relationship shown in Figure 8 ($\Delta\varepsilon_{Hf}$ = 42.2*Al_2O_3/SiO_2 -3.6) and the Al_2O_3/SiO_2 ratios published by Lupker et al. (2012), we estimate that the average $\Delta\varepsilon_{Hf}$ of Himalayan bedloads is close to zero while surface suspended loads should have an average $\Delta\varepsilon_{Hf}$ of about 9 (see the orange and green stars in Figure 8).

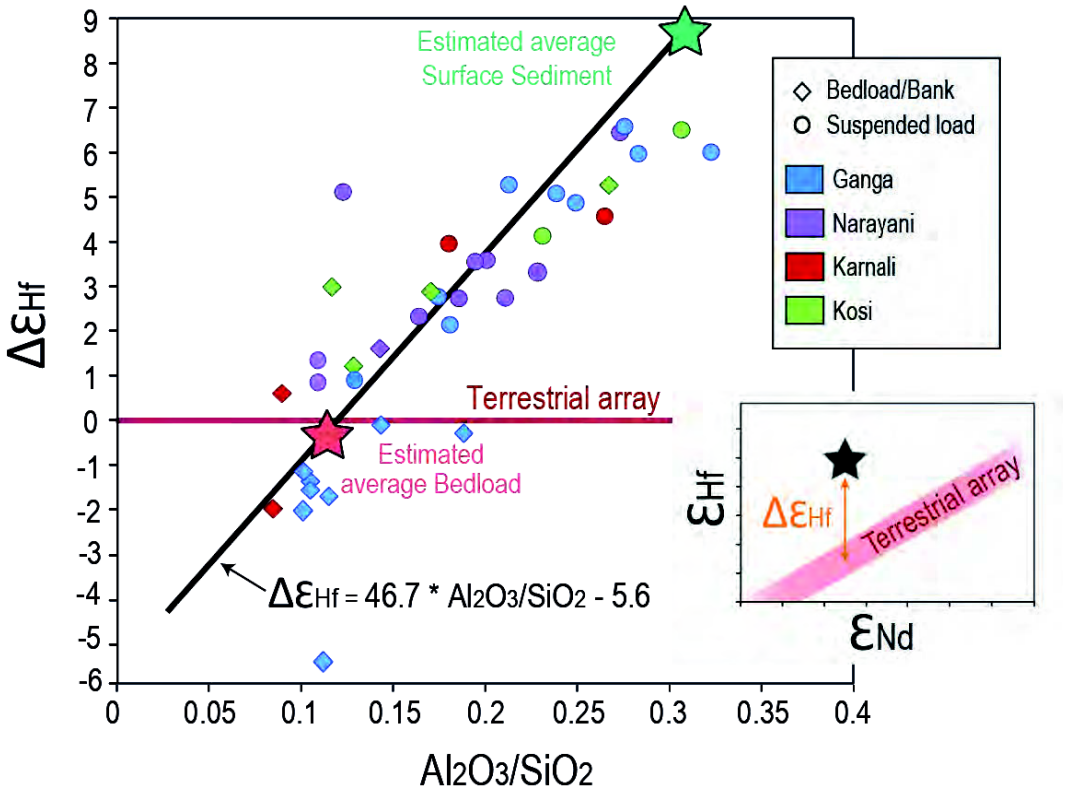

Figure 8: $\Delta\varepsilon_{Hf}$ vs. Al_2O_3/SiO_2 ratio used as grain-size proxy for the Ganga, the Narayani, the Karnali and the Kosi river sediments.
The sketch at the bottom right corner shows how vertical deviations ($\Delta\varepsilon_{Hf}$) from the Terrestrial Array of Vervoort et al. (2011) are calculated. The black line represents the best fit to our data. Green and red stars correspond to our estimates of average Himalayan bedload and surface sediment calculated using the Al_2O_3/SiO_2 ratios published by Lupker et al. (2011) and the regression line through our data.

Similar decoupling of Nd and Hf isotopes through mineralogical sorting processes has already been reported in detrital oceanic materials (see Figure 4 and 5; Chauvel et al., 2008 ; Bayon et al., 2009; Carpentier et al., 2009; Vervoort et al., 2011) but, to our knowledge, it is the first time that it is demonstrated for modern river sediments on continents. We believe

that in both environments, the process that fractionates Hf from Nd isotopes is the same: the sample mineralogy. Zircons host most of the Hf in river sediments and they have a very low Lu/Hf ratios (Kinny and Maas, 2003) compared to any other minerals. Their Hf isotopic compositions is therefore very close to the initial ratio of the material from which they crystallized, and always significantly less radiogenic than the Hf isotopic composition of all other crustal minerals. Because coarse-grained sediments are zircon-rich, they do inherit the unradiogenic Hf isotopic composition of zircons. By contrast, the Hf isotopic composition of fine-grained sediments varies depending on the relative proportion of zircons and other minerals, which are less resistant to erosion and have higher Lu/Hf ratios such as phyllosilicates. The amplitude of the fractionation is of course dependent on the age of the crustal protolith since time is necessary to produce ^{176}Hf as a decay product of ^{176}Lu. In contrast, the mineralogical sorting through river transport has no effect on Nd isotopes because the minerals that host Nd in the bedloads, banks and suspended loads (i.e. phyllosilicates, monazite, etc) have basically similar resistance to erosion and similar Sm/Nd ratios; all sediments share the same Nd isotopic composition, that of their source. This is absolutely not the case for Hf isotopic compositions that cannot be used to trace sources if care is not taken of the sediment mineralogy. Only coarse-grained sediments, rich in zircons, have Hf isotopes that can be representative of their continental sources provided that the age of the zircon population is known (Harrison et al., 2005; Kemp et al., 2007; Garçon et al., 2011).

5.3. Where does decoupling of Nd and Hf isotopes occur on continents?

Mineralogical sorting processes depend heavily on the river hydrodynamics. Thus, chemical and isotopic compositions of river sediments should change as a function of the sampling site, in the steep Himalayan range or in the floodplain. The Nd-Hf isotopic decoupling occurring in fine-grained sediments should also vary depending on the degree of mineral sorting.

In the Himalayan range, no clear downstream variation of ε_{Nd} values occurs in the Marsyandi sediments (Figure 6). Values remain rather constant between -18.0 and -15.4 because they are not significantly affected by source effects, nor mineralogical sorting. The same observation applies to ε_{Hf} values of bedloads even though they are more variable (-25.5 to -19.9). The ε_{Hf} variability does not correlate with the Nd isotopic compositions of

sediments, and it is not related to the geological units on which the river flows (Figure 6). The river profile being relatively steep (Figure 6), we believe that the Hf isotopic composition of the Marsyandi bedloads is rather controlled by local changes in the river hydrodynamic conditions that impact the proportions of heavy minerals (see section 5.2.1. and Garzanti et al., 2007). Unfortunately, we could not measure the isotopic compositions of suspended loads in the Marsyandi River and we ignore how different they are from the bedloads. However, our bedload data alone suggest that the isotopic variability present in sediments sampled in the mountain range is not very predictable and mainly controlled by local hydrodynamic conditions.

The situation is very different in the Ganga floodplain, along the 2500 km of river profile. Figure 9 shows the variations of Nd and Hf isotopic compositions of bedloads, banks and suspended loads from the Ganga and its major tributaries as a function of their sampling location in the floodplain. While ε_{Nd} values are remarkably constant at about -17.8 and do not indicate any downstream change, ε_{Hf} values display interesting variations. As mentioned above, the Hf isotopic compositions of bedloads and banks are less radiogenic than those of corresponding suspended loads sampled at the same location. Figure 9 shows clearly that this difference increases with distance from river source. This is particularly clear for the Ganga sediments in which the Hf isotopic difference is lesser than 5 ε_{Hf} units at about 260 km away from the river source and reaches 12 ε_{Hf} units in the Bay of Bengal, 2600 km away from the source. The decoupling of Nd-Hf isotopes in river sediments thus exists at the front of the mountain range but is much more pronouced at the river mouth. This observation is best explained by a preponderant role of the distance of transport on the efficiency of mineralogical sorting in sediments. Even if Lupker et al. (2012) estimated that sequestration of sediments in the Ganga floodplain is limited to only 10% of the transported sediments, we believe that part of the isotopic decoupling observed at the river mouth could be due to this sequestration process that could help in maintaining coarse-grained sediments at the river bed.

The impact of mineralogical sorting on the overall chemistry of sediments from other large fluvial systems in the world was highlighted by previous work (Dupré et al., 1996; Bouchez et al., 2011) but no study targeted the decoupling of Nd and Hf. We believe however that our observation is not restricted to the Himalayan system but occurs systematically for all detrital sediments that are delivered into the world ocean at the mouth of large rivers. This has major implications for Nd-Hf isotopic systematics in the global

sedimentary system, and particularly to understand why detrital oceanic clays are displaced towards elevated ε_{Hf} relative their ε_{Nd} values.

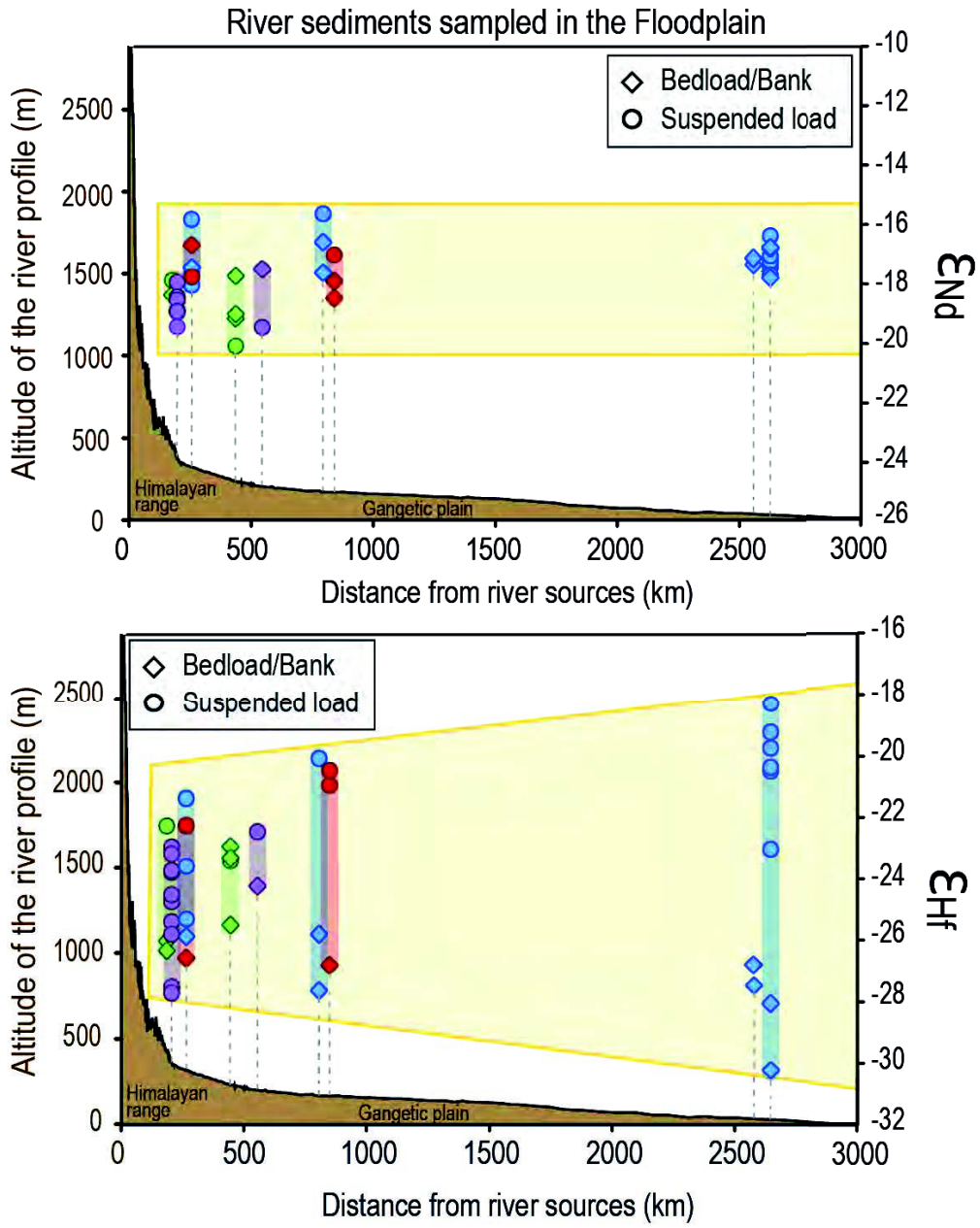

Figure 9: Downstream changes of ε_{Nd} and ε_{Hf} in sediments from the Ganga and its major tributaries in the floodplain, from the Himalayan Mountain front to the Bengal delta.
Footnotes: Same symbols and colors as in previous figures. Color lines link bedloads and banks to their corresponding suspended loads sampled at the same location at different depths in the water column. The topography of the river profile is shown in brown.

5.4. Impact of continental fractionation on oceanic sediments

Detrital sediments delivered into the world ocean at the mouth of large rivers represent a significant part of the terrigenous oceanic sedimentation (e.g. (Milliman and Meade, 1983; Lisitzin, 1996; Hay, 1998). We thus suggest that the Nd-Hf isotopic decoupling known as the “zircon effect” in detrital oceanic sediments originates on continents and is transferred by rivers to the open ocean.

Here we compare the impact of mineralogical sorting processes on river sediments to those observed in worldwide oceanic sediments that are not authigenic. Indeed, biogenic sediments and Fe-Mn crusts and nodules precipitate from seawater and their composition reflects the Nd and Hf isotopic signatures of seawater and most probably not that of detrital particles (e.g. Albarède et al., 1998; Van de Flierdt et al., 2004; 2007; Vervoort et al., 2011). We use the vertical deviation from the Terrestrial Array (ΔεHf) in a Hf-Nd isotopic space as a proxy (cf. Figure 8). However, part of the amplitude of ΔεHf values of worldwide sediments comes from the average age of the continental sources, which can be evaluated using their e_{Nd} value. Sediments eroded from an old evolved crust have very low e_{Nd} values, contain zircons with very low e_{Hf} and phyllosilicates with elevated e_{Hf}. The amplitude of ΔεHf values should thus be very large. In contrast, erosion products of a more juvenile crust have higher e_{Nd} values and the e_{Hf} values of both zircons and phyllosilicates are less extreme because radiogenic decay within minerals lasted a shorter time (see the inset of Figure 10). We thus need to normalize the ε_{Hf} values of worldwide river and ocean sediments for the age effect before comparing them. This correction is explained in the sketch shown in the inset of Figure 10. We choose to project all initial Nd-Hf isotopic compositions of sediments to an arbitrary intermediate ε_{Nd} value of -15 using straight lines that converge at an average depleted mantle value of ε_{Nd} = +8.9 and ε_{Hf} = +14.8 (see caption of Figure 10). We then calculated the vertical deviation ($\Delta\varepsilon_{Hf}$) from the Terrestrial Array of all projected ε_{Hf} values to obtain a parameter that is less influenced by age effect; such projection allows us to compare sediments from everywhere in the world. The range of normalized $\Delta\varepsilon_{Hf}$ is plotted in Figure 10 as a function of Al_2O_3/Zr ratios for river and oceanic sediments. As done previously by (Vervoort et al., 2011), we selected Al_2O_3/Zr instead of Al_2O_3/SiO_2 as proxy to the relative proportions of zircons vs. phyllosilicates because the presence of biogenic silica in oceanic sediments affects Al_2O_3/SiO_2 while this is not the case in continental environments.

Figure 10 shows that river and terrigenous oceanic sediments share a common positive correlation between $\Delta\varepsilon_{Hf}$ and Al_2O_3/Zr.

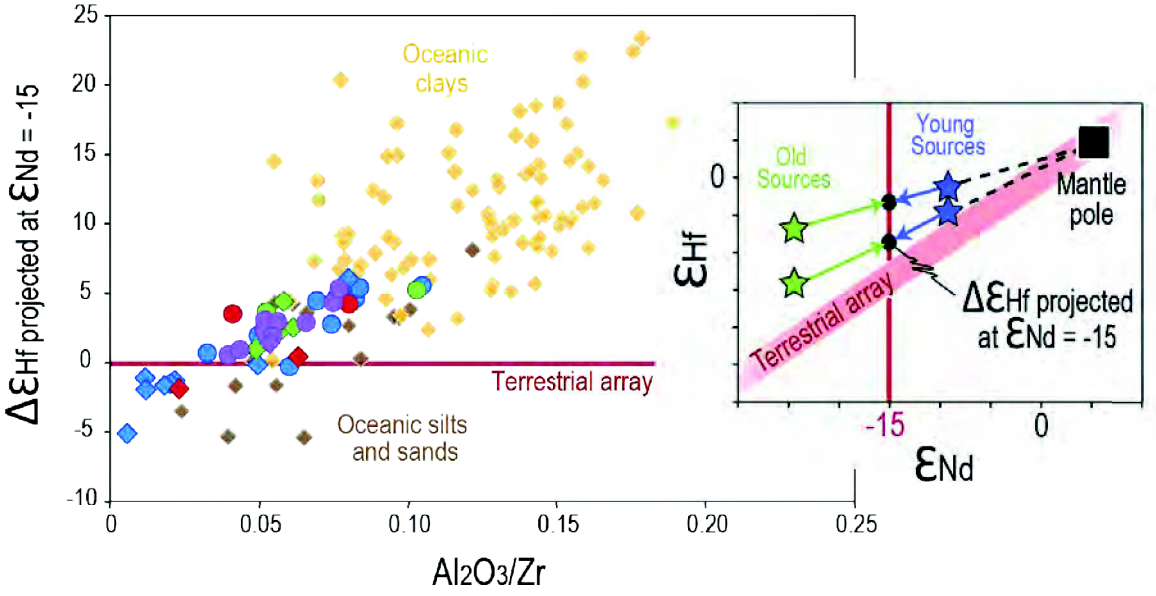

Figure 10: $\Delta\varepsilon_{Hf}$ projected at ε_{Nd}=-15 plotted as a function of Al_2O_3/Zr ratios for river sediments analyzed in this study and worldwide oceanic terrigenous sediments (oceanic sands, silts and clays).
The sketch shown in the inset explains how all measured and published ε_{Hf} are projected to ε_{Nd}=-15 to calculate the vertical deviation from the Terrestrial Array of Vervoort et al. (2011): $\Delta\varepsilon_{Hf}$ that is plotted in the main panel. The ε_{Nd} value of the depleted mantle pole was compiled using data from the PETDB database and its ε_{Hf} was calculated by projecting this ε_{Nd} value on the Terrestrial Array of Vervoort et al. (2011). In the main panel, colors and symbols for river sediments analyzed in this study are the same as in previous figures. Data for oceanic sands, silts and clays correspond to terrigenous sediments poor in volcanic ashes and are from (Plank et al., 2007; Carpentier et al., 2008; 2009; Chauvel et al., 2009; Vervoort et al., 2011). ε_{Hf} and ε_{Nd} of terrigenous sediments have been corrected for subsequent disintegration after their deposition age. It can be noted that $\Delta\varepsilon_{Hf}$ projected at ε_{Nd}=-15 is quite a robust parameter since the trend that we observe for river and oceanic sediments does not significantly change if we choose other reasonable values for the depleted mantle pole or for the εNd value at which the projection is done.

This suggests strongly that the decoupling of Nd and Hf isotopic compositions in river and oceanic sediments results of the same process i.e. mineralogical sorting and variable proportions of zircons in the sediments. In addition, oceanic sands and silts have the same $\Delta\varepsilon_{Hf}$ values as the Himalayan river sediments analyzed in this study, while oceanic clays have generally higher $\Delta\varepsilon_{Hf}$ than the Himalayan suspended loads. This shows that the decoupling that started during transport of sediments in the rivers is amplified in the oceanic basins. It is also consistent with the fact that more than 90% of suspended matter transported by rivers and nearly all bedloads are actually deposited in deltas and estuaries

and never reach the ocean (Lisitzin, 1996). It is particularly true for the heavy mineral fraction that contains zircons and is usually removed from suspended matter during transport from river mouth to open ocean (Stummeyer et al., 2002). Sorting processes at the river/ocean interface thus amplify the chemical fractionation started in rivers, favor the sequestration of zircon-rich sediments with unradiogenic Hf signature and lead to the delivery of sediments with radiogenic Hf in the ocean. It remains nevertheless that almost half of the decoupling job is already done upstream in rivers on continents (see Figure 10). In the oceanic environment, Hf-Nd fractionation most probably continues with segregation of fine particles travelling far from continents while coarser fractions settle down close to source areas, next to continents.

Our study of river sediments demonstrates that mineralogical sorting during transport is the factor controlling Nd-Hf decoupling in both continental and oceanic environments. The anomalous Nd-Hf isotopic compositions of terrigenous oceanic clays displaced above the Terrestrial Array in a ε_{Hf} vs. ε_{Nd} diagram is a feature progressively acquired during transport from sediment sources on continents to the open ocean. This has major implications for the long-term evolution of the Earth's mantle if oceanic sediments with Nd-Hf isotopic compositions different from those of continental crust, are recycled back into the mantle for long periods of time. Indeed, Chauvel et al. (2008) already showed that oceanic sediments affected the overall Nd-Hf isotopic composition of the mantle since the peculiar composition of oceanic sediments is needed to properly explain the Mantle Array and therefore the mantle sources of oceanic island basalts and mid-ocean ridge basalts. Here, we go one step further and propose that reinjection of oceanic sediments into the mantle could have shifted the Mantle Array towards higher e_{Hf} at any given e_{Nd} value through time. In other words, continental crust separated from the mantle in the earliest part of history probably had lower e_{Hf} at any given e_{Nd} than recently formed crust. Evaluating the impact of such a temporal change on the overall composition of continental crust and mantle is difficult because data on old and well-constrained materials are not numerous. Additional Nd and Hf isotopic data on carefully selected rocks with ages covering the Earth history could provide an answer. The Terrestrial Array that describes the overall relationship between Nd and Hf isotopes is based on all available terrestrial data and represents a mixture of materials formed at different times from the mantle (Vervoort et al., 1999, 2011). In addition, it is strongly controlled by recent basalts. The slightly positive e_{Hf} intercept and more significantly the large error on the slope of the Terrestrial Array could be due to the temporal increase of incongruence of the two isotopic systems.

6. Summary and Conclusions

This paper presents the first comprehensive study of Nd and Hf isotopic compositions in bedloads, banks and suspended loads sampled along one of the largest river, the Ganga River that drains the Himalayan range. Because source heterogeneity does not significantly affect the isotopic composition of the studied sediments, we could demonstrate that mineralogical sorting processes control the chemistry of river sediments and account for the entire Hf isotopic variability (>10 ε_{Hf}) measured in sediments from the Ganga and its major tributaries. Bedload and bank sediments always have lower ε_{Hf} than suspended loads sampled at the same location at various depths in the water column. The coarse-grained sediments fall next to the Terrestrial Array in Hf-Nd isotopic space while fine-grained sediments display increasing decoupling of the two isotopic systems as sediment grain size decreases. We attribute these features to hydraulic sorting of minerals during transport in the floodplain with the selective deposition of zircons hosting significant amounts of unradiogenic Hf. We believe that zircons may totally control the Hf isotopic budget of coarse sediments in which they concentrate while their contribution to the Hf isotopic budget of finer sediments is balanced by other minerals with more radiogenic Hf such as phyllosilicates.

We show that the Nd-Hf isotopic decoupling known in oceanic environments also exists in river sediments and that it increases from mountain source to the estuary where it reaches its maximum. When comparing river sediments to worldwide oceanic clays, we estimate that almost half of the Nd-Hf isotopic decoupling displayed by oceanic clays is already acquired on continents. Finally we speculate that transport of fine particles over long distances in the open ocean amplifies the signal to reach the maximum known $\Delta\varepsilon_{Hf}$ values of +20. If significant amounts of oceanic sediments with anomalous Nd-Hf isotopic compositions were sent back into the mantle over Earth history, they could have slowly shifted the overall isotopic composition of the Earth's mantle towards more radiogenic Hf values.

Acknowledgments

We thank S. Bureau for her help in the clean lab, P. Telouk (ENS, Lyon) for assistance during MC-ICP-MS measurements at Lyon and N. Arndt (ISTerre, Grenoble) for constructive discussions that helped improving the content of the manuscript.
This study was supported by funding from CNRS and INSU programs.

References

Ahmad, T., Harris, N., Bickle, M., Chapman, H., Bunbury, J., Prince, C., 2000. Isotopic constraints on the structural relationships between the lesser Himalayan series and the high Himalayan crystalline series, Garhwal Himalaya. Geological Society of America Bulletin 112, 467–477.

Albarède, F., Goldstein, S.L., Dautel, D., 1997. The neodymium isotopic composition of manganese nodules from the Southern and Indian oceans, the global oceanic neodymium budget, and their bearing on deep ocean circulation. Geochimica et Cosmochimica Acta 61, 1277–1291.

Albarède, F., Simonetti, A., Vervoort, J.D., Blichert-Toft, J., Abouchami, W., 1998. A Hf-Nd isotopic correlation in ferromanganese nodules. Geophys. Res. Lett. 25, 3895–3898.

Attal, M., lavé, J., 2006. Changes of bedload characteristics along the Marsyandi River (central Nepal): Implications for understanding hillslope sediment supply, sediment load evolution along fluvial networks, and denudation in active orogenic belts. Geological Society of America Special Paper 398, 143–171.

Bayon, G., Burton, K.W., Soulet, G., Vigier, N., Dennielou, B., Etoubleau, J., Ponzevera, E., German, C.R., Nesbitt, R.W., 2009. Hf and Nd isotopes in marine sediments: Constraints on global silicate weathering. Earth and Planetary Science Letters 277, 318–326.

Bayon, G., Vigier, N., Burton, K.W., Jean Carignan, A.B., Etoubleau, J., Chu, N.-C., 2006. The control of weathering processes on riverine and seawater hafnium isotope ratios. Geology 34, 433.

Ben Othman, D., White, W.M., Patchett, J., 1989. The geochemistry of marine sediments, island arc magma genesis, and crust-mantle recycling. Earth and Planetary Science Letters 94, 1–21.

Bouchez, J., Gaillardet, J., France-Lanord, C., Maurice, L., Dutra-Maia, P., 2011. Grain size control of river suspended sediment geochemistry: Clues from Amazon River depth profiles. Geochem. Geophys. Geosyst. 12, Q03008.

Bouvier, A., Vervoort, J.D., Patchett, P.J., 2008. The Lu–Hf and Sm–Nd isotopic composition of CHUR: constraints from unequilibrated chondrites and implications for the bulk composition of terrestrial planets. Earth and Planetary Science Letters 273, 48–57.

Carignan, J., Hild, P., Mevelle, G., Morel, J., Yeghicheyan, D., 2007. Routine Analyses of Trace Elements in Geological Samples using Flow Injection and Low Pressure On-Line Liquid Chromatography Coupled to ICP-MS: A Study of Geochemical Reference Materials BR, DR-N, UB-N, AN-G and GH. Geostandards and Geoanalytical Research 25, 187–198.

Carpentier, M., Chauvel, C., Mattielli, N., 2008. Pb–Nd isotopic constraints on sedimentary input into the Lesser Antilles arc system. Earth and Planetary Science Letters 272, 199–211.

Carpentier, M., Chauvel, C., Maury, R.C., Mattielli, N., 2009. The “zircon effect” as recorded by the chemical and Hf isotopic compositions of Lesser Antilles forearc sediments. Earth and Planetary Science Letters 287, 86–99.

Chauvel, C., Blichert-Toft, J., 2001. A hafnium isotope and trace element perspective on melting of the depleted mantle. Earth and Planetary Science Letters 190, 137–151.

Chauvel, C., Bureau, S., Poggi, C., 2011. Comprehensive chemical and isotopic analyses of

basalt and sediment reference materials. Geostandards and Geoanalytical Research 35, 125–143.

Chauvel, C., Marini, J.-C., Plank, T., Ludden, J.N., 2009. Hf-Nd input flux in the Izu-Mariana subduction zone and recycling of subducted material in the mantle. Geochem. Geophys. Geosyst. 10, Q01001.

Condie, K.C., 1991. Another look at rare earth elements in shales. Geochimica et Cosmochimica Acta 55, 2527–2531.

David, K., Frank, M., O'Nions, R., Belshaw, N., Arden, J., 2001. The Hf isotope composition of global seawater and the evolution of Hf isotopes in the deep Pacific Ocean from Fe-Mn crusts. Chemical Geology 178, 23–42.

France-Lanord, C., Derry, L., Michard, A., 1993. Evolution of the Himalaya since Miocene time: isotopic and sedimentological evidence from the Bengal Fan. Geological Society of London 74, 603–621.

Galy, A., France-Lanord, C., 1999. Weathering processes in the Ganges–Brahmaputra basin and the riverine alkalinity budget. Chemical Geology 31–60.

Galy, A., France-Lanord, C., 2001. Higher erosion rates in the Himalaya: Geochemical constraints on riverine fluxes. Geology 29, 23–26.

Galy, V., France-Lanord, C., Beyssac, O., Faure, P., Kudrass, H., Palhol, F., 2007. Efficient organic carbon burial in the Bengal fan sustained by the Himalayan erosional system. Nature 450, 407–410.

Galy, V., France-Lanord, C., Lartiges, B., 2008. Loading and fate of particulate organic carbon from the Himalaya to the Ganga–Brahmaputra delta. Geochimica et Cosmochimica Acta 72, 1767–1787.

Garçon, M., Chauvel, C., Bureau, S., 2011. Beach placer, a proxy for the average Nd and Hf isotopic composition of a continental area. Chemical Geology 287, 182–192.

Garzanti, E., Andò, S., France-Lanord, C., Censi, P., Pietro Vignola, Galy, V., Lupker, M., 2011. Mineralogical and chemical variability of fluvial sediments 2. Suspended-load silt (Ganga–Brahmaputra, Bangladesh). Earth and Planetary Science Letters 302, 107–120.

Garzanti, E., Andò, S., France-Lanord, C., Vezzoli, G., Censi, P., Galy, V., Najman, Y., 2010. Mineralogical and chemical variability of fluvial sediments 1. Bedload sand (Ganga–Brahmaputra, Bangladesh). Earth and Planetary Science Letters 299, 368–381.

Garzanti, E., Vezzoli, G., Andò, S., lavé, J., Attal, M., France-Lanord, C., Decelles, P.G., 2007. Quantifying sand provenance and erosion (Marsyandi River, Nepal Himalaya). Earth and Planetary Science Letters 258, 500–515.

Godfrey, L., Lee, D.-C., Sangrey, W., Halliday, A., Salters, V., Hein, J., White, W., 1997. The Hf isotopic composition of ferromanganese nodules and crusts and hydrothermal manganese deposits: Implications for seawater Hf. Earth and Planetary Science Letters 151, 91–105.

Goldstein, S., Jacobsen, S.B., 1988. Nd and Sr isotopic systematics of river water suspended material: implications for crustal evolution. Earth and Planetary Science Letters 87, 249–265.

Govindaraju, K., Mevelle, G., 1987. Fully automated dissolution and separation methods for inductively coupled plasma atomic emission spectrometry rock analysis. Application to the determination of rare earth elements. Plenary lecture. J. Anal. At. Spectrom. 2, 615–621.

Götze, J., Lewis, R., 1994. Distribution of REE and trace elements in size and mineral

fractions of high-purity quartz sands. Chemical Geology 114, 43–57.
Hay, W.W., 1998. Detrital sediment fluxes from continents to oceans. Chemical Geology 145, 287–323.
Islam, M.R., Begum, S.F., Yamaguchi, Y., Ogawa, K., 1999. The Ganges and Brahmaputra rivers in Bangladesh: basin denudation and sedimentation. Hydrol. Process. 13, 2907–2923.
Kinny, P.D., Maas, R., 2003. Lu–Hf and Sm–Nd isotope systems in zircon. Reviews in mineralogy and geochemistry 53, 327–341.
Komar, P.D., 2007. The Entrainment, Transport and Sorting of Heavy Minerals by Waves and Currents, in: Heavy Minerals in Use. Developments in Sedimentology, pp. 3–48.
Lisitzin, A.P., 1996. Oceanic Sedimentation: Lithology and Geochemistry. American Geophysical Union, Washington, D. C.
Lupker, M., France-Lanord, C., Galy, V., lavé, J., Gaillardet, J., Gajurel, A.P., Guilmette, C., Rahman, M., Singh, S.K., Sinha, R., 2012. Predominant floodplain over mountain weathering of Himalayan sediments (Ganga basin). Geochimica et Cosmochimica Acta 84, 410-432.
Lupker, M., France-Lanord, C., lavé, J., Bouchez, J., Galy, V., Métivier, F., Gaillardet, J., Lartiges, B., Mugnier, J.-L., 2011. A Rouse-based method to integrate the chemical composition of river sediments: Application to the Ganga basin. J. Geophys. Res. 116, F04012.
McLennan, S.M., Taylor, S.R., McCulloch, M.T., Maynard, J.B., 1990. Geochemical and Nd-Sr isotopic composition of deep-sea turbidites: Crustal evolution and plate tectonic associations. Geochimica et Cosmochimica Acta 54, 2015–2050.
Milliman, J., Meade, R.H., 1983. World-wide delivery of river sediment to the oceans. The Journal of Geology 91, 1–21.
Parrish, R.R., Hodges, V., 1996. Isotopic constraints on the age and provenance of the Lesser and Greater Himalayan sequences, Nepalese Himalaya. Geological Society of America Bulletin 108, 904–911.
Patchett, P.J., White, W.M., Feldmann, H., Kielinczuk, S., Hofmann, A.W., 1984. Hafnium/rare earth element fractionation in the sedimentary system and crustal recycling into the Earth's mantle. Earth and Planetary Science Letters 69, 365–378.
Pearce, J., Kempton, P., Nowell, G., Noble, S., 1999. Hf-Nd element and isotope perspective on the nature and provenance of mantle and subduction components in Western Pacific arc-basin systems. Journal of Petrology 40, 1579–1611.
Pierson-Wickmann, A.-C., Reisberg, L., France-Lanord, C., 2000. The Os isotopic composition of Himalayan river bedloads and bedrocks: importance of black shales. Earth and Planetary Science Letters 176, 203–218.
Plank, T., Kelley, K.A., Murray, R.W., Stern, L.Q., 2007. Chemical composition of sediments subducting at the Izu-Bonin trench. Geochem. Geophys. Geosyst. 8.
Prytulak, J., Vervoort, J.D., Plank, T., Yu, C., 2006. Astoria Fan sediments, DSDP site 174, Cascadia Basin: Hf–Nd–Pb constraints on provenance and outburst flooding. Chemical Geology 233, 276–292.
Richards, A., Argles, T., Harris, N., Parrish, R., Ahmad, T., Darbyshire, F., Draganits, E., 2005. Himalayan architecture constrained by isotopic tracers from clastic sediments. Earth and Planetary Science Letters 236, 773–796.
Robinson, D.M., Decelles, P.G., Patchett, P.J., Garzione, C.N., 2001. The kinematic

evolution of the Nepalese Himalaya interpreted from Nd isotopes. Earth and Planetary Science Letters 192, 507–521.

Rudnick, R.L., Gao, S., 2003. The Composition of the Crust, in: Rudnick, R.L. (Ed.), The Crust Vol.3 Treatise on Geochemistry. pp. 1–64.

Singh, M., Singh, I.B., Müller, G., 2007. Sediment characteristics and transportation dynamics of the Ganga River. Geomorphology 86, 144–175.

Singh, P., 2009. Major, trace and REE geochemistry of the Ganga River sediments: Influence of provenance and sedimentary processes. Chemical Geology 266, 242–255.

Singh, P., 2010. Geochemistry and provenance of stream sediments of the Ganga River and its major tributaries in the Himalayan region, India. Chemical Geology 269, 220–236.

Singh, S.K., France-Lanord, C., 2002. Tracing the distribution of erosion in the Brahmaputra watershed from isotopic compositions of stream sediments. Earth and Planetary Science Letters 202, 645–662.

Singh, S.K., Rai, S.K., Krishnaswami, S., 2008. Sr and Nd isotopes in river sediments from the Ganga Basin: Sediment provenance and spatial variability in physical erosion. J. Geophys. Res. 113, F03006.

Stummeyer, J., Marchig, V., Knabe, W., 2002. The composition of suspended matter from Ganges–Brahmaputra sediment dispersal system during low sediment transport season. Chemical Geology 185, 125–147.

Taylor, S.R., McLennan, S.M., 1995. The Geochemical evolution of the Continental Crust. Reviews of Geophysics 33, 241–265.

Totten, M., 2007. ScienceDirect.com - Developments in Sedimentology - Chapter 12 Heavy Minerals in Shales. Developments in Sedimentology.

Tripathi, J.K., Ghazanfari, P., Rajamani, V., Tandon, S., 2007. Geochemistry of sediments of the Ganges alluvial plains: Evidence of large-scale sediment recycling. Quaternary International 159, 119–130.

Van de Flierdt, T., Frank, M., Lee, D.-C., Halliday, A.N., Reynolds, B.C., Hein, J.R., 2004. New constraints on the sources and behavior of neodymium and hafnium in seawater from Pacific Ocean ferromanganese crusts. Geochimica et Cosmochimica Acta 68, 3827–3843.

Van de Flierdt, T., Goldstein, S.L., Hemming, S.R., Roy, M., Frank, M., Halliday, A.N., 2007. Global neodymium–hafnium isotope systematics—revisited. Earth and Planetary Science Letters 259, 432–441.

Van De Flierdt, T., Hemming, S.R., Goldstein, S.L., Abouchami, W., 2006. Radiogenic isotope fingerprint of Wilkes Land–Adélie Coast Bottom Water in the circum-Antarctic Ocean. Geophys. Res. Lett. 33, L12606.

Vervoort, J., Plank, T., Prytulak, J., 2011. The Hf-Nd isotopic composition of marine sediments. Geochimica et Cosmochimica Acta 75, 5903-5926.

Vervoort, J.D., Patchett, P.D., Blichert-Toft, J., Albarède, F., 1999. Relationships between Lu–Hf and Sm–Nd isotopic systems in the global sedimentary system. Earth and Planetary Science Letters 168, 79–99.

Vlastélic, I., 2005. Miocene climate change recorded in the chemical and isotopic (Pb, Nd, Hf) signature of Southern Ocean sediments. Geochem. Geophys. Geosyst. 6, Q03003.

White, W.M., Patchett, J., BenOthman, D., 1986. Hf isotope ratios of marine sediments and Mn nodules: evidence for a mantle source of Hf in seawater. Earth and Planetary Science Letters 79, 46–54.

Woodhead, J., Hergt, J., Davidson, J., Eggins, S., 2001. Hafnium isotope evidence for “conservative”element mobility during subduction zone processes. Earth and Planetary Science Letters 192, 331–346.

Supplementary Tables

SupplmentaryTable 1 : Major and Trace element concentrations measured in this study

Footnote : * Major element concentrations already published by Lupker et al. (2012)

** Major element concentrations alreary published by Galy and France-Lanord (2001)

Dup stands for complete duplicates

SupplmentaryTable 2 : Trace element concentrations in rocks standards analyzed as unknown samples

Footnote : Standard deviations (2σ) were calculated between the n measurement compositions of the rock standards analysed as unknown samples and calibrated to the BR or BR 24 standards using the reference values of Chauvel et al. (2011). Differences between the published values and our measurement compositions (Diff) are also reported.

Supplementary Table 1: Major and Trace element concentrations in sediments from rivers draining monolithologic basins

Sample Name	R 94-12	MO 102	MO 112	PB 33	PB 37	MO 207	MO 73	MO 50	MO 59	KN 83	MO 504	NAG 22	MAR-50	MAR-40
River	Tributary of the Bheri	Marsel Khola	Isul Khola	Ghara khola	Beg Khola	Andi Khola	Tributary of the Chepe	Chepe khola	Chepe khola	Tadi khola	Yamkim khola	Marsyandi	Marsyandi	Sabche khola
Sampling date	16-Mar-94	11-May-97	12-May-97	9-Jul-05	9-Jul-05	18-May-97	8-May-97	6-May-97	7-May-97	21-Mar-94		28-Nov-95	15-Nov-00	12-Nov-00
Drained lithology	Lesser Himalaya	Lesser Himalaya	Lesser Himalaya	Lesser Himalaya	Lesser Himalaya	Lesser Himalaya	High Himalayan Crystalline	High Himalayan Crystalline	High Himalayan Crystalline	High Himalayan Crystalline	Tethys Himalaya	Tethys Himalaya	Tethys Himalaya	Tethys Himalaya
Type of sediment	Bedload	Bank	Bank, gravel sample	Suspended Load	Bank	Bedload	Bank	Bank	Bank	Bedload	Suspended Load	Bedload	Bedload	Bedload
Sampling Depth (m)				0							0			
ppm														
Cs	1.97	3.75	2.73	5.37	1.53	2.86	3.18	4.16	6.21	4.24	9.58	30.5	7.72	7.52
Rb	48.8	74.9	60.6	131	29.6	53.9	19.5	56.9	99.6	101	180	144	113	118
Ba	318	269	475	438	97.0	176	181	310	524	452	553	633	351	447
Th	3.14	6.91	15.6	11.3	8.45	9.77	8.41	8.49	11.4	13.3	19.7	26.4	16.7	38.2
U	1.05	1.64	3.13	2.82	1.93	2.30	1.53	1.52	2.36	2.56	2.9	3.29	2.87	3.45
Nb	2.72	9.83	7.89	13.0	9.61	8.19	10.4	10.1	10.6	11.4	16.4	19.8	10.2	23.0
Ta	0.281	0.987	0.893	0.986	0.933	0.837	0.872	0.839	0.853	1.01	1.32	1.50	0.862	1.62
La	8.83	19.7	55.3	25.5	30.9	27.7	13.1	22.4	28.3	29.0	34.6	63.4	39.0	98.4
Ce	17.6	50.5	113	66.5	65.7	66.7	50.8	55.5	61.1	69.4	69.7	131	79.2	215
Pr	1.97	4.36	12.1	6.21	7.25	6.31	3.62	5.48	6.85	6.86	7.72	13.6	8.86	21.6
Pb	87.1	12.4	9.19	17.1	11.6	9.12	8.94	15.1	23.3	17.9	33.9	235	20.9	35.2
Nd	7.08	15.6	42.9	23.5	27.5	22.3	14.1	20.7	25.5	25.2	27.4	48.2	32.1	77.3
Sr	55.0	53.0	41.1	53.8	34.3	27.4	52.1	67.2	111	130	174	217	301	211
Sm	1.22	2.90	7.66	4.86	5.41	4.05	2.99	4.22	5.14	5.03	5.27	8.09	6.02	13.7
Zr	39.1	168	268	216	220	227	146	233	183	255	183	370	263	393
Hf	0.982	4.39	6.62	5.58	5.22	5.76	3.68	5.74	4.91	6.21	4.54	9.12	6.65	9.77
Ti	649	2088	2810	5960	6246	2279	2584	2385	2581	2588	3254	5117	2288	4862
Eu	0.223	0.431	1.28	1.06	1.15	0.653	0.581	0.856	0.948	0.966	1.00	1.42	0.971	2.19
Gd	1.04	2.21	5.84	4.29	4.42	3.10	2.71	4.22	4.70	4.39	4.71	6.15	5.12	10.1
Tb	0.145	0.313	0.865	0.667	0.658	0.472	0.446	0.824	0.888	0.694	0.733	0.889	0.764	1.48
Dy	0.928	1.74	5.42	4.22	3.92	2.92	3.02	6.61	6.28	4.52	4.49	5.28	4.45	8.25
Ho	0.181	0.333	1.10	0.872	0.751	0.614	0.683	1.55	1.45	0.963	0.911	1.01	0.888	1.60
Y	5.26	9.47	31.8	25.2	21.6	18.5	21.5	44.4	40.3	27.7	26.7	28.3	25.9	46.0
Er	0.516	0.943	3.27	2.51	2.06	1.90	2.26	4.94	4.38	2.94	2.66	2.98	2.59	4.55
Li	25.9	3.15	12.6	29.7	8.90	10.1	19.3	28.5	43.2	24.6	57.8	58.2	37.1	83.5
Yb	0.473	0.879	3.24	2.38	1.78	1.94	2.58	5.27	4.70	3.02	2.47	2.90	2.48	4.35
Lu	0.0718	0.128	0.463	0.355	0.253	0.281	0.397	0.78	0.695	0.452	0.359	0.427	0.366	0.63
Sc	2.53	3.6	8.79	17.8	10.4	4.81	3.60	8.70	11.2	7.2	13.3	13.8	7.53	14.7
V	15.4	35.1	34.6	168	65.1	30.3	114	47.4	56.7	49.1	83.7	120	40.7	77.1
Cr	14.7	43.0	25.0	111	33.5	21.9	52.2	31.2	39.1	45.3	65.0	93.9	33.5	76.3
Co	2.74	6.96	5.92	27.2	10.8	5.63	7.71	7.41	8.45	7.56	10.6	16.5	7.54	19.6
Ni	13.8	20.3	10.3	57.5	14.2	10.8	18.9	12.6	15.9	18.9	26.3	30.5	15.6	55.3
Cu	14.0	3.91	11.3	52.0	21.0	4.99	8.50	10.8	13.9	17.7	16.0	12.5	8.59	30.9
Zn	113	36.5	29.3	68.4	34.6	27.6	40.3	53.0	59.6	52.2	85.6	179	36.6	81.9
As	12.4	4.25	2.04	9.47	4.85	4.37	0.404	7.84	10.8	0.712	9.26	20.5	21.3	11.3
wt.%														
SiO2	22.24	81.82	79.89	54.44	83.90	78.27	76.81	72.56	71.52	75.02	46.94	43.33	50.97	58.44
Al2O3	2.78	8.82	6.36	18.12	5.59	6.04	10.69	11.79	13.10	11.85	15.46	15.41	9.13	15.10
Fe2O3	1.02	2.98	3.88	9.81	4.06	2.66	4.27	6.04	5.36	3.76	5.14	5.60	2.95	6.13
MnO	0.03	0.00	0.08	0.09	0.13	0.06	0.08	0.27	0.19	0.07	0.05	0.04	0.03	0.04
MgO	15.31	1.25	1.74	4.66	1.25	2.46	1.34	1.01	1.48	1.05	2.66	2.10	1.58	0.61
CaO	21.69	0.02	2.41	1.74	1.03	2.49	1.50	1.18	1.35	1.39	11.19	13.07	17.24	6.24
Na2O	0.04	0.82	0.68	1.25	1.13	0.16	1.20	1.51	1.87	1.57	0.55	0.51	1.46	0.85
K2O	1.33	1.96	1.40	3.46	0.64	2.19	1.93	1.73	2.37	2.50	4.22	3.72	2.31	2.79
TiO2	0.09	0.33	0.50	1.06	1.03	0.39	0.47	0.42	0.47	0.45	0.56	0.80	0.38	0.73
P2O5	0.10	0.08	0.11	0.15	0.10	0.13	0.12	0.11	0.16	0.08	0.20	0.16	0.06	0.17
LOI	35.10	1.80	2.80	5.65	1.30	5.15	1.53	1.55	2.08	1.26	12.74	14.95	13.42	9.02
Total	99.78	99.89	99.85	100.42	100.16	100.00	99.94	98.17	99.95	98.99	99.71	99.69	99.53	100.12

Supplementary Table 1: Major and Trace element concentrations in sediments from the Ganga and its major tributaries and the Marsyandi River

Sample Name	BR 931	BR 932	BR 922*	BR 924*	BR 943*	BR 946*	BR 946 Dup	BGP 6**	BGP 6 Dup	BR 415*	BR 414*	BR 413*	BR 412*	BR 411*	BR 418*
Locality	Devrapayag, India	Devrapayag, India	Rishikesh, India	Rishikesh, India	Kanpur, India	Kanpur, India	Kanpur, India	Rajshahi, India	Rajshahi, India	Harding bridge, Bangladesh	Harding bridge, Bangladesh	Harding bridge, Bangladesh	Harding bridge, Bangladesh	Harding bridge, Bangladesh	Harding bridge, Bangladesh
Latitude			30.12661	30.12661	26.61306	26.61306	26.61306	24.35833	24.35833	24.05290	24.05290	24.05290	24.05290	24.05290	24.05290
Longitude			78.33044	78.33044	80.27576	80.27576	80.27576	88.60833	88.60833	89.02465	89.02465	89.02465	89.02465	89.02465	89.02465
River	Ganga	Ganga	Ganga	Ganga	Ganga	Ganga	Ganga	Ganga	Ganga	Ganga	Ganga	Ganga	Ganga	Ganga	Ganga
Sampling date	12-Aug-09	12-Aug-09	11-Aug-09	11-Aug-09	18-Aug-09	18-Aug-09	18-Aug-09	2-Aug-93	2-Aug-93	13-Jul-04	13-Jul-04	13-Jul-04	13-Jul-04	13-Jul-04	13-Jul-04
Type of sediment	Suspended Load	Suspended Load	Suspended Load	Bank	Suspended Load	Bedload	Bedload	Bedload	Bedload	Suspended Load	Suspended Load	Suspended Load	Suspended Load	Suspended Load	Bedload
Sampling Depth (m)	0	0	0.2		1.7					0	2	4	6.5	9	10
Cs	16.4	8.00	14.6	8.47	10.8	5.61	4.44	3.83	4.02	15.4	13.6	11.8	11.7	8.08	2.64
Rb	185	115	170	128	125	136	68.4	77.9	85.2	202	186	174	175	107	56.6
Ba	469	344	436	368	391	328	221	294	307	627	562	531	527	372	212
Th	16.1	20.7	16.3	14.4	12.6	35.4	26.3	30.2	31.3	20.0	19.0	19.3	18.0	15.1	29.7
U	6.24	5.75	4.93	3.83	2.89	7.64	4.76	5.41	5.71	4.64	4.08	4.15	3.96	2.92	5.14
Nb	13.6	11.0	13.6	11.0	12.6	13.9	15.5	12.9	12.0	17.4	17.9	16.5	15.7	13.6	18.4
Ta	1.58	1.13	1.60	1.24	1.30	1.65	1.83	1.78	1.44	1.54	1.57	1.45	1.39	1.37	2.08
La	31.6	44.6	32.5	29.2	26.6	91.1	58.4	67.1	70.2	42.0	41.3	42.2	40.0	32.8	71.0
Ce	66.1	90.1	69.9	61.4	58.5	170	128	144	145	89.4	88.1	89.2	84.7	76.3	146
Pr	7.56	10.3	7.65	6.75	6.28	21.2	13.5	15.5	16.4	9.75	9.77	9.87	9.29	7.84	16.7
Pb	29.2	21.0	29.1	21.4	23.5	18.9	15.8	17.8	17.6	30.4	26.2	25.3	25.3	17.4	15.0
Nd	27.7	37.2	28.0	25.0	23.5	76.6	48.3	56.5	60.8	35.0	35.7	35.8	34.0	29.0	60.4
Sr	88.8	90.9	86.5	97.4	71.5	107	69.0	115	117	84.1	91.0	99.3	101	88.6	103
Sm	5.81	7.18	5.77	4.87	4.74	15.1	9.45	10.9	11.4	6.93	6.98	7.01	6.77	5.60	12.0
Zr	205	290	150	202	163	388	417	683	667	178	204	227	199	249	479
Hf	5.59	8.23	3.96	5.20	4.07	10.3	10.6	17.1	17.4	4.73	5.22	5.79	5.17	6.14	12.1
Ti	2750	2619	2836	2510	2841	3407	3675	3155	3166	4137	4198	3976	3833	3314	4355
Eu	0.916	0.972	0.942	0.813	0.891	1.94	1.16	1.39	1.45	1.27	1.26	1.23	1.20	1.04	1.48
Gd	5.22	5.87	5.14	4.16	4.26	12.1	8.19	8.51	9.10	6.19	6.15	6.05	5.80	4.96	10.1
Tb	0.868	0.888	0.789	0.653	0.678	1.98	1.39	1.25	1.29	0.984	0.945	0.93	0.872	0.782	1.64
Dy	5.44	5.06	4.73	3.96	4.25	12.0	9.20	7.24	7.61	5.97	5.74	5.72	5.42	4.81	10.3
Ho	1.10	1.00	0.926	0.784	0.846	2.42	1.94	1.39	1.48	1.17	1.15	1.13	1.06	0.95	2.12
Y	32.5	29.1	26.8	23.0	24.9	72.5	58.8	41.1	43.5	32.7	32.8	32.5	30.9	27.1	62.0
Er	3.16	2.90	2.62	2.25	2.47	7.05	5.88	3.99	4.24	3.33	3.30	3.21	3.07	2.65	6.35
Li	62.9	31.5	56.5	35.2	43.8	29.6	18.4	14.7	16.3	51.8	48.2	43.5	41.9	32.2	15.8
Yb	3.03	2.83	2.47	2.15	2.38	6.83	5.92	3.87	4.16	3.18	3.11	3.06	2.88	2.51	6.23
Lu	0.449	0.428	0.344	0.315	0.339	0.993	0.869	0.587	0.614	0.461	0.45	0.448	0.417	0.366	0.905
Sc	10.1	8.72	7.93	7.61	9.55	12.3	6.65	7.74	9.81	15.0	14.4	13.5	12.8	9.04	13.2
V	56.4	43.4	58.3	44.5	62.1	36.8	37.0	32.7	34.8	93.4	90.7	81.1	79.1	61.8	46.9
Cr	43.3	32.4	38.3	34.2	53.3	27.1	29.5	36.9	38.4	76.6	81.9	67.0	63.4	53.4	40.0
Co	9.52	7.66	10.0	6.87	10.6	5.01	4.94	3.93	4.32	15.5	15.1	13.6	13.4	10.3	5.58
Ni	22.5	14.7	22.5	16.3	29.5	7.70	9.82	11.0	11.3	38.6	40.5	32.4	31.5	26.4	11.7
Cu	19.7	14.4	33.6	17.2	25.3	2.86	6.15	10.9	11.3	33.9	31.7	25.7	23.7	24.3	10.0
Zn	56.4	41.9	70.7	46.0	68.9	31.1	39.8	29.1	28.1	84.9	83.5	73.3	72.1	56.6	38.8
As	15.8	9.01	13.5	7.43	11.9	3.00	3.22	2.32	5.03	9.17	7.33	5.52	5.70	5.41	1.79
wt.%															
SiO2	65.51	73.12	57.94	70.03	69.75	80.14		78.45		57.76	60.42	63.07	63.44	68.36	75.40
Al2O3	12.28	9.37	12.26	9.95	12.09	8.32		7.86		18.57	17.04	15.64	15.06	12.27	8.58
Fe2O3	4.01	3.19	4.40	3.15	4.51	3.59		2.46		6.61	6.31	5.75	5.55	4.20	5.19
MnO	0.07	0.06	0.07	0.05	0.07	0.15		0.05		0.08	0.08	0.07	0.07	0.06	0.19
MgO	2.99	2.24	4.98	2.64	2.09	1.01		0.91		2.39	2.34	2.20	2.07	1.71	1.47
CaO	4.12	3.54	6.11	3.94	1.78	1.80		3.28		1.79	2.36	2.73	2.67	2.77	4.15
Na2O	1.75	1.56	1.46	1.60	1.23	1.41		1.48		1.03	1.13	1.19	1.22	1.37	1.18
K2O	3.25	2.27	3.20	2.57	2.82	1.51		1.83		3.77	3.52	3.28	3.20	2.82	1.26
TiO2	0.48	0.44	0.50	0.42	0.50	0.63		0.57		0.75	0.76	0.72	0.70	0.58	0.91
P2O5	0.13	0.12	0.14	0.11	0.14	0.23		0.12		0.16	0.15	0.15	0.14	0.12	0.27
LOI	6.35	4.60		4.96		1.38		2.57		7.19	6.51	6.07	6.13	4.66	2.15
Total	100.94	100.51	91.06	99.42	94.96	100.16		99.57		100.09	100.62	100.87	100.23	98.89	100.73

Sample Name	BR 8252*	BR 8253*	BR 717*	PB 79*	PB 80*	PB 80 Dup	BR 8113*	BR 8113 Dup	BR 8115*	LO 762*	LO 763*	LO 763 Dup	PB 69*	PB 70*
Locality	Harding bridge, Bangladesh	Harding bridge, Bangladesh	Harding bridge, Bangladesh	Chisapani, Nepal	Chisapani, Nepal	Chisapani, Nepal	Revelganj, India	Revelganj, India	Revelganj, India	Chatara, Nepal	Chatara, Nepal	Chatara, Nepal	Chatara, Nepal	Chatara, Nepal
Latitude	24.05290	24.05290	24.05290	28.63895	28.63895	28.63895	25.77950	25.77950	25.77950	26.84815	26.84815	26.84815	26.84815	26.84815
Longitude	89.02465	89.02465	89.02465	81.28278	81.28278	81.28278	84.63070	84.63070	84.63070	87.15137	87.15137	87.15137	87.15137	87.15137
River	Ganga	Ganga	Ganga	Karnali	Karnali	Karnali	Karnali	Karnali	Karnali	Kosi	Kosi	Kosi	Kosi	Kosi
Sampling date	10-Sep-08	10-Sep-08	17-Aug-07	15-Jul-05	15-Jul-05	15-Jul-05	18-Aug-08	18-Aug-08	18-Aug-08	16-Aug-07	16-Aug-07	16-Aug-07	13-Jul-05	13-Jul-05
Type of sediment	Bedload	Suspended Load	Bedload	Suspended Load	Bank	Bank	Suspended Load	Suspended Load	Bedload	Suspended Load	Bank	Bank	Suspended Load	Bank
Sampling Depth (m)	14	0	11	0			0	0	5.4	0			0	
Cs	3.05	8.92	3.87	8.20	3.50	3.56	11.5	11.7	4.31	11.6	5.26	5.84	13.8	4.77
Rb	34.5	51.7	50.3	141	70.7	71.2	173	176	101	107	77.2	106	177	91.8
Ba	203	240	244	482	255	262	574	586	305	357	290	341	637	294
Th	24.3	16.1	74.2	19.0	12.0	12.3	18.5	18.4	8.06	19.5	12.1	11.8	21.0	14.7
U	3.33	1.85	11.7	3.33	2.92	3.07	3.42	3.47	1.72	4.23	2.15	3.08	4.06	2.75
Nb	13.6	15.8	20.3	16.9	9.79	9.79	15.2	15.2	5.94	17.9	9.23	9.48	18.9	9.21
Ta	2.91	1.31	2.50	1.57	1.04	1.01	1.28	1.27	0.554	1.63	0.878	0.902	1.73	1.08
La	41.6	30.8	141	39.8	27.9	27.9	39.9	40.5	21.5	40.9	28.3	22.3	48.0	32.4
Ce	110	75.4	292	82.0	59.7	59.2	86.0	86.3	36.5	101	61.7	68.5	109	71.1
Pr	10.6	8.12	33.1	8.78	6.52	6.55	9.43	9.53	4.55	9.92	6.70	4.86	11.2	7.59
Pb	10.7	10.5	14.2	12.7	13.9	14.0	30.3	30.5	16.0	17.8	17.6	19.1	17.3	15.3
Nd	39.4	31.2	121	31.6	23.7	23.9	34.7	34.7	16.8	36.4	24.3	17.7	40.0	27.8
Sr	83.6	56.5	98.3	96.3	93.8	94.5	93.5	93.8	86.3	82.2	74.2	88.7	61.9	92.6
Sm	7.63	6.27	22.3	5.69	4.55	4.70	6.72	6.65	3.07	7.25	4.80	3.28	7.60	5.43
Zr	403	196	1550	259	285	337	186	195	112	286	203	206	171	159
Hf	10.5	5.13	40.5	6.43	7.03	8.49	4.81	5.07	3.20	7.79	5.17	5.30	4.62	3.96
Ti	2523	4323	5299	3606	2395	2485	3763	3708	1382	4017	2013	1961	3979	1903
Eu	0.928	1.19	2.24	0.927	0.74	0.817	1.23	1.23	0.576	1.17	0.872	0.601	1.24	0.871
Gd	6.41	5.44	17.7	4.37	3.90	4.38	5.78	5.85	2.70	6.15	4.21	2.88	6.03	4.59
Tb	0.977	0.854	2.52	0.644	0.603	0.746	0.88	0.891	0.376	0.92	0.658	0.447	0.875	0.724
Dy	5.70	5.32	14.7	3.90	3.84	5.02	5.33	5.43	2.40	5.45	4.03	2.76	5.00	4.54
Ho	1.16	1.06	2.83	0.787	0.776	1.02	1.05	1.07	0.468	1.06	0.79	0.571	0.969	0.922
Y	34.5	31.1	85.6	23.0	22.6	30.5	30.3	30.3	13.7	30.8	23.2	18.2	27.2	27.2
Er	3.33	3.04	8.11	2.26	2.24	2.97	2.99	3.03	1.32	3.02	2.29	1.73	2.73	2.76
Li	12.6	45.3	15.7	28.1	16.9	17.0	46.5	46.7	17.0	47.9	17.2	1.23	44.0	17.6
Yb	3.32	2.95	8.17	2.18	2.28	2.79	2.85	2.89	1.27	2.94	2.18	1.67	2.60	2.65
Lu	0.50	0.433	1.25	0.312	0.333	0.416	0.413	0.413	0.179	0.426	0.305	0.25	0.374	0.386
Sc	4.56	11.8	14.3	10.7	6.63	6.95	12.1	13.0	6.08	8.04	4.90	3.49	11.3	5.51
V	34.5	100	53.5	60.6	33.0	32.4	87.1	86.7	24.8	73.2	33.7	33.7	83.9	29.2
Cr	28.2	73.6	44.1	47.2	23.2	22.3	59.3	61.9	18.6	52.1	29.9	29.1	65.2	24.8
Co	4.46	13.8	6.40	4.77	5.15	4.89	13.2	13.8	4.25	13.2	6.20	6.10	13.3	5.82
Ni	9.39	39.4	12.4	12.4	11.0	11.0	30.5	31.0	9.55	28.6	40.4	16.3	32.2	11.9
Cu	7.82	39.4	7.10	6.19	7.33	7.38	26.8	27.1	2.72	26.4	50.2	13.2	20.2	9.31
Zn	24.2	70.4	31.0	30.2	29.2	29.1	71.9	78.6	20.5	83.2	52.8	38.5	59.6	32.7
As	2.21	14.6	2.63	6.24	3.80	3.85	11.4	11.5	3.24	9.01	0.434	0.651	6.17	3.07
wt.%														
SiO2	80.96	56.94	75.03	59.03	77.77		56.24		79.56	64.64	77.58		57.44	79.11
Al2O3	7.68	15.64	8.31	10.57	6.50		14.83		7.03	14.86	9.87		17.54	9.13
Fe2O3	2.57	6.31	4.53	3.94	2.57		5.75		1.72	5.34	2.92		6.00	2.96
MnO	0.06	0.09	0.13	0.06	0.05		0.08		0.03	0.07	0.04		0.07	0.06
MgO	0.90	2.74	1.17	3.46	1.42		3.26		1.17	2.15	1.20		3.78	1.26
CaO	2.50	4.25	3.29	8.69	4.56		4.80		3.41	1.88	1.58		2.24	1.82
Na2O	1.41	0.97	1.29	1.15	0.92		0.87		1.22	1.78	1.72		1.59	1.60
K2O	1.74	3.28	1.72	2.75	1.56		3.50		1.87	3.61	2.35		4.52	1.95
TiO2	0.47	0.75	0.90	0.51	0.45		0.65		0.24	0.68	0.38		0.73	0.34
P2O5	0.10	0.14	0.19	0.12	0.10		0.13		0.06	0.17	0.11		0.15	0.13
LOI	2.19	8.93	2.65	10.51	4.58		9.56		3.79	3.80	1.95		5.83	1.70
Total	100.58	100.04	99.18	100.79	100.49		99.67		100.08	98.98	99.68		99.91	100.05

Sample Name	BR 331*	BR 332*	LO 757*	LO 756*	LO 754*	LO 755*	LO 755 Dup	LO 758 C*	PB 54*	LO 1002	LO 1007
Locality	Dumarighat, India	Dumarighat, India	Narayanghat, Nepal	Narayanghat, Nepal	Narayanghat, Nepal	Narayanghat, Nepal	Narayanghat, Nepal	Narayanghat, Nepal	Narayanghat, Nepal	Narayanghat, Nepal	Narayanghat, Nepal
Latitude	25.54113	25.54113	27.70297	27.70297	27.70297	27.70297	27.70297	27.70297	27.70297		
Longitude	86.72231	86.72231	84.42661	84.42661	84.42661	84.42661	84.42661	84.42661	84.42661		
River	Kosi	Kosi	Narayani	Narayani	Narayani	Narayani	Narayani	Narayani	Narayani	Narayani	Narayani
Sampling date	10-May-04	10-May-04	12-Aug-07	12-Aug-07	12-Aug-07	12-Aug-07	12-Aug-07	12-Aug-07	11-Jul-05	16-Jul-10	16-Jul-10
Type of sediment	Bank	Bank	Suspended Load	Suspended Load	Suspended Load	Suspended Load	Suspended Load	Suspended Load	Suspended Load	Suspended Load	Suspended Load
Sampling Depth (m)			0	3.3	6	8	8	8.5	8	0	0
Cs	11.1	8.43	10.9	10.6	10.3	10.6	10.8	5.02	8.5	12.7	3.43
Rb	107	101	146	142	141	142	148	85.3	123	170	70.4
Ba	362	334	460	454	437	441	457	290	437	510	307
Th	19.4	13.6	14.8	15.2	15.8	15.5	14.9	7.87	11.7	14.4	13.4
U	3.79	2.60	3.18	4.26	3.33	3.26	3.24	2.02	2.69	3.38	3.33
Nb	19.4	13.5	13.6	13.1	12.4	12.6	13.2	6.79	10.7	13.2	14.5
Ta	1.75	1.33	1.25	1.33	1.24	1.23	1.30	0.581	1.01	1.18	1.06
La	40.9	29.7	32.8	35.8	36.9	35.4	33.2	22.2	28.9	32.1	37.5
Ce	97.8	73.5	68.7	73.9	77.1	73.7	69.1	45.8	60.2	66.2	79.9
Pr	10.0	7.14	7.43	8.07	8.48	8.06	7.57	4.95	6.7	7.43	8.82
Pb	15.7	17.2	24.8	72.0	23.6	24.1	25.0	15.5	19.3	27.4	13.6
Nd	36.9	26.7	26.9	29.6	30.9	29.7	27.3	17.8	24.2	27.3	32.9
Sr	60.1	67.2	234	213	197	194	200	112	177	269	68.9
Sm	7.43	5.30	5.26	5.74	6.03	5.82	5.41	3.41	4.70	5.22	6.22
Zr	281	202	217	220	213	200	236	113	188	187	209
Hf	7.57	5.30	5.54	5.63	6.34	5.18	5.88	2.98	4.83	4.85	5.30
Ti	4248	2884	3021	2916	2710	2777	2840	1519	2568	3291	2542
Eu	1.24	0.903	0.984	0.973	1.03	0.997	0.986	0.64	0.894	0.97	1.09
Gd	6.39	4.59	4.52	4.94	5.05	4.81	4.68	2.86	4.10	4.34	5.00
Tb	0.974	0.714	0.712	0.706	0.74	0.734	0.728	0.423	0.627	0.686	0.774
Dy	5.93	4.11	4.20	4.40	4.29	4.44	4.53	2.57	3.87	4.15	4.61
Ho	1.18	0.815	0.838	0.843	0.815	0.875	0.913	0.532	0.786	0.819	0.968
Y	34.9	24.0	25.1	24.0	24.1	25.1	26.9	15.7	22.6	24.0	28.2
Er	3.45	2.31	2.47	2.43	2.29	2.52	2.65	1.61	2.25	2.42	2.83
Li	40.3	27.1	45.9	43.9	41.2	43.7	46.7	22.3	32.1	51.6	14.8
Yb	3.27	2.26	2.36	2.38	2.18	2.34	2.53	1.56	2.17	2.27	2.79
Lu	0.476	0.326	0.343	0.35	0.323	0.344	0.371	0.226	0.307	0.334	0.402
Sc	9.96	5.14	9.72	9.31	8.90	9.24	9.38	5.78	8.52	10.5	5.00
V	78.0	51.8	57.8	55.0	52.0	53.3	54.9	36.1	51.9	69.4	46.6
Cr	61.7	37.0	48.0	44.6	41.9	44.0	45.6	38.3	38.8	58.9	32.0
Co	13.9	9.26	9.07	8.94	8.28	8.37	8.55	4.54	7.64	11.2	7.43
Ni	36.3	20.9	21.5	20.0	18.9	20.1	20.7	18.7	16.7	28.7	17.8
Cu	37.6	34.0	17.6	14.7	16.2	14.9	16.5	11.9	10.1	25.8	25.0
Zn	77.9	56.5	68.2	64.9	60.8	63.4	65.0	37.8	49.7	80.8	42.8
As	11.3	4.04	11.0	11.9	9.86	9.82	9.57	1.68	5.12	14.4	2.84
wt.%											
SiO2	61.28	72.72	53.31	56.78	59.47	57.77		69.39	62.71	53.70	75.74
Al2O3	16.30	12.31	11.17	11.34	10.97	11.17		8.44	10.20	12.22	8.21
Fe2O3	5.96	4.11	3.79	3.82	3.60	3.66		2.55	3.63	4.60	3.62
MnO	0.08	0.06	0.05	0.05	0.05	0.05		0.05	0.06	0.06	0.08
MgO	2.46	1.36	2.19	2.07	2.00	2.05		2.49	2.31	2.50	2.23
CaO	2.29	1.39	11.86	10.91	9.38	9.70		5.90	8.83	12.36	2.92
Na2O	1.31	1.58	1.36	1.38	1.47	1.45		1.36	1.45	1.34	1.33
K2O	3.96	2.95	2.78	2.84	2.72	2.78		1.97	2.61	3.19	1.54
TiO2	0.74	0.49	0.49	0.49	0.46	0.47		0.28	0.45	0.57	0.44
P2O5	0.16	0.13	0.11	0.11	0.11	0.11		0.07	0.11	0.13	0.14
LOI	4.93	2.55	11.64	10.10	8.93	9.40		6.40	8.19		3.73
Total	99.46	99.63	98.74	99.89	99.16	98.60		98.91	100.55	90.65	99.97

Sample Name	LO 1007 Dup	BR 8106*	BR 8107*	MAR-55	MAR-58	MAR-70	MAR-31	MAR-29	MAR-19	MAR-12	MAR-10	MAR-10 Dup
Locality	Narayanghat, Nepal	Hajipur, India	Hajipur, India	Tal, Nepal	Chamje, Nepal	Besi Sahar, Nepal	Philesangu, Nepal	Suribar, Nepal	Turture, Nepal	Anpu, Nepal	Lobrang, Nepal	Lobrang, Nepal
Latitude		25.67933	25.67933									
Longitude		85.19362	85.19362									
River	Narayani	Narayani	Narayani	Marsyandi	Marsyandi	Marsyandi	Marsyandi	Marsyandi	Marsyandi	Marsyandi	Marsyandi	Marsyandi
Sampling date	16-Jul-10	17-Aug-08	17-Aug-08	16-Nov-00	16-Nov-00	18-Nov-00	6-Nov-00	6-Nov-00	4-Nov-00	3-Nov-00	3-Nov-00	3-Nov-00
Type of sediment	Suspended Load	Suspended Load	Bedload	Bedload	Bedload	Bedload	Bedload	Bedload	Bedload	Bedload	Bedload	Bedload
Sampling Depth (m)	0	0										
Cs	3.14	11.1	7.48	17.5	14.4	6.32	5.80	7.30	6.07	8.10	6.85	7.27
Rb	62.0	141	111	194	166	94.6	78	104	84.2	148	106	119
Ba	280	497	390	420	283	328	284	331	279	350	333	366
Th	12.3	17.2	13.6	16.0	16.3	46.3	26.8	8.24	21.0	11.5	10.2	10.7
U	2.96	3.20	2.39	8.37	5.68	8.87	5.58	5.64	5.12	2.87	2.06	2.29
Nb	12.9	15.2	9.14	8.99	12.8	26.5	11.5	9.84	11.7	8.02	8.17	8.85
Ta	0.922	1.28	0.844	0.986	1.79	3.6	1.17	0.865	1.61	0.932	0.738	0.793
La	34.0	38.3	30.9	37.5	38.1	97.1	68.2	22.2	50.7	25.0	27.4	31.8
Ce	72.8	81.8	68.6	60.6	79.0	201	134	44.8	104	49.4	47.6	53.3
Pr	7.99	8.9	7.11	8.85	8.99	22.9	15.4	5.10	11.6	5.41	5.78	6.53
Pb	12.2	26.7	20.9	29.5	28.4	20.4	17.7	17.1	17.8	23.6	18.1	18.9
Nd	29.5	32.4	25.5	32.7	33.4	84.5	56.5	18.8	43.6	20.3	20.9	23.4
Sr	63.0	159	128	276	220	120	146	135	133	155	146	151
Sm	5.45	6.21	4.82	7.63	7.11	16.7	10.9	3.75	8.60	5.04	4.00	4.22
Zr	190	190	189	137	160	154	196	123	159	141	109	56.0
Hf	4.74	5.00	4.78	3.73	4.41	4.33	5.13	3.32	4.41	3.69	2.95	1.62
Ti	2272	3532	2085	1536	1948	4254	2472	2178	2494	1624	1765	1766
Eu	0.98	1.16	0.825	1.48	1.04	2.25	1.61	0.771	1.27	0.817	0.814	0.857
Gd	4.45	5.34	3.93	8.11	6.04	14.1	8.99	3.59	7.34	6.49	3.57	3.84
Tb	0.675	0.825	0.579	1.57	0.981	2.28	1.31	0.614	1.23	1.68	0.619	0.61
Dy	4.23	4.88	3.19	10.9	5.41	15.0	7.95	4.63	8.10	16.8	4.33	4.13
Ho	0.853	0.966	0.605	2.52	1.01	3.13	1.56	1.03	1.79	4.78	0.907	0.889
Y	25.3	28.0	17.5	77.2	28.3	91.6	44.8	29.5	50.9	137	25.5	25.1
Er	2.56	2.76	1.71	7.94	2.65	9.43	4.64	3.21	5.49	18.2	2.75	2.66
Li	13.4	45.3	25.1	72.3	52.5	27.0	24.0	30.8	24.6	28.9	27.8	27.4
Yb	2.50	2.63	1.64	7.58	2.40	9.16	4.54	3.31	5.61	20.2	2.67	2.62
Lu	0.363	0.381	0.239	1.09	0.336	1.29	0.671	0.481	0.812	2.68	0.382	0.38
Sc	5.26	10.6	6.21	7.84	5.99	15.3	13.4	10.2	11.4	9.45	13.8	10.4
V	41.9	79.9	44.6	26.8	29.5	66.7	43.6	49.1	45.0	34.6	38.4	37.4
Cr	28.7	59.5	41.0	35.1	25.2	53.7	41.6	39.7	36.6	30.6	39.0	34.7
Co	6.54	13.4	8.39	4.40	6.22	14.9	9.08	8.44	10.6	5.40	5.93	5.56
Ni	17.3	32.6	22.4	9.98	12.5	24.1	16.5	17.0	15.7	11.3	11.8	11.5
Cu	22.2	112	12.0	5.83	8.38	23.4	11.7	10.9	14.0	6.42	7.37	8.09
Zn	38.2	128	44.4	36.3	41.4	45.7	42.0	46.2	40.2	32.6	38.7	37.4
As	2.52	12.3	2.75	8.92	23.5	52.6	10.2	3.90	14.2	5.55	3.34	3.17
wt.%												
SiO2	53.31	71.09	60.58	61.26	64.74	69.63	70.04	71.31	71.18	71.15		
Al2O3	14.51	10.07	11.20	10.64	11.77	10.22	10.42	10.30	9.93	9.60		
Fe2O3	5.32	3.22	2.11	2.74	7.68	4.17	4.13	4.81	2.85	2.91		
MnO	0.07	0.05		0.03	0.21	0.11	0.09	0.14	0.05	0.05		
MgO	2.86	1.54	1.17	1.39	2.12	1.71	1.88	1.61	1.19	1.49		
CaO	8.13	4.25	10.68	11.14	5.55	6.51	5.36	5.26	5.86	6.04		
Na2O	1.23	1.57	2.35	2.36	1.47	1.66	1.62	1.68	1.81	1.64		
K2O	3.57	2.55	3.13	2.74	1.98	1.58	2.03	1.64	2.01	1.87		
TiO2	0.61	0.38	0.26	0.34	0.73	0.45	0.36	0.45	0.29	0.29		
P2O5	0.14	0.07	0.11	0.15	0.22	0.18	0.11	0.16	0.11	0.14		
LOI	10.28	4.19	8.23	7.04	3.37	3.81	3.78	3.10	4.53	4.63		
Total	100.03	98.98	99.82	99.83	99.84	100.03	99.82	100.46	99.81	99.81		

Supplementary Table 1 (end)

Supplementary Table 2: Trace-element concentrations in rock standards analyzed as unknown samples (ppm)

	BR ref	BR 24 ref	AGV-1		AGV-1		BEN		BEN		JSd-2		JSd-2	
	Chauvel et al. (2011)	*Chauvel et al. (2011)*	n=2	2σ (%)	*Chauvel et al. (2011)*	Diff (%)	n=10	2σ (%)	*Chauvel et al. (2011)*	Diff (%)	n=28	2σ (%)	*Chauvel et al. (2011)*	Diff (%)
Li	15.1	7.15	10.8	9.7	10.9	1.1	13.2	4.1	13.0	-1.2	22.8	5.4	22.1	-3.1
Sc	22.8	25.9	12.2	11.1	12.8	4.5	23.0	6.8	22.5	-2.3	17.8	6.2	17.9	0.8
Ti	15300	17500	5955	5.7	6080	2.0	15492	5.2	15400	-0.6	3569	4.0	3570	0.0
V	226	267	115	1.9	117	1.8	229	5.3	226	-1.4	125	4.4	126	0.9
Cr	338	425	7.91	4.5	8.05	1.7	346	5.7	340	-1.6	104	6.5	106	2.0
Co	56.6	52.6	14.9	0.9	15.3	2.3	61.0	5.7	60.0	-1.6	47.6	5.1	47.5	-0.2
Ni	259	238	14.6	2.8	14.5	-0.7	265	6.4	258	-2.8	91.7	6.2	91.1	-0.7
Cu	68.8	37.0	57.1	5.4	57.2	0.2	68.8	8.9	69.3	0.7	1040	9.0	1060	1.9
Zn	158	109	77.4	6.2	91.7	15.6	122	4.8	119	-2.6	1996	17.3	1980	-0.8
As	2.22		1.03	11.6	0.98	-5.1	2.23	37.6	1.80	-24.1	38.3	45.4	37.8	-1.4
Rb	46.6	80.0	68.0	9.5	66.8	-1.8	47.5	6.1	46.8	-1.6	26.3	8.2	25.8	-2.0
Sr	1340	607	662	1.9	657	-0.8	1381	3.5	1380	-0.1	213	7.6	210	-1.4
Y	28.9	28.5	19.4	1.4	19.5	0.6	29.3	4.4	29.0	-1.2	18.4	2.7	18.2	-1.3
Zr	273	294	237	1.0	237	0.2	278	4.4	274	-1.5	108	7.9	103	-4.7
Nb	115	38.1	14.5	0.2	13.9	-4.6	116	5.0	116	-0.2	4.39	8.3	4.19	-4.8
Cs	0.82	0.648	1.29	2.3	1.29	0.3	0.754	6.0	0.752	-0.2	1.07	3.9	1.05	-2.0
Ba	1090	390	1217	2.7	1230	1.0	1055	2.6	1050	-0.5	1264	4.4	1230	-2.7
La	82.6	33.6	38.3	0.5	38.0	-0.9	83.4	2.1	83.0	-0.5	11.3	4.0	10.8	-4.3
Ce	155	73.9	69.7	1.5	69.0	-1.0	157	2.8	155	-1.2	23.5	7.6	22.1	-6.5
Pr	17.4	9.61	8.39	0.5	8.47	0.9	17.6	3.4	17.4	-1.4	3.03	3.6	2.94	-3.0
Nd	66.4	39.9	31.7	0.5	31.8	0.2	67.2	3.1	67.0	-0.3	12.5	3.5	12.1	-3.3
Sm	12.2	8.36	5.75	4.7	5.77	0.3	12.3	3.5	12.2	-0.8	2.95	3.8	2.86	-3.2
Eu	3.66	2.53	1.61	4.2	1.61	0.3	3.67	3.0	3.67	0.0	0.853	5.8	0.872	2.2
Gd	9.88	7.28	4.68	0.0	4.69	0.1	9.83	2.5	9.87	0.5	3.04	3.7	2.85	-6.5
Tb	1.25	1.03	0.611	0.9	0.632	3.4	1.26	3.0	1.26	0.2	0.479	3.6	0.465	-3.0
Dy	6.42	5.77	3.57	5.1	3.55	-0.7	6.52	2.3	6.44	-1.2	3.10	3.3	3.04	-1.8
Ho	1.08	1.05	0.674	2.0	0.675	0.1	1.09	3.2	1.08	-1.1	0.651	2.5	0.641	-1.5
Er	2.58	2.70	1.85	5.6	1.84	-0.5	2.60	4.3	2.59	-0.4	1.95	2.7	1.91	-1.9
Yb	1.84	2.13	1.66	6.6	1.65	-0.8	1.86	3.8	1.84	-1.2	1.94	3.3	1.91	-1.8
Lu	0.246	0.297	0.247	4.6	0.241	-2.6	0.248	5.9	0.245	-1.3	0.293	4.8	0.288	-1.8
Hf	5.67	6.75	5.09	1.1	5.05	-0.8	5.72	3.2	5.64	-1.5	2.72	8.8	2.74	0.7
Ta	5.55	2.34	0.809	1.9	0.825	2.0	5.83	12.7	5.57	-4.6	0.369	17.7	0.345	-7.0
Pb	4.77	3.69	35.2	0.8	35.9	1.9	4.22	8.7	4.17	-1.2	160	7.2	154	-4.2
Th	10.7	4.75	6.37	2.8	6.35	-0.3	10.8	3.0	10.7	-0.9	2.62	3.3	2.43	-8.0
U	2.39	1.20	1.80	4.0	1.83	1.5	2.42	5.1	2.39	-1.1	1.13	10.2	1.09	-4.0

III.2. Systématiques isotopiques du Pb

Les résultats et interprétations faites dans le manuscrit précédent suggèrent l'existence d'une forte variabilité isotopique en Hf entre les sédiments de fond de rivière et ceux transportés en suspension. Qu'en est-il pour les compositions isotopiques en Pb ? Ce manuscrit se propose d'étudier les isotopes du Pb dans les sédiments de rivère et dans différentes fractions minérales et granulométriques afin de comprendre les systématiques de ce système isotopique.

Les compositions isotopiques en Pb des sédiments de rivière du Ganges et de ses affluents drainant la chaîne Himalayenne sont extrêment variables et présentent des caractéristiques remarquables. Elles sont alignées le long d'une tendance linéaire dans tous les diagrammes Pb-Pb. Dans le manuscrit qui suit, nous cherchons à comprendre l'origine de ces variations en nous appuyant sur les compositions isotopiques en Pb des différentes fractions minérales et granulométriques analysées au cours de cette thèse. Ces dernières nous permettent de (1) contraindre l'importance des certaines espèces minérales dans le budget isotopique en Pb des sédiments de rivière et (2) d'estimer la composition isotopique moyenne en Pb de la croûte Himalayenne. En se basant sur nos interprétations, nous proposons plusieurs estimations pour la composition isotopique moyenne de la croûte contientale supérieure, estimations qui dépendent de son âge d'extraction moyen du réservoir mantellique.

New approach to the average upper continental crust Pb isotopic value

(To be submitted to Nature Geoscience)

Marion Garçon[1], Catherine Chauvel[1], Christian France-Lanord[2], Mara Limonta[3], Eduardo Garzanti[3]

[1] ISTerre, CNRS, Université Joseph Fourier de Grenoble, BP 53, 38041 Grenoble Cedex 09, France

[2] CRPG-CNRS, 15, rue Notre Dame des Pauvres, 54501 Vandoeuvre-lès-Nancy, France

[3] Laboratorio di Petrografia del Sedimentario, Dipartimento di Scienze Geologiche e Geotecnologie, Università di Milano-Bicocca, 20126 Milano, Italy

Note : Figures were integrated in the text to facilitate the reading

Knowing the average Pb isotopic compositions of major Earth reservoirs such as the continental crust is crucial to constrain the evolution of the Earth since its formation. Current estimates are rare and essentially based on data acquired on river or oceanic sediments[1-4]. These estimates assume that sediments are representative of their continental sources. Possible bias introduced by sedimentary mineral sorting is ignored although it was clearly demonstrated that it affects other systems such as Hf isotopes that are fractionated by the so-called “zircon effect”. Retention on continents of unradiogenic Hf-rich zircons in coarse sediments leads to the delivery, into the ocean, of material with Hf isotopes much more radiogenic than their continental sources[5]. Because zircons have extremely radiogenic Pb isotopes, we evaluated the impact of the “zircon effect” on the Pb isotopic compositions of sediments. Using a comprehensive sample set of sediments and minerals from Himalayan Rivers, we demonstrate that the few zircons present in our samples (< 0.5 wt.%) generate a Pb isotopic variability as large as that observed in the entire Earth’s mantle. After careful correction of this effect, we suggest a new average value for upper continental crust.

The Ganga is one of the largest river on Earth, delivering annually ca. 400 million tons of sediments to the Bay of Bengal[6]. Because of its critical role in the world’s sedimentation system[7], this fluvial network constitutes a privileged laboratory to assess the global isotopic systematics of river sediments. The Ganga River carries the erosion products of the Himalayan orogenic belt that can be divided into four main geological units[8] from north to south : (1) the variably metamorphosed sedimentary rocks of the Tethyan Sedimentary Series, (2) the highly metamorphosed crystalline rocks of the High Himalayan Crystalline, (3) the weakly metamorphosed sedimentary rocks of the Lesser Himalaya, and (4) the Siwaliks made of Neogene to Quaternary floodplain deposits (see Figure 1). Here we report the Pb isotopic compositions of (a) sediments eroded from three of these geological units carried by small rivers draining Himalayan monolithologic catchments and (b) of bedload, bank and suspended load sediments sampled in the floodplain at the Himalayan front and further downstream in the Ganga and its major tributaries (Karnali, Narayani and Kosi Rivers) (Supplementary Table 1 ; Figures 1 and 2). Major element data on the same samples were reported by Lupker et al.[9] while trace elements and Nd-Hf isotopes were reported by Garçon et al.[10].

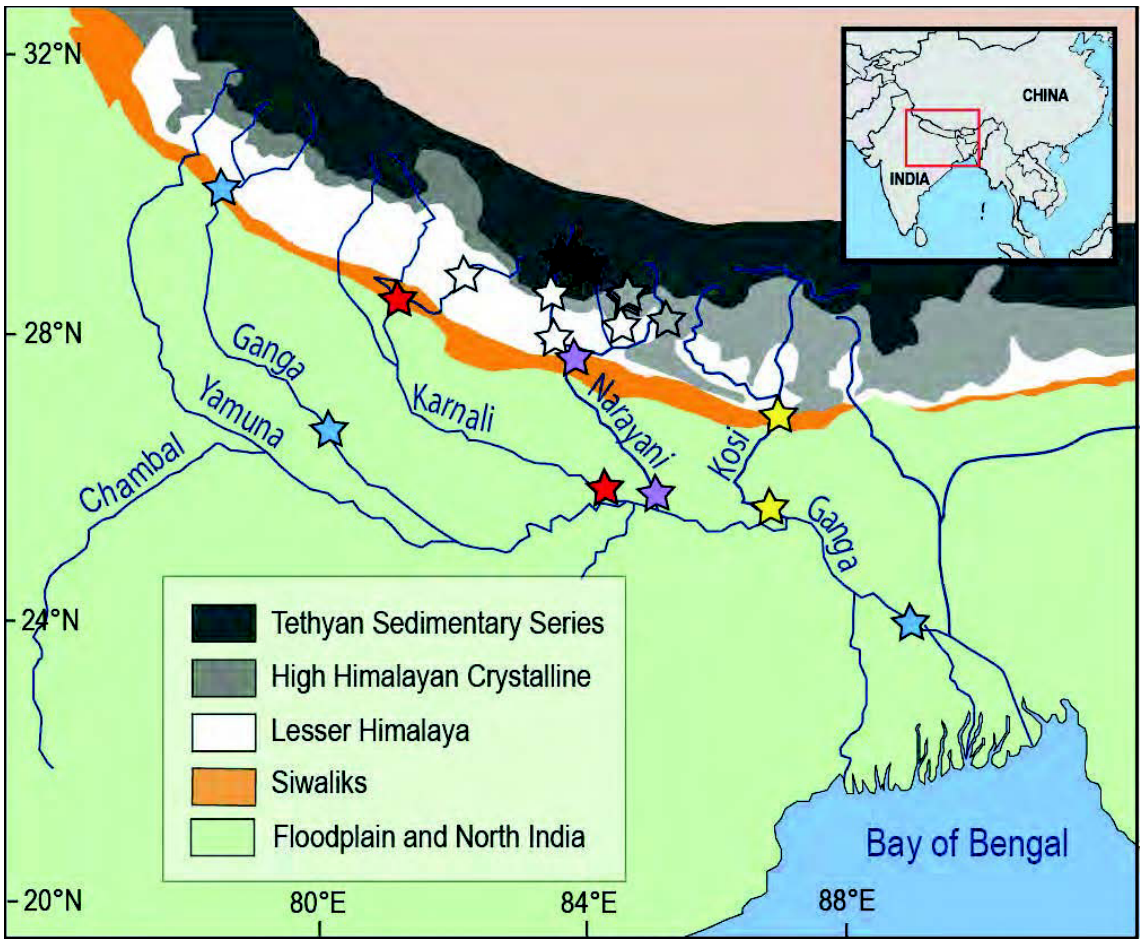

Figure 1: Map of the Ganga fluvial system
Colored stars indicate the sampling locations of river sediments sampled in the floodplain and analyzed in this study. White and grey stars indicate the sampling locations of river sediments sampled in the mountain range. White stars: sampling sites for the Lesser Himalaya-derived sediments. Light grey stars: sampling sites for the High Himalayan Crystalline-derived sediments. Dark grey stars: sampling sites for the Tethyan Sedimentary Series-derived sediments. See Supplementary Tables 1, 2 and 3 for additional information on the location and nature of samples.

The most striking feature seen in Figure 2 is that Himalayan sediments define a remarkable linear trend in both $^{207}Pb/^{204}Pb$ vs. $^{206}Pb/^{204}Pb$ and $^{208}Pb/^{204}Pb$ vs. $^{206}Pb/^{204}Pb$ diagrams, spanning an extremely large range of values compared to what is generally known for terrestrial rocks. Such a linear array in Pb isotopic spaces is quite puzzling and could be interpreted as being an isochron or a mixing line. Because Nd isotopes of Himalayan river sediments and U-Pb ages of individual zircons clearly demonstrate that the sources of sediments are diverse and have different ages [11-13], the isochron case appears very unlikely. Alternatively, the trend could result from mixing of sediments derived from Himalayan sources with different Pb isotopic compositions. We also reject this interpretation because sediments eroded from single geological units have extremely variable Pb compositions and

do not define end member values along the array. This is clearly the case of sediments eroded from the Lesser Himalaya units (white dots and diamonds in Figure 2), a surprising feature for two reasons. First, Lesser Himalaya units include much older rocks than the other geological units[11,12], the expected more radiogenic Pb signatures are however not observed. Secondly, some of the sediments eroded from the Lesser Himalaya have Pb isotopic compositions similar to those derived from the Tethyan Sedimentary Series and the High Himalayan Crystalline units but different Nd and Hf isotopic compositions[10,13-15]. These observations lead us to suggest that the Pb isotopic compositions of river sediments may not faithfully reflect that of their sources.

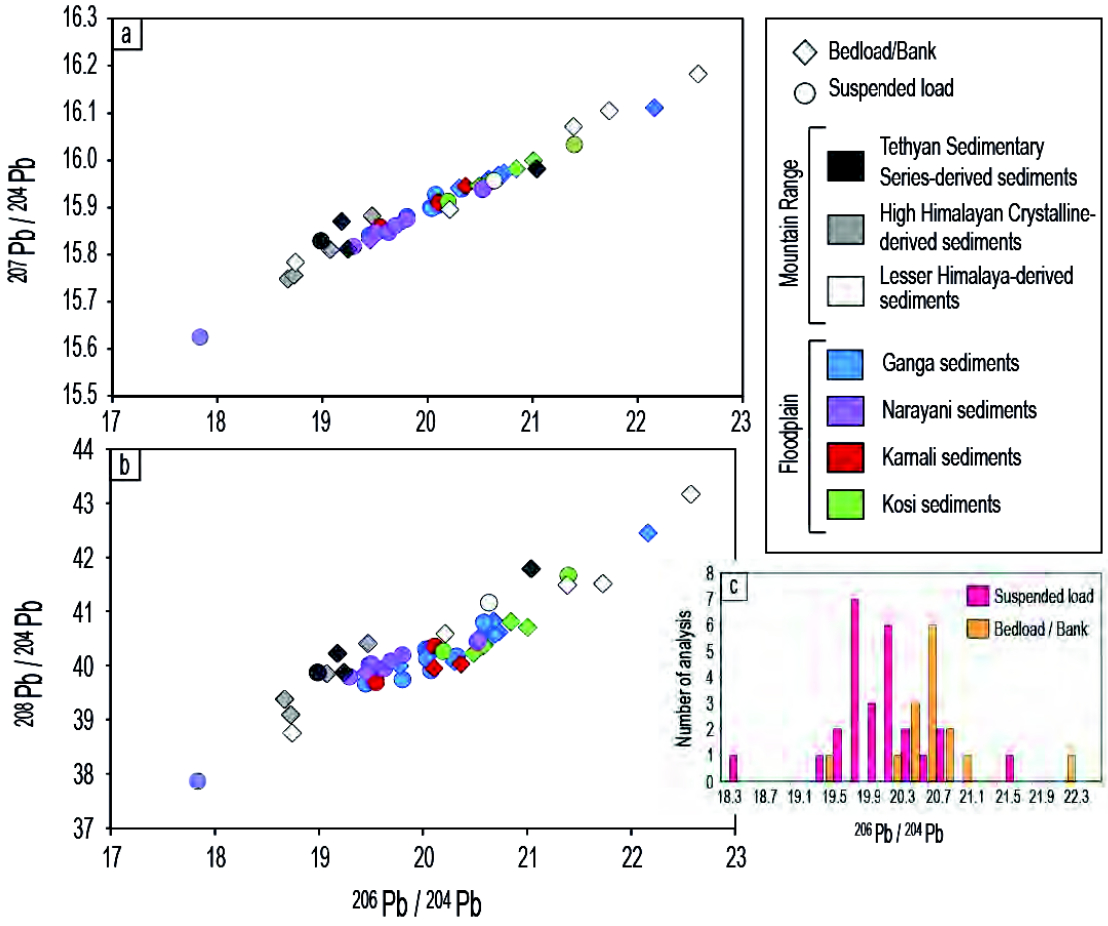

Figure 2: Pb isotopic compositions of Himalayan river sediments
a. b. $^{207}Pb/^{204}Pb$ versus $^{206}Pb/^{204}Pb$ and $^{208}Pb/^{204}Pb$ versus $^{206}Pb/^{204}Pb$ diagrams for the river sediments analyzed in this study. **c.** Histogram of $^{206}Pb/^{204}Pb$ ratios for sediments sampled in the floodplain (Ganga, Narrayani, Karnali, and Kosi Rivers).

Sediments collected in the floodplain also define a large range of Pb isotopic compositions (Figure 2). This is in sharp contrast with their uniform Nd isotopic compositions[10,14,15] indicating that Himalayan detritus is well homogenized before entering the floodplain and that there is no addition of new source-derived material supplied by tributaries along the river courses. It is therefore extremely unlikely that the Pb isotopic variations defined by sediments are due to source variability.

The histogram shown in Figure 2c highlights a systematic difference between suspended load and bedload/bank, the latter generally displaying more radiogenic $^{206}Pb/^{204}Pb$ ratios. The most straightforward explanation is that the observed variability of Pb isotopes results from processes occurring sediment transport and deposiiton in the river.

In order to understand what controls Pb isotopes in river sediments, we analyzed pure mineral separates of biotite, K-feldpar, muscovite, plagioclase, magnetite, epidote, titanite, vermiculite, amphibole and carbonate separated from a bedload sampled at the outflow of the Ganga (BR 717). We also analyzed several grain-size fractions from a suspended load of the Narayani sampled at the Himalayan front (PB 60) and from a bedload collected at the outflow of the Ganga (BGP 6) (Supplementary Tables 2 and 3). The results are shown in Figure 3. Except for titanite, all mineral separates lie at the lower end of the trend defined by the Himalayan sediment samples (Figure 3). The same is true for the clay fractions (<2 µm), shown with dark blue symbols in Figure 3. In contrast, the 2-50 µm and 50-63 µm fractions from BGP 6 (green and yellow diamonds in Figure 3) have extremely radiogenic Pb values, up to 32 for $^{206}Pb/^{204}Pb$, 17.1 for $^{207}Pb/^{204}Pb$ and 52 for $^{208}Pb/^{204}Pb$, and lie on the extension of the array defined by all river sediments. These grain-size fractions also have the highest Zr and Hf contents (8,000-12,000 ppm and 200-300 ppm, see Supplementary Table 3), a feature indicating the presence of relatively high proportions of zircons, as documented by petrologic studies conducted by Garzanti et al.[16,17] on samples collected at the same location. Using a Hf concentration of 3 ppm for the <2 µm fraction from bedload BGP 6 that, we believe, contains negligible zircon, and an Hf content of 10,000 ppm for the pure zircon separate (see Supplementary Tables 2 and 3), we calculate that the 2-50 µm fraction shown with a green diamond in Figure 3 contains about 2 wt.% of zircon. Its elevated Pb isotopic ratios may thus result from the presence of this mineral.

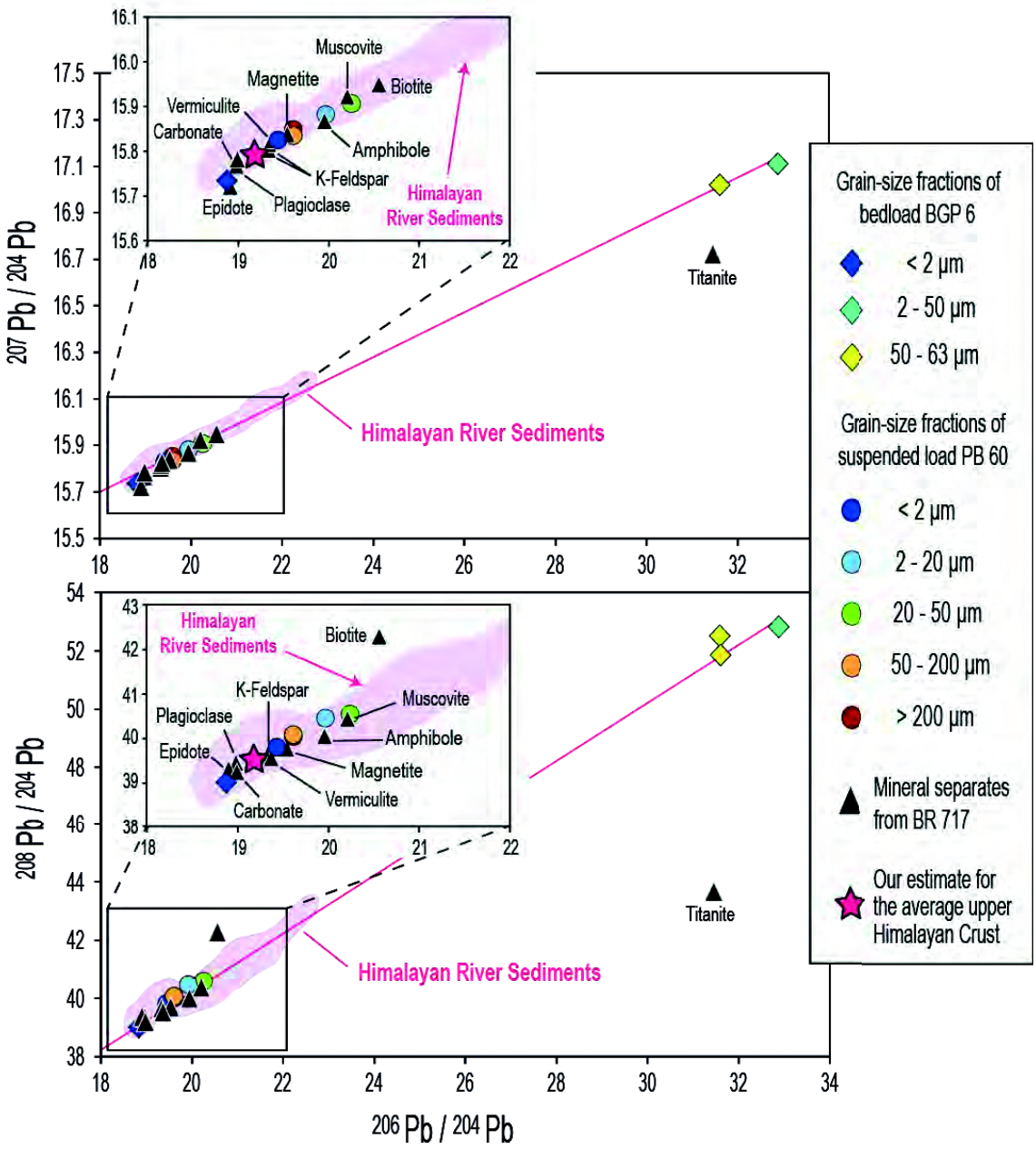

Figure 3: Pb isotopic compositions of mineral separates and grain-size fractions.
The field for Himalayan river sediments was constructed using the data shown in Figure 2. The pink lines show the best linear regressions between Himalayan sediments and grain-size fractions. Titanite is the only one to significantly deviate from this regression.

Due to their chemical istability and their very high U/Pb and Th/Pb ratios, zircons accumulate vast amounts of radiogenic Pb through time and their $^{206}Pb/^{204}Pb$, $^{207}Pb/^{204}Pb$ and $^{208}Pb/^{204}Pb$ ratios are extremely radiogenic compared to most terrestrial rocks. The linear trend displayed by Himalayan river sediments (see Figure 2) may thus be due to the “zircon effect” caused by mineralogical sorting processes during sediment transport and deposition. In other words, the array seen in Figure 2 results from mixing between extremely radiogenic

zircons and a more subdued end member corresponding to the zircon-free composition of the Himalayan crust.

In order to define this latter end-member (shown with a pink star in Figure 3), we calculated an average composition based on all zircon-poor samples (clay fractions <2 µm) as well as the pure K-feldspar separate because K-feldspar hosts most of the Pb present in crustal rocks and its derived sediments together with very little U and Th[4,18]. The Pb isotopic composition of the radiogenic zircon end-member is constrained using sample BGP 6 B, its Pb content and isotopic composition and the fact that it contains 2% zircon. The resulting mixing line is shown in Figure 4a for $^{207}Pb/^{204}Pb$ vs. $^{206}Pb/^{204}Pb$ and in Supplementary File 1 for $^{208}Pb/^{204}Pb$ vs. $^{206}Pb/^{204}Pb$.

The important observations supporting our “zircon effect” interpretation for the linear array displayed by all Himalayan river sediments in Figure 2 are as follows:

(1) Despite the low Pb content of zircons, our calculation demonstrates that a proportion between 0 and 0.5 wt.% of such an extremely radiogenic mineral explains the entire range of Pb isotopic values measured for Himalayan river sediments (Figure 4a).

(2) The isotopic composition of bedload BR 717, the sample from which mineral separates were isolated, indicates addition of 0.5 wt.% zircons to the unradiogenic end member (Figure 4a). This value is identical to the proportion determined independently by [16] on the same sample (see supplementary Table 2).

(3) Addition of radiogenic Pb present in zircons explains why bedloads have more radiogenic Pb isotopes than suspended loads (Figure 2c). Indeed, mineral sorting during sediment transport enriches bedloads in fast-settling coarser and denser minerals, such as ultradense zircons, whereas suspended loads are preferentially enriched in platy phyllosilicates and other slow-setting minerals.

(4) The slope of the array defined by all sediments in $^{207}Pb/^{204}Pb$ vs. $^{206}Pb/^{204}Pb$ isotopic space (Figure 2a) is totally controlled by the very radiogenic isotopic signature of the zircon fraction and provides an age of 1.6 ± 0.1 Ga. This age is consistent with the average U-Pb age of 1.7 Ga that we calculated using data published by DeCelles et al.[19] on detrital zircons found in modern Himalayan rivers.

We are therefore confident that the array defined by Himalayan river sediments in Pb isotopic spaces represents the varying contribution of zircons (0-0.5 wt%) in the sedimentary materials.

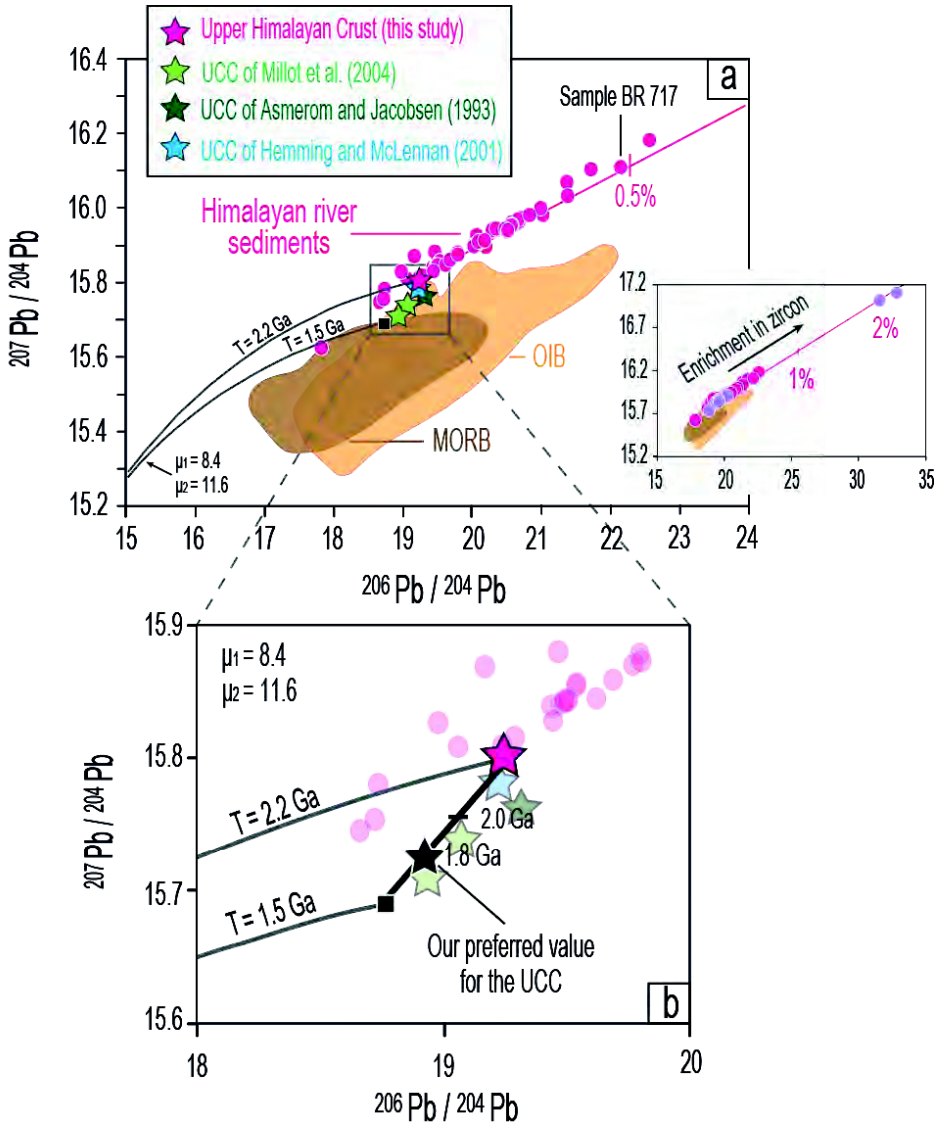

Figure 4: $^{207}Pb/^{204}Pb$ versus $^{206}Pb/^{204}Pb$ diagrams comparing our estimated composition of the upper Himalayan crust and those of the upper continental crust.
UCC: Upper continental crust. Pink dots represent the Himalayan river sediments as shown in Figure 2. Purple dots correspond to the grain-size fractions. **a.** Ticks on the pink mixing line show the proportions of zircons in the binary mixing between the unradiogenic upper Himalayan crust estimate (pink star) and the radiogenic zircon end member. Fields for Ocean Island Basalts (OIB) and Mid-Ocean Ridge Basalts (MORB) show the Pb isotopic variability of the Earth's mantle. These fields were constructed using data from GEOROC and PETDB databases. **b.** Blow-up showing the average Pb isotopic composition of the upper continental crust as a function of its mean age (T). Our preferred value is that corresponding to a mean age of 1.8 Ga.

Going one step further, we use our sediment data to estimate the average Pb isotopic composition of the eroded crust. Assuming that all the upper continental crust zirconium (i.e. 193 ppm after Rudnick and Gao [20]) resides in zircon, we estimate that crustal rocks contain a maximum of 0.03 wt.% of zircon. With this proportion, mixing calculations indicate that the average Pb isotopic composition of the eroded crust is, within errors, similar to our

unradiogenic end member shown as a pink star in Figure 4 ($^{206}Pb/^{204}Pb$ = 19.24; $^{207}Pb/^{204}Pb$ 15.80; $^{208}Pb/^{204}Pb$ = 39.51). This value is less radiogenic than the average Pb composition of the Himalayan-derived suspended loads, bedloads and banks (Figure 2c), indicating that river sediments are more radiogenic than their sources due to the "zircon effect". In addition, it suggests that zircons are present in fine suspended load either as small individual grain or as inclusion in other minerals (e.g. phyllosilicates). We recognize that the "zircon effect" is particularly visible in Himalayan sediments because Himalayan zircons are rather old, and their extremely radiogenic Pb isotopic composition can more easily influence the bulk sediment Pb isotopic budget. A lesser effect would be expected if the eroded sources are on average younger.

Some studies[21,22] showed that sediments are further sorted at the continent/ocean interface due to the lowering of the hydraulic energy. As a consequence, much of the zircons carried by large rivers settle down in the estuary, next to continents. We thus anticipate that zircon-rich materials having more radiogenic Pb compositions than their continental source are retained on continents and continental margins, whereas zircon-poor muds having the same Pb isotopes as their sources preferentially reach and are deposited in the deep ocean, far from continents.

Using our Pb estimate for the upper Himalayan crust, we can evaluate the Pb isotopic composition of upper continental crust at a more global scale. We follow the same two-stage approach as Asmerom et al.[1] using our Pb isotopic values and an average extraction age for the Himalayan crust from the mantle constrained by Nd model ages of Himalayan river sediment samples (ca. 2.2 Ga calculated using data of Garçon et al.[10]). We obtain a mantle-stage μ_1 value of 8.4 followed by a crustal-stage μ_2 value of 11.6 (see Figure 4), values that are in complete agreement with those commonly suggested for mantle and upper continental crust[1,23]. Unfortunately, a similar calculation for κ_1 and κ_2 values (i.e. $^{232}Th/^{238}U$ ratios) using $^{208}Pb/^{204}Pb$ ratios is unconstrained because the two κ values are interdependent, but κ is, on average, around 4. Using our μ_1 and μ_2 values and κ values of 4, we can calculate the Pb isotopic composition of the upper continental crust depending on its average extraction time from the mantle (Figure 4b, Supplementary Figure and Table 1). Nd model ages suggested for average upper continental crust range between 1.5 and 2.2 Ga[24,25] and can be used to estimate the average crustal Pb isotopic composition. For an average crust differentiation age of 1.5 Ga, the $^{206}Pb/^{204}Pb$ ratio is 18.76 and it increases following the black line shown in Figure 4b up to 19.24 for an average age of 2.2 Ga. The total range shown in Figure 4b is consistent but always displaced to the left of former estimates based on suspended river

sediments[1,2] and deep-sea turbidites[4], a discrepancy most likely due to the "zircon effect" on Pb isotopes. Using the commonly preferred average age of 1.8 Ga for upper crust, we suggest the following values: $^{206}Pb/^{204}Pb$ = 18.96, $^{207}Pb/^{204}Pb$ = 15.73 and $^{208}Pb/^{204}Pb$ = 39.16 (Table 1). If, in the future, another average age for crust differentiation is established using independent methods, another value can be easily determined.

Average Model age (Ga)	$^{208}Pb/^{204}Pb$	$^{207}Pb/^{204}Pb$	$^{206}Pb/^{204}Pb$
1.5	38.96	15.69	18.76
1.8	**39.16**	**15.73**	**18.95**
2.0	39.30	15.76	19.09
2.2	39.51	15.80	19.24

Table 1: Our Pb estimates for average upper continental crust
Pb estimates were calculated using $\mu_1 = 8.4$, $\mu_2 = 11.6$ and $\kappa_1 = \kappa_2 = 4$ from the isotope ratios of primeval Pb of Cayon Diablo as published by Tatsumoto et al.[29]

METHODS

Grain-size fractions were separated from two samples (PB 60 and BGP 6) by sieving. Mineral separates were obtained from different grain-size fractions of sample BR 717. We used successive centrifugations in sodium metatungstate and methylene iodide to separate the minerals as a function of their densities and recovered them by partial freezing in liquid nitrogen. Each mineral separate was then carefully purified under the binocular microscope. 5 to 10 mg mineral separates and 50 to 100 mg powder for the bulk sediments and the grain-size fractions were attacked for 2 days in HNO_3 14N on a hot plate at 130°C, evaporated and then digested in a mixture of HF and $HClO_4$ in teflon containers placed in steel PARR bombs for 6 weeks at 140°C or one week at 200°C. Following the analytical procedure described by Chauvel et al.[26], the isolation of Pb was carried out with anion AG1-X8 resin. Pb isotopic ratios were measured on a Nu Plasma MC-ICP-MS at ENS Lyon (France). Mass fractionation bias was corrected using a thallium spike according to White et al.[27]. Analytical drift was corrected by the standard bracketing technique using the measured values for the NBS 981 standard run every two or three samples and those published by Galer and Abouchami[28]. The reproducibility (1σ) of our measurements for the NBS 981 standard, measured 66 times, is better than 270 ppm for $^{208}Pb/^{204}Pb$, 180 ppm for $^{207}Pb/^{204}Pb$ and 420

ppm for $^{206}Pb/^{204}Pb$. Total procedural blanks averages 280 pg and are always negligible relative to the amount of Pb isolated in each sample.

ACKNOLEDGEMENTS

We thank S. Andò for his help during mineral separations, S. Bureau for her help in the clean lab, P. Telouk (ENS, Lyon) for assistance during MC-ICP-MS measurements at Lyon and N. Arndt (ISTerre, Grenoble) for constructive discussions that helped improving the content of the manuscript.

This study was supported by funding from CNRS and INSU programs.

REFERENCES

1. Asmerom, Y. & Jacobsen, S. B. The Pb isotopic evolution of the Earth: inferences from river water suspended loads. *Earth and Planetary Science Letters* **115**, 245–256 (1993).
2. Millot, R., Allègre, C. J., Gaillardet, J. & Roy, S. Lead isotopic systematics of major river sediments: a new estimate of the Pb isotopic composition of the Upper Continental Crust. *Chemical Geology* **203**, 75–90 (2004).
3. Allègre, C. J., Dupré, B., Négrel, P. & Gaillardet, J. Sr-Nd-Pb isotope systematics in Amazon and Congo River systems: constraints about erosion processes. *Chemical Geology* **131**, 93–112 (1996).
4. Hemming, S. & McLennan, S. Pb isotope compositions of modern deep sea turbidites. *Earth and Planetary Science Letters* **184**, 489–503 (2001).
5. Patchett, P. J., White, W. M., Feldmann, H., Kielinczuk, S. & Hofmann, A. W. Hafnium/rare earth element fractionation in the sedimentary system and crustal recycling into the Earth's mantle. *Earth and Planetary Science Letters* **69**, 365–378 (1984).
6. Lupker, M. *et al.* A Rouse-based method to integrate the chemical composition of river sediments: Application to the Ganga basin. *J. Geophys. Res.* **116**, F04012 (2011).
7. Milliman, J. & Meade, R. H. World-wide delivery of river sediment to the oceans. *The Journal of Geology* **91**, 1–21 (1983).
8. Le Fort, P. Himalayas: the collided range. Present knowledge of the continental arc. *American Journal of Science* (1975).
9. Lupker, M. *et al.* Predominant floodplain over mountain weathering of Himalayan sediments (Ganga basin). *Geochimica et Cosmochimica Acta* 84, 410-432 (2012).
10. Garçon, M., Chauvel, C. & France-Lanord, C. Almost half of worldwide sedimentary Nd-Hf isotopic decoupling done on continents. To be submitted to G-cubed.

11. Parrish, R. R. & Hodges, V. Isotopic constraints on the age and provenance of the Lesser and Greater Himalayan sequences, Nepalese Himalaya. *Geological Society of America Bulletin* **108**, 904–911 (1996).
12. DeCelles, P., Gehrels, G., Quade, J., LaReau, B. & Spurlin, M. Tectonic implications of U-Pb zircon ages of the Himalayan orogenic belt in Nepal. *Science* **288**, 497–499 (2000).
13. Richards, A. *et al.* Himalayan architecture constrained by isotopic tracers from clastic sediments. *Earth and Planetary Science Letters* **236**, 773–796 (2005).
14. Galy, A. & France-Lanord, C. Higher erosion rates in the Himalaya: Geochemical constraints on riverine fluxes. *Geol* **29**, 23–26 (2001).
15. Singh, S. K., Rai, S. K. & Krishnaswami, S. Sr and Nd isotopes in river sediments from the Ganga Basin: Sediment provenance and spatial variability in physical erosion. *J. Geophys. Res.* **113**, F03006 (2008).
16. Garzanti, E. *et al.* Mineralogical and chemical variability of fluvial sediments 1. Bedload sand (Ganga–Brahmaputra, Bangladesh). *Earth and Planetary Science Letters* **299**, 368–381 (2010).
17. Garzanti, E. *et al.* Mineralogical and chemical variability of fluvial sediments 2. Suspended-load silt (Ganga–Brahmaputra, Bangladesh). *Earth and Planetary Science Letters* **302**, 107–120 (2011).
18. Patterson, C. & Tatsumoto, M. The significance of lead isotopes in detrital feldspar with respect to chemical differentiation within the earth's mantle. *Geochimica et Cosmochimica Acta* **28**, 1–22 (1964).
19. DeCelles, P. *et al.* Neogene foreland basin deposits, erosional unroofing, and the kinematic history of the Himalayan fold-thrust belt, western Nepal. *Geological Society of America Bulletin* **110**, 2–21 (1998).
20. Rudnick, R. L. & Gao, S. The Composition of the Crust. *The Crust Vol.3 Treatise on Geochemistry* 1–64 (2003).
21. Lisitzin, A. P. *Oceanic Sedimentation: Lithology and Geochemistry*. **44**, 1–400 (American Geophysical Union: Washington, D. C, 1996).
22. Stummeyer, J., Marchig, V. & Knabe, W. The composition of suspended matter from Ganges–Brahmaputra sediment dispersal system during low sediment transport season. *Chemical Geology* **185**, 125–147 (2002).
23. Kramers, J. D. & Tolstikhin, I. N. Two terrestrial lead isotope paradoxes, forward transport modelling, core formation and the history of the continental crust. *Chemical Geology* **139**, 75–110 (1997).
24. Goldstein, S. & Jacobsen, S. B. Nd and Sr isotopic systematics of river water suspended material: implications for crustal evolution. *Earth and Planetary Science Letters* **87**, 249–265 (1988).
25. Jacobsen, S. B. Isotopic constraints on crustal growth and recycling. *Earth and Planetary Science Letters* **90**, 315–329 (1988).
26. Chauvel, C., Bureau, S. & Poggi, C. Comprehensive chemical and isotopic analyses of basalt and sediment reference materials. *Geostandards and Geoanalytical Research* **35**, 125–143 (2011).
27. White, W. M., Albarède, F. & Télouk, P. High-precision analysis of Pb isotope ratios by multi-collector ICP-MS. *Chemical Geology* **167**, 257–270 (2000).
28. Galer, S. J. G. & Abouchami, W. Practical application of lead triple spiking for

correction of instrumental mass discrimination. 491–492 (1998).
29. Tatsumoto, M., Knight, R. J. & Allègre, C. J. Time differences in the formation of meteorites as determined from the ratio of lead-207 to lead-206. *Science* (1973).

SUPPLEMENTARY MATERIALS

Supplementary Tables 1, 2, 3 : Pb isotopes in sediments, pure mineral fractions and grain-size fractions.

Footnote : 1σ are in-run errors. Zr, Hf and Pb concentrations were measured by ICP-MS following the procedure of Chauvel et al. (2011) on the same dissolutions as those used to measure Pb isotopic compositions.

Supplementary Table 1: Pb isotopes in sediments

From rivers draining monolithologic basins in the Himalayan range

Sample Name	Locality	River	Type of sediment	Pb (ppm)	$^{208}Pb/^{204}Pb$	1σ	$^{207}Pb/^{204}Pb$	1σ	$^{206}Pb/^{204}Pb$	1σ
Lesser Himalaya units										
R 94-12	Sarmi, Nepal	Tributary of the Bheri	Bedload	87.1	40.5828	0.0010	15.8958	0.0003	20.2112	0.0004
MO 102	Confluence Darondi/Marsel Khola, Nepal	Marsel Khola	Bank	12.4	41.4861	0.0009	16.0709	0.0004	21.3862	0.0005
MO 102 re-run					41.4857	0.0013	16.0701	0.0004	21.3858	0.0006
MO 112	Confluence Bhuri Gandaki/Isul Khola, Nepal	Isul Khola	Bank, gravel sample	9.19	43.1638	0.0017	16.1832	0.0007	22.5753	0.0008
PB 33	Nepal	Ghara khola	Suspended Load	17.1	41.1620	0.0010	15.9564	0.0004	20.6345	0.0005
PB 37	Nepal	Beg Khola	Bank	11.6	38.7584	0.0012	15.7833	0.0005	18.7442	0.0003
MO 207	Waling, Nepal	Andi Khola	Bedload	9.12	41.5076	0.0019	16.1047	0.0007	21.7295	0.0009
High Himalayan Crystalline units										
MO 73	Nepal	Tributary of the Chepe khola	Bank	8.94	40.4110	0.0016	15.8820	0.0006	19.4708	0.0005
MO 50	Nepal	Chepe khola	Bank	15.1	39.3746	0.0015	15.7486	0.0005	18.6711	0.0004
MO 59	Nepal	Chepe khola	Bank	23.3	39.0933	0.0018	15.7565	0.0006	18.7296	0.0008
KN 83	Ghyangphedi, Nepal	Tadi khola	Bedload	17.9	39.8509	0.0009	15.8109	0.0003	19.0735	0.0003
Tethyan Sedimentary Series										
MO 504	Tukche, Nepal	Yamkim khola	Suspended Load	33.9	39.8670	0.0011	15.8287	0.0004	18.9871	0.0004
NAG 22	Pedi, Nepal	Marsyandi (10 km away from the River Source)	Bedload	235	41.7816	0.0010	15.9819	0.0003	21.0408	0.0004
MAR-50	Temang, Nepal	Marsyandi (60 km away from the River Source)	Bedload	20.9	39.8665	0.0015	15.8117	0.0006	19.2416	0.0006
MAR-40	Sabche, Nepal	Sabche khola	Bedload	35.2	40.2185	0.0017	15.8706	0.0006	19.1799	0.0006
MAR-40 re-run					40.2139	0.0017	15.8676	0.0006	19.1795	0.0007

From the Ganga river and its major tributaries in the floodplain

Sample Name	Locality	Approximative distance from River Source (km)	Type of sediment	Pb (ppm)	$^{208}Pb/^{204}Pb$	1σ	$^{207}Pb/^{204}Pb$	1σ	$^{206}Pb/^{204}Pb$	1σ
Ganga River										
BR 931	Devrapayag, India	260	Suspended Load	29.2	39.6694	0.0019	15.8417	0.0006	19.4498	0.0006
BR 932	Devrapayag, India	260	Suspended Load	21.0	40.1668	0.0020	15.9401	0.0006	20.3250	0.0007
BR 922	Rishikesh, India	260	Suspended Load	29.1	39.9124	0.0019	15.9272	0.0007	20.0784	0.0007
BR 924	Rishikesh, India	260	Bank	21.4	40.0740	0.0014	15.9405	0.0005	20.3010	0.0005
BR 943	Kanpur, India	800	Suspended Load	23.5	39.7368	0.0014	15.8813	0.0005	19.8032	0.0005
BR 946	Kanpur, India	800	Bedload	18.9	40.5941	0.0016	15.9605	0.0005	20.5807	0.0006
BGP 6	Rajshahi, India	2570	Bedload	17.8	40.6213	0.0022	15.9733	0.0007	20.7277	0.0007
BGP 6 Dup	Rajshahi, India	2570	Bedload	17.6	40.5790	0.0020	15.9644	0.0007	20.6899	0.0009
BR 415	Harding bridge, Bangladesh	2640	Suspended Load	30.4	40.3003	0.0009	15.8991	0.0003	20.0301	0.0003
BR 415 re-run					40.2903	0.0011	15.8958	0.0004	20.0256	0.0004
BR 414	Harding bridge, Bangladesh	2640	Suspended Load	26.2	40.3019	0.0012	15.9013	0.0003	20.0574	0.0004
BR 413	Harding bridge, Bangladesh	2640	Suspended Load	25.3	40.2931	0.0017	15.9040	0.0004	20.0912	0.0004
BR 412	Harding bridge, Bangladesh	2640	Suspended Load	25.3	40.2725	0.0008	15.9040	0.0003	20.0756	0.0004
BR 411	Harding bridge, Bangladesh	2640	Suspended Load	17.4	40.1312	0.0014	15.8984	0.0005	20.0387	0.0005
BR 418	Harding bridge, Bangladesh	2640	Bedload	15.0	40.8292	0.0012	15.9684	0.0004	20.6767	0.0005
BR 8252	Harding bridge, Bangladesh	2640	Bedload	10.7	40.8030	0.0013	15.9548	0.0004	20.5845	0.0005
BR 8253	Harding bridge, Bangladesh	2640	Suspended Load	10.5	39.9963	0.0014	15.8730	0.0007	19.7765	0.0005
BR 717	Harding bridge, Bangladesh	2640	Bedload	14.2	42.4525	0.0013	16.1109	0.0004	22.1618	0.0005
Karnali River										
PB 79	Chisapani, Nepal	260	Suspended Load	12.7	40.3508	0.0016	15.9117	0.0006	20.1105	0.0005

PB 80	Chisapani, Nepal	260	Bank	13.9	39.9552	0.0017	15.9101	0.0005	20.1047	0.0006
BR 8113	Revelganj, India	850	Suspended Load	30.3	39.7131	0.0014	15.8585	0.0005	19.5477	0.0006
BR 8113 Dup	Revelganj, India	850	Suspended Load	30.5	39.6936	0.0015	15.8570	0.0004	19.5474	0.0005
Kosi River										
LO 762	Chatara, Nepal	180	Suspended Load	17.8	40.2696	0.0022	15.9136	0.0007	20.1936	0.0005
LO 762 re-run					40.2771	0.0023	15.9163	0.0007	20.1914	0.0009
LO 763	Chatara, Nepal	180	Bank	17.6	40.3778	0.0010	15.9529	0.0003	20.5899	0.0004
LO 763 Dup	Chatara, Nepal	180	Bank	19.1	40.3688	0.0011	15.9535	0.0004	20.5825	0.0006
PB 69	Chatara, Nepal	440	Suspended Load	17.3	41.6645	0.0013	16.0340	0.0004	21.3982	0.0005
PB 70	Chatara, Nepal	440	Bank	15.3	40.7029	0.0014	15.9993	0.0005	21.0066	0.0005
BR 331	Dumarighat, India	440	Bank	15.7	40.8060	0.0013	15.9820	0.0004	20.8453	0.0005
BR 332	Dumarighat, India	440	Bank	17.2	40.2245	0.0014	15.9449	0.0006	20.4868	0.0006
Narayani River										
LO 757	Narayanghat, Nepal	200	Suspended Load	24.8	40.0158	0.0007	15.8437	0.0002	19.4858	0.0003
LO 756	Narayanghat, Nepal	200	Suspended Load	72.0	37.8642	0.0013	15.6249	0.0005	17.8352	0.0005
LO 756 re-run					37.8540	0.0016	15.6222	0.0006	17.8336	0.0006
LO 754	Narayanghat, Nepal	200	Suspended Load	23.6	40.0035	0.0011	15.8452	0.0003	19.5028	0.0004
LO 755	Narayanghat, Nepal	200	Suspended Load	24.1	40.0317	0.0009	15.8467	0.0003	19.5035	0.0003
LO 755 Dup	Narayanghat, Nepal	200	Suspended Load	25.0	40.0043	0.0018	15.8468	0.0003	19.5100	0.0003
LO 758 C	Narayanghat, Nepal	200	Suspended Load	15.5	39.9544	0.0013	15.8476	0.0005	19.6294	0.0005
PB 54	Narayanghat, Nepal	200	Suspended Load	19.3	40.0753	0.0010	15.8614	0.0008	19.6925	0.0008
PB 60	Narayanghat, Nepal	200	Suspended Load	16.6						
LO 1002	Narayanghat, Nepal	200	Suspended Load	27.4	39.7958	0.0024	15.8183	0.0005	19.2935	0.0005
LO 1007	Narayanghat, Nepal	200	Suspended Load	13.6	40.4425	0.0013	15.9385	0.0004	20.5219	0.0004
LO 1007 Dup	Narayanghat, Nepal	200	Suspended Load	12.2	40.4698	0.0012	15.9405	0.0004	20.5304	0.0005
BR 8106	Hajipur, India	550	Suspended Load	26.7	40.1990	0.0015	15.8760	0.0004	19.8046	0.0004
BR 8107	Hajipur, India	550	Bedload	20.9	39.8702	0.0016	15.8310	0.0004	19.4519	0.0005

Supplementary Table 1 (end)

Supplementary Table 2: Pb isotopes in mineral separates from BR 717

Sample Name	Type of mineral	Weight proportion in BR 717 after Garzanti et al. (2010)	Hf (ppm)	Pb (ppm)	$^{208}Pb/^{204}Pb$	1σ	$^{207}Pb/^{204}Pb$	1σ	$^{206}Pb/^{204}Pb$	1σ
BR 717 Msc	Muscovite	8.6		11.1	40.4282	0.0020	15.9237	0.0007	20.2008	0.0008
BR 717 Bio	Biotite			4.96	42.2870	0.0022	15.9514	0.0007	20.5508	0.0013
BR 717 Bio re-run					42.2816	0.0021	15.9486	0.0006	20.5582	0.0015
BR 717 Fd-K	K-Felspar	8.5		61.3	39.5826	0.0014	15.8053	0.0006	19.3257	0.0008
BR 717 Fd-K Dup	K-Felspar			75.1	39.6220	0.0013	15.8174	0.0005	19.3318	0.0006
BR 717 Plg	Plagioclase	7.1		12.6	39.4450	0.0017	15.7695	0.0007	18.9724	0.0009
BR 717Mag	Magnetite			19.1	39.7607	0.0020	15.8403	0.0007	19.5343	0.0007
BR 717 Ep	Epidote	1.1		46.9	39.2848	0.0018	15.7229	0.0007	18.9028	0.0007
BR 717 Ttn	Titanite	0.3		5.52	43.6704	0.0019	16.7220	0.0005	31.4562	0.0011
BR 717 Verm	Vermiculite			75.5	39.5411	0.0018	15.8266	0.0006	19.3597	0.0006
BR 717 Amp	Amphibole	1		24.1	40.0280	0.0016	15.8694	0.0006	19.9482	0.0006
BR 717 Carb	Carbonate			7.28	39.2442	0.0011	15.7839	0.0003	18.9809	0.0004
BR 717 Zrn	Zircon	0.5	10 171	19.3						

Supplementary Table 3: Pb isotopes in grain-size fractions from BGP 6 and PB 60

Sample Name	Type of sediment	Grain-size fractions	Zr (ppm)	Hf (ppm)	Pb (ppm)	$^{208}Pb/^{204}Pb$	1σ	$^{207}Pb/^{204}Pb$	1σ	$^{206}Pb/^{204}Pb$	1σ
BGP 6 A	Bedload	< 2 µm	447	12.2	95.2	39.0244	0.0015	15.7357	0.0005	18.8658	0.0006
BGP 6 C	Bedload	2 - 50 µm	11954	290	24.3	52.8624	0.0024	17.1069	0.0007	32.8786	0.0014
BGP 6 B	Bedload	50 - 63 µm	8328	205	20.9	52.5387	0.0024	17.0178	0.0006	31.6096	0.0010
BGP 6 B Dup	Bedload	50 - 63 µm	8208	203	20.5	51.8890	0.0022	17.0196	0.0007	31.5960	0.0010
PB 60 A	Suspended Load	< 2 µm	119	3.13	67.1	39.8007	0.0018	15.8265	0.0006	19.4227	0.0006
PB 60 LF	Suspended Load	2 - 20 µm	150	3.96	23.2	40.4494	0.0016	15.8843	0.0006	19.9572	0.0006
PB 60 LG	Suspended Load	20 - 50 µm	345	9.44	18.0	40.5608	0.0021	15.9089	0.0007	20.2376	0.0007
PB 60 SF	Suspended Load	50 - 200 µm	119	3.12	17.7	40.0655	0.0023	15.8485	0.0008	19.6105	0.0010
PB 60 SG	Suspended Load	> 200 µm	136	3.63	15.8	40.0589	0.0018	15.8364	0.0006	19.6054	0.0007

Supplementary Figure : $^{208}Pb/^{204}Pb$ versus $^{206}Pb/^{204}Pb$ diagrams comparing our estimated composition of the upper Himalayan crust and those of the upper continental crust.

Footnote : Same colors, symbols and data sources as Figure 4.

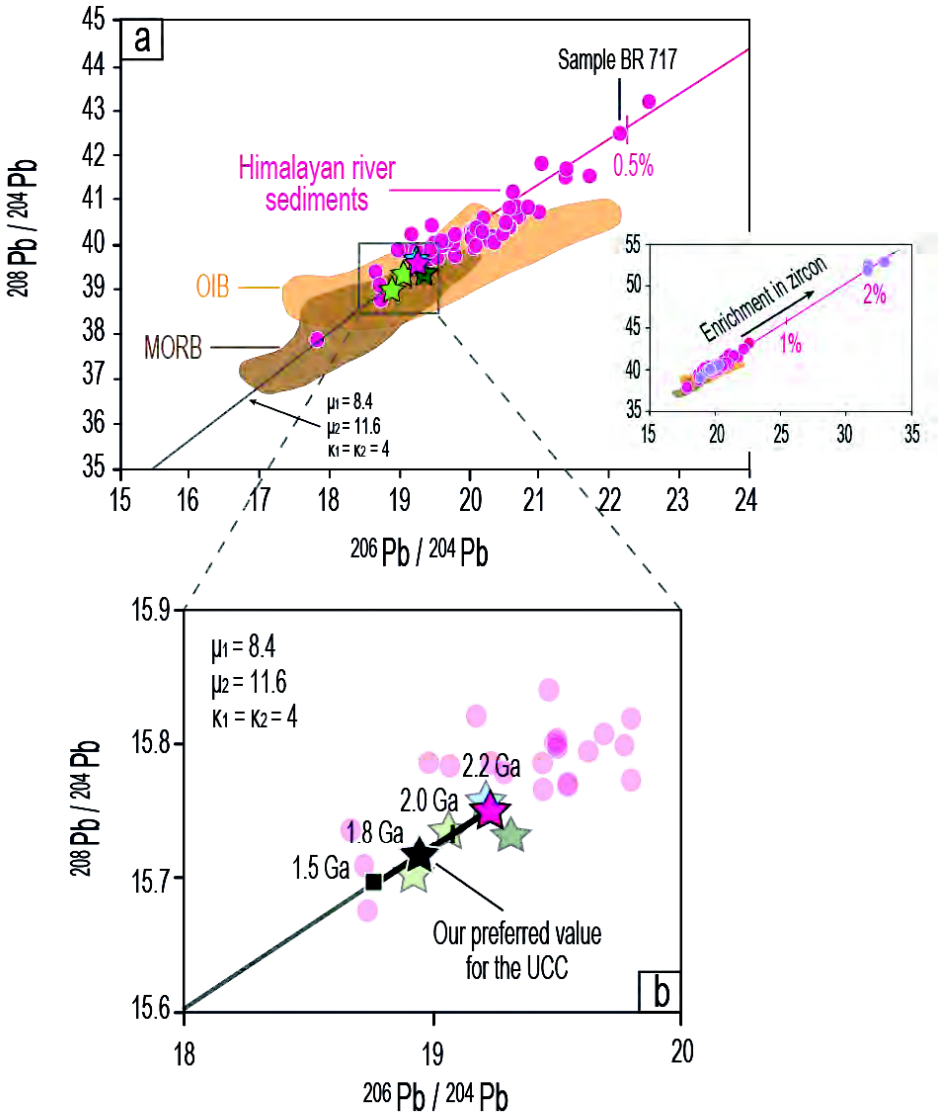

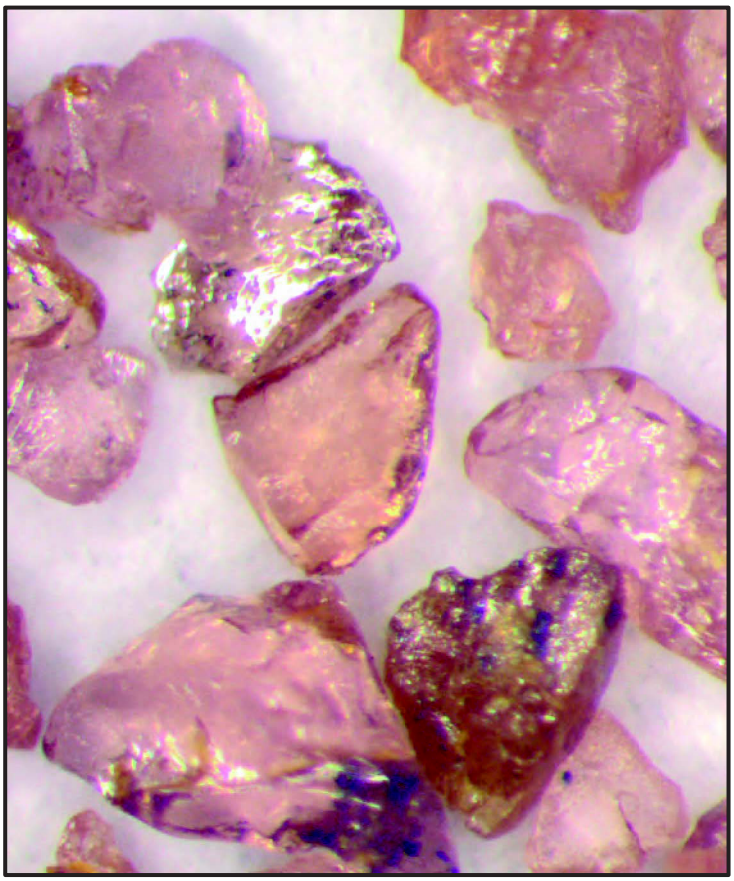

Chapitre 4

Quels Minéraux Contrôlent les Compositions Isotopiques des Sédiments ?

Dans les minéraux, les rapports isotopiques évoluent en système fermé, suivant la quantité d'éléments pères et fils piégés au moment de la cristallisation, jusqu'à ce qu'un événement vienne perturber le système (métamorphisme, fusion, etc…). Chaque espèce minérale a donc une signature isotopique qui lui est propre. Puisque que les sédiments sont, en grande partie, constitués de minéraux, leurs compositions isotopiques résultent du mélange de celles des différentes espèces minérales qu'ils contiennent. L'objectif de ce chapitre, présenté sous la forme d'un manuscrit pour Chemical Geology, est d'évaluer la contribution spécifique de chaque espèce minérale dans le budget isotopique du Nd, de l'Hf, du Pb et du Sr des sédiments de rivières Himalayennes. Pour ce faire, nous utiliserons les résultats présentés dans le chapitre précédent ainsi que les compositions isotopiques en Sr mesurées dans quelques sédiments du Ganges et les concentrations en éléments traces et les compositions isotopiques en Nd, Hf, Pb et Sr mesurés dans différentes fractions de minéraux purs.

Which minerals control the Nd-Hf-Sr-Pb isotopic compositions of river sediments?
(To be submitted to Chemical Geology)

ABSTRACT **123**
1. INTRODUCTION **124**
2. STUDIED AREA AND SAMPLES **125**
3. METHODS **127**
4. RESULTS **129**
5. DISCUSSION **133**
6. SUMMARY AND CONCLUSIONS **147**
ACKNOWLEDGMENTS **148**
REFERENCES **149**
SUPPLEMENTARY MATERIAL **149**

Dans le chapitre précédent, nous avons montré que les variabilités de compositions isotopiques en Hf et Pb des sédiments de rivières Himalayennes étaient liées aux effets du tri minéralogique et plus particulièrement à un " effet zircon ". Au contraire, nous avons montré que les compositions isotopiques en Nd de ces mêmes sédiments étaient relativement peu variables et donc peu affectées par les effets du tri minéralogique. A quel point les zircons contrôlent-ils la composition isotopique en Hf et Pb des différents types de sédiments? Pourquoi n'observe t-on pas de différences isotopiques significatives en Nd entre les sédiments de fond de rivière et ceux transportés en suspension ? L'objectif du manuscrit présenté ci-dessous est de " décortiquer " les compositions isotopiques de ces sédiments afin de quantifier la contribution précise de chaque espèce minérale et déterminer si les variabilités observées peuvent être expliquées ou non par la minéralogie des différents types de sédiments. Nous nous concentrerons exclusivement sur les sédiments échantillonés dans le delta du Bangladesh puisque les différentes fractions minérales ont été séparées à partir d'un sédiment échantillonné à cet endroit et que les très faibles variations isotopiques liées aux effets de provenance dans les autres sédiments du système fluviatile (cf. Section III.1) pourraient biaiser nos interprétations.

La quantification de la contribution des différents minéraux nécessite la prise en compte de nombreux paramètres i.e. les proportions, les concentrations et les compositions isotopiques de chaque espèce minérale. Nous avons donc choisi d'aborder ce sujet en utilisant des procédures Monte-Carlo qui visent à modéliser les compositions isotopiques en Nd, Hf, Pb et Sr de différents mélanges de minéraux. Pour chaque système isotopique, nous comparons les compositions isotopiques modélisées avec celles mesurées dans les sédiments du Ganges au Bangladesh afin de déterminer la nature des espèces minérales qui contrôlent leurs budgets isotopiques. A la fin du manuscrit, nous discutons les implications de nos résultats pour les études de provenance basées sur les traceurs isotopiques Nd, Hf, Pb et Sr et pour les systématiques isotopiques des sédiments exportés vers l'océan.

Which minerals control the Nd-Hf-Sr-Pb isotopic compositions of river sediments?

(To be submitted to Chemical Geology)

Marion Garçon[1], Catherine Chauvel[1], Christian France-Lanord[2], Mara Limonta[3], Eduardo Garzanti[3]

[1] ISTerre, CNRS, Université Joseph Fourier de Grenoble, BP 53, 38041 Grenoble Cedex 09, France

[2] CRPG-CNRS, 15, rue Notre Dame des Pauvres, 54501 Vandoeuvre-lès-Nancy, France

[3] Laboratorio di Petrografia del Sedimentario, Dipartimento di Scienze Geologiche e Geotecnologie, Università di Milano-Bicocca, 20126 Milano, Italy

Note : Figures were integrated in the text to facilitate the reading

Abstract

River sediments naturally sample and average large areas of eroded continental crust. They are ideal targets not only for provenance studies based on isotopic compositions, but also to establish average continental crust isotopic values. However, in large fluvial systems, mineral sorting processes significantly modify the mineralogy, and thus the geochemistry of the transported sediments. We still do not know, in any quantitative way, to what extent mineral sorting affects and fractionates the isotopic compositions of river sediments. Here, we focus on this issue and try to decipher the role of each mineral species in the bulk isotopic compositions of bedloads and suspended loads sampled at the outflow of the Ganga River that drains the Himalayan mountain range.

We analyzed Nd, Hf, Sr and Pb isotopic compositions as well as trace element contents of a large number of pure mineral fractions (K-feldspar, plagioclase, muscovite, biotite, magnetite, zircon, titanite, apatite, monazite/allanite, amphibole, epidote, garnet, carbonate and clay) separated from bedload sediments. We combine these data with mineral proportions typical of the Ganga sediments to perform Monte-carlo simulations that quantifiy the contribution of individual mineral species to the Nd, Hf, Sr and Pb isotopic budgets of bedloads and suspended loads. We show that the isotopic systematic of river sediments is entirely buffered by very few minerals. Despite their extremely low proportions in sediments, zircon and monazite/allanite control Hf and Nd isotopes, respectively. K-feldspar buffers the Sr isotopic budget while clay, feldspar and zircon dominate Pb isotopes. We also demonstrate that the observed difference in Hf, Sr and Pb isotopic compositions between bedloads and suspended loads reflects their different mineral proportions. We anticipate that fractionation of the isotopic systems continues at the river/ocean interface to deliver to the deep oceans sediments that are not always representative of their crustal precursors. This stresses the need to carefully address isotopic compositions of sediments as source proxies.

Keywords: isotopic fractionation, bedload, suspended load, continental crust

1. Introduction

Because they integrate large portion of continental crust exposed to weathering, river sediments from worldwide fluvial systems have been widely used to trace sediment provenance, estimate the average isotopic composition of the upper continental crust and constrain its evolution through time (Goldstein et al., 1984; Goldstein and Jacobsen, 1988; Asmerom and Jacobsen, 1993; Allègre et al., 1996; Clift et al., 2002; Singh and France-Lanord, 2002; Millot et al., 2004; Kamber et al., 2005; Richards et al., 2005; Roddaz et al., 2005; Singh et al., 2008; Cina et al., 2009; Belousova et al., 2010; Hawkesworth et al., 2010; Wu et al., 2010; Dhuime et al., 2011; Padoan et al., 2011). Most studies assume that the isotopic composition of river sediments reflects that of the drained continental area. However, depending on its size, shape and density, detrital material transported by rivers is segregated within the water column by hydrodynamic processes: fast-settling coarse and heavy minerals concentrate in bedloads while fine, platy and light minerals are preferentially transported in suspension, at different depth in the water column depending on their settling velocities (Komar, 2007; Garzanti et al., 2008). Because chemical elements are carried in different amounts by the various minerals, it is now well recognized that mineral sorting processes lead to large chemical variability between bedload and suspended load sediments (Garzanti et al., 2010; Bouchez et al., 2011; Garzanti et al., 2011; Lupker et al., 2011; 2012). In contrast, our knowledge of how such processes affect the Nd, Hf, Sr and Pb isotopic compositions of sediments is relatively limited. While several studies pointed out the existence of Nd, Hf and Sr isotopic fractionations between fine and coarse-grained sediments due to mineral sorting processes (Patchett et al., 1984; McLennan et al., 1989; Revel et al., 1996; Eisenhauer et al., 1999; Chauvel et al., 2008; Bayon et al., 2009; Carpentier et al., 2009; Chauvel et al., 2009; Vervoort et al., 2011), the influence of each mineral species on the isotopic composition of sediments has never been thoroughly quantified.

In this paper, we report trace element contents and Nd, Hf, Sr and Pb isotopic compositions for a large number of pure mineral fractions separated from two bedloads sampled at the outflow of the Ganga fluvial system in the Bangladesh delta. Using Monte-Carlo simulations, we combine these data with mineral proportions estimated by Garzanti et al. (2010; 2011) in river sediments sampled at the same location to (1) evaluate the individual contribution of each mineral species to the Nd, Hf, Sr and Pb isotopic budgets of bedloads and suspended loads and (2) determine if the known mineralogy of bedloads and suspended

loads accounts for the observed difference in isotopic compositions. Finally, we discuss the implications of our results for sediment provenance studies based on isotope data and for large-scale isotopic partitioning between continental and oceanic sediments.

2. Studied Area and Samples

The studied mineral fractions were separated from two bedload sediments (BGP 6 and BR 717) sampled at the outflow of the Ganga River, before the confluence with the Brahmaputra River (Figure 1). The sampling site was selected because it is located downstream, far away from the mountain range. As a consequence, the sediments integrate all materials transported by the Ganga River and its tributaries. These rivers belong to one of the largest fluvial system on Earth (Milliman and Meade, 1983) that stretches over more than 2500 km and deliver several hundred millions tons of sediments to the ocean each year (Lupker et al., 2011). Such sediments contain the erosion products of a large area in the Himalayan mountain range (Galy and France-Lanord, 2001; Lupker et al., 2011), which mainly consists of sedimentary, crystalline and metamorphic rocks (Le Fort, 1975). Because of the large lithological and chemical diversity of Himalayan rocks, the Ganga basin can be considered as a representative portion of the upper continental crust. All minerals analyzed in our study are thus ubiquitous in the erosion products of any upper continental crust exposed to weathering (McLennan, 1989; Taylor and McLennan, 1995; McLennan, 2001) and our results should be relevant for river sediments sampled in other worldwide fluvial systems draining large continental areas.

The second major advantage of the selected site is that these sediments were extensively studied for their mineralogy by Garzanti et al. (2010; 2011) (Supplementary Table 1). These authors showed that bedloads and suspended loads share quite similar type of minerals but in different proportions. Surface suspended loads are generally finer and relatively rich in micas and clays while bedloads tend to be coarser and richer in quartz and heavy minerals. Among all of the heavy minerals that are commonly found in the Ganga sediments, amphibole, epidote and garnet are the most abundant but there are also many others: titanite, zircon, rutile, apatite, monazite, tourmaline and allanite for example (Garzanti et al., 2010; 2011). Mineral proportions as estimated by Garzanti et al. (2010; 2011) in the Ganga bedloads and suspended loads are provided in Supplementary Table 1.

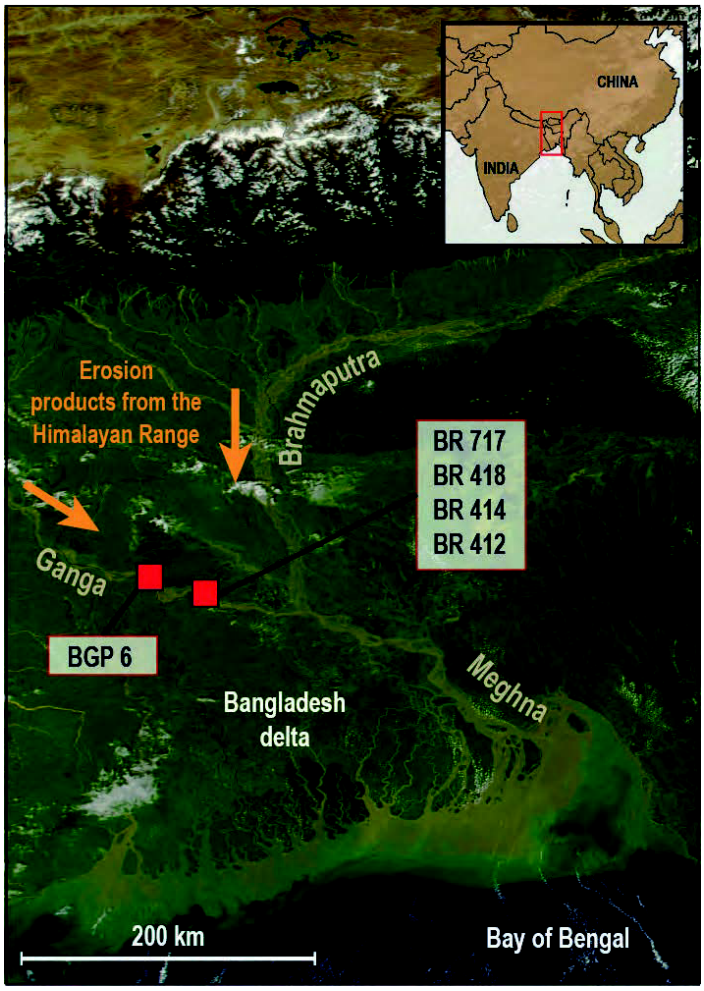

Figure 1: Map of the Bangladesh delta showing sampling sites for river sediments analyzed in this study.

Finally, several studies already reported major and trace element contents as well as Nd, Hf and Pb isotopic compositions of bulk suspended loads and bedloads from this sampling site (Galy and France-Lanord, 2001; Lupker et al., 2011; Garçon et al. 2012a; 2012b; Lupker et al., 2012). These data are absolutely necessary to evaluate the role of individual minerals in the bulk isotopic budget of river sediments. Because no Sr isotopic data exist in the literature for unleached bedloads and suspended loads, we analyzed the bulk Sr isotopic compositions of 3 bedloads (BR 717, BGP 6 and BR 418) and 2 suspended loads (BR 414 and BR 412) sampled in the Bangladesh delta (Figure 1). The major and trace element data, the Nd, Hf and Pb isotopic compositions and the sampling strategy for these samples can be found in Galy and France-Lanord (2001), Lupker et al. (2011; 2012) and Garçon et al. (2012a; 2012b).

3. Methods

3.1. Mineral separation

The starting material consists in several kilos of sediment collected during the monsoon season with a stainless steel tube dropped at the riverbed from a boat. With the exception of the clay fraction, all mineral fractions were separated from bedload BR 717. The sample was first washed and dried, then divided into 3 grain-size fractions by sieving: 63-100 µm, 125-250 µm, >250 µm. For each fraction, we used successive centrifugations in heavy liquids (sodium metatungstate and methylene iodide) to separate minerals and partial freezing in liquid nitrogen to recover them. After this step, some of the minerals were isolated using a hand magnet or the Frantz isodynamic magnet separator. Biotite, muscovite, plagioclase, quartz and K-feldspar were isolated from the >250 µm fraction; magnetite, amphibole, apatite, garnet, epidote, titanite monazite, allanite and zircon from the 63-100 µm and/or the 125-250 µm fractions. Each mineral fraction was finally carefully purified under the binocular and polarizing microscopes to remove impurities.

Because monazite and allanite were very small and too difficult to distinguish from each other, we analyzed an impure fraction containing high amounts of both minerals. In the rest of the paper, this fraction is called the “monazite/allanite fraction”. Similarly, we could not remove all impurities in the apatite fraction; hence we analyzed an impure fraction highly enriched in apatite. Following Galy et al. (1999), the composition of the carbonate fraction was obtained using a 1N acetic acid leaching procedure for one hour in an ultrasonic bath. To insure a pure carbonate fraction and avoid dissolution of other minerals or contamination by clay minerals, we leached a coarse fraction containing only carbonate, quartz, K-feldspar, plagioclase and few phyllosilicates (non-magnetic 125-250 µm fraction with a density < 2.90 $g.cm^{-3}$). The carbonate-rich leachate was then isolated by centrifugation and evaporated on a hot plate. Finally, a clay fraction, selected as the <2 µm fraction, was separated by sieving from bedload BGP 6 because we lacked material to recover it from beldload BR 717.

3.2. Chemistry

For each mineral separate, we performed a single dissolution used to analyze both trace element concentrations and Nd, Hf and Sr isotopes. Note that Pb isotopes have

already been published by Garçon et al. (2012b). Methods used to obtain Pb data are described in this latter paper.

After washing with ultrapure water, 5 to 100 mg of mineral grains or powder were first attacked for 2 days in HNO_3 14N on a hot plate at 130°C, then evaporated and dissolved in a mixture of HF and $HClO_4$ in teflon containers placed in steel PARR bombs for 10 days at 200°C to ensure complete dissolution. For bulk bedloads and suspended loads, 50 to 100 mg of fine powder were dissolved using the same procedure as for the mineral fractions.

We measured trace element concentrations by ICPMS with a dilution factor of 5000 and the equivalent of 2mg of sample. Measurements were performed using an Agilent 7500ce ICP-MS in Grenoble (France). Oxide interference and analytical drift were corrected following the procedure of Chauvel et al. (2011). BR-24 rock standards were measured every four samples to calibrate and convert peak signals into concentrations offline. To ensure the validity of our results international rock standards were run as unknown samples, including sedimentary materials such as JSd-2.

Hf, Nd and Sr were isolated from the same aliquot using the ion resin technique and following the procedure described by Chauvel et al. (2011). Total procedural blanks were < 80 pg for Nd (n=1), < 35 pg for Hf (n=2) and < 140 pg for Sr (n=2). These small amounts can be considered negligible compared to the amount of Nd, Hf and Sr isolated in all samples. Nd and Hf isotopes were measured on a Nu Plasma MC-ICP-MS at the ENS Lyon (France). Nd isotopic compositions were normalized to $^{146}Nd/^{144}Nd=0.7219$ and Hf isotopic compositions to $^{179}Hf/^{177}Hf=0.7325$. The Ames-Rennes Nd and Ames-Grenoble Hf reference standards run every two or three samples yielded average $^{143}Nd/^{144}Nd = 0.511953 \pm 8$ (2σ, n = 15) and $^{176}Hf/^{177}Hf = 0.282157 \pm 18$ (2σ, n = 14), respectively. We used the recommended values published by Chauvel and Blichert-Toft (2001) and Chauvel et al. (2011) for these two standards to correct the analytical drift all through the measurement sequence. Sr isotopic compositions were measured using a solid source Thermo Scientist Triton mass spectrometer in Brest (France) and normalized to $^{86}Sr/^{88}Sr=0.1194$. The NBS 987 reference material yielded average $^{87}Sr/^{86}Sr = 0.710270 \pm 7$ (2σ, n = 10).

4. Results

4.1. Trace element concentrations

Trace element concentrations measured in the mineral fractions are reported in Table 1 and shown in Figure 2 as spidergrams normalized to the average composition of upper continental crust (Rudnick and Gao, 2003). Except for mobile elements such as Cs, Rb, Ba, Sr, Li, Co or Ni, heavy minerals (Figure 2a) generally display higher trace element contents than light minerals (Figure 2b). The trace element pattern of the various minerals are generally consistent with published values (Götze and Lewis, 1994; Bea, 1996; Garçon et al., 2011; Garzanti et al., 2011). Zircon and garnet show typical depletions in light REE while monazite/allanite shows depletion in heavy REE. The REE distributions of other minerals, including light minerals, are rather flat. The monazite/allanite and zircon separates clearly exhibit the highest concentrations in Nd and Hf, respectively, with enrichment factors > 1000 (see Figure 2). The highest Pb contents are found in clay (95 ppm) and K-feldspar (75 ppm). The highest Sr concentrations are found in epidote (1509 ppm), carbonate (526 ppm), K-feldspar (243 ppm) and plagioclase (195 ppm). Both apatite and monazite/allanite fractions display relatively high concentrations in Nb, Ta, Zr and Hf, a feature probably due to the presence in both mineral separates of other minerals such as epidote, titanite or zircon. This can easily be explained by the fact that we were enable to carefully purified the apatite and monazite/allanite fractions under the binocular microscope due to the very small size of the minerals.

4.2. Isotopic compositions

Nd, Hf and Sr isotopic compositions measured for all mineral separates are reported in Table 1. Because of the extremely low Nd, Hf and Sr concentrations associated to the small amount of crystals that could be handpicked, no isotopic data could be obtained for the quartz fraction. Similarly, no Hf isotopic composition could be measured for the carbonate fraction. We also did not measure Hf and Sr isotopes in the monazite/allanite-rich fraction and the apatite-rich separate because the obvious presence of other minerals in both separates could strongly influence the measured Hf and Sr isotopic compositions.

Sample Name	BR 717 Msc	BR 717 Bio	BR 717 Fd-K	BR 717 Fd-K Dup	BR 717 Plg	BR 717 Qtz	BR 717Mag	BR 717 Ep	BR 717 Grt	BR 717 Ttn
Type of mineral	*Muscovite*	*Biotite*	*K-Felspar*	*K-Felspar (Duplicate)*	*Plagioclase*	*Quartz*	*Magnetite*	*Epidote*	*Garnet*	*Titanite*
Cs	15.4	69.9	8.94		0.838	0.209	0.579	0.267	0.153	0.557
Rb	311	425	313		31.1	3.34	7.37	2.54	1.50	9.73
Ba	967	478	1393		146	19.8	33.0	14.9	3.49	39.9
Th	4.58	24.9	4.10		2.37	2.91	13.7	17.8	15.6	151
U	1.54	2.36	0.663		0.692	0.83	3.61	6.49	3.49	50.1
Nb	36.1	87.3	0.992		1.39	0.581	20.8	3.69	3.25	229
Ta	2.78	9.58	0.112		0.106	0.0304	1.66	0.267	0.42	31.0
La	9.99	60.9	4.41		3.74	5.23	19.8	62.2	40.4	172
Ce	27.5	110	14.3		14.4	11.3	41.1	134	91.0	527
Pr	2.34	10.2	1.07		0.933	1.29	4.58	17.2	9.79	93.1
Pb	11.1	4.96	75.1		12.6	3.89	19.1	46.9	0.916	5.52
Nd	8.29	32.0	3.77		3.57	4.59	16.6	71.8	34.5	414
Sr	32.3	7.01	243		195	70.6	11.8	1509	3.31	52.9
Sm	1.57	4.77	0.837		0.684	1.04	3.17	17.6	7.83	105
Zr	210	264	21.9		94.4	22.1	265	183	251	2128
Hf	5.70	7.30	0.658		2.56	0.749	7.01	4.76	6.95	72.8
Ti	4898	16573	185		273	71.4	17180	2706	770	32279
Eu	0.253	0.416	0.744		0.30	0.176	0.54	5.75	1.01	19.4
Gd	1.25	3.41	0.733		0.585	0.921	2.74	18.2	16.4	100
Tb	0.185	0.462	0.118		0.0907	0.155	0.46	2.94	5.95	17.4
Dy	1.14	2.59	0.658		0.537	1.01	2.86	18.6	60.9	113
Ho	0.226	0.474	0.127		0.108	0.214	0.612	3.78	15.7	22.0
Y	6.49	13.6	3.77		3.39	6.65	17.0	110	379	536
Er	0.677	1.32	0.345		0.335	0.645	1.83	10.6	52.0	62.7
Li	24.6	334	11.8		0.461	5.96	3.69	3.42	14.3	8.78
Yb	0.685	1.22	0.322		0.381	0.587	1.92	9.61	58.0	58.9
Lu	0.108	0.192	0.0478		0.062	0.0861	0.296	1.39	8.54	7.91
Sc	13.3	27.3	0.655		0.917	0.299	8.14	90.1	102	33.8
V	171	243	1.89		6.86	8.08	1281	414	54.4	139
Cr	91.3	144	2.74		5.13	3.34	1950	131	76.1	44.8
Co	2.76	47.9	0.691		0.907	0.269	51.0	2.69	23.8	0.683
Ni	6.39	79.7	2.77		3.62	0.464	170	6.34	1.55	3.28
$^{143}Nd/^{144}Nd \pm 2\sigma$	0.511844 ± 15	0.511834 ± 11	0.511834 ± 19		0.511901 ± 33		0.512089 ± 9	0.512235 ± 10	0.511906 ± 11	0.512182 ± 9
Re-run		0.511820 ± 9								
$^{176}Hf/^{177}Hf \pm 2\sigma$	0.282218 ± 9	0.282162 ± 11	0.282400 ± 15	0.282313 ± 15	0.282325 ± 9		0.282602 ± 8	0.282803 ± 12	0.282698 ± 5	0.282055 ± 16
Re-run										0.282077 ± 8
$^{87}Sr/^{86}Sr \pm 2\sigma$	0.831306 ± 10	0.812332 ± 8	0.758656 ± 8	0.755512 ± 7	0.722744 ± 8		0.728827 ± 7	0.712509 ± 7	0.746224 ± 28	0.722704 ± 7
$^{206}Pb/^{204}Pb \pm 2\sigma$ *	20.2008 ± 16	20.5508 ± 26	19.3257 ± 16	19.3318 ± 12	18.9724 ± 18		19.5343 ± 14	18.9028 ± 14		31.4562 ± 22

Table 1: Trace element concentrations and Nd-Hf-Sr-Pb isotopes for the mineral fractions

Sample Name	BR 717 Amp	BR 717 Carb	BR 717 Zrn	BR 717 Mnz	BR 717 Ap	BGP 6 A
Type of mineral	*Amphibole*	*Carbonate*	*Zircon*	*Rich in Monazite and Allanite*	*Rich in Apatite*	*Clay*
Cs	1.80	0.00913	0.214	0.935	0.504	17.0
Rb	23.3	0.846	3.03	12.0	9.16	167
Ba	60.2	16.6	7.01	71.3	427	373
Th	24.0	1.17	219	2374	28.8	62.0
U	7.40	0.522	612	400	28.9	8.55
Nb	403	< DL	171	1068	119	16.7
Ta	43.5	0.013	17.9	162	8.24	1.49
La	32.6	6.89	32.8	3763	71.1	103
Ce	71.6	14.7	113	7785	206	206
Pr	8.76	1.95	16.3	883	30.3	24.3
Pb	24.1	7.28	19.3	81.9	7.98	95.2
Nd	34.1	8.25	79.6	3180	146	90.5
Sr	38.4	526	16.9	274	197	47.9
Sm	7.88	2.07	32.7	670	54.0	17.3
Zr	539	< DL	416415	20849	4240	447
Hf	15.5	< DL	10171	639	119	12.2
Ti	168099	2.29	41321	107327	18799	6416
Eu	1.73	0.523	7.19	59.8	6.20	2.70
Gd	8.96	2.37	65.1	494	74.3	14.3
Tb	1.78	0.414	17.8	61.5	14.1	2.02
Dy	13.3	2.59	178	310	88.5	11.4
Ho	2.83	0.577	55.7	52.5	16.2	2.12
Y	86.1	19.4	1463	1148	432	58.0
Er	8.42	1.76	243	140	42.3	5.84
Li	26.2	0.889	15.7	19.8	13.3	40.8
Yb	8.50	1.82	424	140	33.3	5.21
Lu	1.22	0.283	83.5	21.3	4.47	0.736
Sc	44.8	1.95	3225	211	32.9	19.7
V	943	< DL	99.2	408	128	220
Cr	197	2.00	70.7	236	81.1	143
Co	44.6	0.956	0.443	2.83	1.25	27.3
Ni	35.6	1.40	3.86	4.74	2.50	99.0
$^{143}Nd/^{144}Nd \pm 2\sigma$	0.511929 ± 24	0.511843 ± 10	0.512062 ± 10	0.511732 ± 8	0.511921 ± 7	0.511827 ± 10
Re-run				0.511741 ± 6		
$^{176}Hf/^{177}Hf \pm 2\sigma$	0.282236 ± 8		0.281970 ± 5			0.282234 ± 8
Re-run			0.281979 ± 4			
$^{87}Sr/^{86}Sr \pm 2\sigma$	0.725748 ± 8	0.713942 ± 8	0.734440 ± 20			0.746642 ± 8
$^{206}Pb/^{204}Pb \pm 2\sigma$ *	19.9482 ± 12	18.9809 ± 8	2180 **			18.8658 ± 12

Table 1 (continued): Trace element concentrations and Nd-Hf-Sr-Pb isotopes for the mineral fractions.
±2σ are in-run errors.
* Data already published by Garçon et al. (2012b)
** Estimated using zircon-rich fractions, see Garçon et al. (2012b) for further details

Nd, Hf and Sr isotopic compositions span large ranges of values between 0.511732 and 0.512235 for $^{143}Nd/^{144}Nd$ ratios, 0.281970 and 0.282803 for $^{176}Hf/^{177}Hf$ ratios and 0.712509 and 0.831306 for $^{87}Sr/^{86}Sr$ ratios. The monazite/allanite fraction has the lowest Nd isotopic composition of all minerals while the zircon separate has the lowest Hf isotopic composition of all. Biotite and muscovite, known for their very high Rb/Sr ratios, have accordingly highly radiogenic Sr isotopes (0.812332 and 0.831306, respectively). By

contrast, epidote and carbonate have the least radiogenic Sr isotopic compositions (0.712509 and 0.713942) of all minerals.

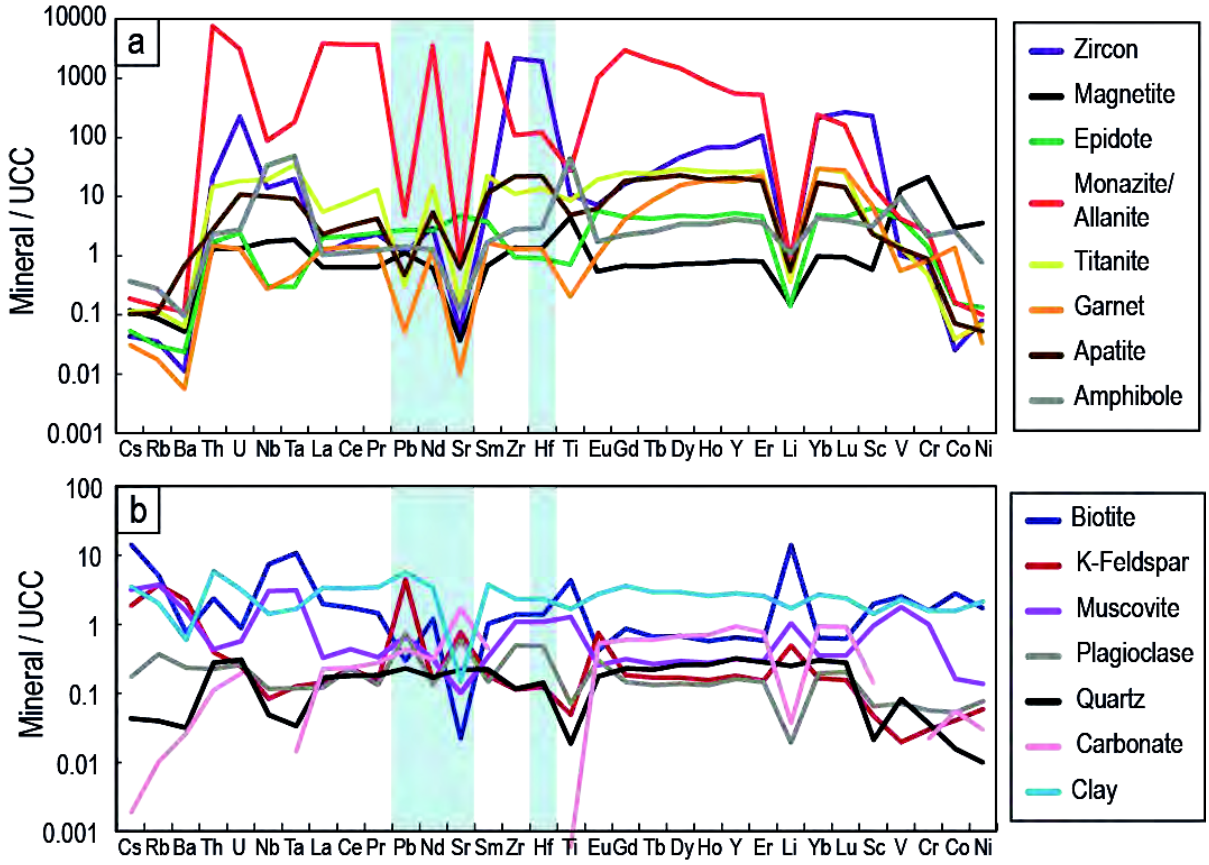

Figure 2: Trace element patterns normalized to the average composition of the upper continental crust (UCC) of Rudnick and Gao (2003).
a. Heavy minerals **b.** Light minerals

Sr isotopic compositions measured in bulk bedloads and suspended loads from the Ganga River are listed in Table 2. They are particularly radiogenic and vary between 0.754593 and 0.773743, with the bedloads tending to have less radiogenic Sr isotopes than suspended loads. These results fall in the large range of Sr isotopes usually measured in the silicate and/or carbonate fractions isolated from Himalayan derived sediments (Harris et al., 1998; Galy et al., 1999; Galy and France-Lanord, 2001; Pierson-Wickmann et al., 2001; Singh et al., 2008). Note that such highly radiogenic isotopic compositions are explained by the remobilization of radiogenic Sr from Rb-rich micas into more weatherable minerals such

as feldspars due to high-grade metamorphism during the Himalayan orogenesis (Edmond, 1992).

Sample Name	Latitude	Longitude	Sampling date	Type of sediment	Sampling depth (m)	$^{86}Sr/^{87}Sr$	± 2σ
BGP 6	24.35833	88.60833	2-Aug-93	Bedload		0.758885	8
BR 414	24.05290	89.02465	13-Jul-04	Suspended Load	2	0.773743	8
BR 412	24.05290	89.02465	13-Jul-04	Suspended Load	6.5	0.768185	12
BR 418	24.05290	89.02465	13-Jul-04	Bedload	10	0.754593	8
BR 717	24.05290	89.02465	17-Aug-07	Bedload	11	0.757160	8

Table 2: Sr isotopes of bedloads and suspended loads sampled at the outflow of the Ganga River
±2σ are in-run errors.

5. Discussion

River sediments are basically mixtures of mineral species. Some minerals, such as quartz, contain virtually no trace elements and their proportion in the sedimentary material influences only the silica content of the sediment but has no impact on most isotopic ratios. In contrast, other minerals very rich in certain trace elements or with very unusual isotopic compositions have the potential to significantly contribute or can even overwhelm the trace element and isotopic budget of river sediments even if they are present in very low proportions. A proper understanding of the role of individual mineral species in the isotopic budget of river sediments thus requires the consideration of several parameters. These include the nature and the proportion of the different mineral species, as well as their trace element concentration and their isotopic composition.

Here, we present Monte-Carlo simulations that quantitatively evaluate the role of individual minerals in the final Nd, Hf, Sr and Pb isotopic budget of river sediments. We simulate the composition of a hundred thousand mixtures between common mineral species that are present in the sedimentary material and that have the potential to significantly influence its isotopic compositions (cf. Supplementary File). Then, we compare our results to the data published on bulk sediments.

Using mineral proportions estimated by Garzanti et al. (2010; 2011) in suspended loads and bedloads sampled in the Bangladesh delta, we first defined a range of possible proportions for each type of mineral (see Supplementary File). For each mineral species, we then randomly sample proportions within this range and associate them with the Nd, Hf, Sr or Pb concentrations and isotopic compositions measured in our mineral separates. Finally, we calculate the isotopic compositions of the resulting mixtures using the following equation, written here for the Nd isotopic system:

$$\left(\frac{^{143}Nd}{^{144}Nd}\right)_{mixture} = \sum_{i=1}^{n}\left[x_i \cdot \frac{C_{Nd,\,i}}{C_{Nd,\,mixture}} \cdot \left(\frac{^{143}Nd}{^{144}Nd}\right)_i\right]$$

where n is the number of minerals involved in the mixture; x_i the weight proportion of mineral i sampled randomly in its defined range; $C_{Nd,i}$ and $\left(\frac{^{143}Nd}{^{144}Nd}\right)_i$ the Nd content and the Nd isotopic composition of mineral i (see Table 1); and $C_{Nd,\,mixture} = \sum_{i=1}^{n}\left[x_i \cdot C_{Nd,\,i}\right]$, the Nd concentration of the mixture.

In the following sections, we compare the modeled Nd, Hf, Sr and Pb isotopic compositions to those measured in both suspended load and bedload sediments as sampled in the Bangladesh delta (data from the literature and our Sr isotope measurements). Using such approach, we can evaluate the role of each mineral in the isotopic budget of all river sediments. We illustrate the results of our Monte-Carlo simulations for each isotopic system in diagrams that show the contribution of the various mineral species as a function of the modeled isotopic composition for all mixtures. The contribution of each mineral i is determined in percentage using the following equation:

$$\text{Mineral contribution} = 100 \cdot x_i \cdot \frac{C_{Nd,\,i}}{C_{Nd,\,mixture}} \cdot \left(\frac{^{143}Nd}{^{144}Nd}\right)_i \Big/ \left(\frac{^{143}Nd}{^{144}Nd}\right)_{mixture}$$

More details on the input parameters and the way simulations were performed can be found in the Supplementary File.

5.1. Which minerals control Nd isotopes of river sediments?

To perform a Monte-Carlo simulation modeling Nd isotopic compositions, we considered the 14 analyzed minerals (K-feldspars, plagioclase, muscovite, biotite, magnetite, zircon, titanite, apatite, monazite/allanite, amphibole, epidote, garnet, carbonate and clay) and we set the mineral proportions within the range known for river sediments sampled in the Bangladesh delta (see Supplementary File and inset in Figure 3). Results are shown in Figure 3.

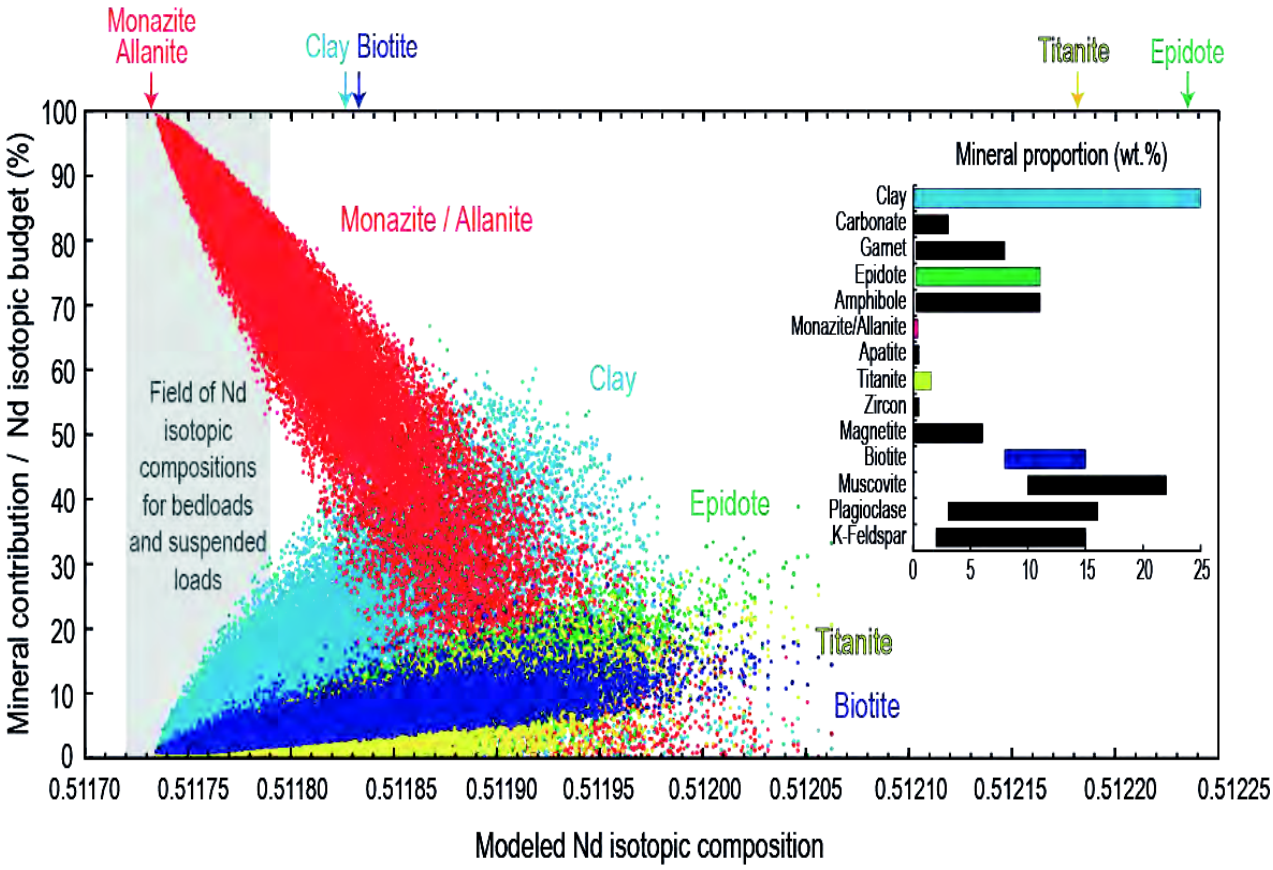

Figure 3: Results of the Monte-carlo simulation for Nd isotopes.
Proportions of minerals used to perform the Monte-carlo simulation are shown in the histogram in the top right corner of the Figure (see Supplementary File for more details). Color dots indicate the contributions of the different minerals to the Nd isotopic compositions of the 100,000 modeled mixings. The contributions of carbonate, garnet, amphibole, apatite, zircon, magnetite, muscovite, plagioclase and K-feldspar are not shown in this Figure because they are lesser than 10% over the whole range of modeled Nd isotopic compositions. The vertical gray field shows the range of Nd isotopic compositions measured in bedloads and suspended loads sampled at the outflow of the Ganga River and was constructed using the data of Garçon et al. (2012a). Arrows on the top axis indicate isotopic compositions of important minerals.

The first important observation is that minerals that significantly contribute to the Nd isotopic budget are very few: monazite/allanite, clay, epidote, titanite and biotite. All other minerals (K-feldspars, plagioclase, muscovite, magnetite, zircon, apatite, amphibole, garnet and carbonate) always contribute to less than 10% of the isotopic budget, over the entire range of modeled Nd isotopic compositions; this is why they are not shown in Figure 3. Because of its extreme enrichment in Nd (Figure 2), the monazite/allanite fraction entirely dominates the Nd isotopic budget of modeled mixtures and it can even control 100% of the isotopic budget (Figure 3) while its proportion in the mineral assemblage never exceeds 0.4 wt.% (see Supplementary File and inset of Figure 3). It is only when the modeled Nd isotopic composition is greater than 0.51185 that the contribution of clay, epidote, titanite and biotite starts being significant (Figure 3).

As shown by the grey field in Figure 3, Nd isotopes reported for bedloads and suspended loads sampled at the outflow of the Ganga River span a limited range of values between 0.51172 and 0.51179 (Garçon et al. 2012a), values similar to those reported by Galy and France-Lanord (2001) for sediments sampled at the same location. According to our Monte-carlo simulation (Figure 3), such compositions correspond to mixtures highly dominated by monazite and allanite (60-100%) with a small but significant contribution from clays (0-30%). We can therefore suggest that the few monazite and allanite present in the sediments (0-0.4 wt%, see Supplementary File) totally overwhelm the Nd isotopic compositions of river sediments in the Bangladesh delta.

In a more classical diagram showing $^{143}Nd/^{144}Nd$ ratios as a function of $^{147}Sm/^{144}Nd$ ratios (Figure 4), it becomes even more obvious that the unradiogenic Nd signature of the monazite/allanite fraction is absolutely necessary to account for the composition of the Ganga sediments since no other mineral has a Nd isotopic composition similar to or lower than the bulk sediments. As suggested by our Monte-carlo simulation, both bedloads and suspended loads are well reproduced by a mixture of monazite, allanite, clay ± biotite (Figure 4).

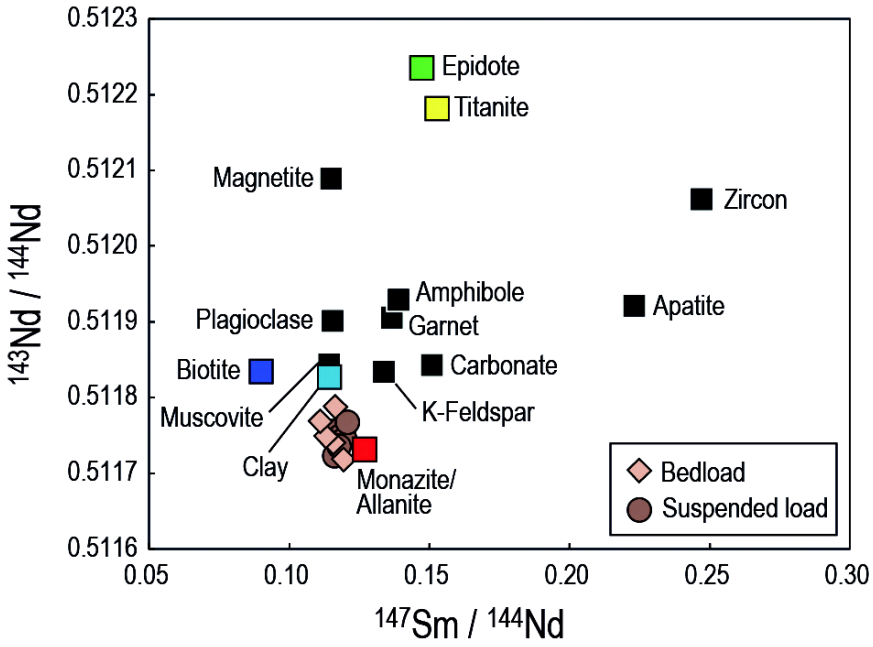

Figure 4: Variations of $^{143}Nd/^{144}Nd$ ratios against $^{147}Sm/^{144}Nd$ ratios for the different mineral fractions.
Bedloads and suspended loads shown in this Figure were sampled at the outflow of the Ganga River. Data are from Garçon et al. (2012a).

5.2. Which minerals control Hf isotopes of river sediments?

The results of the Monte-Carlo simulation for Hf isotopes are shown in Figure 5. Eleven minerals were introduced in the simulation: K-feldspar, plagioclase, muscovite, biotite, magnetite, zircon, titanite, amphibole, epidote, garnet and clay. Quartz and carbonates were ignored because they do not contain any Hf and we did not measure their Hf isotopic compositions. The two impure fractions, rich in monazite and apatite, were also ignored because they contain a lot of small zircons, a feature that explains their high Hf concentrations. We are convinced that if we had measured their Hf isotopic compositions, the results would not have been representative of the composition of the monazite or the apatite but would have reflected that of the zircons present in the fractions.

As for Nd isotopes, only few minerals significantly contribute to the Hf isotopic budget of the modeled mixtures: zircon, clay, amphibole, muscovite, biotite and titanite. By contrast, garnet, epidote, magnetite, plagioclase and K-feldspar contribute to less than 10% of the Hf isotopic budget and are not shown in Figure 5. Modeled Hf isotopic compositions span a relatively large range of values between 0.28197 and 0.28235. One of the most remarkable features is that unradiogenic Hf-rich zircon totally buffers the Hf isotopic budget over a large

range of isotopic compositions (Figure 5) while its proportion in the mineral assemblage is always less than 0.5 wt% (see Supplementary File and inset of Figure 5). Clay is the second important mineral but its contribution never exceeds 45%. Together with amphibole, muscovite, biotite and titanite, the clay fraction accounts for the most radiogenic Hf isotopic compositions in the simulation.

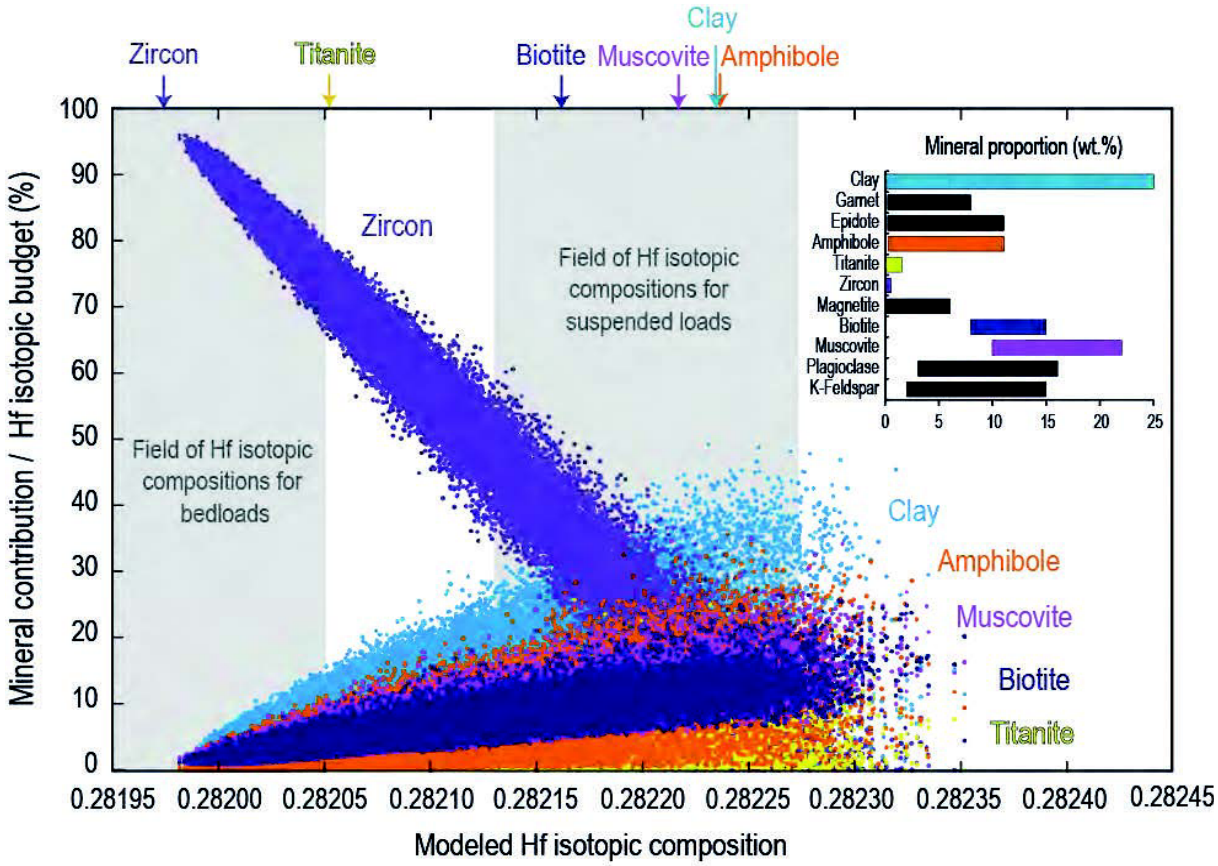

Figure 5: Results of the Monte-carlo simulation for Hf isotopes.
Proportions of minerals used to perform the Monte-carlo simulation are shown in the histogram in the top right corner of the Figure (see Supplementary File for more details). Color dots indicate the contributions of the different minerals to the Hf isotopic compositions of the 100,000 modeled mixings. The contributions of garnet, epidote, magnetite, plagioclase and K-feldspar are not shown in this Figure because they are lesser than 10% over the whole range of modeled Hf isotopic compositions. Vertical gray fields show the range of Hf isotopic compositions measured in bedloads and suspended loads sampled at the outflow of the Ganga River and were constructed using the data of Garçon et al. (2012a). Arrows on the top axis indicate isotopic compositions of important minerals.

In contrast to Nd, there is a difference between the $^{176}Hf/^{177}Hf$ ratio of bedloads and suspended loads sampled at the outflow of the Ganga River (Garçon et al., 2012a). As

shown by grey fields in Figure 5, bedloads are less radiogenic than suspended loads. The results of our Monte-carlo simulation show that the difference is easily explained by different contributions of unradiogenic zircon. The range of $^{176}Hf/^{177}Hf$ measured in bedloads results from a very high contribution of zircon (i.e. 70-100% of their Hf isotopic budget) and the relative contribution of all other minerals remains always below 10%. The higher $^{176}Hf/^{177}Hf$ measured in suspended loads result of a higher contribution of more radiogenic minerals such as clay, amphibole, muscovite, biotite and titanite and a lower contribution of zircon, even if it can still contribute to up to 50% of the isotopic budget (Figure 5).

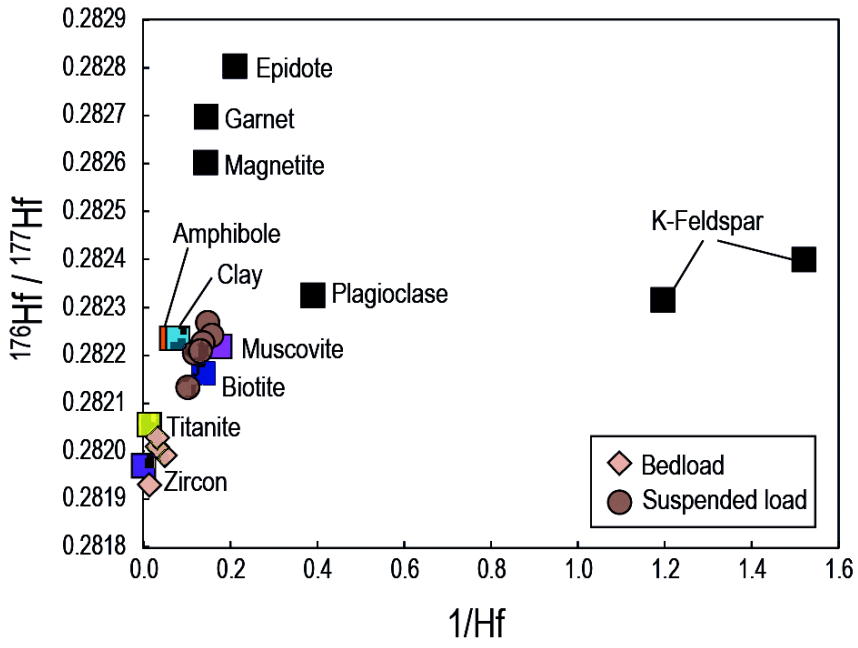

Figure 6: Variations of $^{176}Hf/^{177}Hf$ ratios against 1/Hf ratios for the different mineral fractions. Data for bedloads and suspended loads sampled at the outflow of the Ganga River are from Garçon et al. (2012a). 1/Hf ratios of river sediments have been recalculated on a quartz-free basis by normalizing their SiO_2 contents, as published by Lupker et al. (2011), to that of our clay fraction i.e. 43 wt%.

In Figure 6, we show the relationship between $^{176}Hf/^{177}Hf$ and 1/Hf for minerals, bedloads and suspended loads. In contrast to what we did for the Nd case, we chose to not represent Hf isotopic compositions as a function of their parent/daughter ratios (i.e. $^{176}Lu/^{177}Hf$ ratios) because Lu and Hf are not carried by the same minerals and it would introduce confusion when evaluating the role of individual minerals in the Hf isotopic compositions of sediments. We also normalized the 1/Hf ratio of all sediments to the SiO_2 content of the clay fraction, because dilution by variable amounts of quartz has a drastic

effect on the Hf concentration of river sediments (Lupker et al., 2011, see footnote of Figure 6 for more details). As highlighted by our Monte-Carlo simulations, Figure 6 shows clearly that all bedloads plot close to zircon, confirming that this mineral plays a predominant role in the Hf isotopic budget of bedloads. Figure 6 also shows that the composition of suspended loads requires a mixture of more radiogenic minerals such as biotite, muscovite, clay and amphibole together with less radiogenic titanite and zircon for some of them (Figure 6).

5.3. Which minerals control Sr isotopes of river sediments?

In Figure 7a, we show the modeled $^{87}Sr/^{86}Sr$ for mixing simulations between K-feldspar, plagioclase, muscovite, biotite, magnetite, zircon, titanite, amphibole, epidote, garnet, carbonate and clay. Six minerals (garnet, amphibole, titanite, zircon, magnetite and biotite) are not shown in the figure because they all are minor contributors (<10%) to the Sr isotopic budget. In contrast, because of their high Sr contents (Table 1), epidote, K-feldspar, plagioclase and, to a lesser extent, clay, carbonate and muscovite exert a major role on the $^{87}Sr/^{86}Sr$ of the modeled mixtures.

Using grey fields, we show the range of Sr isotopic compositions measured in bedloads and suspended loads in Figure 7 and their variations as a function of 1/Sr in Figure 8. Figure 7a demonstrates clearly that our Monte-Carlo simulation fails in reproducing the high $^{87}Sr/^{86}Sr$ of all sediments, in particular those of suspended loads. We can think of several reasons to explain this mismatch. The first possibility is that we miss a mineral with high $^{87}Sr/^{86}Sr$ and high Sr content in our Monte-Carlo procedure. Given their high Sr contents (Table 1), potential candidates are apatite, monazite/allanite and quartz. However, they all have low $^{87}Rb/^{86}Sr$ ratios, just like carbonate and epidote, which have the lowest $^{87}Sr/^{86}Sr$ (Figure 8). It seems thus unlikely that these phases could have the elevated $^{87}Sr/^{86}Sr$ that is required to explain the observed mismatch between model and measurements in Figure 7a. A second possibility is that one (or several) of the mineral phases with high Sr content has a $^{87}Sr/^{86}Sr$ ratio higher than the value that we measured. We suspect that it could be the case for K-feldspar and muscovite for the following reason: for convenience, we separated these two minerals from the coarsest fraction (>250 µm) of bedload BR 717 (see section 3.1) and we suspect that smaller minerals might have different isotopic compositions.

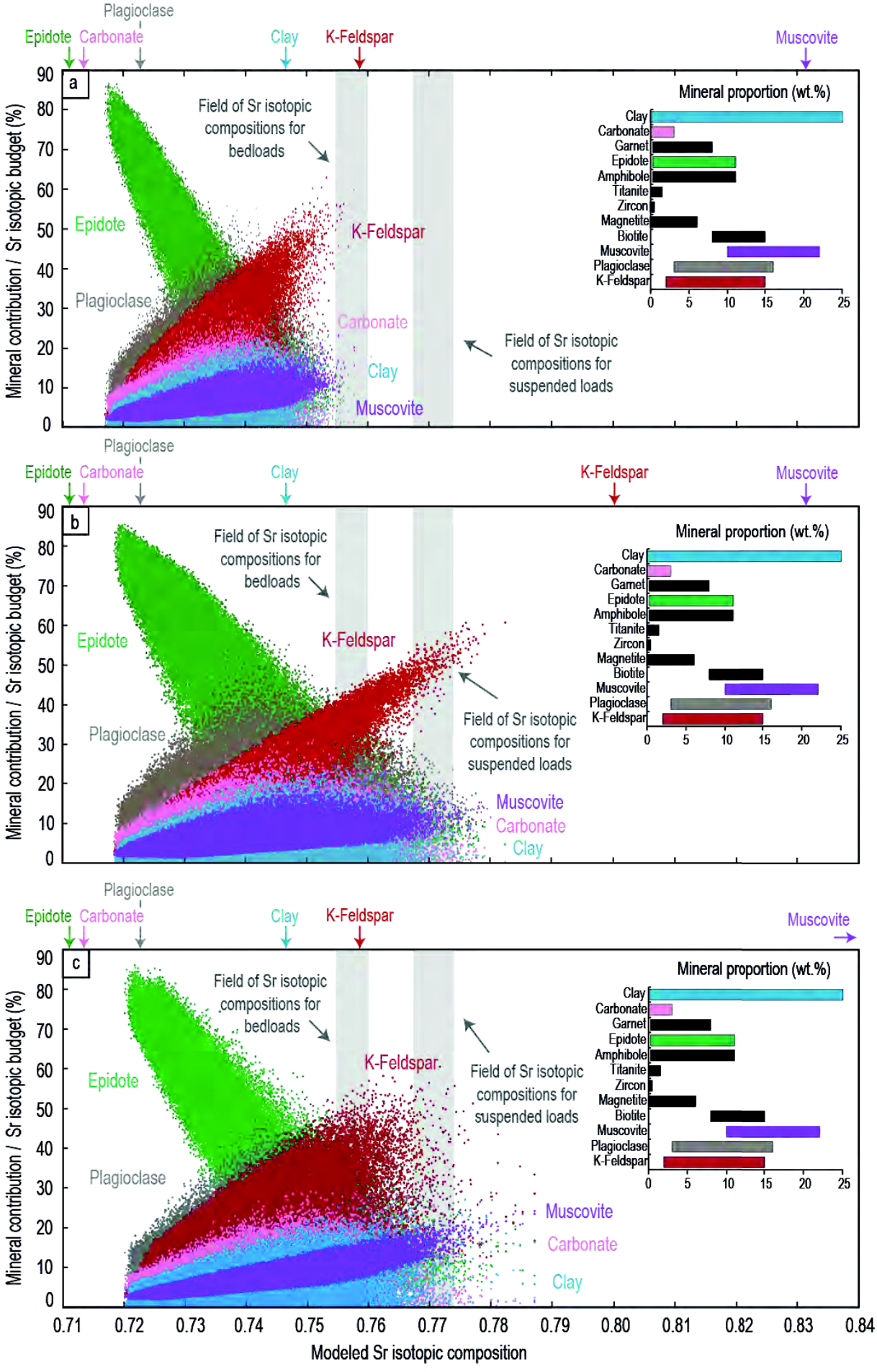
a
b
c
Plagioclase
Epidote
Carbonate
Clay
K-Feldspar
Muscovite
Mineral contribution / Sr isotopic budget (%)
Field of Sr isotopic compositions for bedloads
Field of Sr isotopic compositions for suspended loads
Mineral proportion (wt.%)
Clay
Carbonate
Garnet
Epidote
Amphibole
Titanite
Zircon
Magnetite
Biotite
Muscovite
Plagioclase
K-Feldspar
0 5 10 15 20 25
0 10 20 30 40 50 60 70 80 90
0.71 0.72 0.73 0.74 0.75 0.76 0.77 0.78 0.79 0.80 0.81 0.82 0.83 0.84
Modeled Sr isotopic composition

Figure 7: Results of the Monte-carlo simulation for Sr isotopes.
Proportions of minerals used to perform the Monte-carlo simulation are shown in the histograms in the top right corner of the Figures (see Supplementary File for more details). Color dots indicate the contributions of the different minerals to the Sr isotopic compositions of the 100,000 modeled mixings. The contributions of garnet, amphibole, titanite, zircon, magnetite and biotite are not shown in this Figure because they are lesser than 10% over the whole range of modeled Sr isotopic compositions. Vertical gray fields show the range of Sr isotopic compositions measured in bedloads and suspended loads sampled at the outflow of the Ganga River and analyzed in this study. **a.** Monte-carlo simulation performed using the Sr isotopic compositions as measured in our mineral fractions. **b.** Monte-carlo simulation performed using a $^{86}Sr/^{87}Sr$ ratio of 0.800 for the K-feldspar fraction. **c.** Monte-carlo simulation performed using a $^{86}Sr/^{87}Sr$ ratio of 1.000 for the muscovite fraction. Arrows on the top axis indicate isotopic compositions of important minerals for each simulation.

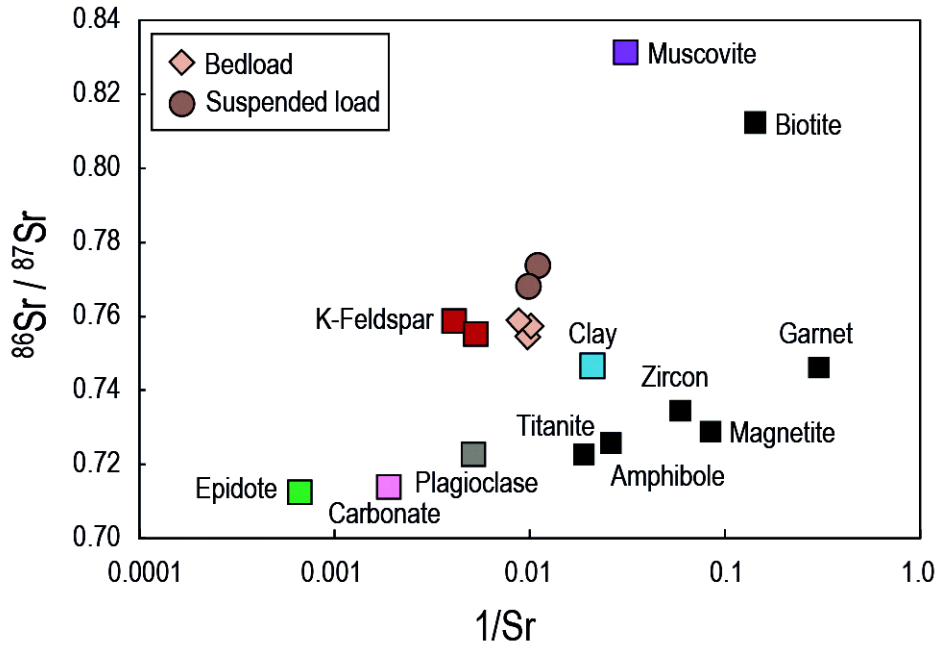

Figure 8: Variations of $^{86}Sr/^{87}Sr$ ratios against 1/Sr ratios (logarithmic scale) for the different mineral fractions and the river sediments analyzed in this study.

Indeed, large ranges of $^{87}Sr/^{86}Sr$ are reported for K-feldspar (0.737 to 0.801) and muscovite (0.765 to 8.353) in Himalayan crystalline rocks (Mehta, 1977; Kai, 1981; Ferrara et al., 1983; Deniel et al., 1987; Johnson and Rogers, 1997) and we believe that the coarse feldspar and muscovite that we isolated might have $^{87}Sr/^{86}Sr$ different from those present in fine suspended loads. We recognize that analyses of finer mineral fractions would help confirm our hypothesis but the separation and purification of a significant quantity of small mineral grains constitutes a difficult challenge. As an alternative, we perform two other Monte-Carlo

simulations, one using a $^{87}Sr/^{86}Sr$ ratio of 0.800 for K-feldspar (Figure 7b) or one using a $^{87}Sr/^{86}Sr$ ratio of 1.0 for muscovite (Figure 7c). In both cases, the mismatch between simulation and data disappears and the simulated mixtures overlap with the fields known for bedloads and suspended loads. Also in both cases, K-feldspar, carbonate, clay, plagioclase, epidote and muscovite control the Sr isotopic budget of sediments (Figure 7b and 7c) with a higher relative contribution of K-feldspar and/or muscovite in the suspended loads compared to bedloads.

5.4. Which minerals control Pb isotopes of river sediments?

To perform the Monte-Carlo simulation for Pb isotopes, we used the values published by Garçon et al. (2012b) but we list them for convenience in Table 1. The results obtained for $^{206}Pb/^{204}Pb$ ratios are shown in Figure 9. Six minerals (biotite, magnetite, titanite, amphibole, garnet and carbonate) always contribute to less than 10% to the Pb isotopic budget and are not shown in Figure 9. In contrast, six other minerals (clay, K-feldspar, epidote, muscovite, plagioclase and zircon) contribute significantly to the final composition. The modeled $^{206}Pb/^{204}Pb$ cover a very large range of values between 19 and 50, the highest values being associated to high contributions of zircon in the mixture (Figure 9). Indeed, if we perform a simulation without zircons, the modeled $^{206}Pb/^{204}Pb$ ratios only range between 19.0 and 19.8. This is because zircon is extremely radiogenic ($^{206}Pb/^{204}Pb$ ratio of about 2200, see Table 1), and even a minute amount of this Pb-poor mineral in the mixture (0-0.5wt%) significantly shifts the modeled Pb isotopic compositions towards very radiogenic values (Figure 9).

The ranges of $^{206}Pb/^{204}Pb$ measured for bedloads (20.6-22.2) and suspended loads (19.8-20.1) are shown using grey fields in Figure 9. Our results show that for both types of sediments, the Pb-rich clay and K-feldspar control up to 70% of the Pb isotopic budget while epidote, muscovite and plagioclase are other significant contributors. Our simulations also show that zircon plays a key role in increasing the Pb isotopic compositions of both bedloads and suspended loads. Indeed, if zircon were not present, the $^{206}Pb/^{204}Pb$ ratio of any mixture could not exceed 19.8, a value significantly lower than what is measured on both bedloads and suspended loads. This implies that the Pb isotopic budget of both bedloads and suspended loads are influenced by a zircon effect, with a stronger impact on bedloads than on suspended loads (see Figure 9 and Garçon et al. (2012b) for further discussion).

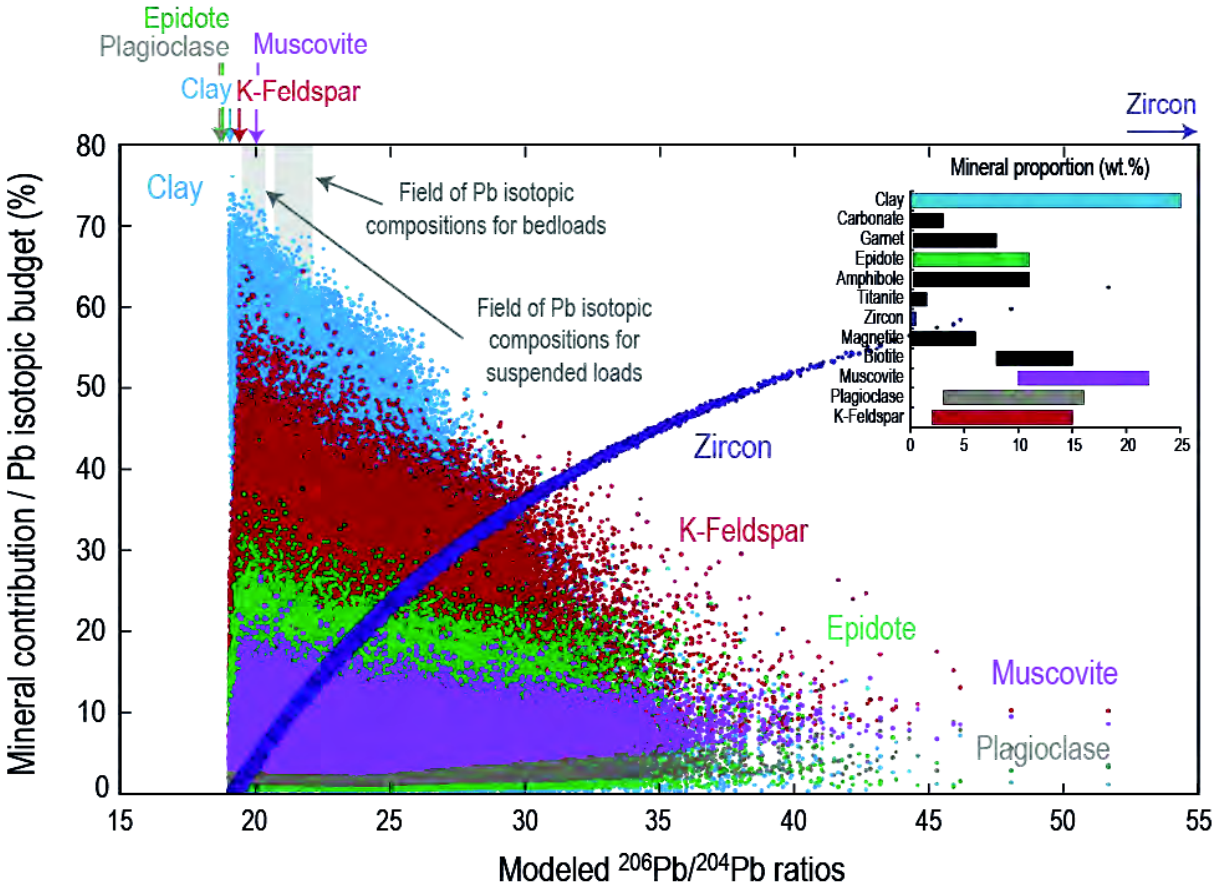

Figure 9: Results of the Monte-carlo simulation for Pb isotopes.
Proportions of minerals used to perform the Monte-carlo simulation are shown in the histograms in the top right corner of the Figures (see Supplementary File for more details). Color dots indicate the contributions of the different minerals to the Pb isotopic compositions of the 100,000 modeled mixings. The contributions of carbonate, garnet, amphibole, titanite, magnetite and biotite are not shown in this Figure because they are lesser than 10% over the whole range of modeled $^{206}Pb/^{204}Pb$ ratios. Vertical gray fields show the range of Pb isotopic compositions measured in bedloads and suspended loads sampled at the outflow of the Ganga River and were constructed using the data of Garçon et al. (2012b). Arrows on the top axis indicate isotopic compositions of important minerals for each simulation.

5.5. Geological implications

We showed above that the difference in Hf, Sr and Pb isotopic compositions between bedloads and suspended loads sampled at the same location are due to different mineral contributions that are ultimately controlled by mineral sorting processes within the water column. We now evaluate the implications of these results for (1) sediment provenance studies based on isotope data and (2) large-scale isotopic partitioning between continental and oceanic sediments.

5.5.1. Sediment provenance studies

Isotopic data are often used to trace changes through time of the source of sedimentary material. This is for example the case for numerous studies that focus on the relation between detrital material and changes of tectonic regimes and/or climate (Walter et al., 2000; Singh and France-Lanord, 2002; Gingele et al., 2007; Yan et al., 2007; Haley et al., 2008; Singh et al., 2008; Cina et al., 2009; Stumpf et al., 2011; Hu et al., 2012). It is also the case for studies focusing on the changes of ocean circulation through time (Revel et al., 1996; Innocent et al., 1997; Stille et al., 1997; Bayon et al., 2002; Frank, 2002; Goldstein and Hemming, 2003; Piotrowski et al., 2004; Gourlan et al., 2008; Haley et al., 2008; Ehlert et al., 2011) or for studies that attend to establish average isotopic compositions or ages for large areas of continental crust (Goldstein et al., 1984; Goldstein and Jacobsen, 1988; Asmerom and Jacobsen, 1993; Allègre et al., 1996; Millot et al., 2004; Kamber et al., 2005; Dhuime et al., 2011). It is therefore important to know which isotopic systems are robust tracers of source compositions and in which conditions.

Nd isotopes are certainly the most popular source tracer. Our study of bedloads, suspended loads and individual minerals clearly confirms that it is very robust. More specifically, we demonstrate that the isotopic budget of both suspended loads and bedloads is buffered by monazite and allanite even when present in extremely small proportions (< 0.4 wt.%) in the sediments. Both types of sediments can be used for provenance studies. We also confirm the conclusions presented by Garçon et al. (2011) who demonstrated that, in beach placers, monazite by itself was a good proxy to estimate the Nd isotopic composition of large continental areas. Analyses of populations of monazite grains or analyses of single grains could be an alternative to whole rock analyses.

Hf isotopic analysis of zircon grains is another very popular approach to trace source compositions (Bodet and Schärer, 2000; Davis et al., 2005; Harrison et al., 2005; Veevers et al., 2005; Flowerdew et al., 2006; Hawkesworth and Kemp, 2006; Kemp et al., 2007; Zeh et al., 2007; Belousova et al., 2010). Using the $^{176}Hf/^{177}Hf$ of bulk sediments as a source tracer of sedimentary material is definitively more tricky in view of the famous “zircon effect” highlighted by numerous previous studies (Patchett et al., 1984; Vervoort et al., 1999; Chauvel et al., 2008; Bayon et al., 2009; Carpentier et al., 2009; Vervoort et al., 2011). However, our study demonstrates and quantifies the fact that since zircon almost entirely controls the $^{176}Hf/^{177}Hf$ ratio of bedloads, these sediments can be used for source provenance studies. In contrast, suspended loads that are depleted in zircon and have their

Hf isotopic budget controlled by radiogenic minerals such as biotite, muscovite, clay or amphibole have isotopic compositions that differ from that of their source and cannot be used to trace sediment provenance.

A surprising feature is that zircon not only affects the Hf isotopic systematic of river sediments but has even more dramatic effects on their Pb isotopic compositions. Indeed, our calculations clearly demonstrate that, because of its extremely radiogenic Pb isotopes, Pb-poor zircon has the potential to significantly influence the Pb isotopic ratios of both bedloads and suspended loads, and increase them to values up to 50 for $^{206}Pb/^{204}Pb$ for example (Figure 9). Both bedloads and suspended loads are not good proxies of the composition of the source areas, but suspended loads are less affected by the zircon effect than bedloads. The best approach to constrain the Pb isotopic composition of source areas is to concentrate on K-feldspars or clays separated from sediments (Garçon et al., 2012b).

Finally using Sr isotopes in river sediments to trace the composition of source areas appears very difficult. Bedloads and suspended loads have different compositions and, according to our calculations, the more radiogenic Sr signature of suspended loads compared to bedloads probably comes from higher contributions of radiogenic K-feldspar and/or muscovite in suspended loads (Figure 7). However, it remains unclear whether either bedloads or suspended loads have compositions similar to that of the source areas.

5.5.2. Difference between what goes into the ocean and what remains on continents

At a global scale, mineral sorting processes are responsible for significant isotopic fractionation between continental sediments and terrigeneous oceanic clays. Patchett et al. (1984) were the first to discuss such effects and showed their impact on the Hf isotopic systematics of sediments. They argued that the “zircon effect”, i.e. retention of unradiogenic Hf-rich zircons on continents, led to the delivery into the oceans of finer detrital material, poor in zircons and with radiogenic Hf isotopes. Numerous other studies confirmed the observation since 1984 (Chauvel et al., 2008; Bayon et al., 2009; Carpentier et al., 2009; Chauvel et al., 2009; Vervoort et al., 2011). Very recently, Garçon et al. (2012a) showed that almost half of the Hf isotopic fractionation observed today between terrigenous oceanic clay and continental sediments was already done on continents during fluvial transport. The

Monte-Carlo simulation presented above and in Figure 5 confirms that suspended loads delivered at the mouth of a river as large as the Ganga still contain zircons and that it must be further sorted in the oceanic environment to reach the maturity of terrigenous oceanic clay and their characteristic highly radiogenic zircon-free Hf signature. We showed in particular that, even if radiogenic minerals such as phyllosilicates control a non-negligible part of the Hf isotopic composition of suspended loads sampled in the Bangladesh delta, the contribution of zircon can still constitute up to 50% of their Hf isotopic budget (Figure 5). Further zircon sorting probably occur in the ocean, next to continental margin due to a rapid change of the hydrodynamic conditions (Lisitzin, 1996; Stummeyer et al., 2002).

Deposition of heavy minerals in the coastal zone is probably a key process that not only affects the Hf isotopic composition of sedimentary material delivered to the ocean, but also affects their Pb and Sr isotopes in a similar way. Our simulations clearly demonstrate that the Pb isotopic composition of suspended loads is bias towards radiogenic values by the “zircon effect”. Thus, we expect terrigeneous oceanic clays to be characterized by less radiogenic Pb isotopic ratios than river suspended loads. Similarly, the deposition of heavy epidote and/or coarse particles in coastal zones should lead to the delivery into the deep oceans of materials with more radiogenic Sr isotopic compositions than river suspended loads. Such a potential Sr isotopic fractionation at the land/ocean interface has already been pointed out by Eisenhauer et al. (1999). Finally, deposition of heavy monazite and allanite in the coastal zone should not modify the Nd isotopic composition of sediments delivered in the deep ocean, since these two minerals have essentially the same $^{147}Sm/^{144}Nd$ as both bulk sediments and continental sources (Patchett et al., 1984; McLennan, 1989; Garçon et al., 2011; Vervoort et al., 2011).

6. Summary and Conclusions

The Monte-Carlo simulations performed in this study provide a framework to decipher the contribution of individual mineral species to the Nd, Hf, Sr and Pb isotopic budget of river sediments. They also provide clues to understand the isotopic differences observed between bedloads and suspended loads. We relate them to mineral sorting processes during the fluvial transport of sediments. We demonstrate that, despite the diversity of mineral species present in river sediments, only few minerals really participate to the isotopic budgets.

Nd isotopes of both bedloads and suspended loads are mainly controlled by monazite and allanite and they are not modified by mineral sorting processes. Hence, they can be used to trace the continental sources of sediments. By contrast, mineral sorting processes lead to significant Hf, Sr and Pb isotopic differences between bedloads and suspended loads. We demonstrate that the Hf isotopic budget of bedloads is totally dominated by the contribution of unradiogenic Hf-rich zircons. The more radiogenic Hf signature of suspended loads results from lower but still significant contribution of zircons combined to higher contributions of more radiogenic minerals such as phyllosilicates. The Pb isotopic budgets of bedloads and suspended loads are dominated by K-feldspar and clay contributions but they are significantly affected by a zircon effect that deviates their Pb isotopic compositions towards very radiogenic values. Sr isotopes in river sediments are controlled by K-feldspar, epidote, plagioclase, muscovite, carbonate and clay. Slightly higher contributions from K-feldspar and/or muscovite explain the more radiogenic Sr isotopic compositions of suspended loads relative to bedloads. Isotopic fractionations caused by mineral sorting processes during sediment transport thus stress the need to carefully address the isotopic compositions of river sediments as provenance proxies.

We anticipate that hydrodynamic sorting in the coastal zone should further fractionate the Hf, Sr and Pb isotopic systems in oceanic sediments. In particular, the continuing deposition of heavy minerals (zircon and epidote) at the river/ocean interface should sequester material with low $^{176}Hf/^{177}Hf$ and $^{87}Sr/^{86}Sr$ and Pb isotopes may and deliver into the deep ocean sediments with higher $^{176}Hf/^{177}Hf$ and $^{87}Sr/^{86}Sr$ and less radiogenic Pb isotopes than river suspended loads.

Acknowledgments

We would like to thank S. Bureau and C. Poggi for their help in the clean lab, P. Telouk and P. Nonnotte for assistance during isotopic measurements in Lyon and Brest, as well as N.T. Arndt and E. Lewin for constructive discussions that helped to develop and interpret the results of the Monte-Carlo simulations. This study was supported by fundings from CNRS and INSU programs.

References

Allègre, C.J., Dupré, B., Négrel, P., Gaillardet, J., 1996. Sr-Nd-Pb isotope systematics in Amazon and Congo River systems: constraints about erosion processes. Chemical Geology 131, 93–112.

Asmerom, Y., Jacobsen, S.B., 1993. The Pb isotopic evolution of the Earth: inferences from river water suspended loads. Earth and Planetary Science Letters 115, 245–256.

Bayon, G., Burton, K.W., Soulet, G., Vigier, N., Dennielou, B., Etoubleau, J., Ponzevera, E., German, C.R., Nesbitt, R.W., 2009. Hf and Nd isotopes in marine sediments: Constraints on global silicate weathering. Earth and Planetary Science Letters 277, 318–326.

Bayon, G., German, C.R., Boella, R.M., Milton, J.A., Taylor, R.N., Nesbitt, R.W., 2002. An improved method for extracting marine sediment fractions and its application to Sr and Nd isotopic analysis. Chemical Geology 187, 179–199.

Bea, F., 1996. Residence of REE, Y, Th and U in granites and crustal protoliths; implications for the chemistry of crustal melts. Journal of Petrology 37, 521–552.

Belousova, E.A., Kostitsyn, Y.A., Griffin, W.L., Begg, G.C., O'reilly, S.Y., Pearson, N.J., 2010. The growth of the continental crust: Constraints from zircon Hf-isotope data. LITHOS 119, 457–466.

Bodet, F., Schärer, U., 2000. Evolution of the SE-Asian continent from U-Pb and Hf isotopes in single grains of zircon and baddeleyite from large rivers. Geochimica et Cosmochimica Acta 64, 2067–2091.

Bouchez, J., Gaillardet, J., France-Lanord, C., Maurice, L., Dutra-Maia, P., 2011. Grain size control of river suspended sediment geochemistry: Clues from Amazon River depth profiles. Geochem. Geophys. Geosyst. 12, Q03008.

Carpentier, M., Chauvel, C., Maury, R.C., Mattielli, N., 2009. The “zircon effect” as recorded by the chemical and Hf isotopic compositions of Lesser Antilles forearc sediments. Earth and Planetary Science Letters 287, 86–99.

Chauvel, C., Blichert-Toft, J., 2001. A hafnium isotope and trace element perspective on melting of the depleted mantle. Earth and Planetary Science Letters 190, 137–151.

Chauvel, C., Bureau, S., Poggi, C., 2011. Comprehensive chemical and isotopic analyses of basalt and sediment reference materials. Geostandards and Geoanalytical Research 35, 125–143.

Chauvel, C., Lewin, E., Carpentier, M., Arndt, N.T., Marini, J.-C., 2008. Role of recycled oceanic basalt and sediment in generating the Hf–Nd mantle array. Nature Geosciences 1, 64–67.

Chauvel, C., Marini, J.-C., Plank, T., Ludden, J.N., 2009. Hf-Nd input flux in the Izu-Mariana subduction zone and recycling of subducted material in the mantle. Geochem. Geophys. Geosyst. 10, Q01001.

Cina, S.E., Yin, A., Grove, M., Dubey, C.S., Shukla, D.P., Lovera, O.M., Kelty, T.K., Gehrels, G.E., Foster, D.A., 2009. Gangdese arc detritus within the eastern Himalayan Neogene foreland basin: Implications for the Neogene evolution of the Yalu–Brahmaputra River system. Earth and Planetary Science Letters 285, 150–162.

Clift, P.D., Lee, J.I., Hildebrand, P., Shimizu, N., Layne, G.D., Blusztajn, J., Blum, J.D., Garzanti, E., Khan, A.A., 2002. Nd and Pb isotope variability in the Indus River System: implications for sediment provenance and crustal heterogeneity in the Western

Himalaya. Earth and Planetary Science Letters 200, 91–106.
Davis, D.W., Amelin, Y., Nowell, G.M., Parrish, R.R., 2005. Hf isotopes in zircon from the western Superior province, Canada: Implications for Archean crustal development and evolution of the depleted mantle reservoir. Precambrian Research 140, 132–156.
Deniel, C., Vidal, P., Fernandez, A., Fort, P., Peucat, J.J., 1987. Isotopic study of the Manaslu granite (Himalaya, Nepal): inferences on the age and source of Himalayan leucogranites. Contrib Mineral Petrol 96, 78–92.
Dhuime, B., Hawkesworth, C.J., Storey, C.D., Cawood, P.A., 2011. From sediments to their source rocks: Hf and Nd isotopes in recent river sediments. Geology 39, 407–410.
Edmond, J.M., 1992. Himalayan Tectonics, Weathering Processes, and the Strontium Isotope Record in Marine Limestones. Science 258, 1594–1597.
Ehlert, C., Frank, M., Haley, B.A., Böniger, U., De Deckker, P., Gingele, F.X., 2011. Current transport versus continental inputs in the eastern Indian Ocean: Radiogenic isotope signatures of clay size sediments. Geochem. Geophys. Geosyst. 12, Q06017.
Eisenhauer, A., Meyer, H., Rachold, V., Tütken, T., Wiegand, B., Hansen, B.T., Spielhagen, R.F., Lindemann, F., Kassens, H., 1999. Grain size separation and sediment mixing in Arctic Ocean sediments: evidence from the strontium isotope systematic. Chemical Geology 158, 173–188.
Ferrara, G., Tonarini, S., Lombardo, B., 1983. Rb/Sr geochronology of granites and gneisses from the Mount Everest region, Nepal Himalaya. Int J Earth Sci (Geol Rundsch) 72, 119–136.
Flowerdew, M.J., Millar, I.L., Vaughan, A.P.M., Horstwood, M.S.A., Fanning, C.M., 2006. The source of granitic gneisses and migmatites in the Antarctic Peninsula: a combined U–Pb SHRIMP and laser ablation Hf isotope study of complex zircons. Contrib Mineral Petrol 151, 751–768.
Frank, M., 2002. Radiogenic isotopes: Tracers of past ocean circulation and erosional input. Reviews of Geophysics 40, 1001.
Galy, A., France-Lanord, C., 2001. Higher erosion rates in the Himalaya: Geochemical constraints on riverine fluxes. Geology 29, 23–26.
Galy, A., France-Lanord, C., Derry, L.A., 1999. The strontium isotopic budget of Himalayan Rivers in Nepal and Bangladesh. Geochimica et Cosmochimica Acta 63, 1905–1925.
Garçon, M., Chauvel, C., Bureau, S., 2011. Beach placer, a proxy for the average Nd and Hf isotopic composition of a continental area. Chemical Geology 287, 182–192.
Garçon, M., Chauvel, C., France-Lanord, C., 2012a. Almost half of worldwide sedimentary Nd-Hf isotopic decoupling done on continents. To be submitted to Geochemistry Geophysics Geosystems.
Garçon, M., Chauvel, C., France-Lanord, C., Limonta, M., Garzanti, E., 2012b. New approach to the average upper continental crust Pb isotopic value. To be submitted to Nature Geosciences.
Garzanti, E., Andò, S., France-Lanord, C., Censi, P., Pietro Vignola, Galy, V., Lupker, M., 2011. Mineralogical and chemical variability of fluvial sediments 2. Suspended-load silt (Ganga–Brahmaputra, Bangladesh). Earth and Planetary Science Letters 302, 107–120.
Garzanti, E., Andò, S., France-Lanord, C., Vezzoli, G., Censi, P., Galy, V., Najman, Y., 2010. Mineralogical and chemical variability of fluvial sediments 1. Bedload sand (Ganga–Brahmaputra, Bangladesh). Earth and Planetary Science Letters 299, 368–381.
Garzanti, E., Andò, S., Vezzoli, G., 2008. Settling equivalence of detrital minerals and grain-

size dependence of sediment composition. Earth and Planetary Science Letters 273, 138–151.

Gingele, F., De Deckker, P., Norman, M., 2007. Late Pleistocene and Holocene climate of SE Australia reconstructed from dust and river loads deposited offshore the River Murray Mouth. Earth and Planetary Science Letters 255, 257–272.

Goldstein, S., Jacobsen, S.B., 1988. Nd and Sr isotopic systematics of river water suspended material: implications for crustal evolution. Earth and Planetary Science Letters 87, 249–265.

Goldstein, S.L., Hemming, S.R., 2003. Long-lived isotopic tracers in oceanography, paleoceanography, and ice-sheet dynamics. Treatise on geochemistry.

Goldstein, S.L., O'nions, R.K., Hamilton, P.J., 1984. A Sm-Nd isotopic study of atmospheric dusts and particulates from major river systems. Earth and Planetary Science Letters 70, 221–236.

Gourlan, A.T., Meynadier, L., Allègre, C.J., 2008. Tectonically driven changes in the Indian Ocean circulation over the last 25 Ma: Neodymium isotope evidence. Earth and Planetary Science Letters 267, 1-2, 353-364.

Götze, J., Lewis, R., 1994. Distribution of REE and trace elements in size and mineral fractions of high-purity quartz sands. Chemical Geology 114, 43–57.

Haley, B.A., Frank, M., Spielhagen, R.F., Fietzke, J., 2008. Radiogenic isotope record of Arctic Ocean circulation and weathering inputs of the past 15 million years. Paleoceanography 23, PA1S13–.

Harris, N., Bickle, M., Chapman, H., Fairchild, I., Bunbury, J., 1998. The significance of Himalayan rivers for silicate weathering rates: Evidence from the Bhote Kosi tributary. Chemical Geology 144, 205–220.

Harrison, T.M., Blichert-Toft, J., Müller, W., Albarède, F., Holden, P., Mojzsis, S.J., 2005. Heterogeneous Hadean Hafnium: Evidence of Continental Crust at 4.4 to 4.5 Ga. Science 310, 1947–1950.

Hawkesworth, C.J., Dhuime, B., Pietranik, A.B., Cawood, P.A., Kemp, A.I.S., Storey, C.D., 2010. The generation and evolution of the continental crust. Journal of the Geological Society 167, 229–248.

Hawkesworth, C.J., Kemp, A., 2006. The differentiation and rates of generation of the continental crust. Chemical Geology 226, 134–143.

Hu, B., Li, G., Li, J., Bi, J., Zhao, J., Bu, R., 2012. Provenance and climate change inferred from Sr–Nd–Pb isotopes of late Quaternary sediments in the Huanghe (Yellow River) Delta, China. Quaternary Research 1–11.

Innocent, C., Fagel, N., Stevenson, R.K., Hillaire-Marcel, C., 1997. Sm-Nd signature of modern and late Quaternary sediments from the northwest North Atlantic: Implications for deep current changes since the Last Glacial Maximum. Earth and Planetary Science Letters 146, 607–625.

Johnson, M., Rogers, G., 1997. Rb-Sr ages of micas from the Kathmandu complex, Central Nepalese Himalaya: Implications for the evolution of the Main Central Thrust. Journal of the Geological Society 154, 863–869.

Kai, K., 1981. Rb-Sr Ages of the Biotite and Muscovite of the Himalayas, Eastern Nepal - Its Implication in the Uplift History. Geochem J 15, 63–68.

Kamber, B.S., Greig, A., Collerson, K.D., 2005. A new estimate for the composition of weathered young upper continental crust from alluvial sediments, Queensland, Australia.

Geochimica et Cosmochimica Acta 69, 1041–1058.
Kemp, A.I.S., Hawkesworth, C.J., Foster, G.L., Paterson, B.A., Woodhead, J.D., Hergt, J.M., Gray, C.M., Whitehouse, M.J., 2007. Magmatic and Crustal Differentiation History of Granitic Rocks from Hf-O Isotopes in Zircon. Science 315, 980–983.
Komar, P.D., 2007. The Entrainment, Transport and Sorting of Heavy Minerals by Waves and Currents, in: Heavy Minerals in Use. Developments in Sedimentology, pp. 3–48.
Le Fort, P., 1975. Himalayas: the collided range. Present knowledge of the continental arc. American Journal of Science.
Lisitzin, A.P., 1996. Oceanic Sedimentation: Lithology and Geochemistry. American Geophysical Union, Washington, D. C.
Lupker, M., Blard, P.-H., lavé, J., France-Lanord, C., Leanni, L., Puchol, N., Charreau, J., Bourlès, D., 2012. 10Be-derived Himalayan denudation rates and sediment budgets in the Ganga basin. Earth and Planetary Science Letters 333-334, 146–156.
Lupker, M., France-Lanord, C., Galy, V., lavé, J., Gaillardet, J., Gajurel, A.P., Guilmette, C., Rahman, M., Singh, S.K., Sinha, R., 2012. Predominant floodplain over mountain weathering of Himalayan sediments (Ganga basin). Geochimica et Cosmochimica Acta 84, 410-432.
Lupker, M., France-Lanord, C., lavé, J., Bouchez, J., Galy, V., Métivier, F., Gaillardet, J., Lartiges, B., Mugnier, J.-L., 2011. A Rouse-based method to integrate the chemical composition of river sediments: Application to the Ganga basin. J. Geophys. Res. 116, F04012.
McLennan, S.M., 1989. Rare earth elements in sedimentary rocks; influence of provenance and sedimentary processes. Reviews in mineralogy and geochemistry 21, 169–200.
McLennan, S.M., 2001. Relationships between the trace element composition of sedimentary rocks and upper continental crust. Geochem. Geophys. Geosyst. 2, 1021–1024.
McLennan, S.M., McCulloch, M.T., Taylor, S.R., Maynard, J.B., 1989. Effects of sedimentary sorting on neodymium isotopes in deep-sea turbidites. Nature 337, 547–549.
Mehta, P.K., 1977. Rb-Sr geochronology of the Kulu-Mandi Belt: Its implications for the Himalayan Tectogenesis. Int J Earth Sci (Geol Rundsch) 66, 156–175.
Milliman, J., Meade, R.H., 1983. World-wide delivery of river sediment to the oceans. The Journal of Geology 91, 1–21.
Millot, R., Allègre, C.J., Gaillardet, J., Roy, S., 2004. Lead isotopic systematics of major river sediments: a new estimate of the Pb isotopic composition of the Upper Continental Crust. Chemical Geology 203, 75–90.
Padoan, M., Garzanti, E., Harlavan, Y., Villa, I.M., 2011. Tracing Nile sediment sources by Sr and Nd isotope signatures (Uganda, Ethiopia, Sudan). Geochimica et Cosmochimica Acta 75, 3627–3644.
Patchett, P.J., White, W.M., Feldmann, H., Kielinczuk, S., Hofmann, A.W., 1984. Hafnium/rare earth element fractionation in the sedimentary system and crustal recycling into the Earth's mantle. Earth and Planetary Science Letters 69, 365–378.
Pierson-Wickmann, A.C., Reisberg, L., France-Lanord, C., 2001. Os-Sr-Nd results from sediments in the Bay of Bengal: Implications for sediment transport. Paleoceanography 16, 435–444.
Piotrowski, A.M., Goldstein, S.L., Hemming, S.R., Fairbanks, R.G., 2004. Intensification and variability of ocean thermohaline circulation through the last deglaciation. Earth and Planetary Science Letters 225, 205–220.

Revel, M., Cremer, M., Grousset, F.E., Labeyrie, L., 1996. Grain-size and Sr-Nd isotopes as tracer of paleo-bottom current strength, Northeast Atlantic Ocean. Marine Geology 131, 233–249.

Richards, A., Argles, T., Harris, N., Parrish, R., Ahmad, T., Darbyshire, F., Draganits, E., 2005. Himalayan architecture constrained by isotopic tracers from clastic sediments. Earth and Planetary Science Letters 236, 773–796.

Roddaz, M., Viers, J., Brusset, S., Baby, P., Hérail, G., 2005. Sediment provenances and drainage evolution of the Neogene Amazonian foreland basin. Earth and Planetary Science Letters 239, 57–78.

Rudnick, R.L., Gao, S., 2003. The Composition of the Crust, in: Rudnick, R.L. (Ed.), The Crust Vol.3 Treatise on Geochemistry. pp. 1–64.

Singh, S.K., France-Lanord, C., 2002. Tracing the distribution of erosion in the Brahmaputra watershed from isotopic compositions of stream sediments. Earth and Planetary Science Letters 202, 645–662.

Singh, S.K., Rai, S.K., Krishnaswami, S., 2008. Sr and Nd isotopes in river sediments from the Ganga Basin: Sediment provenance and spatial variability in physical erosion. J. Geophys. Res. 113, F03006.

Stille, P., Steinmann, M., Riggs, S.R., 1997. Nd isotope evidence for the evolution of the paleocurrents in the Atlantic and Tethys oceans during the past 180 Ma. Oceanographic Literature Review 44, 698–698.

Stummeyer, J., Marchig, V., Knabe, W., 2002. The composition of suspended matter from Ganges–Brahmaputra sediment dispersal system during low sediment transport season. Chemical Geology 185, 125–147.

Stumpf, R., Frank, M., Schönfeld, J., Haley, B.A., 2011. Climatically driven changes in sediment supply on the SW Iberian shelf since the Last Glacial Maximum. Earth and Planetary Science Letters 312, 80–90.

Taylor, S.R., McLennan, S.M., 1995. The Geochemical evolution of the Continental Crust. Reviews of Geophysics 33, 241–265.

Veevers, J.J., Saeed, A., Belousova, E.A., Griffin, W., 2005. U-Pb ages and source composition by Hf-isotope and trace-element analysis of detrital zircons in Permian sandstone and modern sand from southwestern Australia and a review of the paleogeographical and denudational history of the Yilgam Craton. Earth Science Reviews 68, 245–279.

Vervoort, J., Plank, T., Prytulak, J., 2011. The Hf-Nd isotopic composition of marine sediments. Geochimica et Cosmochimica Acta 75, 5903-5926.

Vervoort, J.D., Patchett, P.D., Blichert-Toft, J., Albarède, F., 1999. Relationships between Lu–Hf and Sm–Nd isotopic systems in the global sedimentary system. Earth and Planetary Science Letters 168, 79–99.

Walter, H.J., Hegner, E., Diekmann, B., Kuhn, G., 2000. Provenance and transport of terrigenous sediment in the South Atlantic Ocean and their relations to glacial and interglacial cycles: Nd and Sr isotopic evidence. Geochimica et Cosmochimica Acta 64, 3813–3827.

Wu, W., Xu, S., Yang, J., Yin, H., Lu, H., Zhang, K., 2010. Isotopic characteristics of river sediments on the Tibetan Plateau. Chemical Geology 269, 406–413.

Yan, Y.I., Xia, B., Lin, G.E., Carter, A., Hu, X., Cui, X., Liu, B., Yan, P., Song, Z., 2007. Geochemical and Nd isotope composition of detrital sediments on the north margin of

the South China Sea: provenance and tectonic implications. Sedimentology 54, 1–17.
Zeh, A., Gerdes, A., Klemd, R., Barton, J.M., 2007. Archaean to Proterozoic Crustal Evolution in the Central Zone of the Limpopo Belt (South Africa-Botswana): Constraints from Combined U-Pb and Lu-Hf Isotope Analyses of Zircon. Journal of Petrology 48, 1605–1639.

Supplementary File

Input parameters for the Monte-Carlo simulations

Based on mineral proportions estimated in suspended loads and bedloads from the Bangladesh delta by Garzanti et al. (2010, 2011), we defined a range of possible proportions for each mineral species analyzed in this study (see the Table below).

Range of proportions used for Monte-Carlo simulations

(wt.%)	Minimum proportion	Maximum proportion
K-feldspar	2	15
Plagioclase	3	16
Muscovite	10	22
Biotite	5	15
Magnetite	0.05	6
Zircon	0	0.5
Titanite	0	1.5
Apatite	0	0.5
Monazite/Allanite	0	0.4
Amphibole	0.3	11
Epidote	0.2	11
Garnet	0.2	8
Carbonate	0	3
Clay	0	25

For the magnetite and carbonate fractions, we used, respectively, the weight proportions of opaques+Fe oxides and calcite as estimated by Garzanti et al. (2010, 2011). The proportions indicated for the monazite/allanite fraction correspond to that of monazite alone. For each mineral species, proportions were randomly sampled (n=100,000) in uniform distributions defined by minimum and maximum proportions indicated above. Then, using these proportions together with the concentrations and the isotopic compositions that we

measured in our mineral fractions, we calculated the isotopic compositions of different mixtures. Note that, since we didn't not separate pure fractions of monazite, allanite and apatite, we used the monazite and apatite Nd concentrations published by Garzanti et al. (2010, 2011) for our Nd simulation (i.e. 94, 000 ppm and 635 ppm, respectively).

Not all of the minerals identified by Garzanti et al. (2010, 2011) (see Supplementary Table 1) were taken into account in the Monte-carlo procedures. The contributions of quartz, chlorite, tourmaline, rutile, Ti oxide, pyroxene, spinel, chloritoid, staurolite, kyanite, sillimanite, fibrolite, olivine and xenotime were always neglected in our calculations because we did not separate those minerals. However, except quartz for Sr, none of these minerals do contribute to more than 2% in the Nd, Hf, Sr and Pb elemental budgets of the Ganga sediments after Garzanti et al. (2010, 2011). We are thus rather confident in the fact that these latter minerals do not play a preponderant role in the Nd, Hf, Sr and Pb isotopic budgets of the sediments.

Note that Nd, Hf, Pb and Sr concentrations modeled by our Monte-Carlo simulations are always higher than those measured in sediments because we didn't take into account quartz that significantly dilute concentrations. However, we performed several other simulations aiming to model the concentrations of the sediments alone. The results of these simulations show that we perfectly reproduce the range of concentrations in Nd, Hf, Sr and Pb measured in the Ganga sediments, when taking into account quartz and the minerals listed above in the Table.

Supplementary Table 1

Supplementary Table 1: Weight mineral proportions in Ganga sediments modified after Garzanti et al. (2010, 2011)

Surface suspended loads (<3m)			Deep suspended loads (>8m)			Bedloads		
	Average	**2σ**		**Average**	**2σ**		**Average**	**2σ**
Quartz	34.3	22.8	**Quartz**	48.7	10.6	**Quartz**	55.4	14.9
K-feldspar	2.6	1.6	**K-feldspar**	5.7	2.3	**K-Feldspar**	6.6	3.1
Albite	4.6	2.4	**Albite**	5.9	4.0	**Plagioclase**	6.0	2.9
Ca-plagioclase	2.4	2.3	**Ca-plagioclase**	4.2	2.8			
Lithic grain	ND		**Lithic grain**	ND		**Lithic grain**	14.5	5.2
Calcite	1.2	0.3	**Calcite**	2.9	1.6	**Calcite**	ND	
Dolomite	1.8	0.2	**Dolomite**	2.3	2.1	**Dolomite**	ND	
Muscovite	17.5	9.2	**Muscovite**	8.9	5.4	**Mica**	9.8	21.9
Biotite	10.4	4.3	**Biotite**	5.5	3.0			
Chlorite	2.8	1.4	**Chlorite**	1.7	1.1	**Chlorite**	ND	
Clay	19.5	18.6	**Clay**	9.8	3.6	**Clay**	ND	
Fe-oxides	0.2	0.2	**Fe-oxides**	0.1	0.1	**Fe-oxides**	ND	
Fibrolite	ND		**Fibrolite**	ND		**Fibrolite**	0.1	0.2
Opaques	1.3	0.1	**Opaques**	1.0	0.7	**Opaques**	1.1	2.8
Zircon	0.1	0.0	**Zircon**	0.1	0.3	**Zircon**	0.1	0.4
Tourmaline	0.2	0.1	**Tourmaline**	0.2	0.1	**Tourmaline**	0.3	0.7
Rutile	0.2	0.2	**Rutile**	0.2	0.2	**Rutile**	0.1	0.2
Ti oxide	0.4	0.1	**Ti oxide**	0.2	0.2	**Ti oxide**	0.0	0.1
Titanite	0.1	0.1	**Titanite**	0.2	0.3	**Titanite**	0.3	0.5
Apatite	0.1	0.0	**Apatite**	0.1	0.1	**Apatite**	0.1	0.4
Monazite	ND		**Monazite**	ND		**Monazite**	0.1	0.3
Amphibole	0.5	0.6	**Amphibole**	1.1	0.6	**Amphibole**	1.4	2.0
Pyroxene	0.2	0.1	**Pyroxene**	0.3	0.2	**Pyroxene**	0.3	0.5
Spinel	ND		**Spinel**	ND		**Cr-spinel**	ND	
Epidote	1.4	0.8	**Epidote**	1.0	0.3	**Epidote**	1.0	1.5
Allanite	ND		**Allanite**	0.0	0.1	**Allanite**	ND	
Chloritoid	ND		**Chloritoid**	ND		**Chloritoid**	ND	
Garnet	0.4	0.5	**Garnet**	1.2	1.9	**Garnet**	2.8	6.5
Staurolite	ND		**Staurolite**	0.0	0.0	**Staurolite**	0.1	0.1
Kyanite	0.0	0.1	**Kyanite**	0.1	0.1	**Kyanite**	0.2	0.5
Sillimanite	ND		**Sillimanite**	0.1	0.1	**Sillimanite**	0.0	0.1
Sum	*102.2*		*Sum*	*101.4*		*Sum*	*100.3*	

ND: not determined or under detection limit

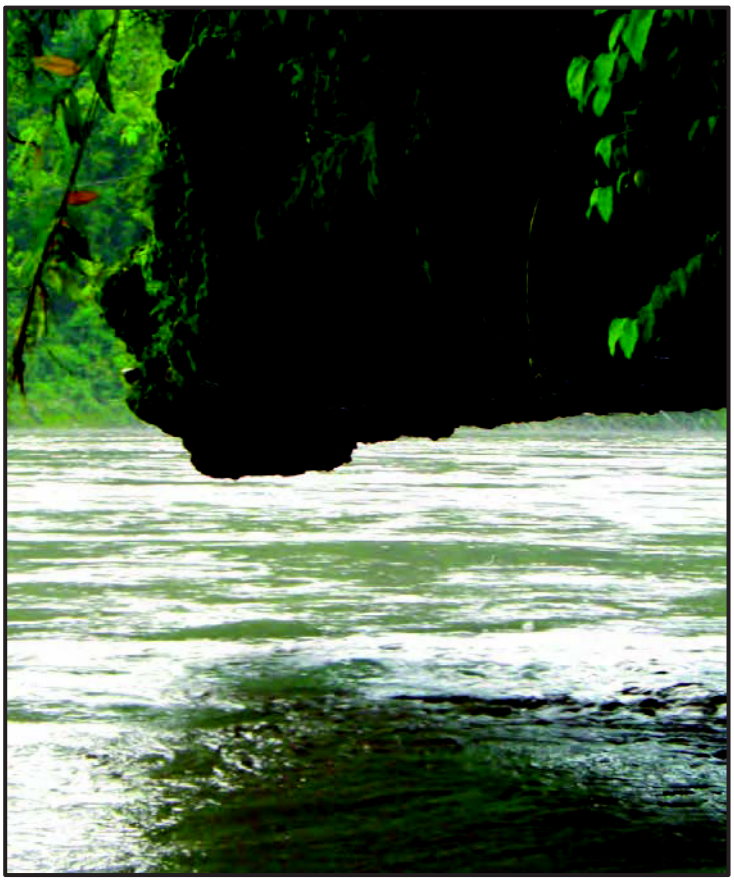

Chapitre 5

Effet de l'Erosion Différentielle sur les Compositions Isotopiques des Sédiments

Les bassins de drainage des rivières sont souvent constitués de différentes lithologies qui peuvent présenter d'importants contrastes d'érodabilité. Celles-ci pourraient générer différents types de sédiments en fonction de leur résistance aux processus d'altération et d'érosion. Dans ce chapitre, présenté sous la forme d'un article que nous souhaiterions soumettre à Geology, nous nous intéressons aux effets de couplage entre les processus d'érosion différentielle dans le bassin versant et les processus de tri sédimentaire au cours du transport fluviatile sur les compositions isotopiques en Nd, Hf et Pb des sédiments. Pour ce faire, nous comparerons les systématiques isotopiques de sédiments de rivières drainant d'importantes quantités de roches cristallines et sédimentaires (chaîne Himalayenne et bouclier nord Indien) à ceux drainant d'importantes quantités de basaltes (Traps du Deccan) dans le sud de la plaine Indo-Gangétique.

Isotopic data suggest strong bias towards basalts in river surface sediments
(To be submitted to Geology)

ABSTRACT **163**
INTRODUCTION **164**
GEOLOGICAL SETTING **164**
RESULTS AND DISCUSSION **166**
ACKNOWLEDGMENTS **171**
REFERENCES **171**
SUPPLEMENTARY MATERIAL **175**

L'ensemble des échantillons étudiés dans les deux chapitres précédents provenait du Ganges et de ses affluents drainant la chaîne Himalayenne c'est à dire, en majeure partie, des roches cristallines et sédimentaires variablement métamorphisées (cf. Chapitre 1 ; Le Fort, 1975). Nous avons montré que la variabilité isotopique observée dans ces sédiments était quasi exclusivement liée à des processus de tri sédimentaire qui modifient leur composition minéralogique au cours du transport fluviatile. Dans ce chapitre, nous nous intéressons à d'autres sédiments, échantillonnés au Sud du Système Himalayen, dans des rivières dont les bassins de drainage sont constitués de roches sédimentaires et cristallines (chaîne Himalayenne et bouclier nord Indien) mais également d'importantes quantités de basaltes appartenant aux Traps du Deccan. Le but du manuscrit présenté ci dessous est d'évaluer les effets du tri sédimentaire dans les sédiments de rivière lorsque les lithologies exposées à l'altération et l'érosion dans le bassin de drainage présentent d'importants contrastes d'érodabilité i.e. roches cristallines relativement résistantes vs. basaltes plus altérables.

Ce manuscrit est essentiellement basé sur la comparaison des compositions isotopiques en Nd, Hf et Pb de sédiments échantillonnés à différentes profondeurs dans la colonne d'eau au niveau du delta du Bangladesh (résultats d'ores et déjà présentés et interprétés dans les deux chapitres précédents) et au sud du système fluviatile du Ganges. La contribution des produits d'érosion basaltique dans les sédiments échantillonnés au sud est précisément quantifiée en utilisant des mélanges isotopiques impliquant les systèmes Sm-Nd et Lu-Hf. Les implications potentielles de nos résultats pour les systématiques isotopiques des sédiments océaniques détritiques sont évaluées à la fin du manuscrit.

Isotopic data suggest strong bias towards basalts in river surface sediments

(To be submitted to Geology)

Marion Garçon[1], Catherine Chauvel[1], Christian France-Lanord[2]

[1] ISTerre, CNRS, Université Joseph Fourier de Grenoble, BP 53, 38041 Grenoble Cedex 09, France

[2] CRPG-CNRS, 15, rue Notre Dame des Pauvres, 54501 Vandoeuvre-lès-Nancy, France

Note : Figures were integrated in the text to facilitate the reading

ABSTRACT

Weathering, erosion and sedimentary processes significantly modify the chemical and isotopic compositions of river sediments relative to those of their source rocks. The extent to which those processes affect the geochemistry of the sediments is however not yet fully understood. Here, we report Nd, Hf and Pb isotopic compositions of sediments sampled at different water depths in the Ganga, Yamuna and Chambal Rivers draining the Deccan Traps basalts and the crystalline and sedimentary rocks from the Himalayan mountain range and the northern Indian shield. Isotopic differences between surface and bed sediments sampled at the same location reach 6 ε_{Nd} and about 15 ε_{Hf} units. We demonstrate that when contrasted lithologies are eroded, bedloads and suspended loads do not carry similar provenance information because of differential erosion coupled with hydrodynamic sorting during sediment transport. Materials eroded from basalts are preferentially transported in suspension near the river surface while materials eroded from more crystalline precursors are preferentially transported near the bottom of the river. We suggest that this depth-dependent provenance within the river channel leads to an overrepresentation of basaltic materials in fine-grained suspended loads that are delivered into the ocean and become part of the oceanic terrigenous clays. By contrast, their proportion in coarser oceanic sediments such as turbidites is underestimated.

INTRODUCTION

River sediments are essentially mixtures of solid materials eroded from the different types of rocks present in the catchment area. Their chemical and isotopic compositions are therefore often used to trace sources, estimate the average composition of the drained area or determine chemical and physical erosion rates in large basins (Goldstein et al., 1984; Goldstein and Jacobsen, 1988; Asmerom and Jacobsen, 1993; Allègre et al., 1996; Clift et al., 2002; Singh et al., 2008; Singh, 2009; Millot et al., 2004; Kamber et al., 2005; Richards et al., 2005; Roddaz et al., 2005; Cina et al., 2009; Belousova et al., 2006; Wu et al., 2010; Dhuime et al., 2011; Padoan et al., 2011). However, using sediments as such proxies requires a proper understanding of biases introduced by erosion and sedimentary processes on chemical compositions. Several studies already showed that the proportions of source rocks estimated using the isotopic compositions of sediments often do not match their geographical extend in the catchment area (Dhuime et al., 2011; Goldstein and Jacobsen, 1988; Kramers and Tolstikhin, 1997; Tricca et al., 1999; Steinmann and Stille, 2008). This is because some lithologies are more erodible than others. In addition, hydrodynamic sorting of particles within the water column during fluvial transport introduces large fractionation of the chemical and isotopic messages of the various types of river sediments (Lupker et al., 2011; Bouchez et al., 2011; Garzanti et al., 2010; Garzanti et al., 2011; Garçon et al., 2012a; Garçon et al., 2012b). Here, we go one step further and evaluate the combined effects of (a) contrasting erodibility of crystalline, sedimentary versus basaltic rocks and (b) isotopic fractionation caused by hydrodynamic sorting in the water column. We focus on the Nd, Hf and Pb isotopic compositions of sediments sampled at different water depths in the Ganga fluvial system that drains the Himalayan range, the northern Indian shield and the Deccan Traps basalts. We show that bedloads and suspended loads carry very different provenance information and we evaluate the implications for worldwide terrigenous oceanic sediments.

GEOLOGICAL SETTING

Here, we compare the composition of sediments recovered at three different sampling sites along the large Ganga fluvial system (Figure 1). The first sampling site is located in Bangladesh at the outflow of the Ganga River (yellow star in Figure 1); given its location downstream along the river, it integrates all sediments transported by the Ganga and its tributaries. The drainage basin covers about one million km^2 and includes reworked fluvial

deposits from the Indo-Gangetic floodplain, materials eroded from the crystalline and variably metamorphosed sedimentary rocks from both the Himalayan mountain range and the northern Indian shield, and few materials eroded from the Deccan Traps (Le Fort, 1975; Krishnan, 1982). Indeed, at this location, the Deccan Traps basalts represent about 4% of the total drained area.

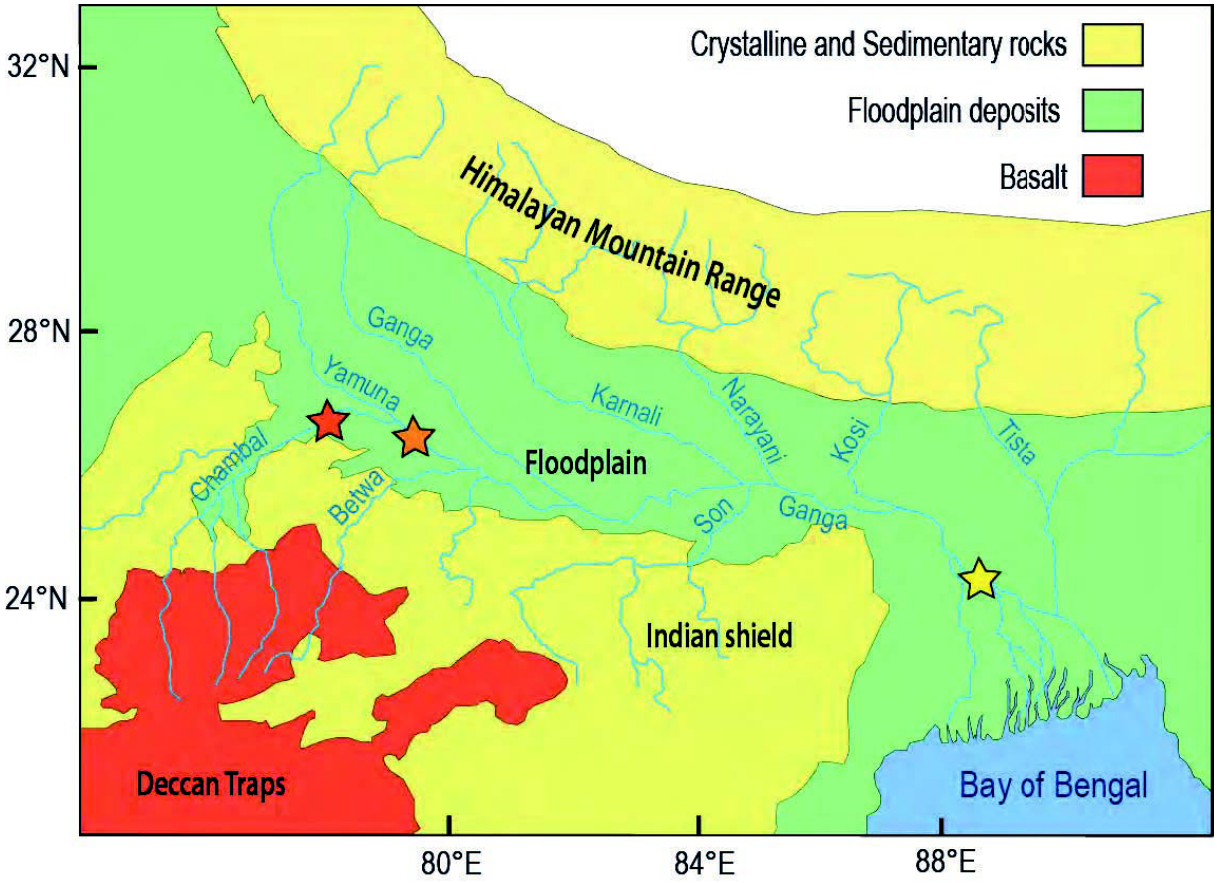

Figure 1: Map of the Ganga fluvial system
Colored stars indicate the sampling locations of the sediments analyzed in this study. In the Ganga and Yamuna Rivers, sediments were sampled in a depth profile from the water surface to the bottom of the river. See Supplementary Table 1 for additional information on the location and nature of the different samples.

The two other sampling sites are both located upstream in the floodplain, one in the Yamuna River and the other in the Chambal River (light and dark orange stars in Figure 1). At the Chambal sampling site, the Deccan Traps basalts constitute 30% of the basin area and at the Yamuna sampling site, they represent 20% (Lupker et al., 2012; Jha et al., 1988); the other 70 or 80% of the drained area consist of reworked fluvial deposits from the Indo-

Gangetic floodplain and/or crystalline and sedimentary rocks from both the Himalayan mountain range and the northern Indian shield (Figure 1).

RESULTS AND DISCUSSION

Nd, Hf and Pb isotopic compositions of sediments sampled at different water depths in Bangladesh are shown in yellow in Figure 2 and can be found in Supplementary Table 1. Nd isotopes do not change with water depth and exhibit a constant value at $\varepsilon_{Nd} \approx -17$, value similar to the isotopic signature of the Himalayan units (Singh et al., 2008; Richards et al., 2005; Robinson et al., 2001; Galy and France-Lanord, 2001; Garçon et al., 2012a). The contribution from the Deccan Traps is estimated to be less than 4% in our particular samples (Lupker et al., 2011) and a quick mass balance calculation between an $\varepsilon_{Nd} \approx +5$ typical of Deccan basalts and the low ε_{Nd} typical of the Himalayan units shows that the resulting value is indistinguishable from that of the Himalayan sources. Note that the contribution of few erosion products from the northern Indian shield should not modify the isotopic composition of the Ganga sediments since this area is isotopically equivalent to the Himalayan units because it represents their protolith (Parrish and Hodges, 1996). In contrast to Nd, as can be seen in Figure 2, ε_{Hf} and Pb isotopic ratios do change with water depth in the Ganga profile: bottom sediments have lower ε_{Hf} and more radiogenic Pb isotopic ratios than the overlying suspended loads. We attribute these differences to the "zircon effect", i.e. the concentration of coarse and dense minerals, such as zircons, in the bottom of the river through hydrodynamic sorting processes (Garçon et al., 2012a; Garçon et al., 2012b).

Upstream in the floodplain, sediments from the Yamuna and Chambal Rivers are isotopically very different from the Ganga River samples (Supplementary Table 1, Figure 2). They have much higher ε_{Nd} and ε_{Hf} values and less radiogenic Pb isotopic ratios. We explain the difference by the contribution of eroded basalts from the Indian Deccan Traps (Figure 2). The isotopic changes of the Yamuna and Chambal sediments as a function of depth within the water column are however surprising. First, ε_{Nd} dramatically decreases with depth, from -10 at the surface to about -16 at the bottom of the river when no such change exists in the Ganga sediments. Second, the downward decrease of ε_{Hf} and increase of Pb isotopic ratios are much larger than those observed for the Ganga sediments. For example, the difference between surface and bottom sediments sampled in the Yamuna reaches almost 15 ε_{Hf} units

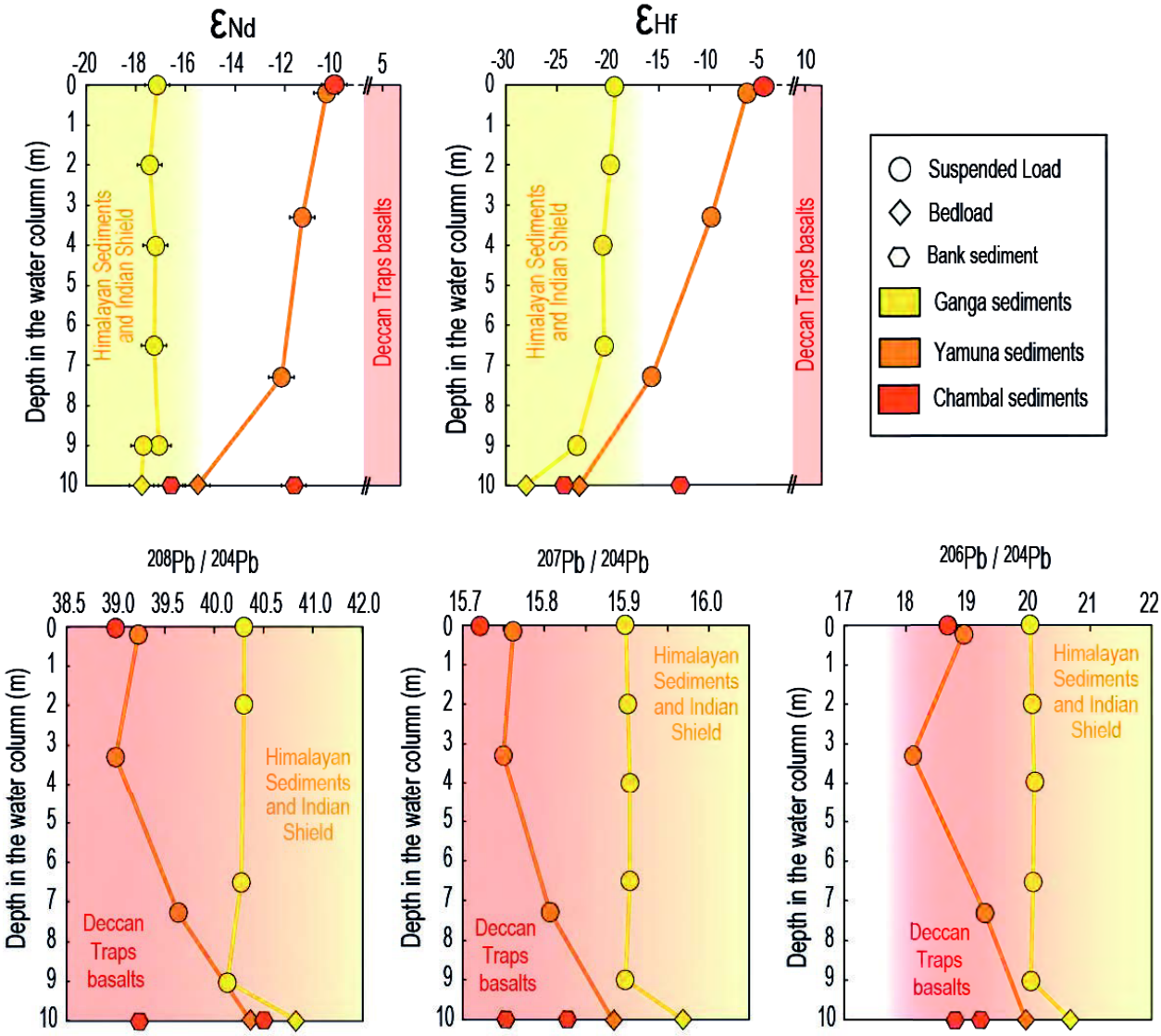

Figure 2: Nd, Hf and Pb isotopic variations of sediments sampled at different water depths in the Ganga, Yamuna and Chambal Rivers.
For the Ganga sediments, only the samples recovered along the depth profile are shown in the diagrams (see Supplementary Table 1). The entire Nd and Hf isotopic variability of the Himalayan sediments i.e. samples from the Ganga and its major tributaries collected at different locations in the floodplain, from the Himalayan mountain front to the delta in Bangladesh are indicated by a yellow field (data from Garçon et al. 2012a). River bank sediments from the Chambal were plot at an arbitrarily depth of 10m in each diagram. Red fields show the Nd, Hf and Pb isotopic compositions of the northern Deccan Traps basalts (data from GEOROC database). ε_{Nd} and ε_{Hf} were calculated using the CHUR composition of Bouvier et al. (2008). Analytical errors are smaller than the symbol size except for Nd isotopes, for which they are shown by horizontal bars at ± 0.5 ε units.

and we are convinced that the huge Nd, Hf and Pb isotopic changes seen in Figure 2 cannot result from hydrodynamic processes alone. Instead, we suggest that surface suspended loads from both Yamuna and Chambal rivers include much higher proportions of basaltic erosion products from the Deccan Traps than the bed sediments, a feature that we explain

by the contrasting erodibility of basalts vs. crystalline and sedimentary rocks from both Himalayan range and Indian shield. Indeed, several authors already showed that the Deccan Traps basalts weather more easily than the surrounding crystalline and sedimentary rocks (Dessert et al., 2001; Das et al., 2005; Rengarajan et al., 2009). Jha et al. (1993) even showed that the Deccan basalts contribute to significant amounts of clays, essentially montmorillonite, that are preferentially transported in suspension in the Yamuna River. By contrast, we expect the erosion products of the crystalline and sedimentary rocks from the Himalayan range and Indian shield to be coarser, thus to take more easily part of the bedload sediments. In summary, the erosion products of the more weatherable basalts are preferentially transported in suspension near the river surface whereas the erosion products of the more resistant crystalline and sedimentary rocks are preferentially transported near the bottom of the river.

We can quantify the proportion of eroded basalts present at different water depths in the Yamuna and Chambal sediments by using the relationship between ε_{Nd} vs. ε_{Hf} and calculating mixing arrays (Supplementary Table 2, Figure 3). Figure 3 shows clearly that the Nd and Hf isotopic compositions of the Yamuna and Chambal sediments can easily be reproduced through mixing between radiogenic material eroded from the Deccan Traps and diverse grain fractions of sedimentary material similar to the Ganga River sediments that represent the erosion products of the Himalayan range and the northern Indian shield. Surface suspended loads from both Yamuna and Chambal Rivers have the the highest ε_{Nd} and ε_{Hf}, values explained by a contribution of 60 to 70% of Ganga surface suspended loads and 30 to 40% Deccan Traps basalts. The slightly lower ε_{Nd} and ε_{Hf}, values of deeper suspended loads only require 20 to 30% of basaltic material. Finally, the bedloads from Yamuna and Chambal rivers resemble those of the Ganga River and include less than 10% of Deccan Traps basalts. Our calculations clearly demonstrate that the proportion of basaltic erosion products significantly decreases with depth in both rivers and show that bedloads and suspended loads record different provenance information. We believe that this feature certainly occurs also in other areas in the world when both basalts and granitoïds occur in the drainage basin of large rivers. To our knowledge, no publication reports similar data but consistent conclusions were reached by Bouchez et al. (Bouchez et al., 2011) when interpreting the Sr isotopic variations of sediments located at different water depths in the Amazon river.

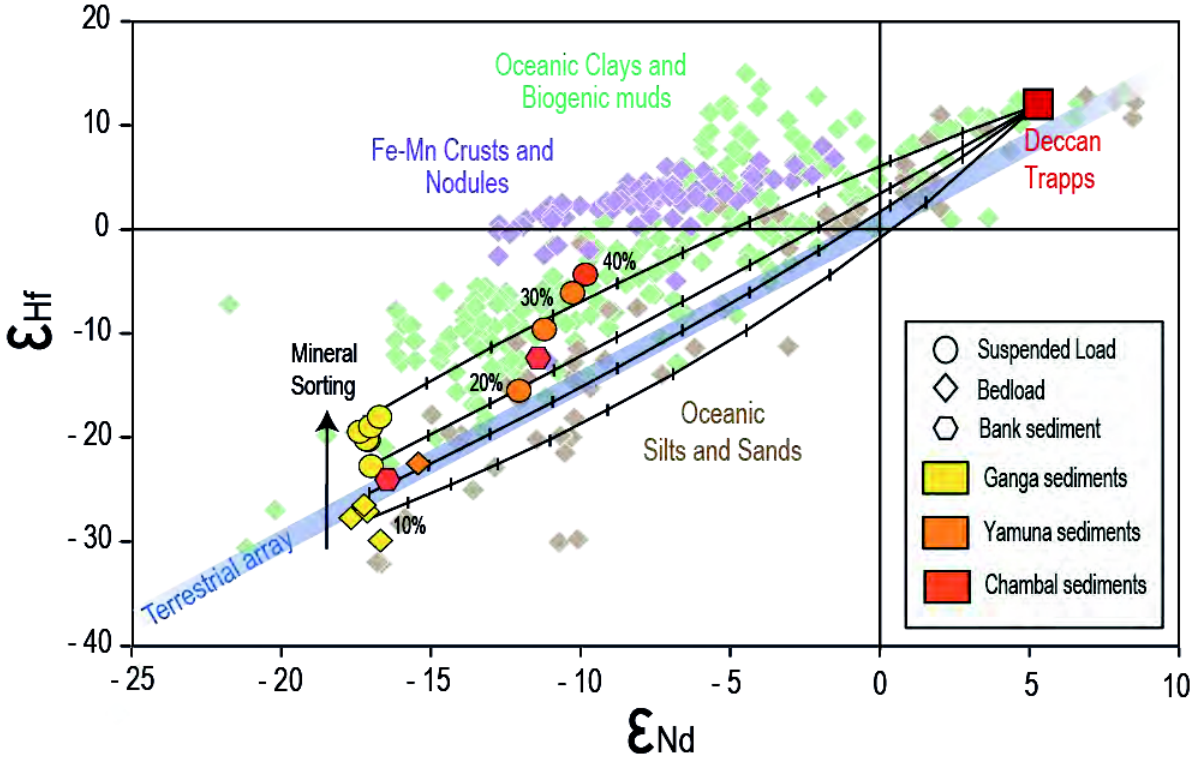

Figure 3: ε_{Nd} and ε_{Hf} diagrams showing the composition of the Ganga, Yamuna and Chambal sediments.
Mixing curves between the Deccan Traps basalts and the sediments sampled at different water depths in the Ganga River in Bangladesh are shown by black lines. Ticks indicate the proportion of Deccan Traps basalts involved in the mixings. The composition of the different endmembers used to calculate the mixing hyberbolas are summarized in Supplementary Table 2. The Terrestrial Array is that of (Vervoort et al., 2011). Nd-Hf isotopic compositions of worldwide oceanic sediments are also shown. Data for Fe-Mn crusts and nodules are from (Albarède et al., 1998; Godfrey et al., 1997; David et al., 2001; Van De Flierdt et al., 2006; Albarède et al., 1997); oceanic clays and biogenic muds are from (Bayon et al., 2009; McLennan et al., 1990; Ben Othman et al., 1989; Vervoort et al., 1999; White et al., 1986; Vlastélic, 2005; Pearce et al., 1999; Woodhead et al., 2001; Prytulak et al., 2006; Carpentier et al., 2009; Chauvel et al., 2009; Vervoort et al., 2011; Carpentier et al., 2008) and oceanic silts and sands are from (Carpentier et al., 2008; Carpentier et al., 2009; McLennan et al., 1990; Vervoort et al., 1999; Bayon et al., 2009; Prytulak et al., 2006; Vervoort et al., 2011). All of the ε_{Nd} and ε_{Hf} presented in this Figure have been recalculated using the CHUR composition of Bouvier et al. (2008).

Variations of Pb isotopic ratios in the studied sediments are globally in agreement with the observation based on e_{Nd} and e_{Hf} even if things are slightly more ambiguous (Supplementary Figure). The Deccan Traps basalts have relatively low $^{206}Pb/^{204}Pb$ while sediments from the Himalayan Range have generally higher but mainly more variable $^{206}Pb/^{204}Pb$. The Yamuna and Chambal sediments have generally less radiogenic signatures than the Ganga River sediments, a feature consistent with a higher involvement of material deriving from the Deccan Traps basalts. However, the influence of the different sources on

Pb isotopic ratios is blurred by the effect of hydrodynamic sorting that concentrates zircon with extremely radiogenic Pb isotopic ratios in the coarse sediments while fine grain sediments poorer in zircon have less radiogenic values (Garçon et al., 2012b). In addition, the large range of Pb isotopic compositions reported for the Deccan Traps basalts makes it impossible to calculate proportions of basaltic materials in the Yamuna and Chambal sediments.

Using the comparison between proportions of basaltic material estimated using the sediment Nd and Hf isotopic compositions and proportions of basalt exposed to the surface in the catchment area, we can evaluate the isotopic bias generated by erosion and sedimentary processes. Our calculations indicate that the Deccan Traps basalts contribute to less than 10% in the bedload of the Yamuna River (Figure 3) whereas this lithology covers about 20% of the drained area. This implies that basaltic material in coarse sediments is significantly underrepresented. By contrast, we showed that surface suspended load from the same river consists of 30 to 40% of material eroded from the Deccan Traps basalts; hence, basaltic material is overrepresented in fine suspended loads. These results have major implications at the scale of the global sedimentary system, particularly for oceanic sediments because most authors use the Nd, Hf or Pb isotopic compositions of oceanic terrigenous sediments as a proxy for their continental provenance (Plank and Langmuir, 1998; Vervoort et al., 2011; Hemming and McLennan, 2001). If basaltic erosion products are effectively overrepresented in fine suspended loads delivered into the ocean at the mouths of large rivers, the contribution of basaltic material in pelagic terrigenous clays could be overestimated relative to the proportion of basalts effectively exposed to weathering at the surface of the Earth. Conversely, the basaltic precursor is certainly underestimated in coarse terrigenous sediments such as turbidites deposited next to continental margins. The overrepresentation of volcanic sources in oceanic sediments was already highlighted 20 years ago by McLennan (1989) and more recent work also demonstrated the preponderant role of chemical weathering of basalts on the composition of the seawater (Dessert et al., 2003; Dessert et al., 2001). What our new results demonstrate is that the controlling factors are particle grain-size and transport processes that decouple sources as a function of depth within the river. They also clearly show that the erosion products of basaltic rocks exposed to weathering above sea level must be overrepresented in the oceanic sedimentation because fine sedimentary particles find more easily their way from continents to open ocean.

ACKNOLEDGEMENTS

We thank S. Bureau for her help in the clean lab, P. Telouk (ENS, Lyon) for assistance during MC-ICP-MS measurements at Lyon and N. Arndt (ISTerre, Grenoble) for constructive discussions that helped improving the content of the manuscript.
This study was supported by funding from CNRS and INSU programs.

REFERENCES

Albarède, F., Goldstein, S.L., and Dautel, D., 1997, The neodymium isotopic composition of manganese nodules from the Southern and Indian oceans, the global oceanic neodymium budget, and their bearing on deep ocean circulation: Geochimica et Cosmochimica Acta, v. 61, no. 6, p. 1277–1291.

Albarède, F., Simonetti, A., Vervoort, J.D., Blichert-Toft, J., and Abouchami, W., 1998, A Hf-Nd isotopic correlation in ferromanganese nodules: Geophysical Research Letters, v. 25, no. 20, p. 3895–3898.

Allègre, C.J., Dupré, B., Négrel, P., and Gaillardet, J., 1996, Sr-Nd-Pb isotope systematics in Amazon and Congo River systems: constraints about erosion processes: Chemical Geology, v. 131, no. 1, p. 93–112.

Asmerom, Y., and Jacobsen, S.B., 1993, The Pb isotopic evolution of the Earth: inferences from river water suspended loads: Earth and Planetary Science Letters, v. 115, no. 1-4, p. 245–256.

Bayon, G., Burton, K.W., Soulet, G., Vigier, N., Dennielou, B., Etoubleau, J., Ponzevera, E., German, C.R., and Nesbitt, R.W., 2009, Hf and Nd isotopes in marine sediments: Constraints on global silicate weathering: Earth and Planetary Science Letters, v. 277, no. 3-4, p. 318–326, doi: 10.1016/j.epsl.2008.10.028.

Belousova, E.A., Preiss, W.V., Schwarz, M.P., and Griffin, W.L., 2006, Tectonic affinities of the Houghton Inlier, South Australia: U – Pb and Hf-isotope data from zircons in modern stream sediments: Australian Journal of Earth Sciences, v. 53, no. 6, p. 971–989, doi: 10.1080/08120090600880875.

Ben Othman, D., White, W.M., and Patchett, J., 1989, The geochemistry of marine sediments, island arc magma genesis, and crust-mantle recycling: Earth and Planetary Science Letters, v. 94, no. 1-2, p. 1–21.

Bouchez, J., Gaillardet, J., France-Lanord, C., Maurice, L., and Dutra-Maia, P., 2011, Grain size control of river suspended sediment geochemistry: Clues from Amazon River depth profiles: Geochemistry Geophysics Geosystems, v. 12, no. 3, p. Q03008, doi: 10.1029/2010GC003380.

Bouvier, A., Vervoort, J.D., and Patchett, P.J., 2008, The Lu–Hf and Sm–Nd isotopic composition of CHUR: constraints from unequilibrated chondrites and implications for the bulk composition of terrestrial planets: Earth and Planetary Science Letters, v. 273, no. 1, p. 48–57, doi: 10.1016/j.epsl.2008.06.010.

Carpentier, M., Chauvel, C., and Mattielli, N., 2008, Pb–Nd isotopic constraints on

sedimentary input into the Lesser Antilles arc system: Earth and Planetary Science Letters, v. 272, no. 1-2, p. 199–211, doi: 10.1016/j.epsl.2008.04.036.

Carpentier, M., Chauvel, C., Maury, R.C., and Mattielli, N., 2009, The "zircon effect" as recorded by the chemical and Hf isotopic compositions of Lesser Antilles forearc sediments: Earth and Planetary Science Letters, v. 287, no. 1-2, p. 86–99, doi: 10.1016/j.epsl.2009.07.043.

Chauvel, C., Marini, J.-C., Plank, T., and Ludden, J.N., 2009, Hf-Nd input flux in the Izu-Mariana subduction zone and recycling of subducted material in the mantle: Geochemistry Geophysics Geosystems, v. 10, no. 1, p. Q01001, doi: 10.1029/2008GC002101.

Cina, S.E., Yin, A., Grove, M., Dubey, C.S., Shukla, D.P., Lovera, O.M., Kelty, T.K., Gehrels, G.E., and Foster, D.A., 2009, Gangdese arc detritus within the eastern Himalayan Neogene foreland basin: Implications for the Neogene evolution of the Yalu–Brahmaputra River system: Earth and Planetary Science Letters, v. 285, no. 1-2, p. 150–162, doi: 10.1016/j.epsl.2009.06.005.

Clift, P.D., Lee, J.I., Hildebrand, P., Shimizu, N., Layne, G.D., Blusztajn, J., Blum, J.D., Garzanti, E., and Khan, A.A., 2002, Nd and Pb isotope variability in the Indus River System: implications for sediment provenance and crustal heterogeneity in the Western Himalaya: Earth and Planetary Science Letters, v. 200, no. 1, p. 91–106.

Das, A., Krishnaswami, S., Sarin, M.M., and Pande, K., 2005, Chemical weathering in the Krishna Basin and Western Ghats of the Deccan Traps, India: Rates of basalt weathering and their controls: Geochimica et Cosmochimica Acta, v. 69, no. 8, p. 2067–2084, doi: 10.1016/j.gca.2004.10.014.

David, K., Frank, M., O'Nions, R., Belshaw, N., and Arden, J., 2001, The Hf isotope composition of global seawater and the evolution of Hf isotopes in the deep Pacific Ocean from Fe-Mn crusts: Chemical Geology, v. 178, no. 1-4, p. 23–42.

Dessert, C., Dupré, B., François, L.M., Schott, J., Gaillardet, J., Chakrapani, G., and Bajpai, S., 2001, Erosion of Deccan Traps determined by river geochemistry: impact on the global climate and the 87Sr/86Sr ratio of seawater: Earth and Planetary Science Letters, v. 188, no. 3-4, p. 459–474, doi: 10.1016/S0012-821X(01)00317-X.

Dessert, C., Dupré, B., Gaillardet, J., François, L.M., and Allègre, C.J., 2003, Basalt weathering laws and the impact of basalt weathering on the global carbon cycle: Chemical Geology, v. 202, no. 3-4, p. 257–273, doi: 10.1016/j.chemgeo.2002.10.001.

Dhuime, B., Hawkesworth, C.J., Storey, C.D., and Cawood, P.A., 2011, From sediments to their source rocks: Hf and Nd isotopes in recent river sediments: Geology, v. 39, no. 4, p. 407–410, doi: 10.1130/G31785.1.

Galy, A., and France-Lanord, C., 2001, Higher erosion rates in the Himalaya: Geochemical constraints on riverine fluxes: Geology, v. 29, no. 1, p. 23–26.

Garçon, M., Chauvel, C., and France-Lanord, C., 2012a, Almost half of worldwide sedimentary Nd-Hf isotopic decoupling done on continents: To be submitted to Geochemistry Geophysics Geosystems.

Garçon, M., Chauvel, C., France-Lanord, C., Limonta, M., and Garzanti, E., 2012b, New approach to the average upper continental crust Pb isotopic value: To be submitted to Nature Geoscience.

Garzanti, E., Andò, S., France-Lanord, C., Censi, P., Pietro Vignola, Galy, V., and Lupker, M., 2011, Mineralogical and chemical variability of fluvial sediments 2. Suspended-load

silt (Ganga–Brahmaputra, Bangladesh): Earth and Planetary Science Letters, v. 302, no. 1-2, p. 107–120, doi: 10.1016/j.epsl.2010.11.043.

Garzanti, E., Andò, S., France-Lanord, C., Vezzoli, G., Censi, P., Galy, V., and Najman, Y., 2010, Mineralogical and chemical variability of fluvial sediments 1. Bedload sand (Ganga–Brahmaputra, Bangladesh): Earth and Planetary Science Letters, v. 299, no. 3-4, p. 368–381, doi: 10.1016/j.epsl.2010.09.017.

Godfrey, L., Lee, D.-C., Sangrey, W., Halliday, A., Salters, V., Hein, J., and White, W., 1997, The Hf isotopic composition of ferromanganese nodules and crusts and hydrothermal manganese deposits: Implications for seawater Hf: Earth and Planetary Science Letters, v. 151, no. 1, p. 91–105.

Goldstein, S., and Jacobsen, S.B., 1988, Nd and Sr isotopic systematics of river water suspended material: implications for crustal evolution: Earth and Planetary Science Letters, v. 87, p. 249–265.

Goldstein, S.L., O'nions, R.K., and Hamilton, P.J., 1984, A Sm-Nd isotopic study of atmospheric dusts and particulates from major river systems: Earth and Planetary Science Letters, v. 70, no. 2, p. 221–236.

Hemming, S., and McLennan, S., 2001, Pb isotope compositions of modern deep sea turbidites: Earth and Planetary Science Letters, v. 184, no. 2, p. 489–503.

Jha, P.K., Subramanian, V., and Sitasawad, R., 1988, Chemical and sediment mass transfer in the Yamuna River-A tributary of the Ganges system: Journal of Hydrology, v. 104, no. 1-4, p. 237–246.

Jha, P.K., Vaithiyanathan, P., and Subramanian, V., 1993, Mineralogical characteristics of the sediments of a Himalayan river: Yamuna River - a tributary of the Ganges: Environmental Geology, no. 22, p. 13–20.

Kamber, B.S., Greig, A., and Collerson, K.D., 2005, A new estimate for the composition of weathered young upper continental crust from alluvial sediments, Queensland, Australia: Geochimica et Cosmochimica Acta, v. 69, no. 4, p. 1041–1058, doi: 10.1016/j.gca.2004.08.020.

Kramers, J.D., and Tolstikhin, I.N., 1997, Two terrestrial lead isotope paradoxes, forward transport modelling, core formation and the history of the continental crust: Chemical Geology, v. 139, no. 1, p. 75–110.

Krishnan, M.S., 1982, Geology of India and Burna: CBS Publishers and Distributors, New Delhi.

Le Fort, P., 1975, Himalayas: the collided range. Present knowledge of the continental arc: American Journal of Science.

Lupker, M., Blard, P.-H., lavé, J., France-Lanord, C., Leanni, L., Puchol, N., Charreau, J., and Bourlès, D., 2012, 10Be-derived Himalayan denudation rates and sediment budgets in the Ganga basin: Earth and Planetary Science Letters, v. 333-334, no. C, p. 146–156, doi: 10.1016/j.epsl.2012.04.020.

Lupker, M., France-Lanord, C., lavé, J., Bouchez, J., Galy, V., Métivier, F., Gaillardet, J., Lartiges, B., and Mugnier, J.-L., 2011, A Rouse-based method to integrate the chemical composition of river sediments: Application to the Ganga basin: Journal of Geophysical Research, v. 116, no. F4, F04012, doi: 10.1029/2010JF001947.

McLennan, S.M., McCulloch, M.T., Taylor, S.R., and Maynard, J.B., 1989, Effects of sedimentary sorting on neodymium isotopes in deep-sea turbidites: Nature, v. 337, no. 6207, p. 547–549, doi: 10.1038/337547a0.

McLennan, S.M., Taylor, S.R., McCulloch, M.T., and Maynard, J.B., 1990, Geochemical and Nd-Sr isotopic composition of deep-sea turbidites: Crustal evolution and plate tectonic associations: Geochimica et Cosmochimica Acta, v. 54, no. 7, p. 2015–2050, doi: 10.1016/0016-7037(90)90269-Q.

Millot, R., Allègre, C.J., Gaillardet, J., and Roy, S., 2004, Lead isotopic systematics of major river sediments: a new estimate of the Pb isotopic composition of the Upper Continental Crust: Chemical Geology, v. 203, no. 1, p. 75–90, doi: 10.1016/j.chemgeo.2003.09.002.

Padoan, M., Garzanti, E., Harlavan, Y., and Villa, I.M., 2011, Tracing Nile sediment sources by Sr and Nd isotope signatures (Uganda, Ethiopia, Sudan): Geochimica et Cosmochimica Acta, v. 75, no. 12, p. 3627–3644, doi: 10.1016/j.gca.2011.03.042.

Parrish, R.R., and Hodges, V., 1996, Isotopic constraints on the age and provenance of the Lesser and Greater Himalayan sequences, Nepalese Himalaya: Geological Society of America Bulletin, v. 108, no. 7, p. 904–911.

Pearce, J., Kempton, P., Nowell, G., and Noble, S., 1999, Hf-Nd element and isotope perspective on the nature and provenance of mantle and subduction components in Western Pacific arc-basin systems: Journal of Petrology, v. 40, no. 11, p. 1579–1611.

Plank, T., and Langmuir, C.H., 1998, The chemical composition of subducting sediment and its consequences for the crust and mantle: Chemical Geology, v. 145, no. 3-4, p. 325–394.

Prytulak, J., Vervoort, J.D., Plank, T., and Yu, C., 2006, Astoria Fan sediments, DSDP site 174, Cascadia Basin: Hf–Nd–Pb constraints on provenance and outburst flooding: Chemical Geology, v. 233, no. 3-4, p. 276–292, doi: 10.1016/j.chemgeo.2006.03.009.

Rengarajan, R., Singh, S.K., Sarin, M.M., and Krishnaswami, S., 2009, Strontium isotopes and major ion chemistry in the Chambal River system, India: Implications to silicate erosion rates of the Ganga: Chemical Geology, v. 260, no. 1-2, p. 87–101, doi: 10.1016/j.chemgeo.2008.12.013.

Richards, A., Argles, T., Harris, N., Parrish, R., Ahmad, T., Darbyshire, F., and Draganits, E., 2005, Himalayan architecture constrained by isotopic tracers from clastic sediments: Earth and Planetary Science Letters, v. 236, no. 3, p. 773–796, doi: 10.1016/j.epsl.2005.05.034.

Robinson, D.M., Decelles, P.G., Patchett, P.J., and Garzione, C.N., 2001, The kinematic evolution of the Nepalese Himalaya interpreted from Nd isotopes: Earth and Planetary Science Letters, v. 192, no. 4, p. 507–521.

Roddaz, M., Viers, J., Brusset, S., Baby, P., and Hérail, G., 2005, Sediment provenances and drainage evolution of the Neogene Amazonian foreland basin: Earth and Planetary Science Letters, v. 239, no. 1-2, p. 57–78, doi: 10.1016/j.epsl.2005.08.007.

Singh, P., 2009, Major, trace and REE geochemistry of the Ganga River sediments: Influence of provenance and sedimentary processes: Chemical Geology, v. 266, no. 3-4, p. 242–255, doi: 10.1016/j.chemgeo.2009.06.013.

Singh, S.K., Rai, S.K., and Krishnaswami, S., 2008, Sr and Nd isotopes in river sediments from the Ganga Basin: Sediment provenance and spatial variability in physical erosion: Journal of Geophysical Research, v. 113, no. F3, p. F03006, doi: 10.1029/2007JF000909.

Steinmann, M., and Stille, P., 2008, Controls on transport and fractionation of the rare earth elements in stream water of a mixed basaltic–granitic catchment basin (Massif Central, France): Chemical Geology, v. 254, no. 1, p. 1–18, doi: 10.1016/j.chemgeo.2008.04.004.

Tricca, A., Stille, P., Steinmann, M., Kiefel, B., Samuel, J., and Eikenberg, J., 1999, Rare earth elements and Sr and Nd isotopic compositions of dissolved and suspended loads from small river systems in the Vosges mountains (France), the river Rhine and groundwater: Chemical Geology, v. 160, no. 1, p. 139–158.

Van De Flierdt, T., Hemming, S.R., Goldstein, S.L., and Abouchami, W., 2006, Radiogenic isotope fingerprint of Wilkes Land–Adélie Coast Bottom Water in the circum-Antarctic Ocean: Geophysical Research Letters, v. 33, no. 12, p. L12606, doi: 10.1029/2006GL026020.

Vervoort, J., Plank, T., and Prytulak, J., 2011, The Hf-Nd isotopic composition of marine sediments: Geochimica et Cosmochimica Acta, p. 1–70, doi: 10.1016/j.gca.2011.07.046.

Vervoort, J.D., Patchett, P.D., Blichert-Toft, J., and Albarède, F., 1999, Relationships between Lu–Hf and Sm–Nd isotopic systems in the global sedimentary system: Earth and Planetary Science Letters, v. 168, p. 79–99.

Vlastélic, I., 2005, Miocene climate change recorded in the chemical and isotopic (Pb, Nd, Hf) signature of Southern Ocean sediments: Geochemistry Geophysics Geosystems, v. 6, no. 3, p. Q03003, doi: 10.1029/2004GC000819.

White, W.M., Patchett, J., and BenOthman, D., 1986, Hf isotope ratios of marine sediments and Mn nodules: evidence for a mantle source of Hf in seawater: Earth and Planetary Science Letters, v. 79, no. 1-2, p. 46–54.

Woodhead, J., Hergt, J., Davidson, J., and Eggins, S., 2001, Hafnium isotope evidence for "conservative"element mobility during subduction zone processes: Earth and Planetary Science Letters, v. 192, no. 3, p. 331–346.

Wu, W., Xu, S., Yang, J., Yin, H., Lu, H., and Zhang, K., 2010, Isotopic characteristics of river sediments on the Tibetan Plateau: Chemical Geology, v. 269, no. 3-4, p. 406–413, doi: 10.1016/j.chemgeo.2009.10.015.

SUPPLEMENTARY MATERIAL

Supplementary Table 1: Trace element concentrations and Nd-Hf-Pb of the Chambal, Yamuna and Ganga sediments

Footnote : * Data already published by Garçon et al. (2012a ; 2012b)

Uncertainties (± 2σ) reported in the Table correspond to in-run errors

εNd and εHf were calculated using the CHUR composition of Bouvier et al. (2008)

Trace element concentrations and Nd, Hf, Pb isotopic compositions were measured using ICP-MS and MC-ICP-MS, respectively, following analytical procedures described by Garçon et al. (2012a ; 2012b)

Supplementary Table 1: Trace element concentrations and Nd-Hf-Pb of the Chambal, Yamuna and Ganga sediments

				Depth profile				
Sample Name	BR 935	BR 937	BR 938	BR 913	BR 912	BR 911	BR 914	BR 717*
Sampling date	14-Aug-09	14-Aug-09	14-Aug-09	9-Aug-09	9-Aug-09	9-Aug-09	9-Aug-09	17-Aug-07
Latitude (°N)	26.657	26.657	26.657	26.1306	26.1306	26.1306	26.1306	24.0529
Longitude (°E)	77.903	77.903	77.903	79.7539	79.7539	79.7539	79.7539	89.0247
River	Chambal	Chambal	Chambal	Yamuna	Yamuna	Yamuna	Yamuna	Ganga
Type of sediment	Suspended load	Bank sediment	Bank sediment	Suspended load	Suspended load	Suspended load	Bedload	Bedload
Sampling depth (m)	0			0.2	3.3	7.3	≈10	11
Cs	7.84	1.30	5.02	7.99	7.65	6.15	2.22	3.87
Rb	105	44.2	77.2	110	109	95.0	57.8	50.3
Ba	346	267	325	394	389	362	293	244
Th	12.0	15.8	9.50	11.6	12.8	13.5	20.1	74.2
U	1.95	2.29	1.69	2.73	2.23	2.62	3.69	11.7
Nb	13.6	8.24	10.5	14.1	14.2	14.9	14.6	20.3
Ta	1.00	0.655	0.783	1.05	1.08	1.15	1.35	2.50
La	28.7	34.0	24.2	27.5	30.5	35.8	51.1	141
Ce	62.6	68.7	54.1	61.0	69.2	78.5	107	292
Pr	6.95	8.06	6.03	6.66	7.52	8.64	11.8	33.1
Pb	23.1	14.0	17.5	24.9	28.0	21.3	16.6	14.2
Nd	27.2	30.2	23.2	25.3	28.6	32.2	43.1	121
Sr	204	132	180	193	172	167	160	98.3
Sm	5.57	5.69	4.65	5.20	5.71	6.50	8.24	22.3
Zr	133	383	159	144	177	276	621	1550
Hf	3.53	9.74	4.10	3.75	4.43	6.95	15.3	40.5
Ti	5415	3588	4334	5038	5118	5216	5019	5299
Eu	1.23	0.902	1.08	1.16	1.18	1.26	1.29	2.24
Gd	4.86	4.63	4.39	4.76	5.18	5.53	6.61	17.7
Tb	0.751	0.69	0.664	0.754	0.78	0.839	1.01	2.52
Dy	4.74	4.24	4.12	4.52	4.75	5.03	5.96	14.7
Ho	0.935	0.814	0.809	0.898	0.911	0.999	1.14	2.83
Y	25.9	23.8	23.3	24.9	25.5	28.0	33.7	85.6
Er	2.62	2.34	2.33	2.59	2.59	2.82	3.40	8.11
Li	48.5	9.60	30.2	46.6	43.9	35.5	13.4	15.7
Yb	2.44	2.28	2.17	2.44	2.44	2.79	3.36	8.17
Lu	0.358	0.344	0.316	0.354	0.356	0.400	0.506	1.25
Sc	22.0	7.01	12.3	20.4	18.8	16.9	10.7	14.3
V	162	60.8	115	142	138	120	64.1	53.5
Cr	123	72.2	83.1	113	108	112	88.5	44.1
Co	25.7	6.00	18.1	22.5	20.6	17.1	6.82	6.40
Ni	83.5	19.5	52.3	74.1	67.4	53.1	19.1	12.4
Cu	106	20.5	54.8	98.2	73.0	47.0	16.9	7.10
Zn	125	23.5	57.2	157	187	73.9	34.2	31.0
$^{143}Nd/^{144}Nd \pm 2\sigma$	0.512122 ± 8	0.511779 ± 8	0.512038 ± 6	0.512101 ± 8	0.512051 ± 7	0.512008 ± 6	0.511835 ± 5	0.511769 ± 7
ε_{Nd}	-9.9	-16.6	-11.6	-10.3	-11.3	-12.1	-15.5	-16.8
Duplicate								
$^{176}Hf/^{177}Hf \pm 2\sigma$	0.282656 ± 7	0.282101 ± 7	0.282426 ± 9	0.282605 ± 7	0.282506 ± 5	0.282340 ± 6	0.282140 ± 9	0.281930 ± 6
ε_{Hf}	-4.5	-24.2	-12.7	-6.4	-9.9	-15.7	-22.8	-30.2
Re-run		0.282112 ± 9						
Duplicate							0.282139 ± 9	
$^{208}Pb/^{204}Pb \pm 2\sigma$	39.0273 ± 42	40.4987 ± 36	39.2603 ± 38	39.2302 ± 74	39.0014 ± 28	39.6362 ± 24	40.3682 ± 40	42.4525 ± 26
Re-run			39.2661 ± 26					
$^{207}Pb/^{204}Pb \pm 2\sigma$	15.7228 ± 12	15.8277 ± 14	15.7527 ± 12	15.7618 ± 24	15.7500 ± 8	15.8067 ± 8	15.8824 ± 12	16.1109 ± 8
Re-run			15.7536 ± 8					
$^{206}Pb/^{204}Pb \pm 2\sigma$	18.7124 ± 12	19.2689 ± 10	18.8164 ± 12	18.9519 ± 22	18.1184 ± 8	19.2948 ± 8	19.9554 ± 10	22.1618 ± 10
Re-run			18.8193 ± 8					

Supplementary Table 1 (continued)

	Depth profile							
Sample Name	BR 415*	BR 414*	BR 413*	BR 412*	BR 411*	BR 418*	BGP 6*	BR 8253*
Sampling date	13-Jul-04	13-Jul-04	13-Jul-04	13-Jul-04	13-Jul-04	13-Jul-04	2-Aug-93	10-Sep-08
Latitude (°N)	24.0529	24.0529	24.0529	24.0529	24.0529	24.0529	24.3583	24.0529
Longitude (°E)	89.0247	89.0247	89.0247	89.0247	89.0247	89.0247	88.6083	89.0247
River	Ganga	Ganga	Ganga	Ganga	Ganga	Ganga	Ganga	Ganga
Type of sediment	Suspended Load	Suspended Load	Suspended Load	Suspended Load	Suspended Load	Bedload	Bedload	Suspended Load
Sampling depth (m)	0	2	4	6.5	9	10		0
Cs	15.4	13.6	11.8	11.7	8.08	2.64	3.83	8.92
Rb	202	186	174	175	107	56.6	77.9	51.7
Ba	627	562	531	527	372	212	294	240
Th	20.0	19.0	19.3	18.0	15.1	29.7	30.2	16.1
U	4.64	4.08	4.15	3.96	2.92	5.14	5.41	1.85
Nb	17.4	17.9	16.5	15.7	13.6	18.4	12.9	15.8
Ta	1.54	1.57	1.45	1.39	1.37	2.08	1.78	1.31
La	42.0	41.3	42.2	40	32.8	71.0	67.1	30.8
Ce	89.4	88.1	89.2	84.7	76.3	146	144	75.4
Pr	9.75	9.77	9.87	9.29	7.84	16.7	15.5	8.12
Pb	30.4	26.2	25.3	25.3	17.4	15.0	17.8	10.5
Nd	35.0	35.7	35.8	34.0	29.0	60.4	56.5	31.2
Sr	84.1	91.0	99.3	101	88.6	103	115	56.5
Sm	6.93	6.98	7.01	6.77	5.60	12.0	10.9	6.27
Zr	178	204	227	199	249	479	683	196
Hf	4.73	5.22	5.79	5.17	6.14	12.1	17.1	5.13
Ti	4137	4198	3976	3833	3314	4355	3155	4323
Eu	1.27	1.26	1.23	1.20	1.04	1.48	1.39	1.19
Gd	6.19	6.15	6.05	5.80	4.96	10.1	8.51	5.44
Tb	0.984	0.945	0.93	0.872	0.782	1.64	1.25	0.854
Dy	5.97	5.74	5.72	5.42	4.81	10.3	7.24	5.32
Ho	1.17	1.15	1.13	1.06	0.95	2.12	1.39	1.06
Y	32.7	32.8	32.5	30.9	27.1	62.0	41.1	31.1
Er	3.33	3.3	3.21	3.07	2.65	6.35	3.99	3.04
Li	51.8	48.2	43.5	41.9	32.2	15.8	14.7	45.3
Yb	3.18	3.11	3.06	2.88	2.51	6.23	3.87	2.95
Lu	0.461	0.45	0.448	0.417	0.366	0.905	0.587	0.433
Sc	15.0	14.4	13.5	12.8	9.04	13.2	7.74	11.8
V	93.4	90.7	81.1	79.1	61.8	46.9	32.7	100
Cr	76.6	81.9	67.0	63.4	53.4	40	36.9	73.6
Co	15.5	15.1	13.6	13.4	10.3	5.58	3.93	13.8
Ni	38.6	40.5	32.4	31.5	26.4	11.7	11.0	39.4
Cu	33.9	31.7	25.7	23.7	24.3	10.0	10.9	39.4
Zn	84.9	83.5	73.3	72.1	56.6	38.8	29.1	70.4
$^{143}Nd/^{144}Nd \pm 2\sigma$	0.511752 ± 6	0.511736 ± 8	0.511748 ± 6	0.511745 ± 7	0.511755 ± 6	0.511719 ± 5	0.511758 ± 9	0.511767 ± 8
ε_{Nd}	-17.1	-17.4	-17.2	-17.3	-17.1	-17.8	-17.0	-16.8
Duplicate					0.511723 ± 7			
$^{176}Hf/^{177}Hf \pm 2\sigma$	0.282241 ± 9	0.282226 ± 6	0.282205 ± 6	0.282209 ± 6	0.282133 ± 7	0.281992 ± 11	0.282027 ± 11	0.282268 ± 7
ε_{Hf}	-19.2	-19.8	-20.5	-20.4	-23.0	-28.1	-26.8	-18.3
Re-run								
Duplicate								
$^{208}Pb/^{204}Pb \pm 2\sigma$	40.3003 ± 18	40.3019 ± 24	40.2931 ± 34	40.2725 ± 16	40.1312 ± 28	40.8292 ± 24	40.6213 ± 44	39.9963 ± 28
Re-run								
$^{207}Pb/^{204}Pb \pm 2\sigma$	15.8991 ± 6	15.9013 ± 6	15.9040 ± 8	15.9040 ± 6	15.8984 ± 10	15.9684 ± 8	15.9733 ± 14	15.8730 ± 14
Re-run								
$^{206}Pb/^{204}Pb \pm 2\sigma$	20.0301 ± 6	20.0574 ± 8	20.0912 ± 8	20.0756 ± 8	20.0387 ± 10	20.6767 ± 10	20.7277 ± 14	19.7765 ± 10
Re-run								

Supplementary Table 2 : Endmembers for Nd-Hf isotopic mixings

Footnote : The composition of the different mixing endmembers were constrained using the data of Garçon et al. (2012) for the Ganga sediments and the GEOROC database for the Deccan Traps. ε_{Nd} and ε_{Hf} are calculated using the CHUR composition of Bouvier et al. (2008)

Supplementary Table 2: Endmembers for Nd-Hf isotopic mixings

	Hf (ppm)	ε_{Hf}	Nd (ppm)	ε_{Nd}
Ganga surface suspended load	4.5	-18.2	34	-17.2
Ganga intermediate suspended load	6	-23.1	34	-17.2
Ganga deep suspended load	7	-25.6	34	-17.2
Ganga bedload	14	-28.1	54	-17.2
Deccan Traps	5	11.8	30	5.3

Supplementary Figure : Pb isotopic compositions of the Ganga, Yamuna and Chambal sediments.

Footnote : Red triangles : Northern Deccan Traps basalts (GEOROC database). The black star shows the composition of the Himalayan crust as estimated by Garçon et al. (2012b)

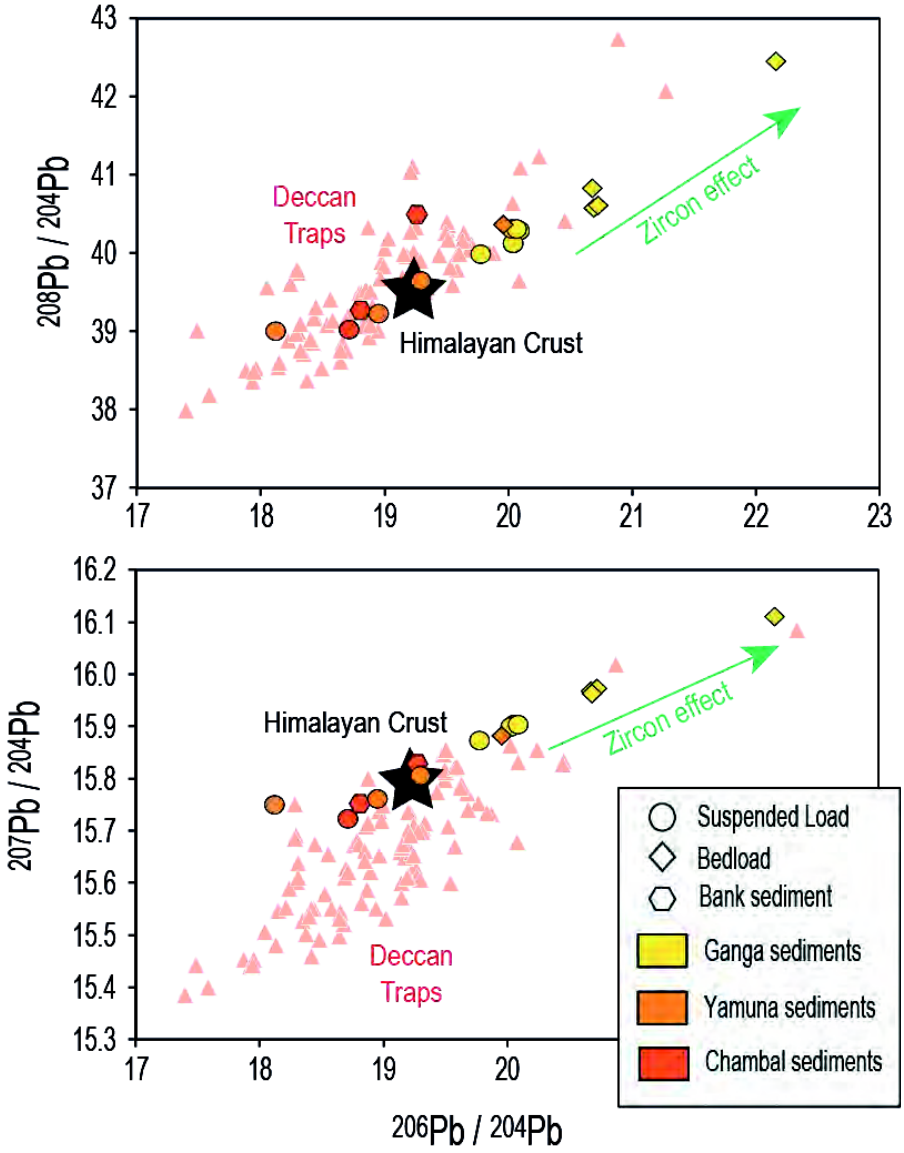

Conclusion

L'étude réalisée au cours de ces trois années de thèse est construite autour de l'analyse des concentrations en éléments traces et des compositions isotopiques en Nd, Hf, Pb et Sr de plusieurs types de sédiments provenant du Ganges et de ses principaux affluents drainant la chaîne Himalayenne, le nord du bouclier Indien et une partie des Traps du Deccan. Ces données permettent de mieux comprendre l'influence des processus sédimentaires sur les compositions chimiques et isotopiques des sédiments transportés par les rivières sur le continent ainsi que leurs conséquences, à plus grande échelle, sur le système sédimentaire globale incluant la sédimentation océanique. Les données acquises sur les fractions de minéraux purs séparés à partir d'un échantillon situé à une position stratégique, à l'embouchure du Ganges, constituent l'une des premières bases de données complètes répertoriant les compositions chimiques et isotopiques d'espèces minérales séparées. Ces données offrent de nouvelles perspectives pour la compréhension des systématiques isotopiques dans les sédiments Himalayens mais elles pourront également être utilisées pour caractériser celles d'autres matériaux ou roches affleurant à la surface de la Terre.

Les chapitres 3 et 4 de cette thèse sont consacrés à la variabilité chimique et isotopique générée par les processus de tri minéralogique au cours du transport des sédiments, de leur source jusqu'à l'océan. Dans le système fluviatile du Ganges, les produits d'érosion de la chaîne Himalayenne sont caractérisés par des compositions isotopiques en Nd très peu variables (ε_{Nd} = -17.8 ± 1.9, 2σ) quelque soit le type de sédiments et le lieu d'échantillonnage i.e. en sortie de chaîne ou plus en aval dans la plaine Indo-Gangétique jusqu'au delta du Bangladesh. Cette stabilité du signal Nd indique, d'une part, que les sédiments sont homogénéisés bien avant leur entrée dans la plaine alluviale et, d'autre part, que le système isotopique Sm-Nd est très peu affecté par les effets de tri minéralogique au cours du transport fluviatile. En effet, les simulations Monte-Carlo, réalisées à partir des données acquises sur les fractions de minéraux purs, montrent que la plus grande partie du budget isotopique du Nd (60 à 100%) dans les sédiments de fond de rivière et dans ceux transportés en suspension est contrôlé par les mêmes minéraux, en l'occurrence la monazite et l'allanite. Ces deux espèces minérales sont présentes en très faibles proportions dans les sédiments du Ganges (< 0.4 wt%) mais ont la particularité d'être extrêmement riches en Nd (concentrations entre 10 000 et 100 000 ppm), d'où leur importance dans le budget isotopique des sédiments.

Les systématiques isotopiques de l'Hf dans les produits d'érosion de la chaîne Himalayenne sont beaucoup plus variables. Les sédiments de fond de rivière sont

généralement caractérisés par des signatures moins radiogéniques que celles des sédiments transportés en suspension, proche de la surface de l'eau. Ces différences entre les sédiments profonds et ceux de surface augmentent significativement avec la distance de transport, du front de chaîne au delta du Bangladesh où elles atteignent plus de 10 ε_{Hf} au même lieu d'échantillonnage. Ces larges variations résultent de l'expression des processus hydrodynamiques qui ségréguent les minéraux en fonction de leur taille, de leur densité et de leur forme dans la colonne d'eau. Malgré la faible proportion de zircons présents dans les sédiments du Ganges (<0.5 wt%), nos résultats montrent que ces minéraux très denses, extrêmement riches en Hf (concentration > 10 000 ppm) et très peu radiogéniques, contrôlent la quasi totalité du budget isotopique en Hf des sédiments de fond de rivières (65 à 95%). La signature plus radiogénique des sédiments transportés en suspension s'explique par une contribution plus faible, mais significative, des zircons (< 60%) et par les contributions d'autres minéraux plus radiogéniques, tels que les micas ou les argiles.

Les compositions isotopiques en Pb des produits d'érosion de la chaîne Himalayenne sont relativement radiogéniques et s'étendent sur une gamme de variabilité aussi grande que celle connue pour le manteau Terrestre. Comme pour l'Hf, des variations systématiques de composition isotopique sont observées entre les sédiments de fond de rivière et ceux transportés en suspension. De manière générale, ces derniers sont caractérisés par des valeurs moins radiogéniques que les sédiments profonds. Une grande partie du budget isotopique du Pb apparaît être contrôlé par les feldspaths et les argiles mais les simulations Monte-Carlo montrent que les zircons sont indispensables pour reproduire les compositions radiogéniques des différents types de sédiments transportés par le Ganges. La composition isotopique en Pb de ces derniers est donc largement affectée par les processus de tri minéralogique dans la colonne d'eau qui produisent un " effet zircon " beaucoup plus marqué que celui affectant les isotopes de l'Hf. Cet effet des zircons a été largement sous-estimé par les études précédentes puisque ces minéraux ne contiennent qu'une dizaine de ppm de Pb et ne sont généralement présents qu'en très faibles proportions dans les sédiments de rivière. Cependant, cette étude démontre que leur composition extrêmement radiogénique en Pb (rapports $^{206}Pb/^{204}Pb$ et $^{208}Pb/^{204}Pb$ > 1 000 et $^{207}Pb/^{204}Pb$ > 100), est suffisante pour significativement influencer la signature isotopique globale des sédiments de rivière.

Les quelques compositions isotopiques en Sr, qui ont été mesurées sur des sédiments échantillonnés à l'embouchure du Ganges, sont extrêmement radiogéniques (0.754593 < $^{86}Sr/^{87}Sr$ < 0.773743). Comme pour l'Hf et le Pb, les résultats montrent que les isotopes du Sr sont sensibles aux processus de tri minéralogique puisque les sédiments de

fonds de rivière sont caractérisés par des compositions moins radiogéniques que ceux transportés en suspension. Les simulations Monte-Carlo indiquent que le budget isotopique du Sr dans les sédiments du Ganges est principalement contrôlé par les feldspath-K, les plagioclases, les muscovites, les argiles et les carbonates. Même si les compositions très radiogéniques en Sr des sédiments transportés en suspension sont difficiles à modéliser, il apparaît réaliste de penser que ces dernières s'expliquent par une contribution plus importante des minéraux radiogéniques tels que les muscovites et les feldspath-K par rapport aux sédiments de fond de rivière.

Les résultats présentés dans le dernier chapitre de cette thèse montrent que d'importantes variations isotopiques de provenance peuvent s'associer aux variations générées par le tri minéralogique dans la colonne d'eau. Ces variations de provenance sont uniquement observées au sud du système Himalayen, dans les sédiments de la Yamuna et de la Chambal qui drainent des bassins versants constitués de 20 à 30% de basaltes appartenant aux Traps du Deccan. A la différence des sédiments du Ganges et de ses affluents drainant, en majeure partie, des roches cristallines et sédimentaires, les sédiments de la Yamuna et de la Chambal présentent des compositions isotopiques en Nd plus radiogéniques en surface ($\varepsilon_{Nd} \approx -10$) qu'en profondeur ($\varepsilon_{Nd} \approx -16$). Les différences isotopiques en Hf et Pb entre les sédiments de surface et ceux de fond de rivière sont également beaucoup plus prononcées que celles observées pour les sédiments du Ganges puisqu'elles atteignent, par exemple, 15 ε_{Hf} au même lieu d'échantillonnage dans la Yamuna. Les calculs de mélange isotopique réalisés à partir des données Nd et Hf montrent que les produits d'érosion des basaltes du Deccan sont transportés en plus grande quantité dans les sédiments en suspension, à la surface de l'eau (30-40%), que dans le fond de la rivière (<10%). Au contraire, les produits d'érosion des roches cristallines et sédimentaires de la chaîne Himalayenne et du bouclier nord-Indien impriment préférentiellement leur signature isotopique dans les sédiments transportés au fond de la rivière sous forme de bedload. Ces différences de provenance sont expliquées par les contrastes d'érodabilité importants existant entre les basaltes, facilement altérables et formant des produits d'érosion relativement fins, et les roches cristallines et sédimentaires, plus résistantes et formant des produits d'érosion plus grossiers.

L'ensemble des résultats obtenus au cours de cette thèse montre que les processus d'érosion et de tri minéralogique au cours du transport fluviatile peuvent conduire à un fractionnement majeur du message isotopique porté par les sédiments de rivières. Ces

résultats soulèvent donc quelques interrogations quant à l'utilisation des compositions isotopiques des sédiments pour tracer leurs sources ou en tant que proxys représentatifs de la composition isotopique moyenne du bassin drainé.

Dans le cas où les lithologies principales exposées dans le bassin versant présentent de forts contrastes d'érodabilité i.e. des basaltes et des roches plus cristallines comme c'est le cas pour la Yamuna et la Chambal, la signature isotopique en Nd, Hf et Pb des sédiments apparaît inévitablement biaisée par les processus d'érosion différentielle. Les proportions de matériel basaltique sont sur-représentées dans les sédiments transportés en suspension, près de la surface de l'eau, et sous-représentées dans les sédiments de fond de rivières.

Lorsque le bassin versant est principalement constitué de roches sédimentaires et cristallines, comme pour le Ganges et ses affluents drainant la chaîne Himalayenne, nos résultats confirment que les compositions isotopiques en Nd mesurés dans les sédiments de surface ou de fond de rivière constituent de très bons traceurs de sources. Quelques précautions sont cependant à prendre pour utiliser les systèmes isotopiques de l'Hf, du Pb et du Sr qui sont significativement fractionnés par les processus de tri minéralogique au cours du transport des sédiments dans le réseau fluviatile. Les compositions isotopiques en Hf des sédiments de fond de rivière apparaissent quasiment entièrement contrôlées par les zircons et peuvent donc être utilisées au même titre que les compositions isotopiques en Hf directement mesurées sur des grains individuels pour tracer la provenance des sédiments. Au contraire, les isotopes de l'Hf dans les sédiments de surface sont contrôlées par des minéraux plus radiogéniques (micas, argiles, etc…) dont les compositions isotopiques sont peu représentatives de celles de leurs roches sources dans le bassin versant. Pour le Pb, nous avons montré que les signatures isotopiques des sédiments de surface et de fond de rivière peuvent être toutes les deux significativement biaisées par un " effet zircon " qui limite donc leur utilisation pour tracer la provenance des sédiments. Une solution alternative consiste à mesurer les compositions isotopiques des fractions de feldspath-K et/ou d'argiles séparées du sédiment. Enfin, la variabilité isotopique du Sr semble être liée aux différentes proportions de muscovite et de feldspath-K dans les sédiments de surface et dans ceux de fond de rivière. Ce système isotopique apparait relativement compliqué à utiliser pour tracer la provenance des sédiments. Une étude plus complète sur les compositions isotopiques en Sr des sédiments de rivière (partie sillicatée + partie carbonatée) et dans des fractions de minéraux purs plus fines pourrait permettre de mieux comprendre l'origine des variabilités isotopiques observées.

L'importance du réseau fluviatile du Ganges dans le système sédimentaire mondial permet d'interpréter les systématiques isotopiques observées dans ses sédiments dans un contexte plus global impliquant les sédiments océaniques et leur recyclage dans le manteau Terrestre au niveau des zones de subduction. Nous avons montré l'existence d'importantes variabilités isotopiques causées par les processus sédimentaires dans le domaine continental. A l'interface continent/océan, la diminution significative de l'énergie hydraulique, qui permet la mise en suspension de certains sédiments en milieu fluviatile, pourrait accentuer davantage les effets du tri minéralogique déjà amorcés sur le continent. Ainsi, nous suggérons que le matériel détritique fin, exporté loin des marges continentales dans l'océan profond, pourrait être caractérisé par des compositions isotopiques encore plus radiogéniques en Hf et moins radiogéniques en Pb et Sr que celles mesurées dans les sédiments transportés en suspension dans les rivières. L'étude des systématiques isotopiques des sédiments en suspension au niveau de l'estuaire et lorsque que l'on s'éloigne des marges continentales pourrait permettre de confirmer cette hypothèse et de mieux contraindre les processus mis en œuvre à l'interface continent/océan.

Pour le système isotopique de l'Hf, plusieurs études avaient, auparavant, souligné l'importance du fractionnement causé par l'effet zircon dans les sédiments argileux de grands fonds océaniques qui présentent des signatures isotopiques en Hf plus radiogéniques que la croûte continentale moyenne. Ici, nous montrons que la moitié de ce fractionnement a lieu sur le continent lorsque les sédiments sont transportés et triés hydrodynamiquement dans le réseau fluviatile. La seconde moitié pourrait être causée par le changement de conditions hydrodynamiques à l'estuaire. A l'échelle de la planète Terre, les conséquences sur l'évolution isotopique à long terme du réservoir mantellique pourraient être importantes si la composition très radiogénique en Hf des sédiments argileux de grands fonds océaniques est transmise au manteau dans les zones de subduction depuis plusieurs millions d'années. Nous suggérons que ce processus de recyclage des sédiments océaniques pourrait notamment être à l'origine d'une légère déviation de la composition isotopique en Hf du manteau au cours des temps géologiques. Malheureusement, cette hypothèse est difficilement vérifiable en raison de la faible quantité de données isotopiques en Hf disponible pour les roches ayant été formées au début de l'histoire de la Terre. Une étude ciblée sur la mesure des isotopes de l'Hf dans des roches soigneusement sélectionnées et dont les âges couvriraient l'histoire de la terre apporterait peut-être des réponses sur ce sujet délicat.

Bibliographie

A

Ahmad, T., Harris, N., Bickle, M., Chapman, H., Bunbury, J., Prince, C., 2000. Isotopic constraints on the structural relationships between the lesser Himalayan series and the high Himalayan crystalline series, Garhwal Himalaya. Geological Society of America Bulletin 112, 467–477.

Albarède, F., Goldstein, S.L., Dautel, D., 1997. The neodymium isotopic composition of manganese nodules from the Southern and Indian oceans, the global oceanic neodymium budget, and their bearing on deep ocean circulation. Geochimica et Cosmochimica Acta 61, 1277–1291.

Albarède, F., Simonetti, A., Vervoort, J.D., Blichert-Toft, J., Abouchami, W., 1998. A Hf-Nd isotopic correlation in ferromanganese nodules. Geophys. Res. Lett. 25, 3895–3898.

Allègre, C.J., Dupré, B., Négrel, P., Gaillardet, J., 1996. Sr-Nd-Pb isotope systematics in Amazon and Congo River systems: constraints about erosion processes. Chemical Geology 131, 93–112.

Armstrong, R.L., 1981. Radiogenic Isotopes: The Case for Crustal Recycling on a Near-Steady-State No-Continental-Growth Earth. Philosophical Transactions of the Royal Society of London 301, 443–472.

Asmerom, Y., Jacobsen, S.B., 1993. The Pb isotopic evolution of the Earth: inferences from river water suspended loads. Earth and Planetary Science Letters 115, 245–256.

Attal, M., lavé, J., 2006. Changes of bedload characteristics along the Marsyandi River (central Nepal): Implications for understanding hillslope sediment supply, sediment load evolution along fluvial networks, and denudation in active orogenic belts. Geological Society of America Special Paper 398, 143–171.

B

Bayon, G., Burton, K.W., Soulet, G., Vigier, N., Dennielou, B., Etoubleau, J., Ponzevera, E., German, C.R., Nesbitt, R.W., 2009. Hf and Nd isotopes in marine sediments: Constraints on global silicate weathering. Earth and Planetary Science Letters 277, 318–326.

Bayon, G., German, C.R., Boella, R.M., Milton, J.A., Taylor, R.N., Nesbitt, R.W., 2002. An improved method for extracting marine sediment fractions and its application to Sr and Nd isotopic analysis. Chemical Geology 187, 179–199.

Bayon, G., Vigier, N., Burton, K.W., Jean Carignan, A.B., Etoubleau, J., Chu, N.-C., 2006. The control of weathering processes on riverine and seawater hafnium isotope ratios. Geology 34, 433.

Bea, F., 1996. Residence of REE, Y, Th and U in granites and crustal protoliths; implications for the chemistry of crustal melts. Journal of Petrology 37, 521–552.

Belousova, E.A., Kostitsyn, Y.A., Griffin, W.L., Begg, G.C., O'reilly, S.Y., Pearson, N.J., 2010. The growth of the continental crust: Constraints from zircon Hf-isotope data. LITHOS 119, 457–466.

Belousova, E.A., Preiss, W.V., Schwarz, M.P., Griffin, W.L., 2006. Tectonic affinities of the Houghton Inlier, South Australia: U – Pb and Hf-isotope data from zircons in modern

stream sediments. Australian Journal of Earth Sciences 53, 971–989.
Ben Othman, D., White, W.M., Patchett, J., 1989. The geochemistry of marine sediments, island arc magma genesis, and crust-mantle recycling. Earth and Planetary Science Letters 94, 1–21.
Bennett, V.C., Nutman, A.P., McCulloch, M.T., 1993. Nd isotopic evidence for transient, highly depleted mantle reservoirs in the early history of the Earth. Earth and Planetary Science Letters 119, 299–317.
Berner, E.K., Berner, R.A., 2012. Global Environment, 2nd ed. Princeton University Press.
Blichert-Toft, J., 2003. Hawaiian hot spot dynamics as inferred from the Hf and Pb isotope evolution of Mauna Kea volcano. Geochem. Geophys. Geosyst. 4, 8704.
Blichert-Toft, J., Albarède, F., Rosing, M., Frei, R., Bridgwater, D., 1999. The Nd and Hf isotopic evolution of the mantle through the Archean. Results from the Isua supracrustals, West Greenland, and from the Birimian terranes of West Africa. Geochimica et Cosmochimica Acta 63, 3901–3914.
Blichert-Toft, J., Chauvel, C., Albar x000E8 de, F., 1997. Separation of Hf and Lu for high-precision isotope analysis of rock samples by magnetic sector-multiple collector ICP-MS. Contrib Mineral Petrol 127, 248–260.
Bodet, F., Schärer, U., 2000. Evolution of the SE-Asian continent from U-Pb and Hf isotopes in single grains of zircon and baddeleyite from large rivers. Geochimica et Cosmochimica Acta 64, 2067–2091.
Bookhagen, B., Thiede, R.C., Strecker, M.R., 2005a. Late Quaternary intensified monsoon phases control landscape evolution in the northwest Himalaya. Geology 33, 149.
Bookhagen, B., Thiede, R.C., Strecker, M.R., 2005b. Abnormal monsoon years and their control on erosion and sediment flux in the high, arid northwest Himalaya. Earth and Planetary Science Letters 231, 131–146.
Bouchez, J., Gaillardet, J., France-Lanord, C., Maurice, L., Dutra-Maia, P., 2011. Grain size control of river suspended sediment geochemistry: Clues from Amazon River depth profiles. Geochem. Geophys. Geosyst. 12, Q03008.
Bouvier, A., Vervoort, J.D., Patchett, P.J., 2008. The Lu–Hf and Sm–Nd isotopic composition of CHUR: constraints from unequilibrated chondrites and implications for the bulk composition of terrestrial planets. Earth and Planetary Science Letters 273, 48–57.

C

Carignan, J., Hild, P., Mevelle, G., Morel, J., Yeghicheyan, D., 2007. Routine Analyses of Trace Elements in Geological Samples using Flow Injection and Low Pressure On-Line Liquid Chromatography Coupled to ICP-MS: A Study of Geochemical Reference Materials BR, DR-N, UB-N, AN-G and GH. Geostandards and Geoanalytical Research 25, 187–198.
Carpentier, M., 2007. Compoition chimique des sédiments entrant dans la zone de subduction des Petites Antilles. Thèse LGCA, Grenoble.
Carpentier, M., Chauvel, C., Mattielli, N., 2008. Pb–Nd isotopic constraints on sedimentary input into the Lesser Antilles arc system. Earth and Planetary Science Letters 272, 199–211.

Carpentier, M., Chauvel, C., Maury, R.C., Mattielli, N., 2009. The “zircon effect” as recorded by the chemical and Hf isotopic compositions of Lesser Antilles forearc sediments. Earth and Planetary Science Letters 287, 86–99.

Chakrapani, G.J., Saini, R.K., 2009. Temporal and spatial variations in water discharge and sediment load in the Alaknanda and Bhagirathi Rivers in Himalaya, India. Journal of Asian Earth Sciences 35, 545–553.

Chamley, H., 1989. Clay sedimentology, 1st ed. Springer. 623 pp.

Chauvel, C., Blichert-Toft, J., 2001. A hafnium isotope and trace element perspective on melting of the depleted mantle. Earth and Planetary Science Letters 190, 137–151.

Chauvel, C., Bureau, S., Poggi, C., 2011. Comprehensive chemical and isotopic analyses of basalt and sediment reference materials. Geostandards and Geoanalytical Research 35, 125–143.

Chauvel, C., Lewin, E., Carpentier, M., Arndt, N.T., Marini, J.-C., 2008. Role of recycled oceanic basalt and sediment in generating the Hf–Nd mantle array. Nature Geosciences 1, 64–67.

Chauvel, C., Marini, J.-C., Plank, T., Ludden, J.N., 2009. Hf-Nd input flux in the Izu-Mariana subduction zone and recycling of subducted material in the mantle. Geochem. Geophys. Geosyst. 10, Q01001.

Chen, M., Tu, X., Zheng, F., Yan, W., Tang, X., Lu, J., Wang, B., Lu, M., 2000. Relations between sedimentary sequence and paleoclimatic changes during last 200 ka in the southern South China Sea. Chin.Sci.Bull. 45, 1334–1340.

Cina, S.E., Yin, A., Grove, M., Dubey, C.S., Shukla, D.P., Lovera, O.M., Kelty, T.K., Gehrels, G.E., Foster, D.A., 2009. Gangdese arc detritus within the eastern Himalayan Neogene foreland basin: Implications for the Neogene evolution of the Yalu–Brahmaputra River system. Earth and Planetary Science Letters 285, 150–162.

Clift, P.D., Lee, J.I., Hildebrand, P., Shimizu, N., Layne, G.D., Blusztajn, J., Blum, J.D., Garzanti, E., Khan, A.A., 2002. Nd and Pb isotope variability in the Indus River System: implications for sediment provenance and crustal heterogeneity in the Western Himalaya. Earth and Planetary Science Letters 200, 91–106.

Condie, K.C., 1991. Another look at rare earth elements in shales. Geochimica et Cosmochimica Acta 55, 2527–2531.

Covault, J.A., 2011. Submarine Fans and Canyon-Channel Systems: A Review of Processes, Products, and Models | Learn Science at Scitable. Nature Education Knowledge.

Curray, J.R., 1994. Sediment volume and mass beneath the Bay of Bengal. Earth and Planetary Science Letters 125, 371–383.

Curray, J.R., Emmel, F.J., Moore, D.G., 2003. The Bengal Fan: morphology, geometry, stratigraphy, history and processes. Marine and Petroleum Geology 19, 1191–1223.

D

Das, A., Krishnaswami, S., Sarin, M.M., Pande, K., 2005. Chemical weathering in the Krishna Basin and Western Ghats of the Deccan Traps, India: Rates of basalt weathering and their controls. Geochimica et Cosmochimica Acta 69, 2067–2084.

David, K., Frank, M., O'Nions, R., Belshaw, N., Arden, J., 2001. The Hf isotope composition of global seawater and the evolution of Hf isotopes in the deep Pacific Ocean from Fe-Mn crusts. Chemical Geology 178, 23–42.

Davis, D.W., Amelin, Y., Nowell, G.M., Parrish, R.R., 2005. Hf isotopes in zircon from the western Superior province, Canada: Implications for Archean crustal development and evolution of the depleted mantle reservoir. Precambrian Research 140, 132–156.

DeCelles, P., Gehrels, G., Quade, J., LaReau, B., Spurlin, M., 2000. Tectonic implications of U-Pb zircon ages of the Himalayan orogenic belt in Nepal. Science 288, 497–499.

DeCelles, P., Gehrels, G., Quade, J., Ojha, T., Kapp, P., Upreti, B., 1998. Neogene foreland basin deposits, erosional unroofing, and the kinematic history of the Himalayan fold-thrust belt, western Nepal. Geological Society of America Bulletin 110, 2–21.

Deniel, C., Vidal, P., Fernandez, A., Fort, P., Peucat, J.J., 1987. Isotopic study of the Manaslu granite (Himalaya, Nepal): inferences on the age and source of Himalayan leucogranites. Contrib Mineral Petrol 96, 78–92.

Dessert, C., Dupré, B., François, L.M., Schott, J., Gaillardet, J., Chakrapani, G., Bajpai, S., 2001. Erosion of Deccan Traps determined by river geochemistry: impact on the global climate and the 87Sr/86Sr ratio of seawater. Earth and Planetary Science Letters 188, 459–474.

Dessert, C., Dupré, B., Gaillardet, J., François, L.M., Allègre, C.J., 2003. Basalt weathering laws and the impact of basalt weathering on the global carbon cycle. Chemical Geology 202, 257–273.

Dhuime, B., Hawkesworth, C.J., Storey, C.D., Cawood, P.A., 2011. From sediments to their source rocks: Hf and Nd isotopes in recent river sediments. Geology 39, 407–410.

Dia, A., Allègre, C.J., Erlank, A.J., 1990. The development of continental crust through geological time: the South African case. Earth and Planetary Science Letters 98, 74–89.

Dupré, B., Gaillardet, J., Rousseau, D., Allègre, C.J., 1996. Major and trace elements of river-borne material: The Congo Basin. Geochimica et Cosmochimica Acta 60, 1301–1321.

E

Edmond, J.M., 1992. Himalayan Tectonics, Weathering Processes, and the Strontium Isotope Record in Marine Limestones. Science 258, 1594–1597.

Ehlert, C., Frank, M., Haley, B.A., Böniger, U., De Deckker, P., Gingele, F.X., 2011. Current transport versus continental inputs in the eastern Indian Ocean: Radiogenic isotope signatures of clay size sediments. Geochem. Geophys. Geosyst. 12, Q06017–.

Eisenhauer, A., Meyer, H., Rachold, V., Tütken, T., Wiegand, B., Hansen, B.T., Spielhagen, R.F., Lindemann, F., Kassens, H., 1999. Grain size separation and sediment mixing in Arctic Ocean sediments: evidence from the strontium isotope systematic. Chemical Geology 158, 173–188.

Elliott, T., Plank, T., Zindler, A., White, W., Bourdon, B., 1997. Element transport from slab to volcanic front at the Mariana arc.

F

Ferrara, G., Tonarini, S., Lombardo, B., 1983. Rb/Sr geochronology of granites and gneisses from the Mount Everest region, Nepal Himalaya. Int J Earth Sci (Geol Rundsch) 72, 119–136.

Flowerdew, M.J., Millar, I.L., Vaughan, A.P.M., Horstwood, M.S.A., Fanning, C.M., 2006. The source of granitic gneisses and migmatites in the Antarctic Peninsula: a combined U–Pb SHRIMP and laser ablation Hf isotope study of complex zircons. Contrib Mineral Petrol 151, 751–768.

France-Lanord, C., Derry, L., Michard, A., 1993. Evolution of the Himalaya since Miocene time: isotopic and sedimentological evidence from the Bengal Fan. Geological Sociiety of London 74, 603–621.

Frank, M., 2002. Radiogenic isotopes: Tracers of past ocean circulation and erosional input. Reviews of Geophysics 40, 1001.

Friedman, G.M., Sanders, J.E., 1978. Principles of Sedimentology. John Wiley & Sons Inc. 808 pp.

G

Gadgil, S., 2003. The Indian Monsoon and its Variability. Annu. Rev. Earth Planet. Sci. 31, 429–467.

Gaillardet, J., Viers, J., Dupré, B., 2003. Trace Elements in River Waters, in: Treatise on Geochemistry Vol.5 Surface and Ground Water, Weathering, and Soils. Elsevier, . 225–272.

Galer, S.J.G., Abouchami, W., 1998. Practical application of lead triple spiking for correction of instrumental mass discrimination. Mineralogical Magazine 491–492.

Galy, A., France-Lanord, C., 1999. Weathering processes in the Ganges–Brahmaputra basin and the riverine alkalinity budget. Chemical Geology 31–60.

Galy, A., France-Lanord, C., 2001. Higher erosion rates in the Himalaya: Geochemical constraints on riverine fluxes. Geology 29, 23–26.

Galy, A., France-Lanord, C., Derry, L.A., 1999. The strontium isotopic budget of Himalayan Rivers in Nepal and Bangladesh. Geochimica et Cosmochimica Acta 63, 1905–1925.

Galy, V., France-Lanord, C., Beyssac, O., Faure, P., Kudrass, H., Palhol, F., 2007. Efficient organic carbon burial in the Bengal fan sustained by the Himalayan erosional system. Nature 450, 407–410.

Galy, V., France-Lanord, C., Lartiges, B., 2008. Loading and fate of particulate organic carbon from the Himalaya to the Ganga–Brahmaputra delta. Geochimica et Cosmochimica Acta 72, 1767–1787.

Garçon, M., Chauvel, C., Bureau, S., 2011. Beach placer, a proxy for the average Nd and Hf isotopic composition of a continental area. Chemical Geology 287, 182–192.

Garçon, M., Chauvel, C., France-Lanord, C., 2012a. Almost half of worldwide sedimentary Nd-Hf isotopic decoupling done on continents. To be submitted to Geochemistry Geophysics Geosystems.

Garçon, M., Chauvel, C., France-Lanord, C., Limonta, M., Garzanti, E., 2012b. New approach to the average upper continental crust Pb isotopic value. To be submitted to Nature Geoscience.

Garzanti, E., 1999. Stratigraphy and sedimentary history of the Nepal Tethys Himalaya passive margin. Journal of Asian Earth Sciences 17, 805–827.

Garzanti, E., Andò, S., France-Lanord, C., Censi, P., Pietro Vignola, Galy, V., Lupker, M., 2011. Mineralogical and chemical variability of fluvial sediments 2. Suspended-load silt (Ganga–Brahmaputra, Bangladesh). Earth and Planetary Science Letters 302, 107–120.

Garzanti, E., Andò, S., France-Lanord, C., Vezzoli, G., Censi, P., Galy, V., Najman, Y., 2010. Mineralogical and chemical variability of fluvial sediments 1. Bedload sand (Ganga–Brahmaputra, Bangladesh). Earth and Planetary Science Letters 299, 368–381.

Garzanti, E., Andò, S., Vezzoli, G., 2008. Settling equivalence of detrital minerals and grain-size dependence of sediment composition. Earth and Planetary Science Letters 273, 138–151.

Garzanti, E., Vezzoli, G., Andò, S., lavé, J., Attal, M., France-Lanord, C., Decelles, P.G., 2007. Quantifying sand provenance and erosion (Marsyandi River, Nepal Himalaya). Earth and Planetary Science Letters 258, 500–515.

Gingele, F., De Deckker, P., Norman, M., 2007. Late Pleistocene and Holocene climate of SE Australia reconstructed from dust and river loads deposited offshore the River Murray Mouth. Earth and Planetary Science Letters 255, 257–272.

Godfrey, L., Lee, D.-C., Sangrey, W., Halliday, A., Salters, V., Hein, J., White, W., 1997. The Hf isotopic composition of ferromanganese nodules and crusts and hydrothermal manganese deposits: Implications for seawater Hf. Earth and Planetary Science Letters 151, 91–105.

Goldstein, S., Jacobsen, S.B., 1988. Nd and Sr isotopic systematics of river water suspended material: implications for crustal evolution. Earth and Planetary Science Letters 87, 249–265.

Goldstein, S.L., Hemming, S.R., 2003. Long-lived isotopic tracers in oceanography, paleoceanography, and ice-sheet dynamics. Treatise on geochemistry.

Goldstein, S.L., O'nions, R.K., Hamilton, P.J., 1984. A Sm-Nd isotopic study of atmospheric dusts and particulates from major river systems. Earth and Planetary Science Letters 70, 221–236.

Gourlan, A.T., Meynadier, L., Allègre, C.J., 2008. ScienceDirect.com - Earth and Planetary Science Letters - Tectonically driven changes in the Indian Ocean circulation over the last 25 Ma: Neodymium isotope evidence. Earth and Planetary Science Letters.

Govindaraju, K., Mevelle, G., 1987. Fully automated dissolution and separation methods for inductively coupled plasma atomic emission spectrometry rock analysis. Application to the determination of rare earth elements. Plenary lecture. J. Anal. At. Spectrom. 2, 615–621.

Götze, J., Lewis, R., 1994. Distribution of REE and trace elements in size and mineral fractions of high-purity quartz sands. Chemical Geology 114, 43–57.

Granet, M., Chabaux, F., Stille, P., Dosseto, A., France-Lanord, C., Blaes, E., 2010. U-series disequilibria in suspended river sediments and implication for sediment transfer time in alluvial plains: The case of the Himalayan rivers. Geochimica et Cosmochimica Acta 74, 2851–2865.

Granet, M., Chabaux, F., Stille, P., France-Lanord, C., Pelt, E., 2007. Time-scales of

sedimentary transfer and weathering processes from U-series nuclides: clues from the Himalayan rivers. Earth and Planetary Science Letters 261, 389–406.
Guillot, S., 2003. Reconstructing the total shortening history of the NW Himalaya. Geochem. Geophys. Geosyst. 4, 1064.
Guillot, S., Replumaz, A., 2012. Importance of continental subductions for the growth of the Tibetan plateau. Bulletin de la Société Géologique de France, in press.

H

Haley, B.A., Frank, M., Spielhagen, R.F., Fietzke, J., 2008. Radiogenic isotope record of Arctic Ocean circulation and weathering inputs of the past 15 million years. Paleoceanography 23, PA1S13–.
Harris, N., Bickle, M., Chapman, H., Fairchild, I., Bunbury, J., 1998. The significance of Himalayan rivers for silicate weathering rates: Evidence from the Bhote Kosi tributary. Chemical Geology 144, 205–220.
Harrison, T.M., Blichert-Toft, J., Müller, W., Albarède, F., Holden, P., Mojzsis, S.J., 2005. Heterogeneous Hadean Hafnium: Evidence of Continental Crust at 4.4 to 4.5 Ga. Science 310, 1947–1950.
Hawkesworth, C.J., Dhuime, B., Pietranik, A.B., Cawood, P.A., Kemp, A.I.S., Storey, C.D., 2010. The generation and evolution of the continental crust. Journal of the Geological Society 167, 229–248.
Hawkesworth, C.J., Kemp, A., 2006. The differentiation and rates of generation of the continental crust. Chemical Geology 226, 134–143.
Hay, W.W., 1998. Detrital sediment fluxes from continents to oceans. Chemical Geology 145, 287–323.
Hemming, S., McLennan, S., 2001. Pb isotope compositions of modern deep sea turbidites. Earth and Planetary Science Letters 184, 489–503.
Hu, B., Li, G., Li, J., Bi, J., Zhao, J., Bu, R., 2012. Provenance and climate change inferred from Sr–Nd–Pb isotopes of late Quaternary sediments in the Huanghe (Yellow River) Delta, China. Quaternary Research 1–11.

I-J

Innocent, C., Fagel, N., Stevenson, R.K., Hillaire-Marcel, C., 1997. Sm-Nd signature of modern and late Quaternary sediments from the northwest North Atlantic: Implications for deep current changes since the Last Glacial Maximum. Earth and Planetary Science Letters 146, 607–625.
Islam, M.R., Begum, S.F., Yamaguchi, Y., Ogawa, K., 1999. The Ganges and Brahmaputra rivers in Bangladesh: basin denudation and sedimentation. Hydrol. Process. 13, 2907–2923.
Jacobsen, S.B., 1988. Isotopic constraints on crustal growth and recycling. Earth and Planetary Science Letters 90, 315–329.

Jha, P.K., Subramanian, V., Sitasawad, R., 1988. Chemical and sediment mass transfer in the Yamuna River--A tributary of the Ganges system. Journal of Hydrology 104, 237–246.

Jha, P.K., Vaithiyanathan, P., Subramanian, V., 1993. Mineralogical characteristics of the sediments of a Himalayan river: Yamuna River - a tributary of the Ganges. Environ Geol 22, 13–20.

Johnson, M., Rogers, G., 1997. Rb-Sr ages of micas from the Kathmandu complex, Central Nepalese Himalaya: Implications for the evolution of the Main Central Thrust. Journal of the Geological Society 154, 863–869.

K

Kai, K., 1981. Rb-Sr Ages of the Biotite and Muscovite of the Himalayas, Eastern Nepal - Its Implication in the Uplift History. Geochem J 15, 63–68.

Kamber, B.S., Greig, A., Collerson, K.D., 2005. A new estimate for the composition of weathered young upper continental crust from alluvial sediments, Queensland, Australia. Geochimica et Cosmochimica Acta 69, 1041–1058.

Kemp, A.I.S., Hawkesworth, C.J., Foster, G.L., Paterson, B.A., Woodhead, J.D., Hergt, J.M., Gray, C.M., Whitehouse, M.J., 2007. Magmatic and Crustal Differentiation History of Granitic Rocks from Hf-O Isotopes in Zircon. Science 315, 980–983.

Kinny, P.D., Maas, R., 2003. Lu–Hf and Sm–Nd isotope systems in zircon. Reviews in mineralogy and geochemistry 53, 327–341.

Klootwijk, C.T., Gee, J.S., Peirce, J.W., Smith, G.M., McFadden, P.L., 1992. An early India-Asia contact: Paleomagnetic constraints from Ninetyeast Ridge, ODP Leg 121. Geology 20, 5, 395-398.

Komar, P.D., 2007. The Entrainment, Transport and Sorting of Heavy Minerals by Waves and Currents, in: Heavy Minerals in Use. Developments in Sedimentology, pp. 3–48.

Kramers, J.D., Tolstikhin, I.N., 1997. Two terrestrial lead isotope paradoxes, forward transport modelling, core formation and the history of the continental crust. Chemical Geology 139, 75–110.

Krishnan, M.S., 1982. Geology of India and Burna, 6th ed. CBS Publishers and Distributors, New Delhi.

L

Labanieh, S., Chauvel, C., Germa, A., Quidelleur, X., Lewin, E., 2010. Isotopic hyperbolas constrain sources and processes under the Lesser Antilles arc. Earth and Planetary Science Letters 298, 35–46.

Le Fort, P., 1975. Himalayas: the collided range. Present knowledge of the continental arc. American Journal of Science.

Lisitzin, A.P., 1996. Oceanic Sedimentation: Lithology and Geochemistry. American Geophysical Union, Washington, D. C.

Lupker, M., 2011. Dynamique sédimentaire, érosion physique et altération chimique dans le système himalayen. Thèse CRPG, Nancy.

Lupker, M., Blard, P.-H., lavé, J., France-Lanord, C., Leanni, L., Puchol, N., Charreau, J., Bourlès, D., 2012. 10Be-derived Himalayan denudation rates and sediment budgets in the Ganga basin. Earth and Planetary Science Letters 333-334, 146–156.

Lupker, M., France-Lanord, C., Galy, V., lavé, J., Gaillardet, J., Gajurel, A.P., Guilmette, C., Rahman, M., Singh, S.K., Sinha, R., 2012. Predominant floodplain over mountain weathering of Himalayan sediments (Ganga basin). Geochimica et Cosmochimica Acta 84, 410-432.

Lupker, M., France-Lanord, C., lavé, J., Bouchez, J., Galy, V., Métivier, F., Gaillardet, J., Lartiges, B., Mugnier, J.-L., 2011. A Rouse-based method to integrate the chemical composition of river sediments: Application to the Ganga basin. J. Geophys. Res. 116, F04012.

M-N

Manhès, G., Allègre, C.J., Provost, A., 1984. U-Th-Pb systematics of the eucrite “Juvinas”: Precise age determination and evidence for exotic lead. Geochimica et Cosmochimica Acta 48, 2247–2264.

Marini, J.-C., Chauvel, C., Maury, R.C., 2005. Hf isotope compositions of northern Luzon arc lavas suggest involvement of pelagic sediments in their source. Contrib Mineral Petrol 149, 216–232.

Mascle, G., Herail, G., 1982. Les Siwaliks: le prisme d'accrétion tectonique associé à la subduction intracontinentale himalayenne. Géol Alpine.

Mascle, G., Pêcher, A., Guillot, S., 2010. Himalaya-Tibet, la collision continentale Inde-Eurasie. Vuibert, Paris, 176 p.

McLennan, S.M., 1988. Recycling of the continental crust. Pure and applied geophysics, 128, 3-4, 683-724.

McLennan, S.M., 1989. Rare earth elements in sedimentary rocks; influence of provenance and sedimentary processes. Reviews in mineralogy and geochemistry 21, 169–200.

McLennan, S.M., 2001. Relationships between the trace element composition of sedimentary rocks and upper continental crust. Geochem. Geophys. Geosyst. 2, 1021–1024.

McLennan, S.M., McCulloch, M.T., Taylor, S.R., Maynard, J.B., 1989. Effects of sedimentary sorting on neodymium isotopes in deep-sea turbidites. Nature 337, 547–549.

McLennan, S.M., Taylor, S.R., McCulloch, M.T., Maynard, J.B., 1990. Geochemical and Nd-Sr isotopic composition of deep-sea turbidites: Crustal evolution and plate tectonic associations. Geochimica et Cosmochimica Acta 54, 2015–2050.

Mehta, P.K., 1977. Rb-Sr geochronology of the Kulu-Mandi Belt: Its implications for the Himalayan Tectogenesis. Int J Earth Sci (Geol Rundsch) 66, 156–175.

Milliman, J., 2001. River Inputs. in: Encyclopedia of Ocean Sciences, Elsevier, 2419–2427.

Milliman, J., Meade, R.H., 1983. World-wide delivery of river sediment to the oceans. The Journal of Geology 91, 1–21.

Millot, R., Allègre, C.J., Gaillardet, J., Roy, S., 2004. Lead isotopic systematics of major river sediments: a new estimate of the Pb isotopic composition of the Upper Continental

Crust. Chemical Geology 203, 75–90.
Mugnier, J.L., Leturmy, P., Mascle, G., Huyghe, P., Chalaron, E., Vidal, G., Husson, L., Delcaillau, B., 1999. The Siwaliks of western Nepal: I. Geometry and kinematics. Journal of Asian Earth Sciences 17, 629–642.

P-Q

Padoan, M., Garzanti, E., Harlavan, Y., Villa, I.M., 2011. Tracing Nile sediment sources by Sr and Nd isotope signatures (Uganda, Ethiopia, Sudan). Geochimica et Cosmochimica Acta 75, 3627–3644.
Parrish, R.R., Hodges, V., 1996. Isotopic constraints on the age and provenance of the Lesser and Greater Himalayan sequences, Nepalese Himalaya. Geological Society of America Bulletin 108, 904–911.
Patchett, P.J., White, W.M., Feldmann, H., Kielinczuk, S., Hofmann, A.W., 1984. Hafnium/rare earth element fractionation in the sedimentary system and crustal recycling into the Earth's mantle. Earth and Planetary Science Letters 69, 365–378.
Patriat, P., Achache, J., 1984. India–Eurasia collision chronology has implications for crustal shortening and driving mechanism of plates. Nature 311, 615–621.
Patterson, C., Tatsumoto, M., 1964. The significance of lead isotopes in detrital feldspar with respect to chemical differentiation within the earth's mantle. Geochimica et Cosmochimica Acta 28, 1–22.
Pearce, J., Kempton, P., Nowell, G., Noble, S., 1999. Hf-Nd element and isotope perspective on the nature and provenance of mantle and subduction components in Western Pacific arc-basin systems. Journal of Petrology 40, 1579–1611.
Pierson-Wickmann, A.-C., Reisberg, L., France-Lanord, C., 2000. The Os isotopic composition of Himalayan river bedloads and bedrocks: importance of black shales. Earth and Planetary Science Letters 176, 203–218.
Pierson-Wickmann, A.C., Reisberg, L., France-Lanord, C., 2001. Os-Sr-Nd results from sediments in the Bay of Bengal: Implications for sediment transport. Paleoceanography 16, 435–444.
Piotrowski, A.M., Goldstein, S.L., Hemming, S.R., Fairbanks, R.G., 2004. Intensification and variability of ocean thermohaline circulation through the last deglaciation. Earth and Planetary Science Letters 225, 205–220.
Plank, T., Kelley, K.A., Murray, R.W., Stern, L.Q., 2007. Chemical composition of sediments subducting at the Izu-Bonin trench. Geochem. Geophys. Geosyst. 102, B7.
Plank, T., Langmuir, C.H., 1998. The chemical composition of subducting sediment and its consequences for the crust and mantle. Chemical Geology 145, 325–394.
Prytulak, J., Vervoort, J.D., Plank, T., Yu, C., 2006. Astoria Fan sediments, DSDP site 174, Cascadia Basin: Hf–Nd–Pb constraints on provenance and outburst flooding. Chemical Geology 233, 276–292.

R

Radhakrishna, M., Subrahmanyam, C., Damodharan, T., 2010. Thin oceanic crust below Bay of Bengal inferred from 3-D gravity interpretation. Tectonophysics 493, 93–105.

Rengarajan, R., Singh, S.K., Sarin, M.M., Krishnaswami, S., 2009. Strontium isotopes and major ion chemistry in the Chambal River system, India: Implications to silicate erosion rates of the Ganga. Chemical Geology 260, 87–101.

Revel, M., Cremer, M., Grousset, F.E., Labeyrie, L., 1996. Grain-size and Sr-Nd isotopes as tracer of paleo-bottom current strength, Northeast Atlantic Ocean. Marine Geology 131, 233–249.

Richards, A., Argles, T., Harris, N., Parrish, R., Ahmad, T., Darbyshire, F., Draganits, E., 2005. Himalayan architecture constrained by isotopic tracers from clastic sediments. Earth and Planetary Science Letters 236, 773–796.

Robinson, D.M., Decelles, P.G., Patchett, P.J., Garzione, C.N., 2001. The kinematic evolution of the Nepalese Himalaya interpreted from Nd isotopes. Earth and Planetary Science Letters 192, 507–521.

Roddaz, M., Viers, J., Brusset, S., Baby, P., Hérail, G., 2005. Sediment provenances and drainage evolution of the Neogene Amazonian foreland basin. Earth and Planetary Science Letters 239, 57–78.

Rudnick, R.L., Gao, S., 2003. The Composition of the Crust, in: Rudnick, R.L. (Ed.), The Crust Vol.3 Treatise on Geochemistry. pp. 1–64.

S

Schärer, U., Hamet, J., Allègre, C.J., 1984. The Transhimalaya (Gangdese) plutonism in the Ladakh region: a UPb and RbSr study. Earth and Planetary Science Letters 67, 327–339.

Shimoda, G., Tatsumi, Y., Nohda, S., Ishizaka, K., Jahn, B.M., 1998. Setouchi high-Mg andesites revisited: geochemical evidence for melting of subducting sediments. Earth and Planetary Science Letters 160, 479–492.

Singh, M., Singh, I.B., Müller, G., 2007. Sediment characteristics and transportation dynamics of the Ganga River. Geomorphology 86, 144–175.

Singh, P., 2009. Major, trace and REE geochemistry of the Ganga River sediments: Influence of provenance and sedimentary processes. Chemical Geology 266, 242–255.

Singh, P., 2010. Geochemistry and provenance of stream sediments of the Ganga River and its major tributaries in the Himalayan region, India. Chemical Geology 269, 220–236.

Singh, S.K., France-Lanord, C., 2002. Tracing the distribution of erosion in the Brahmaputra watershed from isotopic compositions of stream sediments. Earth and Planetary Science Letters 202, 645–662.

Singh, S.K., Rai, S.K., Krishnaswami, S., 2008. Sr and Nd isotopes in river sediments from the Ganga Basin: Sediment provenance and spatial variability in physical erosion. J. Geophys. Res. 113, F03006.

Steinmann, M., Stille, P., 2008. Controls on transport and fractionation of the rare earth

elements in stream water of a mixed basaltic–granitic catchment basin (Massif Central, France). Chemical Geology 254, 1–18.
Stille, P., Steinmann, M., Riggs, S.R., 1997. Nd isotope evidence for the evolution of the paleocurrents in the Atlantic and Tethys oceans during the past 180 Ma. Oceanographic Literature Review 44, 698–698.
Stummeyer, J., Marchig, V., Knabe, W., 2002. The composition of suspended matter from Ganges–Brahmaputra sediment dispersal system during low sediment transport season. Chemical Geology 185, 125–147.
Stumpf, R., Frank, M., Schönfeld, J., Haley, B.A., 2011. Climatically driven changes in sediment supply on the SW Iberian shelf since the Last Glacial Maximum. Earth and Planetary Science Letters 312, 80–90.

T

Takada, Y., Matsu'ura, M., 2007. Geometric evolution of a plate interface–branch fault system: Its effects on the tectonic development of the Himalayas. Journal of Asian Earth Sciences 29, 490–503.
Tatsumoto, M., Knight, R.J., Allègre, C.J., 1973. Time differences in the formation of meteorites as determined from the ratio of lead-207 to lead-206. Science.
Taylor, S.R., McLennan, S.M., 1995. The Geochemical evolution of the Continental Crust. Reviews of Geophysics 33, 241–265.
Totten, M., 2007. ScienceDirect.com - Developments in Sedimentology - Chapter 12 Heavy Minerals in Shales. Developments in Sedimentology.
Tricca, A., Stille, P., Steinmann, M., Kiefel, B., Samuel, J., Eikenberg, J., 1999. Rare earth elements and Sr and Nd isotopic compositions of dissolved and suspended loads from small river systems in the Vosges mountains (France), the river Rhine and groundwater. Chemical Geology 160, 139–158.
Tripathi, J.K., Ghazanfari, P., Rajamani, V., Tandon, S., 2007. Geochemistry of sediments of the Ganges alluvial plains: Evidence of large-scale sediment recycling. Quaternary International 159, 119–130.

U-V

Upreti, B.N., 1999. An overview of the stratigraphy and tectonics of the Nepal Himalaya. Journal of Asian Earth Sciences 17, 577–606.
Van de Flierdt, T., Frank, M., Lee, D.-C., Halliday, A.N., Reynolds, B.C., Hein, J.R., 2004. New constraints on the sources and behavior of neodymium and hafnium in seawater from Pacific Ocean ferromanganese crusts. Geochimica et Cosmochimica Acta 68, 3827–3843.
Van de Flierdt, T., Goldstein, S.L., Hemming, S.R., Roy, M., Frank, M., Halliday, A.N., 2007. Global neodymium–hafnium isotope systematics—revisited. Earth and Planetary Science Letters 259, 432–441.

Van De Flierdt, T., Hemming, S.R., Goldstein, S.L., Abouchami, W., 2006. Radiogenic isotope fingerprint of Wilkes Land–Adélie Coast Bottom Water in the circum-Antarctic Ocean. Geophys. Res. Lett. 33, L12606.

Veevers, J.J., Saeed, A., Belousova, E.A., Griffin, W., 2005. U-Pb ages and source composition by Hf-isotope and trace-element analysis of detrital zircons in Permian sandstone and modern sand from southwestern Australia and a review of the paleogeographical and denudational history of the Yilgam Craton. Earth Science Reviews 68, 245–279.

Vervoort, J., Plank, T., Prytulak, J., 2011. The Hf-Nd isotopic composition of marine sediments. Geochimica et Cosmochimica Acta 75, 5903-5926.

Vervoort, J.D., Blichert-Toft, J., 1999. Evolution of the depleted mantle: Hf isotope evidence from juvenile rocks through time. Geochimica et Cosmochimica Acta 63, 533–556.

Vervoort, J.D., Jonathan Patchett, P., 1996. Behavior of hafnium and neodymium isotopes in the crust: constraints from Precambrian crustally derived granites. Geochimica et Cosmochimica Acta 60, 3717–3733.

Vervoort, J.D., Patchett, P.D., Blichert-Toft, J., Albarède, F., 1999. Relationships between Lu–Hf and Sm–Nd isotopic systems in the global sedimentary system. Earth and Planetary Science Letters 168, 79–99.

Vervoort, J.D., Patchett, P.J., Albarède, F., Blichert-Toft, J., Rudnick, R., Downes, H., 2000. Hf–Nd isotopic evolution of the lower crust. Earth and Planetary Science Letters 181, 115–129.

Vlastélic, I., 2005. Miocene climate change recorded in the chemical and isotopic (Pb, Nd, Hf) signature of Southern Ocean sediments. Geochem. Geophys. Geosyst. 6, Q03003.

W

Walling, D.E., 2006. Human impact on land–ocean sediment transfer by the world's rivers. Geomorphology 79, 192–216.

Walter, H.J., Hegner, E., Diekmann, B., Kuhn, G., 2000. Provenance and transport of terrigenous sediment in the South Atlantic Ocean and their relations to glacial and interglacial cycles: Nd and Sr isotopic evidence. Geochimica et Cosmochimica Acta 64, 3813–3827.

Weis, D., Kieffer, B., Maerschalk, C., Barling, J., de Jong, J., Williams, G.A., Hanano, D., Pretorius, W., Mattielli, N., Scoates, J.S., Goolaerts, A., Friedman, R.M., Mahoney, J.B., 2006. High-precision isotopic characterization of USGS reference materials by TIMS and MC-ICP-MS. Geochem. Geophys. Geosyst. 7, Q08006.

Weis, D., Kieffer, B., Pretorius, W., Barling, J., 2005. High-precision Pb-Sr-Nd-Hf isotopic characterization of USGS BHVO-1 and BHVO-2 reference materials.

Wen, D.-R., Chung, S.-L., Song, B., Iizuka, Y., Yang, H.-J., Ji, J., Liu, D., Gallet, S., 2008. Late Cretaceous Gangdese intrusions of adakitic geochemical characteristics, SE Tibet: Petrogenesis and tectonic implications. Lithos 105, 1–11.

White, W.M., Albarède, F., Télouk, P., 2000. High-precision analysis of Pb isotope ratios by multi-collector ICP-MS. Chemical Geology 167, 257–270.

White, W.M., Dupré, B., 1986. Sediment Subduction and Magma Genesis in the Lesser

Antilles: Isotopic and Trace Element Constraints. J. Geophys. Res. 91, 5927–5941.
White, W.M., Patchett, J., BenOthman, D., 1986. Hf isotope ratios of marine sediments and Mn nodules: evidence for a mantle source of Hf in seawater. Earth and Planetary Science Letters 79, 46–54.
Woodhead, J., Hergt, J., Davidson, J., Eggins, S., 2001. Hafnium isotope evidence for “conservative”element mobility during subduction zone processes. Earth and Planetary Science Letters 192, 331–346.
Wu, W., Xu, S., Yang, J., Yin, H., Lu, H., Zhang, K., 2010. Isotopic characteristics of river sediments on the Tibetan Plateau. Chemical Geology 269, 406–413.
Wulf, H., Bookhagen, B., Scherler, D., 2010. Seasonal precipitation gradients and their impact on fluvial sediment flux in the Northwest Himalaya. Geomorphology 118, 13–21.

X-Y-Z

Yan, Y.I., Xia, B., Lin, G.E., Carter, A., Hu, X., Cui, X., Liu, B., Yan, P., Song, Z., 2007. Geochemical and Nd isotope composition of detrital sediments on the north margin of the South China Sea: provenance and tectonic implications. Sedimentology 54, 1–17.
Zeh, A., Gerdes, A., Klemd, R., Barton, J.M., 2007. Archaean to Proterozoic Crustal Evolution in the Central Zone of the Limpopo Belt (South Africa-Botswana): Constraints from Combined U-Pb and Lu-Hf Isotope Analyses of Zircon. Journal of Petrology 48, 1605–1639.

Annexes

PROCEDURE DE SEPARATION DES MINERAUX A PARTIR DE DIFFERENTES FRACTIONS GRANULOMETRIQUES

Organigramme présentant la procédure de séparation des minéraux à partir de la fraction granulométrique > 250 µm

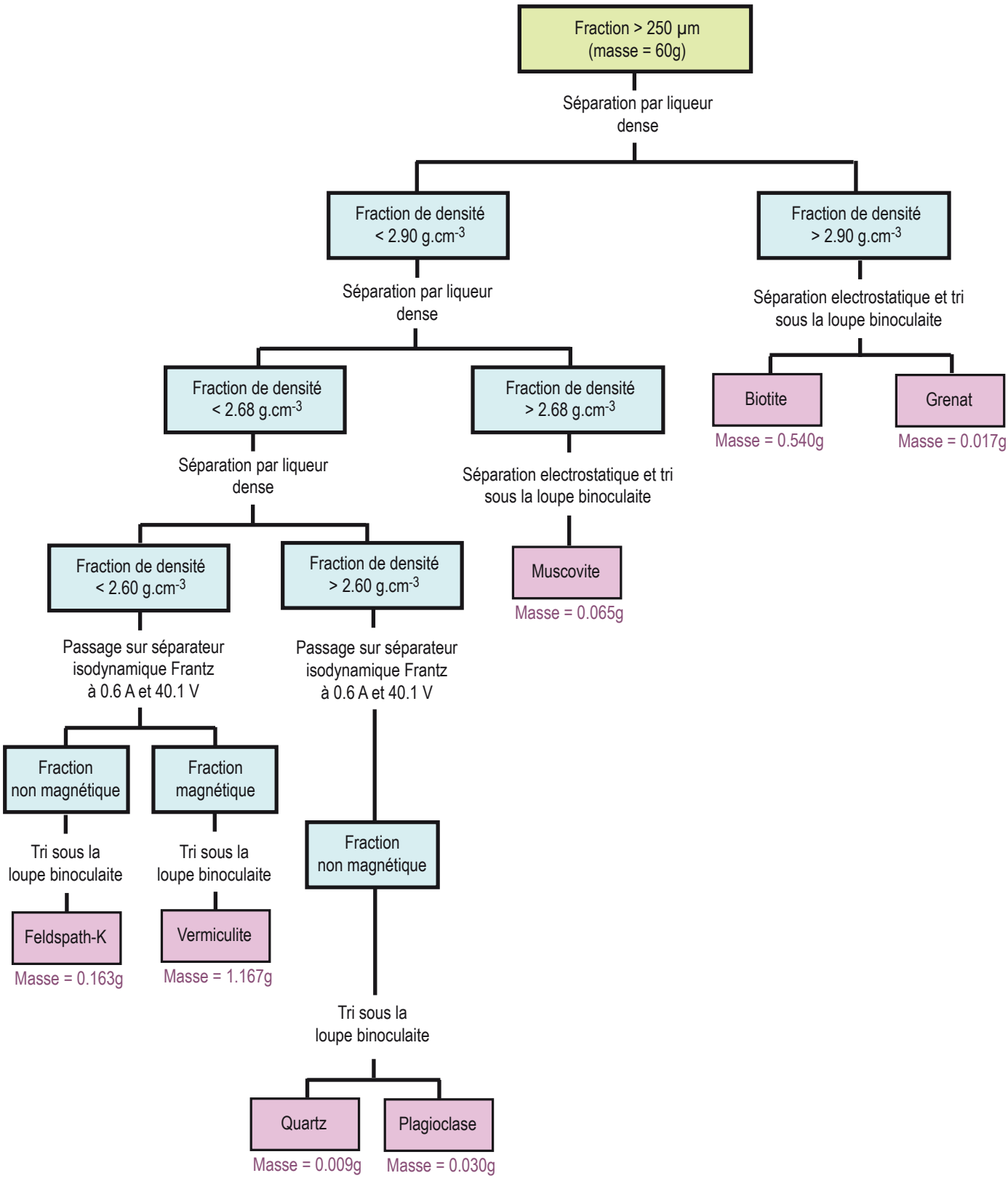

Organigramme présentant la procédure de séparation des minéraux à partir de la fraction granulométrique 125-250 µm

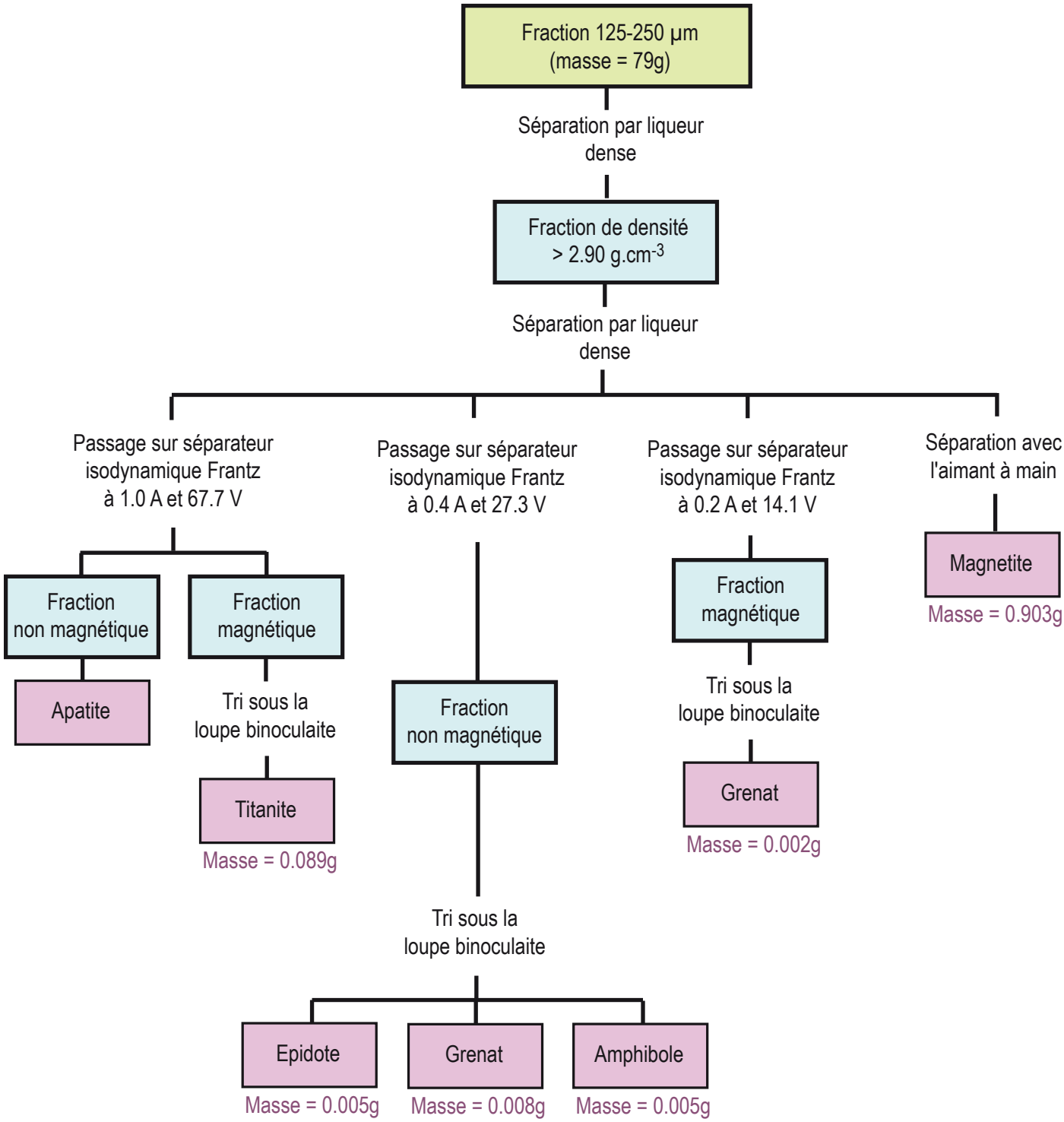

Organigramme présentant la procédure de séparation des minéraux à partir de la fraction granulométrique 63-100 µm

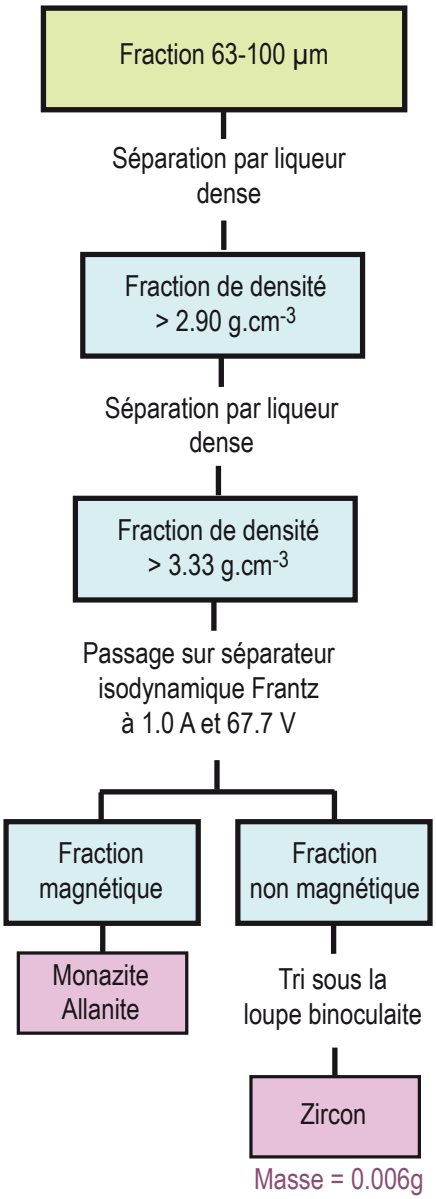

ARTICLES PUBLIÉS AU COURS DE MA THÈSE SUR MES TRAVAUX DE MASTER 1 ET 2

Chemical Geology 287 (2011) 182–192

Contents lists available at ScienceDirect

Chemical Geology

journal homepage: www.elsevier.com/locate/chemgeo

Research papers

Beach placer, a proxy for the average Nd and Hf isotopic composition of a continental area

Marion Garçon, Catherine Chauvel *, Sarah Bureau

ISTerre, CNRS, Université Joseph Fourier de Grenoble, BP 53, 38041 Grenoble Cedex 09, France

ARTICLE INFO

Article history:
Received 1 December 2010
Received in revised form 3 June 2011
Accepted 17 June 2011
Available online 25 June 2011

Editor: L. Reisberg

Keywords:
Neodymium
Hafnium
Monazite
Zircon
Continental crust

ABSTRACT

Beach placer deposits concentrate detrital heavy minerals which are the erosion products of large areas of continental crust. Here, we report the first analyses of Nd–Hf isotopic ratios and trace element concentrations that we measured in a beach placer from Camargue, France and in its pure mineral separates. Both the bulk composition of the placer and those of its pure mineral separates were determined. We also report mineral proportions obtained using observations under a binocular microscope and micro X-ray fluorescence mapping.

Our results indicate that monazite totally controls the placer's Nd isotopic composition ($\varepsilon_{Nd} = -9.3$) while zircon dominates its Hf isotopes ($\varepsilon_{Hf} = -13.0$) even though both mineral phases represent only a small proportion of the heavy mineral assemblage (3.5 and 10% respectively). We demonstrate that the Camargue placer provides a good estimate of the average Nd and Hf isotopic composition of the continental area drained by the Rhone River in Western Europe ($\varepsilon_{Nd} \approx -9$ and $\varepsilon_{Hf} \approx -13$). Using these values, we calculate two stage model ages and show that almost all the placer minerals are derived from Proterozoic crustal protoliths. This provides valuable information on the history of the continental crust drained by the Rhone River. In particular, it suggests that little juvenile crust was created during the recent geological events that formed the Alps and the Massif Central, the two main massifs from which the placer minerals originate.

More generally, we propose that similar measurements made on other worldwide beach placer deposits could provide estimates of the present-day Nd and Hf isotopic composition of large continental areas, values that are difficult to obtain due to the well-known heterogeneity of continental material but are essential to model the growth of continental crust through Earth history or to model the impact of crustal material when recycled into the mantle.

1. Introduction

Modern beach placer deposits are surficial accumulations of clastic heavy minerals that mostly form in the foreshore of sandy beaches by gravity separation under the action of waves and currents. In some regions, beach placers contain valuable heavy minerals such as ilmenite, zircon or monazite and have been studied to identify economically viable deposits (e.g. Patyk-Kara, 2002; Levchenko, 2006; Patyk-Kara, 2008) or to better understand the mechanisms responsible for mineral sorting and depositional patterns (e.g. Komar and Wang, 1984; Frihy et al., 1995; Roy, 1999; Hughes et al., 2000; Hou et al., 2003; Paine et al., 2005). Apart from Götze and Lewis (1994) who studied a few trace elements in pure mineral fractions separated from mature quartz sands, no study has focused on the isotope and trace-element geochemistry of placers and their heavy minerals, even though this type of sediment obviously has the potential to provide valuable insights on broader issues such as fluvial transport processes, crust–mantle recycling or the composition of the upper continental crust.

Several previous studies (see for example, Goldstein and Jacobsen, 1988; Gaillardet et al., 1995; Allègre et al., 1996; Millot et al., 2004; Kamber et al., 2005) used river sediments as proxies to evaluate either the trace element content or the Nd and Pb isotopic compositions of the upper continental crust and its evolution through time. Other studies used Hf and Pb isotopes on individual zircon grains to constrain the timing of major crustal growth episodes as well as their mantle versus crustal sources (Gehrels et al., 1995; Amelin et al., 1999; Bodet and Schärer, 2000; Griffin et al., 2006; Hawkesworth and Kemp, 2006; Dhuime et al., 2011). However, no study ever considered taking advantage of the natural processes leading to the formation of zircon-rich placers to place constraints on both the composition and history of large-scale continental areas.

Here we present the first Nd and Hf isotopic analyses, as well as trace element concentrations, of several pure mineral separates that were isolated from a beach placer sampled near the Rhone delta in Camargue, France. The proportion of each heavy mineral species was

* Corresponding author.
E-mail address: Catherine.chauvel@ujf-grenoble.fr (C. Chauvel).

0009-2541/$ – see front matter © 2011 Elsevier B.V. All rights reserved.
doi:10.1016/j.chemgeo.2011.06.007

estimated as precisely as possible using observations under a binocular microscope and micro X-ray fluorescence mapping. Using all these data, we (a) quantify the influence of the individual minerals on the trace element and isotopic composition of the entire placer, (b) we discuss and interpret the chemical characteristics of beach placers and (c) we demonstrate that placers are good proxies of the average Nd–Hf isotopic composition of large regions of the continental crust exposed to weathering and erosion.

2. Materials and methods

2.1. Brief setting and placer sampling

The studied placer was sampled in 2003 next to the Rhone River delta on the Espiguette Beach in Camargue, France (see Fig. 1) within the zone of wave swash where black-sand deposits are regularly observed after storms. Several kilos of mature sand, rich in black heavy minerals and mixed with very small proportions of light minerals, were collected using a spade on the beach. Previous studies (BRGM, 2000) showed that the Espiguette black-sands usually contain variable abundances of about twenty heavy minerals that are commonly found in beach placer deposits. These include ilmenite, magnetite, rutile, garnet, zircon, monazite and epidote (see Supplementary Table 1 for the complete list of minerals).

As shown in Fig. 1, Espiguette beach is about 10 km long and grows by accumulation of sediments transported from east to west by longshore currents (Vella et al., 2005; Sabatier et al., 2006). The accumulated sediments essentially originate from the reworking of relict pro-deltaic lobes of the Rhone River and consist of materials directly eroded from the massifs drained by the Rhone River and its tributaries. Several studies (BRGM, 2000; Vassas et al., 2006) and more importantly the analyses of zircon typologies and apatite fission track densities performed by Thomassin et al. (2007) demonstrated that the Alps and the Massif Central are the two main sources for the heavy minerals that accumulate in the Camargue beach placers.

2.2. Separation of the mineral fractions

Before analysis and mineral separation, the placer sand was washed, placed in an ultra-sonic bath and oven-dried to remove organic material and seawater. Using heavy liquids (bromoform and methylene iodide), the minerals were separated into three different fractions according to their density. In the heaviest fraction ($d>3.3\ g.cm^{-3}$), the main minerals were isolated according to their magnetic susceptibility using a hand magnet and a Frantz Isodynamic Magnet Separator. Due to their similar magnetic properties, monazite, epidote and titanite were relatively difficult to separate from one another. However, the epidote and titanite grains were generally larger than the monazite grains and we separated them by collecting the fine and coarse fractions after simple 80 μm-sieving. The isolated fractions were then purified by handpicking under a binocular microscope. We obtained six pure mineral separates consisting of garnet, ilmenite, rutile, zircon, epidote and monazite. However, due to the optical similarities of ilmenite and magnetite and because it is impossible to completely eliminate impurities with a hand magnet, we suspect that the pure ilmenite separate likely refers to a fraction containing a few magnetite grains.

2.3. Heavy mineral abundances

Mineral proportions were determined under a binocular microscope in a fraction containing all the heavy minerals isolated from the Camargue placer ($d>2.9\ g.cm^{-3}$) using standard optical characteristics

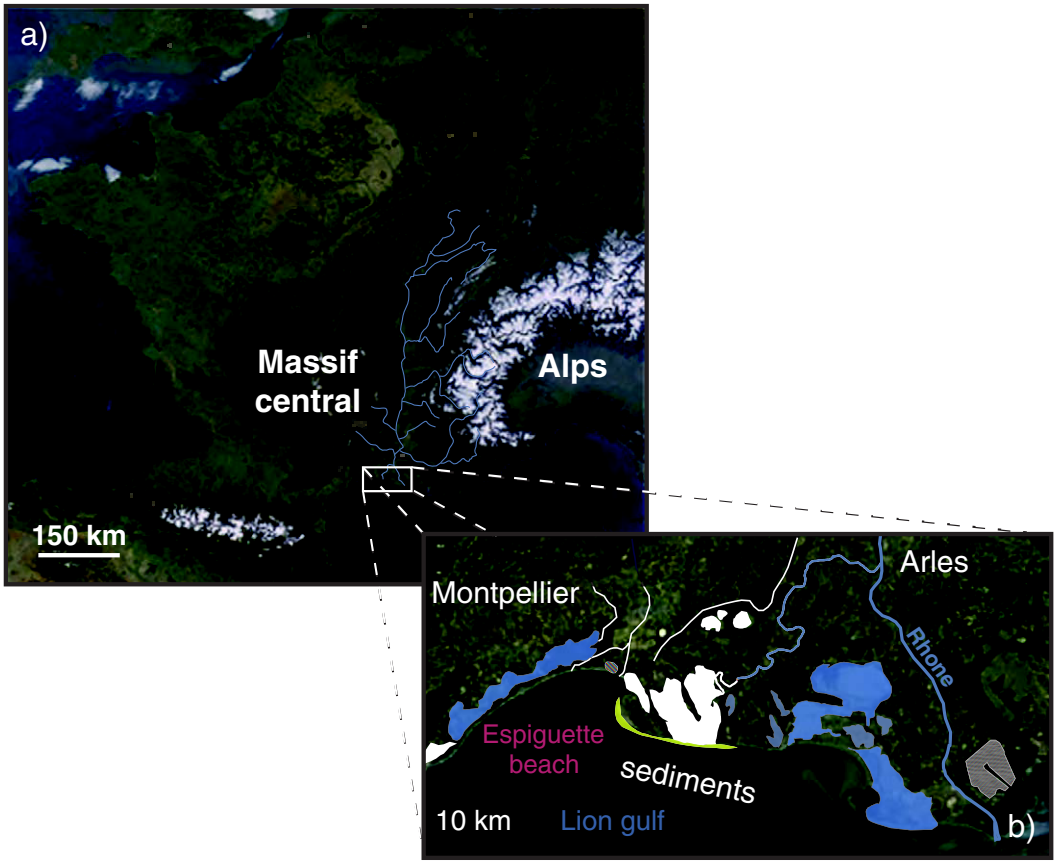

Fig. 1. Location map of the studied area in France. The massifs drained by the Rhone river and its tributaries are indicated in the map (a). The sampling site of the Camargue placer and the sediment transport direction alongside the coast are shown in the inset (b).

such as grain colour or grain shape. In this heavy mineral fraction, the mineral abundances were estimated as a percentage of the total counted grains.

As the identification of certain heavy minerals can be ambiguous in placers because of altered or rounded grains, we also developed a method that uses micro X-ray fluorescence mapping (μXRF EDAX Eagle III) to quantify the mineral abundances in the heavy fraction ($d>2.9$ g.cm^{-3}). Several hundred grains were analysed by μXRF in order to identify their spectral signature and their mineralogical characteristics (see Supplementary File A). Then, using this information, we calculated the relative abundance of each mineral species as a percentage of the total grains analysed by μXRF.

Combining the observations under the binocular microscope with the results obtained by μXRF mapping, we estimated mineral abundances and converted them to mass percentage using specific mineral densities and average grain sizes.

2.4. Chemical analyses of the mineral fractions

Trace element concentrations and Nd–Hf isotopic compositions were measured in bulk fractions to evaluate the influence of each mineral on the geochemistry of the Camargue placer. Measurements were performed on the six mineral separates (monazite, garnet, ilmenite, zircon, epidote and rutile), the total placer and on two fractions, one containing all the light minerals ($d<2.9$ g.cm^{-3}) and the other containing all the heavy minerals ($d>2.9$ g.cm^{-3}). To assess the efficiency of the purification by handpicking under a binocular microscope, the impure monazite, garnet, ilmenite and zircon fractions were also analysed.

2.4.1. Sample dissolution

The samples were first ground to fine powder by hand in an agate mortar to facilitate dissolution. They were then dissolved by acid attack in steel PARR bombs for at least 2 weeks at 135 °C. Because of the well-known resistance of most placer minerals, we used sample-specific dissolution procedures in which the sample quantity, the acid mixture and the dissolution time in bombs were adapted to the mineral species (see Supplementary File B). In addition, in order to improve the efficiency of the dissolution, acid-mixtures were regularly removed from the bomb and stored in separated beakers and new acids were added every week. After complete dissolution, two aliquots were taken from each dissolved sample, one to measure trace element concentrations and the other for Nd–Hf isotopic compositions.

2.4.2. Trace element concentrations

Trace element concentrations were measured in mineral fractions using an Agilent 7500ce ICP-MS in Grenoble, France following a procedure similar to that published by Chauvel et al. (2011). High precision measurements on ICP-MS were obtained by diluting samples in 2% HNO_3 with traces of HF at a specific dilution factor that depends on the sample and the chemical element (see Supplementary File B). As described by Chauvel et al. (2011), ICP-MS analytical drift was corrected by adding an internal standard (a multispike containing Be, Ge, In, Tm, Bi) to all samples. After correction for drift and oxide interferences, trace element concentrations were calculated using an external calibration based on the repeated measurements of the BR rock standard diluted 5000 times. To ensure the validity and the reproducibility of our measurements, rock standards AGV-1 and BR 24 were measured several times as unknown samples and several duplicates were performed (see Supplementary Tables 2 and 3).

2.4.3. Nd and Hf isotopic compositions

Following the method described by Chauvel et al. (2011), Hf and Nd were isolated from the same aliquot using ion exchange resins. For the pure mineral separates, the Hf isolation procedure was slightly modified since the standard method was not suitable for minerals that are much more concentrated in trace elements than usual rocks or sediments (see Supplementary File B). The total procedural blanks were always less than 20 pg for Nd and 120 pg for Hf and can thus be considered as negligible relative to the amount of Nd and Hf present in the samples. Nd and Hf isotopic ratios were measured on a Nu Plasma MC-ICP-MS at the ENS Lyon, France. The mass fractionation bias was corrected using the constant values of the ratios $^{146}Nd/^{144}Nd = 0.7219$ and $^{179}Hf/^{177}Hf = 0.7325$. Analytical drift was monitored by measuring the Ames–Rennes Nd and Ames–Grenoble Hf standards every two or three samples and was corrected using the recommended values published by Chauvel and Blichert-toft (2001) and Chauvel et al. (2011). These two standards yielded a mean $^{143}Nd/^{144}Nd$ value of 0.511962 ± 13 (2σ, $n = 18$) and $^{176}Hf/^{177}Hf$ value of 0.282160 ± 10 (2σ, $n = 11$).

3. Results

3.1. Mineralogical composition of the heavy and light mineral fractions

Using the weight of each separated fraction, we estimated that the light minerals ($d<2.9$ g.cm^{-3}) represent only 5 wt.% of the total placer whereas the heavy minerals ($d>2.9$ g.cm^{-3}) constitute about 95 wt.% of the sample. Observation of the light mineral fraction under the binocular microscope shows that it mainly contains calcite, feldspar and quartz, but also a few residual heavy minerals (ilmenite, zircon, etc.) that were not properly separated from the light minerals by the heavy liquid separation procedure. Fig. 2 shows the mineral abundances in the heavy mineral fraction determined under the binocular microscope and using the μXRF mapping. The mineral proportions estimated by combining the results from the two methods are given in the grey-coloured inset as a percentage of the total counted grains and as a mass percentage. The uncertainties on the mineral proportions and the details about mass percentage calculations are given in the figure caption. As shown in Fig. 2, the results obtained by μXRF mapping are remarkably consistent with the observations done under the binocular microscope. The heavy mineral fraction mainly contains ilmenite–magnetite (44%) and garnet (28%) but also significant proportions of zircon (10%), rutile (7%), monazite (3.5%) and epidote (2%).

The μXRF determination provides precise abundances when the minerals are present in significant proportions (>5%) and has the advantage of being quick and inexpensive. However, when the analysed grains have complex spectral signatures with too many peaks or variable proportions of chemical elements, as is the case for garnet and epidote, the method cannot accurately identify and quantify mineral abundances. In such a case, observation under the binocular microscope provides better results. Unfortunately, for ilmenite and magnetite, both methods remain inefficient because the two minerals are optically similar and their μXRF spectral signatures are highly variable depending on the degree of alteration (Suresh-Babu et al., 1994; Nair et al., 2009), hence indistinguishable with μXRF. The ilmenite percentage calculated in the heavy mineral fraction is probably overestimated because it includes some magnetite.

3.2. Trace-element concentrations

Trace-element concentrations measured in the placer, in the pure mineral separates and in the light and heavy mineral fractions are given in Table 1 and concentrations in the impure fractions of monazite, garnet, ilmenite and zircon are given in Supplementary Table 3. Except for garnet, the composition of the impure fractions is similar to that of the pure mineral separate but generally less concentrated in trace elements. To compare the composition of the entire placer with that of the pure mineral separates and the light and heavy mineral fractions, the concentrations of REE and other trace elements were normalised to the average chondrite composition of

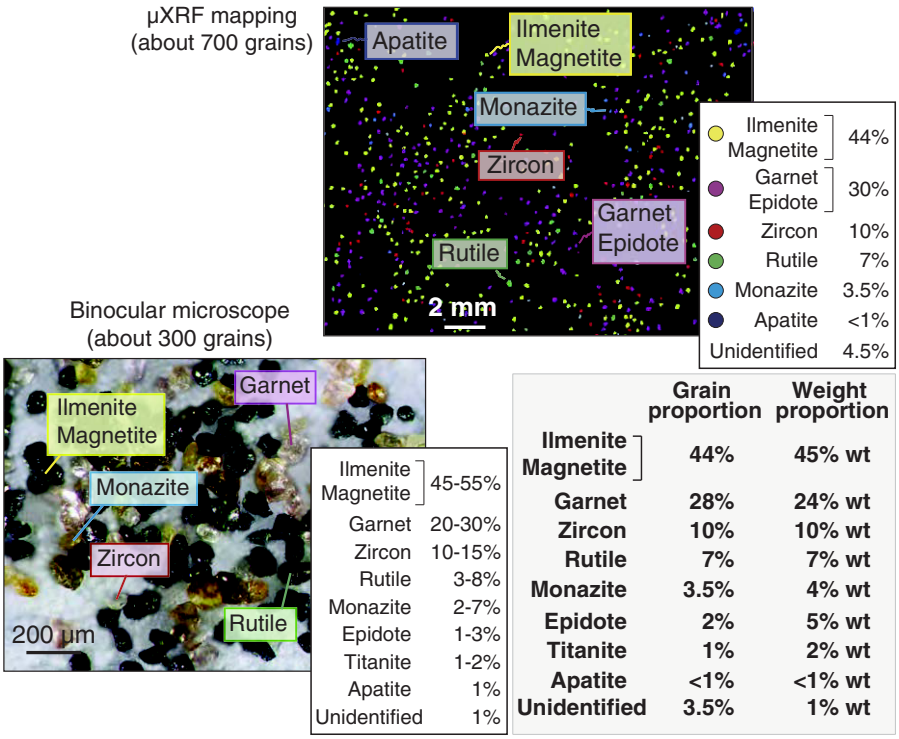

Fig. 2. Mineral abundances in the heavy fraction (d>2.9). A picture of the heavy fraction and the mineral proportions estimated as a percentage of the total grains counted under the binocular microscope are reported in the bottom left corner. The µXRF mapping showing the mineral species of the analysed grains on the adhesive surface and the mineral abundances calculated using this method as a percentage of the counted grains are presented in the top right corner. The heavy mineral abundances determined by combining the results from both methods are shown in the grey-coloured inset as a percentage of the total counted grains and as a mass percentage. For mass percentage calculations, we used the characteristic mineral densities given by Deer et al. (1992) and we estimated, based on binocular microscope observations, that all the grains had roughly the same volume except for the epidote and titanite for which the radius were considered to be 1.5 times larger than that of the other grains. Taking into account all sources of errors, the uncertainties on the mass percentages are estimated at about 3%.

Evensen et al. (1978) in Fig. 3a and to the average upper continental crust values of McLennan (2001) in Fig. 3b. Compared to chondrites, the REE enrichment factors span several orders of magnitude from 10 to almost 400 000 (Fig. 3a). All samples are characterised by a negative Eu anomaly. Compared to upper continental crust, enrichment factors range from about 0.01 to 4000 (Fig. 3b) and almost all samples display

Table 1
Trace-element concentrations measured in the various fractions (ppm). Concentrations were calibrated to the BR standard composition using the reference values recommended by Eggins et al. (1997). Precision on the measured concentrations of most elements is usually better than 5% as described in details by Chauvel et al. (2011) and values obtained for the rock standards analysed as unknown samples are similar to published values within 3% (see Supplementary Table 2).

Sample	CAM Mnz	CAM Grt	CAM Il	CAM Zr	CAM Ru	CAM Ep	CAM HMC	CAM fd NT	Plac7
Description	Monazite	Garnet	Ilmenite	Zircon	Rutile	Epidote	Heavy minerals d>2.9	Light minerals d<2.9	Total placer
Li	4.49	25.6	4.45	18.4	7.04	10.5	16.7	24.2	17.9
Rb	3.48	2.09	4.22	2.53	8.23	5.95	6.53	19.9	9.09
Sr	143	5.60	14.1	23.0	53.5	1525	108	509	170
Y	17 419	414	68.1	2137	285	313	1969	55.5	2363
Zr	1509	2090	528	501 294	23 353	581	45 508	1494	39 432
Nb	3.44	4.44	303	21.5	1366	42.7	295	2.29	360
Cs	0.356	0.181	0.489	0.145	0.749	0.379	0.572	0.643	0.694
Ba	10.3	4.32	22.5	6.70	67.2	19.7	26.7	85.0	50.0
La	90 255	7.28	56.7	17.7	433	350	2788	26.7	2345
Ce	182 339	15.4	113	60.6	866	699	5635	53.0	4833
Pr	22 283	1.87	12.8	7.19	104	84.6	652	6.69	569
Nd	80 352	7.42	46.2	35.2	374	312	2363	25.2	2039
Sm	14 649	2.85	11.0	18.9	68.7	62.6	432	5.27	360
Eu	439	0.96	0.987	4.69	4.30	8.09	19.4	0.571	17.0
Gd	9927	16.0	11.3	59.9	52.9	55.0	324	4.66	271
Tb	1227	4.79	2.05	15.3	7.87	8.66	49.5	0.673	39.7
Dy	4968	46.1	11.7	171	42.8	49.4	279	3.66	221
Ho	656	12.7	2.40	60.1	8.90	9.60	58.0	0.725	45.5
Er	1081	44.6	7.09	276	28.6	26.5	173	2.23	135
Yb	344	50.6	7.05	495	39.1	23.6	168	2.94	134
Lu	33.0	7.78	1.07	99.5	7.38	3.37	26.6	0.569	21.3
Hf	50.0	47.0	14.6	11 230	579	13.1	1012	42.2	889
Ta	2.14	0.549	30.2	4.40	113	7.80	31.0	0.280	30.3
Pb	1268	2.38	18.4	17.2	24.5	60.5	62.7	6.87	55.3
Th	40 663	4.58	20.1	284	306	142	1154	38.2	1006
U	7233	5.33	5.54	720	146	42.4	265	3.96	217

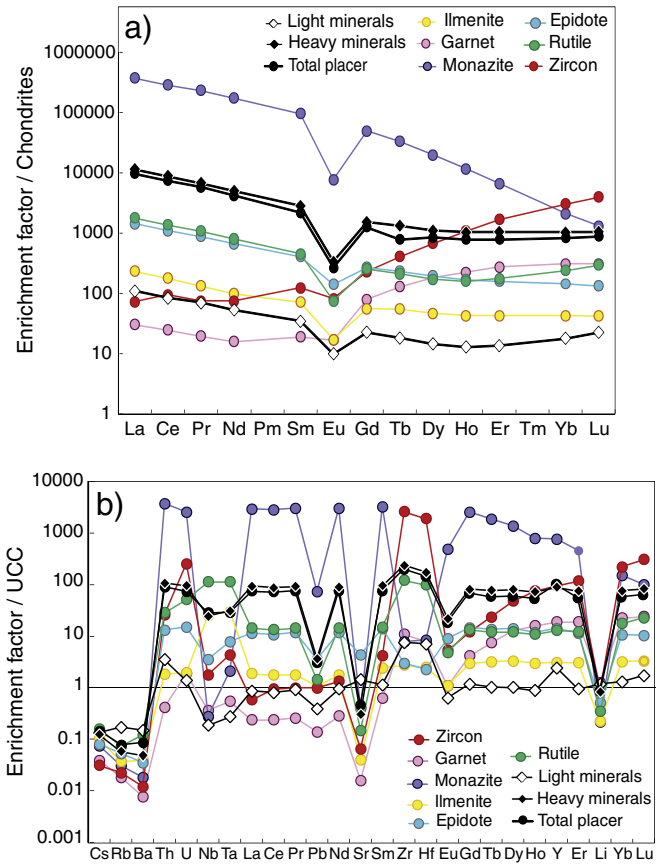

Fig. 3. REE and trace elements in the mineral fractions isolated from the Camargue placer. (a) REE patterns normalised to the average composition of chondrites as given by Evensen et al. (1978). (b) Trace element patterns normalised to the average composition of the upper continental crust given by McLennan (2001).

significant depletions in Cs, Rb, Ba, Sr and Li elements that are all known to be highly mobile during alteration.

As can be seen in Fig. 3b, trace-element concentrations measured in the total placer are about 100 times those of upper continental crust and are quasi-similar to those of the heavy mineral fraction. In contrast, the light mineral fraction has much lower trace element concentrations, quite similar to upper continental crust values. These three fractions display the same small negative anomalies in Nb, Ta and positive anomalies in Hf and Zr (Fig. 3b).

Except for garnet, trace-element concentrations measured in the pure mineral separates strongly resemble those published in the literature when available and/or are consistent with partition coefficients determined in many studies.

- Monazite is extremely rich in Th–U and all REE but particularly the light REE (LREE) (e.g. Kamineni et al., 1991; Ayres and Harris, 1997; Zhu and O'Nions, 1999; Nagy et al., 2002; Thöni et al., 2008; Radulescu et al., 2009).
- Ilmenite is characterised by positive anomalies in Nb–Ta that are consistent with the partition coefficients determined by Klemme et al. (2006) and Melluso et al. (2008) for these two elements.
- Rutile and epidote display quite similar trace-element concentrations except for their anomalies in Nb–Ta and in Zr–Hf which are positive for rutile and negative for epidote. These features are in agreement with the partition coefficients determined by Foley et al. (2000) and Klemme et al. (2005) for these four elements.
- Zircon differs from other minerals because of its strong depletion in LREE and its significant enrichment in Hf and Zr (Fig. 3; see Hoskin and Schaltegger, 2003 for a review).
- Garnet is more enriched in HREE than in LREE (Fig. 3a) and displays unusual positive Zr and Hf anomalies (Fig. 3b). Its LREE concentrations are not as low as usually measured in typical metamorphic or magmatic garnets (Jung and Hellebrand, 2006). In the pure garnet separate, the higher LREE concentrations associated with the Hf and Zr anomalies might be due to the presence of zircon inclusions and/or to an incomplete sorting of the fraction.

3.3. Nd and Hf isotopic compositions

Nd and Hf isotopic ratios measured in the placer, the pure mineral separates and the heavy and light mineral fractions are given in Table 2 and are plotted in a ε_{Hf} vs. ε_{Nd} diagram in Fig. 4. The isotopic compositions of the impure fractions of monazite, garnet, ilmenite and zircon are given in Supplementary Table 3. Except for garnet, the compositions of the impure separates resemble those of their respective pure mineral separates. Nd and Hf isotopic compositions measured in the placer, the pure mineral separates and the heavy and light mineral fractions span a large range of values from 0.512150 ($\varepsilon_{Nd} = -9.4$) to 0.512594 ($\varepsilon_{Nd} = -0.7$) for Nd and from 0.282358 ($\varepsilon_{Hf} = -15.1$) to 0.282942 ($\varepsilon_{Hf} = +5.6$) for Hf. The pure zircon separate has the highest Nd isotopic ratio and one of the lowest Hf isotopic ratios whereas the pure monazite separate has the highest Hf isotopic ratio and one of the lowest Nd isotopic ratios. Considering the analytical uncertainties on the measurements, the total placer, the rutile and the light and heavy mineral fractions have similar Nd and Hf

Table 2
Nd and Hf isotopic compositions of various fractions. Re-run stands for run duplicates. Uncertainties ($\pm 2\sigma$) reported in the table correspond to in-run errors. Nd and Hf isotopes were calculated relative to the Ames–Rennes Nd and Ames–Grenoble Hf standard values given by Chauvel and Blichert-toft (2001) and Chauvel et al. (2011) ($^{143}Nd/^{144}Nd = 0.511961 \pm 13$ (2σ) and $^{176}Hf/^{177}Hf = 0.282160 \pm 12$ (2σ)). The reproducibility calculated using re-run analyses and duplicates (see Supplementary Table 3) is 0.000013 (2σ, n = 7) for the $^{176}Hf/^{177}Hf$ ratios and 0.000037 (2σ, n = 7) for the $^{143}Nd/^{144}Nd$ ratios. ε_{Nd} and ε_{Hf} are calculated using the CHUR composition given by Bouvier et al. (2008). Considering the reproducibility of the entire analytical procedure, uncertainties are estimated at $\pm 0.7\varepsilon$ units for ε_{Nd} and ε_{Hf} values.

Sample	Description	$^{143}Nd/^{144}Nd$	$\pm 2\sigma$	ε_{Nd}	$^{176}Hf/^{177}Hf$	$\pm 2\sigma$	ε_{Hf}
CAM Mnz	Monazite	0.512158	±9	−9.2	0.282942	±9	+5.6
CAM Mnz re-run		0.512166	±7	−9.0			
CAM Grt	Garnet	0.512363	±9	−5.2	0.282559	±6	−8.0
CAM Il	Ilmenite	0.512359	±8	−5.3	0.282593	±7	−6.8
CAM Il re-run		0.512390	±7	−4.7			
CAM Zr	Zircon	0.512594	±5	−0.7	0.282417	±5	−13.0
CAM Zr re-run					0.282409	±6	−13.3
CAM Ru	Rutile	0.512150	±13	−9.4	0.282358	±5	−15.1
CAM Ep	Epidote	0.512279	±5	−6.9	0.282743	±19	−1.5
CAM HMC	Heavy minerals d>2.9	0.512169	±5	−9.0	0.282374	±5	−14.5
CAM HMC re-run		0.512183	±9	−8.7	0.282378	±6	−14.4
CAM fd NT	Light minerals d<2.9	0.512181	±8	−8.8	0.282440	±5	−12.2
CAM fd NT re-run					0.282441	±7	−12.2
Plac7	Total placer	0.512190	±10	−8.6	0.282406	±11	−13.4

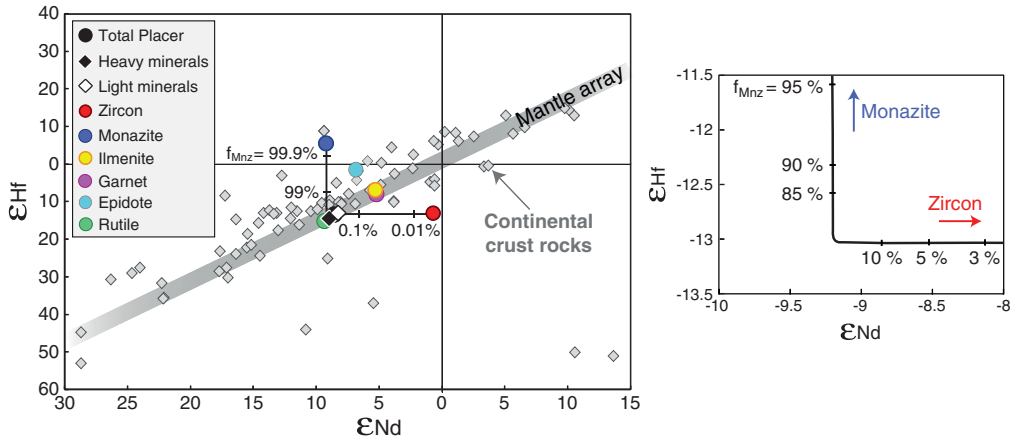

Fig. 4. Nd and Hf isotopes in the mineral fractions isolated from the Camargue placer. The mantle array is that defined by Chauvel et al. (2008) associated with the CHUR composition given by Bouvier et al. (2008). The proportions of monazite (f_{Mnz}) in the binary mixing between zircon and monazite are shown by ticks on the mixing hyperbola connecting the two endmembers. The proportions of monazite in the point of maximum curvature of the mixing hyperbola are shown in more detail in the inset. Continental crust rock data are from Bennett et al. (1993), Vervoort et al. (1996), Vervoort and Patchett (1996), Vervoort and Blichert-Toft (1999) and Vervoort et al. (2000) and plot along an array of $\varepsilon_{Hf} = 1.50 \times \varepsilon_{Nd} - 0.60$. Note that this Nd–Hf relation has the same slope as the mantle array of Chauvel et al. (2008) but passes below the BSE value defined by Bouvier et al. (2008). Analytical errors are smaller than the symbol size.

isotopic compositions which all lie on the mantle array in the ε_{Hf} vs. ε_{Nd} diagram (Fig. 4). Ilmenite and garnet have more radiogenic Nd and Hf isotopic ratios that also fall on the mantle array in Fig. 4. In contrast, epidote lies well above the mantle array due to the radiogenic decay associated to its high Lu/Hf ratio.

4. Discussion

4.1. Geochemical characteristics of the Camargue placer

As heavy minerals are important carriers of trace elements (e.g. Götze and Lewis, 1994; Preston et al., 2002; Totten and Hanan, 2007), we first decipher the contribution of each mineral species to the overall chemistry of the Camargue placer in order to further investigate the Sm–Nd and Lu–Hf systematics of beach placers.

4.1.1. The heavy minerals control the trace element budget of the placer

In Fig. 5, we normalised the trace element concentrations of the heavy (high density, $d > 2.9\ g.cm^{-3}$) and light (low density, $d < 2.9\ g.cm^{-3}$) mineral fractions to the bulk composition of the Camargue placer to assess their respective contributions to the chemical budget of the placer. The enrichment factors calculated for the heavy mineral fraction are very close to 1 whereas they are quite low for the light mineral fraction — usually <0.1. This clearly shows

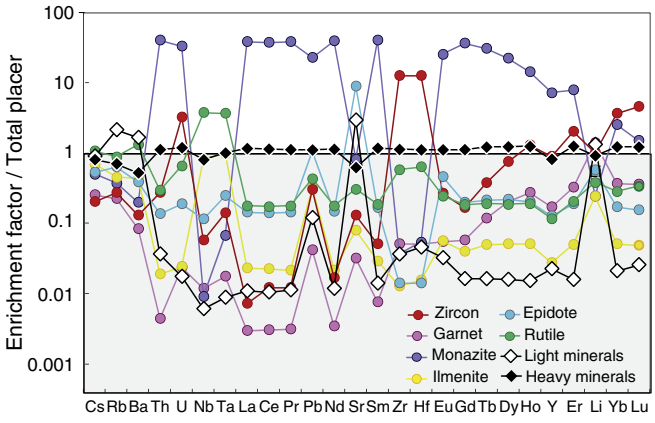

Fig. 5. Trace-element patterns of the mineral fractions normalised to the composition of the Camargue placer.

that heavy minerals almost totally control the bulk geochemistry of the placer by hosting most trace elements. Except for some mobile elements such as Cs, Rb, Ba, Sr and Li, the light minerals do not sequester large amounts of trace elements. The very low concentrations measured in this fraction indicate that it contributes to very little of the overall chemical budget of the placer but it still has the potential to significantly dilute overall concentrations (Götze and Lewis, 1994; Vervoort et al., 1999). We also see that the spectrum for the light mineral fraction in Fig. 3b is not really consistent with those usually found in the literature for quartz, feldspar or calcite, the main mineral species present in this fraction (see Götze and Lewis, 1994; Govindaraju, 1994; Korotev, 1996; Monecke et al., 2000; Strnad et al., 2009). The light mineral fraction displays unusual HFSE contents that strongly resemble those found in the heavy mineral fraction (negative anomaly in Nb and Ta and positive anomaly in Zr and Hf, see Fig. 3). This feature is best explained by the presence of few heavy minerals in the light mineral fraction, a feature not surprising since, unlike the pure mineral separates analysed in this study, the light mineral fraction was not carefully purified by hand-picking under a binocular microscope.

4.1.2. Trace elements hosted by pure mineral separates

In Fig. 5, the placer-normalised patterns reflect the contribution of each heavy mineral to the bulk trace-element budget of the placer. With its very high concentrations, monazite obviously is the major carrier of Th, U and REE. Zircon mainly controls Zr, Hf and to a lesser extent U and HREE while rutile and ilmenite host most Nb and Ta in the placer. The other trace elements such as Cs, Rb, Ba, Sr, Pb or Li are carried in variable proportions by several mineral species and their concentrations in the total placer are not controlled by one or two specific mineral species (Fig. 5).

To ensure that we isolated and analysed all the heavy mineral species that significantly contribute to the trace-element budget of the placer, we use the concentrations measured in the pure mineral separates and the mineral proportions estimated as mass percentages in Fig. 2 to calculate a theoretical trace element pattern for the heavy mineral fraction. In Fig. 6, we compare it to the measured values. We also take into account the uncertainties estimated on the mineral proportions (see footnote of Fig. 6 for more detail) and we model a field of variability for the calculated heavy mineral fraction concentrations (blue field in Fig. 6). With the exception of the HREE and some mobile elements, our results show that the measured trace-element pattern of the heavy mineral fraction is extremely well reproduced

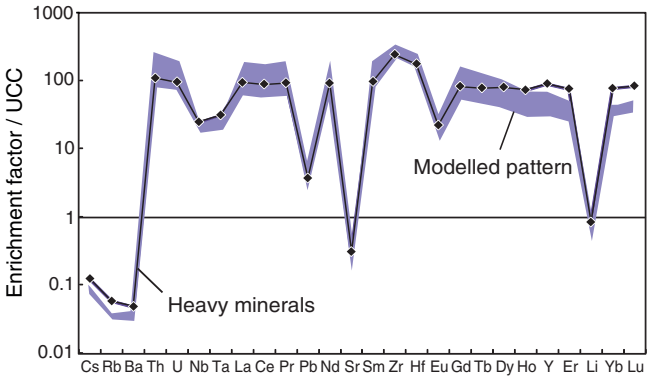

Fig. 6. Modelling of the heavy-mineral trace-element pattern. The concentrations in the heavy mineral fraction were modelled by summing the concentrations of the pure mineral separates multiplied by their mass proportions (estimates done under the binocular microscope and using the μXRF method for each mineral — see Fig. 2). To take into account the uncertainties on mineral percentages, the proportion of the different phases was taken as variable within 2 limits: ilmenite + magnetite: 42–48 wt.%, garnet: 21–27 wt.%, zircon: 8–12 wt.%, rutile: 5–9 wt.%, epidote: 3–7 wt.% and monazite: 2–6 wt.%. The blue field represents the entire range of modelled patterns obtained by sampling different mineral proportions within the ranges of values given above.

using the combined proportions of pure monazite, zircon, ilmenite, garnet, rutile and epidote. This confirms that, except for the HREE, the pure mineral separates account for the trace element budget of the heavy mineral fraction. For Nd and Hf, our calculation shows that their concentrations in the heavy mineral fraction are completely reproduced using only the mass proportions and contents measured in the pure monazite and zircon separates. Other minerals play close to no role in the overall abundance of Nd and Hf in the heavy mineral fraction. Monazite contains such high amounts of LREE and zircon contains such high amounts of Zr and Hf that even though they constitute only small percentages of the mineral assemblage, they are the controlling carriers of Nd and Hf in the beach placer. Finally, we interpret the misfit between calculated and measured concentrations for Cs, Rb, Ba and heavy REE (Fig. 6) as being due to impurities in the garnet separate and/or to the presence of a mineral such as titanite, which we did not separate and analyse.

4.1.3. What controls the Nd and Hf isotopic systematic of beach placer?

Given that monazite and zircon are the carriers of Nd and Hf in the placer, they should control the isotopic compositions. To confirm this hypothesis, we calculated a mixing curve between these two minerals using the equation established by Faure (1977). This mixing curve and the mass proportion of monazite in the binary mixture are shown in Fig. 4. Because monazite controls the Nd content and zircon the Hf content, the mixing hyperbola has such a strong curvature that it resembles two perpendicular straight lines in the ε_{Hf} vs. ε_{Nd} diagram. The first important observation is that, within uncertainties, the bulk composition of the placer, as well as those of the light and heavy mineral fractions plots at the point of maximum curvature on the mixing curve. A simple binary mixture of monazite and zircon without all the other mineral species thus properly reproduces their Nd and Hf isotopic compositions. This confirms that monazite totally controls the Nd isotopic composition in the placer as well as that of the heavy and the light mineral fractions while zircon totally dominates the Hf isotopic composition.

As a consequence of the concentration contrast between monazite and zircon for Nd and Hf, the proportion of monazite in the monazite–zircon mixture varies widely near the point of maximum curvature on the hyperbola (see the inset of Fig. 4). Considering an uncertainty of 0.7ε units on the isotopic compositions, mixing calculations demonstrate that as long as there is 5 to 90% of monazite in the monazite–zircon mixture, the ε_{Nd} of the mixture remains similar to that of the monazite and the ε_{Hf} to that of the zircon. A very wide range of monazite–zircon ratio will thus produce Nd and Hf isotopic compositions that lie at the point of maximum curvature on the mixing hyperbola. This, together with the fact that heavy mineral proportions determined in the studied Camargue placer are comparable to those usually found in mature beach placer deposits, makes us very confident in the reproducibility of our results. Hence, we are convinced that similar isotopic compositions would characterise placer samples taken from various locations on the same beach even if heavy mineral proportions vary locally.

This latter observation potentially has major implications for beach-placer deposits in other parts of the world. Indeed, monazite and zircon are very common minerals in most coastal-marine placers (Patyk-Kara and Shevelev, 2000; Patyk-Kara, 2002) where they usually represent 1–5 wt.% and 5–20 wt.% of the heavy mineral assemblage, respectively (e.g. Carpenter and Carpenter, 1991; Force, 1991; Rao, 1994; Roy, 1999; Paine et al., 2005; Levchenko, 2006), proportions that are comparable to those estimated in the Camargue placer. Given that zircon is unequivocally the major carrier of Hf among common heavy minerals, we suggest that, as for the Camargue placer, the Hf elemental and isotopic budget of worldwide beach placers is likely entirely controlled by zircon. For Nd content and isotopic composition, the situation is more ambiguous because the percentage of monazite in the heavy mineral assemblages can sometimes be low and other minerals will influence the placer Nd isotopic composition if they are present in sufficiently large proportions. Apatite probably constitutes the most serious competitor to monazite in the REE budget of placers because it contains significant amounts of REE and is sometimes present at the percent level in some beach placers. However, the normal Nd content of monazite is at least 100 times that of typical apatite (see Ayres and Harris, 1997 and Belousova et al., 2002 for Nd concentrations in apatites) and 1000 times that of other common placer minerals (cf Fig. 3a; Götze and Lewis, 1994). A simple calculation shows that even if a placer contains only 0.5% monazite, 5% apatite and 94.5% other minerals, 80% of the overall Nd budget is still control by monazite. We therefore suggest that the Nd and Hf isotopic compositions of worldwide beach placers should be controlled by monazite and zircon even though their abundances in the heavy mineral assemblage are often low.

4.2. Present-day Nd and Hf isotopic compositions of continental areas

4.2.1. The continental area drained by the Rhone River

Previous studies showed clearly that the present-day Hf–Nd isotopic compositions of crustal rocks plot on the extension of the mantle array in a Hf–Nd isotopic space and thus on the same trend as rocks coming from the mantle (Vervoort and Patchett, 1996; Vervoort et al., 1999; Vervoort et al., 2000) (Fig. 4). In Fig. 4, data for the Camargue placer lie on the mantle array and also fall in the field of crustal rocks, suggesting that its present-day ε_{Nd} at −9 and its ε_{Hf} at −13 are quite comparable to that of continental crust materials. Our ε_{Hf} value is the first published estimate for the Hf isotopic composition of crustal rocks from Western Europe since no Hf data are available for the source rocks in the region drained by the Rhone River. This is not the case for ε_{Nd}, however. Fig. 7 shows that our ε_{Nd} value is identical to the average value calculated from a compilation of ε_{Nd} reported in the literature for continental crust rocks – granitoids and orthogneiss essentially – from the Massif Central and the Western and Central Alps. It also corresponds to the average Nd isotopic composition of metamorphic rocks, sediments and granitoids of the Hercynian fold belt of Central Europe (Liew and Hofmann, 1988). We conclude that the placer's Nd and Hf isotopic compositions represent those of the average source region of the sediment, allowing us to provide the following estimate for the Western European crust: $\varepsilon_{Hf} \approx -13$ and $\varepsilon_{Nd} \approx -9$.

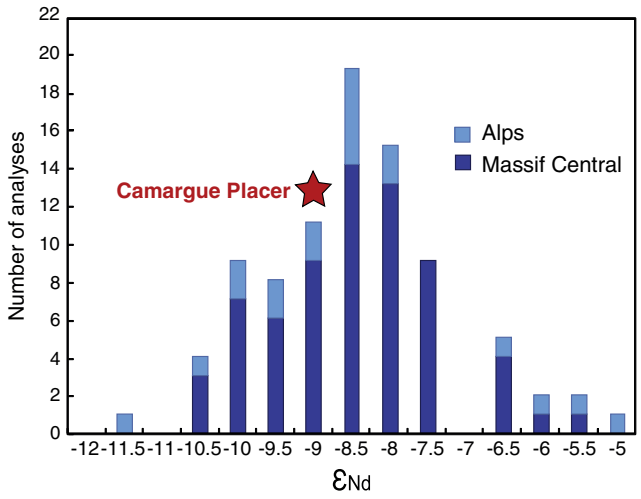

Fig. 7. Histogram of ε_{Nd} values for crustal rocks from the Massif Central and the Alps. Whole-rock Nd isotope data are from Downes (1984), Bossart et al. (1986), Downes and Duthou (1988), Paquette et al. (1989), Pin and Duthou (1990), Tilton et al. (1991), Downes et al. (1997), Duchene et al. (1997), Henry et al. (1997) and Steinmann and Stille (2008). ε_{Nd} values are calculated using the CHUR composition of Bouvier et al. (2008).

4.2.2. Can beach placers be used as proxies for other continental areas?

While we believe that the Camargue placer might be a good proxy for the average Nd and Hf isotopic composition of the continental area drained by the Rhone river, this might not be the case for other beach placers. For an estimate based on placer data to be robust requires a number of conditions that we will now examine. We demonstrated above that the Nd and Hf isotopic compositions of the Camargue placer are controlled by monazite and zircon, ubiquitous minerals that host most of the LREE and Hf in crustal rocks. However, it is also known that parent/daughter ratios such as Sm/Nd and Lu/Hf change when minerals crystallise from a magma (Faure, 1977) and that sedimentary rocks do not necessarily have the same ratios as their sources (Patchett et al., 1984). As time passes after formation of the minerals, the isotopic compositions of minerals evolve following their parent/daughter ratios, which might be significantly different from those of the whole rock. The impact of the difference in parent/daughter ratio needs therefore to be quantitatively evaluated before we can conclude that placers represent proxies for the average Nd and Hf isotopic composition of their crustal precursors.

In continental crust granitoids, Nd resides not only in monazite but also in other minerals such as apatite, allanite or feldspar (Taylor and McLennan, 1995; Bea, 1996) that are not systematically concentrated in beach placers when continental crust is eroded. Nevertheless, as for most common granite-forming minerals (e.g. Taylor and McLennan, 1995; Bayon et al., 2006), monazite has the same $^{147}Sm/^{144}Nd$ ratio as continental crust (see McLennan, 2001 and Rudnick and Gao, 2003 for continental crust ratios and Ayres and Harris, 1997; Thöni et al., 2008 and our own measurement for monazite ratios). Consequently, the monazite Nd isotopic composition never significantly differs from that of crustal rocks and can be considered as a good estimate of the average crustal value even if monazite does not dominate the Nd content of crustal rocks. In contrast, most of the Hf in continental crust granitoids is hosted in resistant zircons (Patchett et al., 1984; Candela, 2003), which have low $^{176}Lu/^{177}Hf$ ratios compared to that of continental crust (0.002 versus 0.013) (see McLennan, 2001 and Rudnick and Gao, 2003 for continental crust ratios and Kinny and Maas, 2003 for zircon ratios). As a consequence, significant isotopic differences develop between mineral and crustal precursor if the zircon crystallisation age is old. In practice, using a $^{176}Lu/^{177}Hf$ ratio of 0.002 for the zircon and 0.013 for the continental crust, our calculations show that if the zircon crystallisation age is younger than 500 Ma, its isotopic composition differs from that of its crustal precursor by less than two ε_{Hf}. This is simply because time is not sufficient for the difference in Lu/Hf to produce a Hf isotopic composition in the zircon very different from that of the crust. As a result, the Hf isotopic composition of a young zircon population, such as that in the Camargue placer, can be considered as a valuable proxy for the average crustal value of the drained area. In the case of an older zircon population, a correction could be applied provided that the average age of the population is known.

In summary, we believe that placers have the potential to provide naturally averaged information about the isotopic composition of large portions of the crust exposed to weathering and erosion, information that is not always available as revealed by the numerous papers that aim to estimate the composition of the continental crust (e.g. Taylor and McLennan, 1995; McLennan, 2001; Rudnick and Gao, 2003). Although we recognise that analytical procedure, particularly for sample dissolution, is sometimes difficult, we suggest that analyses of worldwide beach placer deposits may constitute a fairly simple way to constrain the Nd–Hf systematics of large continental areas. We recognise that this estimate does not take into account mafic and ultramafic materials that could exist in the drainage area because monazite and zircon, the two minerals controlling the Nd and Hf isotopic compositions of beach placers, are not ubiquitous in mafic and ultramafic rocks. Beach placer deposits approximate therefore the average isotopic composition of materials of continental affinity. Interesting sampling sites could be the deltas of large rivers where vast amounts of terrigenous material are deposited and where sea currents facilitate the formation of heavy mineral concentrates (Komar, 2007).

4.3. Nd and Hf model ages of the drained continental area

4.3.1. Two stage model age calculations

Since minerals do not necessarily have Sm/Nd and Lu/Hf ratios similar to those of their whole rocks, Nd and Hf model ages of their crustal protolith must be calculated using a two stage-model, a first stage for the time spent in the crust and a second for the evolution of the mineral itself since crystallisation. For this calculation, we assume that the Sm–Nd and Lu–Hf isotopic systems evolved first in a continental crust-type reservoir extracted from the depleted mantle and then, after crystallisation, in the minerals themselves. An example of the calculation for the Lu–Hf isotopic system is shown in Fig. 8 and the calculated Hf model ages are shown as a function of the Nd model ages in Fig. 9. For the placer and for each mineral fraction, model ages were estimated using a Monte-Carlo procedure to propagate uncertainties related to (1) the isotopic composition of the depleted mantle (mean MORB-pole from the compilation made by Chauvel et

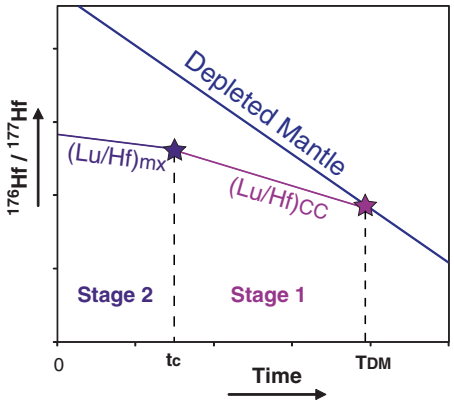

Fig. 8. Sketch of Hf two stage model age calculations. CC: continental crust. mx: mineral. T_{DM}: Hf two stage model age (extraction time from the depleted mantle). t_c: crystallisation age of the mineral.

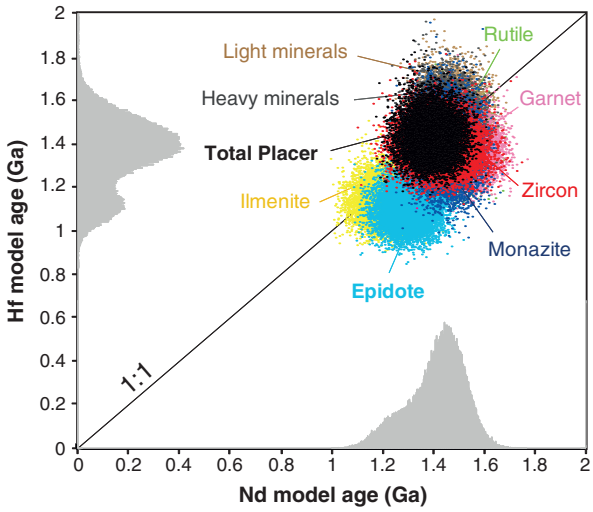

Fig. 9. Hf model ages versus Nd model ages obtained from 10 000 Monte Carlo simulations. As illustrated in Fig. 8, model ages were calculated using two stages and the following equation (here for Hf):

$$T_{DM} = t_c + \frac{1}{\lambda_{Hf}} ln \left[\frac{\left(^{176}Hf/^{177}Hf\right)^{t_c}_{mx} - \left(^{176}Hf/^{177}Hf\right)^{t_c}_{DM}}{\left(^{176}Hf/^{177}Hf\right)^{t_c}_{CC} - \left(^{176}Hf/^{177}Hf\right)^{t_c}_{DM}} + 1 \right]$$

The acronyms used in this equation are similar to those of Fig. 8. All the model ages were calculated using a Monte-Carlo procedure (n = 10 000 for each mineral fraction and for the placer) to propagate the input parameter uncertainties. The distribution of crystallisation ages (t_c) follows a Gaussian law with a mean value of 300 Ma and a standard deviation (2σ) of 50 Ma. After having randomly sampled a crystallisation age in the latter distribution, $\left(^{143}Nd/^{144}Nd\right)^{t_c}_{DM}$, $\left(^{147}Sm/^{144}Nd\right)^{t_c}_{DM}$, $\left(^{176}Hf/^{177}Hf\right)^{t_c}_{DM}$ and $\left(^{176}Lu/^{177}Hf\right)^{t_c}_{DM}$ were calculated using the following parameters: (a) we assume that the depleted mantle has linearly evolved from a bulk Earth value at Earth formation, (b) we use the CHUR values published by Bouvier et al. (2008) and (c) we sample randomly the $\left(^{143}Nd/^{144}Nd\right)^{0}_{DM}$ and $\left(^{176}Hf/^{177}Hf\right)^{0}_{DM}$ isotopic ratios in Gaussian distributions centred at the mean-MORB pole of Chauvel et al. (2008) with a standard deviation (2σ) of 2ε units. $\left(^{143}Nd/^{144}Nd\right)^{t_c}_{mx}$ and $\left(^{176}Hf/^{177}Hf\right)^{t_c}_{mx}$ were calculated back in time using the Nd and Hf isotopic ratios and the Lu, Hf, Sm and Nd concentrations measured in this study. Finally, $\left(^{147}Sm/^{144}Nd\right)^{t_c}_{CC}$ and $\left(^{176}Lu/^{177}Hf\right)^{t_c}_{CC}$ were calculated using $\left(^{147}Sm/^{144}Nd\right)^{0}_{CC}$ and $\left(^{176}Lu/^{177}Hf\right)^{0}_{CC}$ ratios randomly sampled in Gaussian distributions centred at 0.115 ± 0.005 (2σ) and 0.013 ± 0.004 (2σ), respectively (values from McLennan, 2001 and Rudnick and Gao, 2003). $\lambda_{Nd} = 6.54\ 10^{-12}\ yr^{-1}$ and $\lambda_{Hf} = 1.87\ 10^{-11}\ yr^{-1}$. For each mineral fraction and for the placer, colour dots show the location of model ages as calculated using the Monte Carlo simulation. The distribution of Nd and Hf model ages for all fractions together, are shown as histograms along the x and y axes.

al., 2008), (2) the $^{147}Sm/^{144}Nd$ and $^{176}Lu/^{177}Hf$ ratios of average continental crust and (3) the crystallisation ages of the placer minerals (see caption of Fig. 9 for more details). As a primary hypothesis, we considered that the crystallisation age of all minerals was, on average, Hercynian (300 ± 50 (2σ) Ma) given that (1) this period corresponds to the last major magmatic event forming widespread plutonic bodies and occurring both in the Eastern Massif Central and in the Western Alps (Pin and Duthou, 1990; Debon and Lemmet, 1999), the two main sources of the placer minerals and (2) numerous studies have reported crystallisation ages between 290 Ma and 340 Ma for monazite and zircon populations from the Massif Central and the Western-Central Alps (e.g. Bossart et al., 1986; Sergeev et al., 1995; Bruguier et al., 2003; Mezeme et al., 2006; Rossi et al., 2006; Gébelin et al., 2009). Using this assumption, similar model ages are calculated for the two isotopic systems for the placer, the light and heavy mineral fractions and for each pure mineral separate, as shown by the distribution in Fig. 9. In contrast, if we assume an average Alpine crystallisation age of about 30–50 Ma or any age younger than 250 Ma or older than 350 Ma, large discrepancies occur between the Nd and Hf model ages. This would imply a systematic decoupling of the Sm–Nd and Lu–Hf isotopic systems in every mineral species, a situation that is obviously unrealistic. As an example for the pure zircon separate, taking a crystallisation age of 50 Ma leads to Nd model ages (0.7 to 1 Ga) much younger than the Hf model ages (1.3 to 1.7 Ga) while taking a crystallisation age of 500 Ma provides Nd model ages (1.7 to 2.0 Ga) that are far older than the Hf model ages (1.2 to 1.5 Ga). We are therefore confident that calculating model ages using a mean crystallisation age of 300 ± 50 (2σ) Ma for all the placer minerals provides robust information about the Nd and Hf isotopic systematics of the source region. Note that the bulk placer and some of the mineral fractions, such as the light and heavy mineral fractions, the pure ilmenite for Hf and the pure rutile for Nd, have parent/daughter ratios that resemble those of the continental crust, hence they have robust model ages that do not depend on the age of crystallisation we chose to calculate them.

4.3.2. Implications for the history of the drained continental area

Almost all mineral fractions, and the placer itself, display consistent Nd and Hf model ages (Fig. 9) grouped around 1.4–1.5 Ga, suggesting that they derive from similar crustal protoliths. The only exceptions are epidote and ilmenite both of which are characterised by slightly younger ages around 1.1 to 1.3 Ga. Assuming a younger crystallisation age for these two minerals does not significantly raise the Hf and Nd model ages. As a consequence, epidote and ilmenite may record more recent geological events or their parent/daughter ratios may have been disturbed by secondary processes.

Our calculated Nd and Hf model ages are fully consistent with the Proterozoic Nd model ages reported for granitoids from the Massif Central and the Alps (e.g. Bossart et al., 1986; Paquette et al., 1989; Downes et al., 1990) and strongly resemble those of metamorphic rocks, sediments and granitoids from the European Hercynian fold belt whose model ages vary mainly between 1.4 and 1.7 Ga (Liew and Hofmann, 1988). This suggests that the bulk composition of the Camargue placer provides a true estimate of both the Nd and Hf model ages of the large continental area drained by the Rhone River. More generally, Nd and Hf model ages obtained on placer sands from continents could provide similar information for the crustal evolution of large continental areas.

According to our measurements and calculations, the mean crustal residence age of the Nd and Hf now residing in the Camargue placer minerals is Proterozoic, hence far older than the age of the main orogenies that produced the Hercynian and Alpine terranes. As discussed by many authors studying the Hercynian magmatism in the Massif Central and the Alps (e.g. Bossart et al., 1986; Paquette et al., 1989; Pin and Duthou, 1990; Sergeev et al., 1995; Downes et al., 1997), such model ages are best explained in terms of a two-component mixing between new crust and an older component at least Early Proterozoic in age. This suggests strongly that the main process occurring during the Hercynian and Alpine orogenies was reworking of old continental crust with little addition of new material. Considering that the mean age of the old crustal component is 1.8–2.0 Ga (Peucat et al., 1988) and that of the placer minerals is about 1.5 Ga, a simple calculation shows that a maximum of 20–30% juvenile crust could have been added over the last 400 Ma i.e. during the recent Hercynian and Alpine events. Both Sm–Nd and Lu–Hf isotopic systems thus record clear evidence that the continental area drained by the Rhone River had a long history prior to the known Hercynian and Alpine events and that large amounts of old crustal material with a mean Proterozoic age were reworked during the genesis of rocks currently forming the Massif Central and the Alps.

5. Conclusions

This study provides the first analyses of Nd and Hf isotopes and associated trace element concentrations for a placer and the main

mineral species it contains. Our results show that heavy minerals host most trace elements while light minerals only dilute concentrations. More specifically, we show that monazite and zircon control the Nd and Hf isotopic compositions, respectively, of the Camargue placer. A simple mixture of only these two minerals reproduces not only the isotopic compositions but also the Nd and Hf concentrations of the bulk placer. As the mass percentages of heavy minerals in the studied placer are typical of those commonly found in worldwide beach placer deposits, we suggest that monazite and zircon always dominate the Nd and Hf isotopic compositions of beach placer even though they are usually present in low proportions in the mineral assemblage.

Our data indicate that present-day Nd–Hf isotopic compositions of the Camargue placer are representative of the crustal rocks found in the Massif Central and the Alps and provide therefore a reliable estimate of the average isotopic composition of the continental area drained by the Rhone River ($\varepsilon_{Nd} \approx -9$, $\varepsilon_{Hf} \approx -13$). The calculated Nd and Hf model ages for all placer minerals are consistent and provide an average Proterozoic age for the history of this part of the continental crust. We finally suggest that other beach placers formed at the mouths of large rivers in other parts of the world could provide reliable estimates of the average Nd–Hf compositions of other large continental areas, values that are usually not easy to obtain.

Supplementary materials related to this article can be found online at doi:10.1016/j.chemgeo.2011.06.007.

Acknowledgements

We thank F. Senebier (LGCA, Grenoble) for the first separation and recognition of the mineral grains, P. Telouk (ENS, Lyon) for its assistance during Nd and Hf isotopic measurements in Lyon, M. Muñoz and M. Corrazi (LGCA, Grenoble) for their precious help to measure and process µXRF data and Nicholas Arndt (LGCA, Grenoble) for constructive discussions that help to improve the content of this paper. Constructive comments provided by Jonathan Patchett, Laurie Reisberg and an anonymous reviewer greatly helped improving the overall quality of the manuscript. Financial support for this study was provided by the Observatoire des Sciences de l'Univers de Grenoble (OSUG) and an INSU-CNRS grant.

References

Allègre, C.J., Dupré, B., Négrel, P., Gaillardet, J., 1996. Sr–Nd–Pb isotope systematics in Amazon and Congo River systems: constraints about erosion processes. Chemical Geology 131 (1–4), 93–112.

Amelin, Y., Lee, D.C., Halliday, A.N., Pidgeon, R.T., 1999. Nature of the Earth's earliest crust from hafnium isotopes in single detrital zircons. Nature 399 (6733), 252–255.

Ayres, M., Harris, N., 1997. REE fractionation and Nd-isotope disequilibrium during crustal anatexis: constraints from Himalayan leucogranites. Chemical Geology 139, 249–269.

Bayon, G., Vigier, N., Burton, K.W., Brenot, A., Carignan, J., Etoubleau, J., Chu, N.-C., 2006. The control of weathering processes on riverine and seawater hafnium isotope ratios. Geology 34 (6), 433–436.

Bea, F., 1996. Residence of REE, Y, Th and U in granites and crustal protoliths; implications for the chemistry of crustal melts. Journal of Petrology 37 (5), 521–552.

Belousova, E.A., Griffin, W.L., O'Reilly, S.Y., Fisher, N.I., 2002. Apatite as an indicator mineral for mineral exploration: trace-element compositions and their relationship to host rock type. Journal of Geochemical Exploration 76, 45–69.

Bennett, V.C., Nutman, A.P., McCulloch, M.T., 1993. Nd isotopic evidence for transient, highly depleted mantle reservoirs in the early history of the Earth. Earth and Planetary Science Letters 119, 299–317.

Bodet, F., Schärer, U., 2000. Evolution of the SE-Asian continent from U–Pb and Hf isotopes in single grains of zircon and baddeleyite from large rivers. Geochimica et Cosmochimica Acta 64 (12), 2067–2091.

Bossart, P.J., Meier, M., Oberli, F., Steiger, R.H., 1986. Morphology versus U–Pb systematics in zircon: a high-resolution isotopic study of a zircon population from a Variscan dike in the Central Alps. Earth and Planetary Science Letters 78, 339–354.

Bouvier, A., Vervoort, J.D., Patchett, J., 2008. The Lu–Hf and Sm–Nd isotopic composition of CHUR: constraints from unequilibrated chondrites and implications for the bulk composition of terrestrial planets. Earth and Planetary Science Letters 273, 48–57.

BRGM, 2000. Expertise géologique des anomalies radioactives des plages de Camargue. 21 p.

Bruguier, O., Becq-Giraudonb, J.F., Champenoisc, M., Deloulec, E., Luddenc, J., Manginc, D., 2003. Application of in situ zircon geochronology and accessory phase chemistry to constraining basin development during post-collisional extension: a case study from the French Massif Central. Chemical Geology 201, 319–336.

Candela, P.A. 2003. Ore in the Earth's Crust. pp 411–431. In The Crust (ed. R.L. Rudnick) Vol. 3, Treatise on Geochemistry (eds. H.D. Holland and K.K. Turekian), Elsevier-Pergamon, Oxford.

Carpenter, R.H., Carpenter, S.F., 1991. Heavy mineral deposits in the upper coastal plain of North Carolina and Virginia. Economic Geology 86, 1657–1671.

Chauvel, C., Blichert-Toft, J., 2001. A hafnium isotope and trace element perspective on melting of the depleted mantle. Earth and Planetary Science Letters 190, 137–151.

Chauvel, C., Lewin, E., Carpentier, M., Arndt, N.T., 2008. Role of recycled oceanic basalt and sediment in generating the Hf–Nd mantle array. Nature Geoscience 1, 64–67.

Chauvel, C., Bureau, S., Poggi, C., 2011. Comprehensive chemical and isotopic analyses of basalt and sediment reference materials. Geostandards and Geoanalytical Research 35, 125–143.

Debon, F., Lemmet, M., 1999. Evolution of the Mg/Fe ratios in late Variscan plutonic rocks from the external crystalline massifs of the Alps (France, Italy, Switzerland). Journal of Petrology 40 (7), 1151–1185.

Deer, W.A., Howie, R.A., Zussman, J., 1992. An Introduction to the Rock-Forming Minerals.

Dhuime, B., Hawkesworth, C.J., Storey, C.D., Cawood, P.A., 2011. From sediments to their source rocks: Hf and Nd isotopes in recent river sediments. Geology 39 (4), 407–410.

Downes, H., 1984. Sr and Nd isotope geochemistry of coexisting alkaline magma series, Cantal, Massif Central, France. Earth and Planetary Science Letters 69, 321–334.

Downes, H., Duthou, J.L., 1988. Isotopic and trace element arguments for the lower crustal origin of Hercynian granitoids and pre-Hercynian orthogneisses, Massif Central (France). Chemical Geology 68, 291–308.

Downes, H., Dupuy, C., Leyreloup, A.F., 1990. Crustal evolution of the Hercynian belt of Western Europe: evidence for lower-crustal granulitic xenoliths (French Massif Central). Chemical Geology 83, 209–231.

Downes, H., Shaw, A., Williamson, B.J., Thirlwall, M.F., 1997. Sr, Nd and Pb isotopic evidence for the lower crustal origin of Hercynian granodiorites and monzogranites, Massif Central, France. Chemical Geology 136, 99–122.

Duchene, S., Blichert-Toft, J., Luais, B., Telouk, P., Lardeaux, J.M., Albarede, F., 1997. The Lu–Hf dating of garnets and the ages of the Alpine high-pressure metamorphism. Nature 387 (6633), 586–589.

Eggins, S.M., Woodhead, J.D., Kinsley, L.P.J., Mortimer, G.E., Sylvester, P., McCulloch, M.T., Hergt, J.M., Handler, M.R., 1997. A simple method for the precise determination of >40 trace elements in geological samples by ICPMS using enriched isotope internal standardisation. Chemical Geology 134, 311–326.

Evensen, N.M., Hamilton, P.J., O'Nions, R.K., 1978. Rare earth abundances in chondritic meteorites. Geochimica Cosmochimica Acta 42, 1199–1212.

Faure, G., 1977. Principles of Isotope Geology. Wiley, New York.

Foley, S.F., Barth, M.G., Jenner, G.A., 2000. Rutile/melt partition coefficients for trace elements and an assessment of the influence of rutile on the trace element characteristics of subduction zone magmas. Geochimica et Cosmochimica Acta 64 (5), 933–938.

Force, E.R., 1991. Geology of Titanium-Mineral Deposits. Boulder, Colo, Geological Society of America.

Frihy, O.E., Lotfy, M.F., Komar, P.D., 1995. Spatial variations in heavy minerals and patterns of sediment sorting along the Nile Delta, Egypt. Sedimentary Geology 97 (1–2), 33–41.

Gaillardet, J., Dupré, B., Allègre, C.J., 1995. A global geochemical mass budget applied to the Congo basin rivers: erosion rates and continental crust composition. Geochimica et Cosmochimica Acta 59 (17), 3469–3485.

Gébelin A, Roger F and Brunel M. 2009. Syntectonic crustal melting and high-grade metamorphism in a transpressional regime, Variscan Massif Central, France. Tectonophysics 477 (3-4), 229–243.

Gehrels, G.E., Dickinson, W.R., Ross, G.M., Stewart, J.H., Howell, D.G., 1995. Detrital zircon reference for Cambrian to Triassic miogeoclinal strata of western North America. Geology 23 (9), 831–834.

Goldstein, S.J., Jacobsen, S.B., 1988. Nd and Sr isotopic systematics of river water suspended material: implications for crustal evolution. Earth and Planetary Science Letters 87 (3), 249–265.

Götze, J., Lewis, R., 1994. Distribution of REE and trace elements in size and mineral fractions of high-purity quartz sands. Chemical Geology 114, 43–57.

Govindaraju, K., 1994. 1994 Compilation of working values and sample description for 383 geostandards. Geostandards Newsletter 18, 1–158.

Griffin, W.L., Belousova, E.A., Walters, S.G., O'Reilly, S.Y., 2006. Archaean and Proterozoic crustal evolution in the Eastern Succession of the Mt Isa district, Australia: U–Pb and Hf-isotope studies of detrital zircons. Australian Journal of Earth Sciences 53, 125–149.

Hawkesworth, C.J., Kemp, A.I.S., 2006. Using hafnium and oxygen isotopes in zircons to unravel the record of crustal evolution. Chemical Geology 226 (3–4), 144–162.

Henry, P., Deloule, E., Michard, A., 1997. The erosion of the Alps: Nd isotopic and geochemical constraints on the sources of the peri-Alpine molasse sediments. Earth and Planetary Science Letters 146, 627–644.

Hoskin, P.W.O., Schaltegger, U., 2003. The composition of zircon and igneous and metamorphic petrogenesis. Reviews in Mineralogy and Geochemistry 53, 27–62.

Hou, B., Frakes, L.A., Alley, N.F., Heithersay, P., 2003. Evolution of beach placer shorelines and heavy-mineral deposition in the eastern Eucla Basin, South Australia. Australian Journal of Earth Sciences 50 (6), 955–965.

Hughes, M.G., Keene, J.B., Joseph, R.G., 2000. Hydraulic sorting of heavy-mineral grains by swash on a medium-sand beach. Journal of Sedimentary Research 70 (5), 994–1004.
Jung, S., Hellebrand, E., 2006. Trace element fractionation during high-grade metamorphism and crustal melting — constraints from ion microprobe data of metapelitic, migmatitic and igneous garnets and implications for Sm–Nd garnet chronology. Lithos 87, 193–213.
Kamber, B.S., Greig, A., Collerson, K.D., 2005. A new estimate for the composition of weathered young upper continental crust from alluvial sediments, Queensland, Australia. Geochimica et Cosmochimica Acta 69 (4), 1041–1058.
Kamineni, D.C., Rao, A.T., Bonardi, M., 1991. The geochemistry of monazite types from the Eastern Ghats granulite terrain, India. Mineralogy and Petrology 45, 119–130.
Kinny, P.D., Maas, R., 2003. Lu–Hf and Sm–Nd isotope systems in zircon. Reviews in Mineralogy and Geochemistry 53 (1), 327–341.
Klemme, S., Prowatke, S., Hametner, K., Günther, D., 2005. Partitioning of trace elements between rutile and silicate melts: implications for subduction zones. Geochimica et Cosmochimica Acta 69 (9), 2361–2371.
Klemme, S., Günther, D., Hametner, K., Prowatke, S., Zack, T., 2006. The partitioning of trace elements between ilmenite, ulvospinel, armalcolite and silicate melts with implications for the early differentiation of the moon. Chemical Geology 234, 251–263.
Komar, P.D., 2007. The entrainment, transport and sorting of heavy minerals by waves and currents. In: Mange, M.A., Wright, D.T. (Eds.), Heavy Minerals in Use. Developments in Sedimentology, 58. Elsevier, pp. 3–48.
Komar, P.D., Wang, C., 1984. Processes of selective grain transport and the formation of placers on beaches. Journal of Geology 92 (6), 637–655.
Korotev, R.L., 1996. A self-consistent composition of elemental concentration data for 93 geochemical reference samples. Geostandards Newsletter 20 (2), 217–245.
Levchenko, E.N., 2006. Specific features of the mineral composition of titanium–zirconium placers in Russia. Lithology and Mineral Resources 41 (2), 117–136.
Liew, T.C., Hofmann, A.W., 1988. Precambrian crustal components, plutonic associations, plate environment of the Hercynian Fold Belt of central Europe: indications from a Nd and Sr isotopic study. Contributions to Mineralogy and Petrology 98, 129–138.
McLennan, S.M., 2001. Relationships between the trace element composition of sedimentary rocks and upper continental crust. Geochemistry Geophysics Geosystems 2 April 20.
Melluso, L., Lustrino, M., Ruberti, E., Brotzu, P., Gomes, C. d B., Morbidelli, L., Morra, V., Svisera, D.P., d'Amelio, F., 2008. Major and trace-element composition of olivine, perovskite, clinopyroxene, Cr–Fe–Ti oxides, phlogopite and host kamafugites and kimberlites, Alto Paranaiba, Brazil. The Canadian Mineralogist 46, 19–40.
Mezeme, E.B., Cocherie, A., Faure, M., Legendre, O., Rossi, P., 2006. Electron microprobe monazite geochronology of magmatic events: examples from Variscan migmatites and granitoids, Massif Central, France. Lithos 87, 276–288.
Millot, R., Allègre, C.-J., Gaillardet, J., Roy, S., 2004. Lead isotopic systematics of major river sediments: a new estimate of the Pb isotopic composition of the Upper Continental Crust. Chemical Geology 203 (1–2), 75–90.
Monecke, T., Bombach, G., Klemm, W., Kempe, U., Götze, J., Wolf, D., 2000. Determination of trace elements in the quartz reference material UNS-SpS and in natural quartz samples by ICP-MS. Geostandards Newsletter 24 (1), 73–81.
Nagy, G., Draganits, E., Demeny, A., Panto, G., Arkai, P., 2002. Genesis and transformations of monazite, florencite and rhabdophane during medium grade metamorphism: examples from the Sopron Hills, Eastern Alps. Chemical Geology 191, 25–46.
Nair, A.G., Suresh-Babu, D.S., Damodaran, K.T., Shankar, R., Prabhu, C.N., 2009. Weathering of ilmenite from Chavara deposit and its comparison with Manavalakurichi placer ilmenite, southwestern India. Journal of Asian Earth Sciences 34, 115–122.
Paine, M.D., Anand, R.R., Aspandiar, M., Fitzpatrick, R.R., R.Verrall, M., 2005. Quantitative heavy-mineral analysis of a Pliocene beach placer deposit in southeastern Australia using the autogeosem. Journal of Sedimentary Research 75, 742–759.
Paquette, J.-L., Chopin, C., Peucat, J.-J., 1989. U–Pb zircon, Rb–Sr and Sm–Nd geochronology of high- to very-high-pressure meta-acidic rocks from the western Alps. Contributions to Mineralogy and Petrology 101, 280–289.
Patchett, P.J., White, W.M., Feldmann, H., Kielinczuk, S., Hofmann, A.W., 1984. Hafnium/rare earth element fractionation in the sedimentary system and crustal recycling into the Earth's mantle. Earth and Planetary Science Letters 69, 365–378.
Patyk-Kara, N.G., 2002. Placers in the system of sedimentogenesis. Lithology and Mineral Resources 37 (5), 429–441.
Patyk-Kara, N.G., 2008. Sedimentogenesis and placer formation. Lithology and Mineral Resources 43 (4), 318–325.
Patyk-Kara, N.G., Shevelev, A.G., 2000. Inhomogeneity of the mineral field of complex polymineral placers. Lithology and Mineral Resources 35 (2), 109–120.
Peucat, J.J., Jegouzo, P., vidal, P., Bernard-Griffiths, J., 1988. Continental crust formation seen through the Sr and Nd isotope systematics of S-type granites in the Hercynian belt of western France. Earth and Planetary Science Letters 88, 60–68.
Pin, C., Duthou, J.-L., 1990. Sources of Hercynian granitoids from the French Massif Central: inferences from Nd isotopes and consequences for crustal evolution. Chemical Geology 83 (3/4), 281–296.
Preston, J., Hartley, A., Mange-Rajetzky, M., Hole, M., May, G., Buck, S., Vaughan, L., 2002. The provenance of Triassic continental sandstones from the Beryl field, northern north sea: mineralogical, geochemical and sedimentological constraints. Journal of Sedimentary Research 72 (1), 18–29.
Radulescu, I.G., Rubatto, D., Gregory, C., Compagnoni, R., 2009. The age of HP metamorphism in the Gran Paradiso Massif, Western Alps: a petrological and geochronological study of “silvery micaschists”. Lithos 110 (95–108).
Rao, B.N., 1994. Significance of heavy mineral ratios in some beach placers of Andhra Pradesh, East Coast of India. Current Science 67 (7), 535–537.
Rossi, P., Cocherie, A., Fanning, C.M., Deloule, E., 2006. Variscan to eo-Alpine events recorded in European lower-crust zircons sampled from the French Massif Central and Corsica, France. Lithos 87, 235–260.
Roy, P.S., 1999. Heavy mineral beach placer in southeastern Australia: their nature and genesis. Economic Geology 94, 567–588.
Rudnick R L and Gao S. 2003. Composition of the Continental Crust. pp 1–64. In The Crust (ed. R.L. Rudnick) Vol. 3, Treatise on Geochemistry (eds. H.D. Holland and K.K. Turekian), Elsevier-Pergamon, Oxford.
Sabatier, F., Maillet, G., Provansal, M., Fleury, T.-J., Suanez, S., Vella, C., 2006. Sediment budget of the Rhône delta shoreface since the middle of the 19th century. Marine Geology 234, 143–157.
Sergeev, S.A., Meier, M., Steiger, R.H., 1995. Improving the resolution of single-grain U/Pb dating by use of zircon extracted from feldspar: application to the Variscan magmatic cycle in the central Alps. Earth and Planetary Science Letters 134, 37–51.
Steinmann, M., Stille, P., 2008. Controls on transport and fractionation of the rare earth elements in stream water of a mixed basaltic–granitic catchment basin (Massif Central, France). Chemical Geology 254, 1–18.
Strnad, L., Ettler, V., Mihaljevic, M., Hladil, J., Chrastny, V., 2009. Determination of trace elements in calcite using solution and laser ablasion ICP-MS: calibration to NIST SRM glass and USGS MACS carbonate, and application to real landfill calcite. Geostandards Newsletter 33 (3), 347–355.
Suresh-Babu, D.S., Thomas, K.A., Mohan-Das, P.N., Damodaran, A.D., 1994. Alteration of ilmenite in the Manavalakurichi deposit, India. Clays and Clay Minerals 42 (5), 567–571.
Taylor, S.R., McLennan, S.M., 1995. The geochemical evolution of the continental crust. Reviews of Geophysics 33 (2), 241–265.
Thomassin, A., Blanchardon, E., Bottolier-Depois, J.-F., Bouisset, P., Cagnat, X., Chazel, V., Clairand, I., Frelon, S., Gurriaran, R., Huet, C., Paquet, F., Pourcelot, L., Tourlonias, E., 2007. Evaluations dosimétriques de l'exposition potentielle liée à l'accumulation naturelle d'uranium et de thorium dans les sables de certaines plages du littoral de Camargue. Rapport IRSN n°2007/01.
Thöni, M., Miller, C., Zanetti, A., Habler, G., Goessler, W., 2008. Sm–Nd isotope systematics of high-REE accessory minerals and major phases: ID-TIMS, LA-ICP-MS and EPMA data constrain multiple Permian–Triassic pegmatite emplacement in the Koralpe, Eastern Alps. Chemical Geology 254, 216–237.
Tilton, G.R., Schreyer, W., Schertl, H.-P., 1991. Pb–Sr–Nd isotopic behavior of deeply subducted crustal rocks from the Dora Maira Massif, Western Alps, Italy—II: what is the age of the ultrahigh-pressure metamorphism? Contributions to Mineralogy and Petrology 108, 22–33.
Totten, M.W., Hanan, M.A., 2007. Heavy minerals in shales. In: Mange, M.A., Wright, D.T. (Eds.), Heavy Mineral in Use. Developments in Sedimentology, 58. Elsevier, pp. 323–343.
Vassas, C., Pourcelot, L., Vella, C., Carpéna, J., Pupin, J.P., Bouisset, P., Guillot, L., 2006. Mechanisms of enrichment of natural radioactivity along the beaches of the Camargue, France. Journal of Environmental Radioactivity 91, 146–159.
Vella, C., Fleury, T.-J., Raccasi, G., Provansal, M., Sabatier, F., Bourcier, M., 2005. Evolution of the Rhône delta plain in the Holocene. Marine Geology 222–223, 235–265.
Vervoort, J.D., Blichert-Toft, J., 1999. Evolution of the depleted mantle: Hf isotope evidence from juvenile rocks through time. Geochimica et Cosmochimica Acta 63 (3/4), 533–556.
Vervoort, J.D., Patchett, P., 1996. Behavior of hafnium and neodymium isotopes in the crust: constraints from Precambrian crustally derived granites. Geochimica et Cosmochimica Acta 60 (19), 3717–3733.
Vervoort, J.D., Patchett, P.J., Gehrels, G.E., Nutman, A.P., 1996. Constraints on early Earth differentiation from hafnium and neodymium isotopes. Nature 379, 624–627.
Vervoort, J.D., Patchett, P.J., Blichert-Toft, J., Albarède, F., 1999. Relationships between Lu–Hf and Sm–Nd isotopic systems in the global sedimentary system. Earth and Planetary Science Letters 168, 79–99.
Vervoort, J.D., Patchett, P.J., Albarède, F., Blichert-Toft, J., Rudnick, R., Downes, H., 2000. Hf–Nd isotopic evolution of the lower crust. Earth and Planetary Science Letters 181 (1–2), 115–129.
Zhu, X.K., O'Nions, R.K., 1999. Monazite chemical composition: some implications for monazite geochronology. Contributions to Mineralogy and Petrology 137, 351–363.

Applied Geochemistry 27 (2012) 760–773

Contents lists available at SciVerse ScienceDirect

Applied Geochemistry

journal homepage: www.elsevier.com/locate/apgeochem

Silver and lead in high-altitude lake sediments: Proxies for climate changes and human activities

Marion Garçon [a], Catherine Chauvel [a,*], Emmanuel Chapron [b], Xavier Faïn [c], Mingfang Lin [a], Sylvain Campillo [a], Sarah Bureau [a], Marc Desmet [d], Marie-Christine Bailly-Maître [e], Laurent Charlet [a]

[a] ISTerre, Université de Grenoble 1, CNRS, BP 53, 38041 Grenoble Cedex 09, France
[b] Université d'Orléans, CNRS/INSU, Université François Rabelais-Tours, Institut des Sciences de la Terre d'Orléans (ISTO) – UMR 6113, 1A rue de la Férollerie, 45071 Orléans Cedex 2, France
[c] Laboratoire de Glaciologie et Géophysique de l'Environnement, Université de Grenoble 1,CNRS, BP 96, 38402 Saint-Martin d'Hères Cedex, France
[d] Université de Lyon – Ecole Nationale des Travaux Publics de l'Etat, rue Maurice Audin, 69518 Vaulx en Velin Cedex, France
[e] Laboratoire d'Archéologie Médiévale Méditerranéenne, UMR 6572 CNRS – Université de Provence, Aix en Provence, France

ARTICLE INFO

Article history:
Received 25 November 2010
Accepted 16 December 2011
Available online 3 January 2012
Editorial handling by R.B. Wanty

ABSTRACT

High-altitude lake sediments are often used as archives for environmental changes and their chemical and isotopic compositions provide significant constraints on natural and anthropogenic long-term changes that have occurred in their catchment area. Here, trace-element concentrations and Pb isotopes are presented for two sedimentary cores from Lake Blanc Huez in the French Alps, to trace the impact of climate changes and human activities over the Holocene. Lead and Ag contents are very high and clearly dominated by input from a Pb–Ag vein located a few meters from the lakeshore, a vein that also buffers the Pb isotopes. Mining of this vein in medieval times is recorded in the corresponding lake sediments with high Ag content coupled with high Pb/U ratio. These chemical characteristics can be used to constrain the major Holocene climate changes. Significant advances of glaciers next to the lake produced sediments with Ag and Pb concentration peaks and high Pb/U ratios due to accelerated erosion of the Pb–Ag vein, similar to the effects of the medieval mining. In contrast, reduced glacier activity led to the formation of organic-rich sediments with high U and As contents and low Pb/U ratios. More generally, the observed combination of chemical changes could be used elsewhere to decipher environmental changes over long periods of time.

1. Introduction

Because of their location remote from civilization and human activities, high-altitude lakes provide excellent records of an isolated and well-preserved natural environment. Their location at high altitude results in mechanical, chemical and biological conditions that vary drastically between warm and cold periods (e.g. Beniston et al., 1997; Sommaruga-Wögrath et al., 1997; Koinig et al., 1998; Mosello et al., 2002; Eggermont et al., 2007). Therefore, high-altitude lake sediments constitute a valuable tool to investigate climate variability and glacier dynamics over decadal to millennial timescales (e.g. Leemann and Niessen, 1994; Battarbee et al., 2002; Brown et al., 2002; Dhal et al., 2003; Schmidt et al., 2006). In addition, these sediments also record human-induced environmental changes via the accumulation of atmospheric deposits or accelerated erosion resulting from land-use in the catchment area (Ohlendorf et al., 2003; Arnaud et al., 2004; Guyard et al., 2007). High-altitude lake sediments may thus be considered as archives of past environmental changes and as an important source of information on climate change and anthropogenic impacts on the environment.

Previous studies have used multi-trace element geochemistry of lake sediments to investigate past environment (e.g. Koinig et al., 2003; Lavilla et al., 2006). Since the chemical composition of lake sediments reflects the origin of the material accumulated through time, such sediments have the potential to provide valuable insights into the long-term history of the catchment area. For example, the presence of glaciers in the catchment area favors the abrasion of the bedrock (Leemann and Niessen, 1994; Dhal et al., 2003; Piotrowski, 2006; Swift, 2006; Tranter, 2006), changes that are recorded in the geochemistry of proglacial lakes. Similarly, human activities such as mining, industrial activities or intensive land-use lead to deforestation, soil destabilization and atmospheric pollution even in remote ecosystems. These activities should also be recorded in the chemical composition of high-altitude lake sediments.

This paper is based on a geochemical study on high-altitude lake sediments from Lake Blanc Huez, which is located next to

* Corresponding author.
E-mail address: catherine.chauvel@ujf-grenoble.fr (C. Chauvel).

0883-2927/$ - see front matter © 2011 Elsevier Ltd. All rights reserved.
doi:10.1016/j.apgeochem.2011.12.010

the Alpe d'Huez ski resort in the French North-Western Alps. Using trace-element concentrations, Pb isotopic compositions and previous work done by Chapron et al. (2007) on the sediment lithology, how sediments record environmental changes over the last 13 ka was investigated. Trace-element concentrations vary as a function of the erosion regime of the catchment and their changes can be used to identify glacier fluctuations as well as human activities in the catchment. In addition, Pb isotopic compositions can be used to trace sources of sediments and to monitor human activities and atmospheric pollution (Camarero et al., 1998; Kober et al., 1999; Monna et al., 1999, 2000; Eades et al., 2002; Renberg et al., 2002; Arnaud et al., 2004; Geraldes et al., 2006). The combination of trace-element and isotopic data should, therefore, be a powerful tool to trace the impacts of medieval mining activities next to the lake (Bailly-Maitre and Bruno-Dupraz, 1994), to evaluate the impact of the recent development of the Alpe d'Huez ski resort and more generally, to decipher the way the Quaternary climate fluctuations are recorded in high altitude mountain lake sediments.

2. Setting

Lake Blanc Huez is a proglacial lake located at an altitude of 2543 m on the western side of the Grandes Rousses Massif in the French Alps (Fig. 1). It is dammed by a N–S glacial rock bar made of resistant rocks on its eastern shore and has a surface area of about 0.13 km^2 with a maximum depth of 37 m (Fig. 2). The catchment area of Lake Blanc Huez is small (less than 4 km^2), relatively steep with almost no vegetation cover. The bedrock comprises metamorphic Permian rhyolitic ashes (leptynites), chlorite schists (metamorphic Permian flysch) and sedimentary rocks (Fig. 1; Barbier et al., 1973). Lead–Ag veins with quartz–barite gangue occur in various places in the catchment.

From November to June, the catchment area is totally or partly covered by snow and Lake Blanc Huez is frozen. During summer, melt waters from the Rousses glacier feed the lake (see Fig. 1). A relatively large amount of silt and clay particles formed by glacial abrasion of the bedrock are transported as suspended particles in melt water and are deposited in the lake (Chapron et al., 2007).

Previous studies documented have several climate changes that have caused significant glacier fluctuations in the Grandes Rousses Massif over the past 1 ka (Flusin et al., 1909; Chardon, 1991; Valla, 1993; Torinesi et al., 2002; Vincent, 2002; Chapron et al., 2007; Guyard et al., 2007). While the main valleys in this part of the Alps were deglaciated around 17,500 cal. BP, glaciers still totally covered Lake Blanc Huez at this time. Mapping of former moraine belts indicates that the lake was totally deglaciated at termination I (14,500 ka cal BP) and that it was not covered by glaciers during the Holocene.

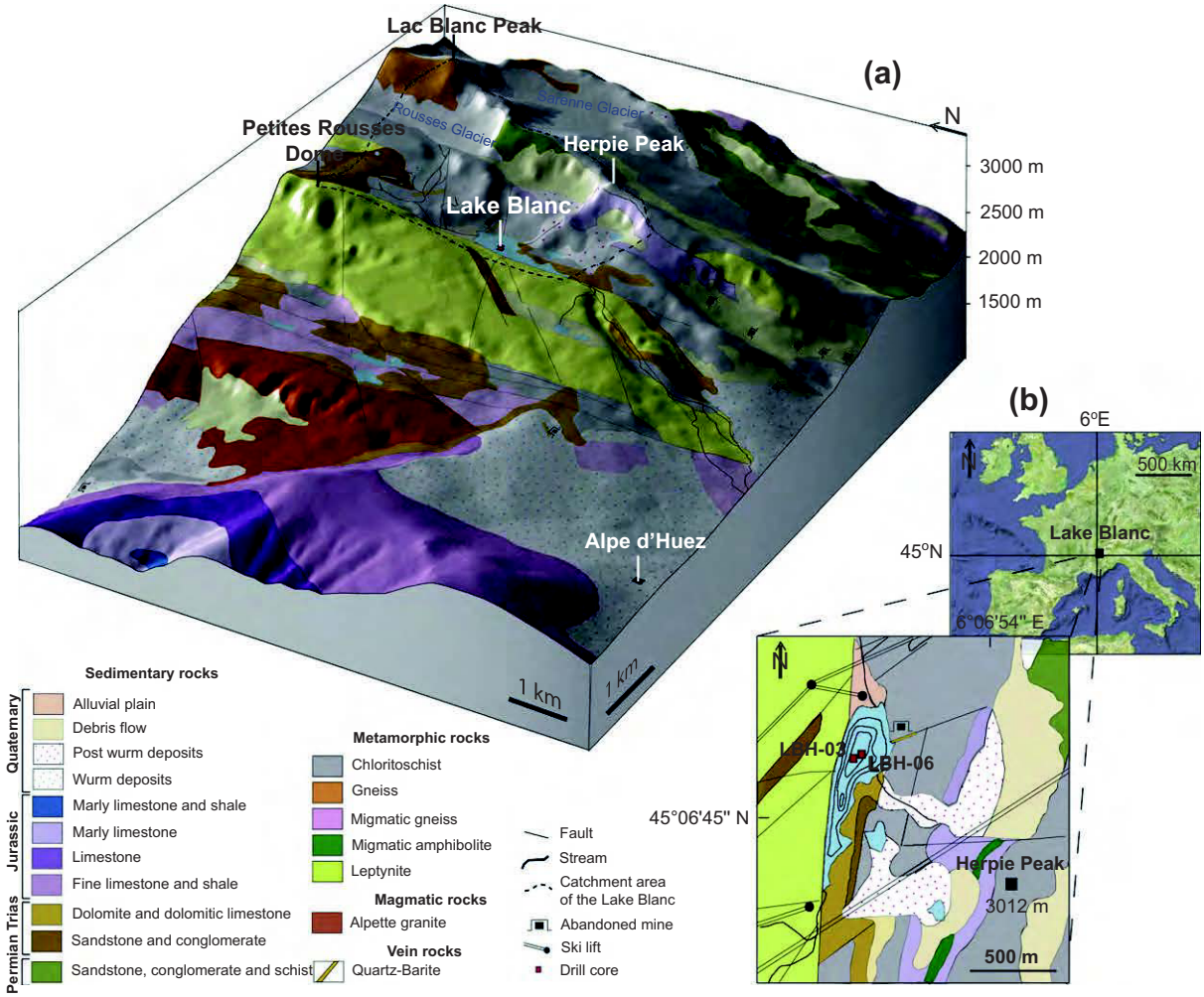

Fig. 1. Map showing the location of Lake Blanc Huez in the western French Alps and its geological context in the Grandes Rousses Massif. Major lithologic units as well as faults, streams and glaciers characterizing the Grandes Rousses Massif are shown in (a). Ski lift locations, coring sites, bathymetry of the lake and more detailed information about lithologic units around Lake Blanc Huez are presented in (b). Isobaths in Lake Blanc Huez are 10 m.

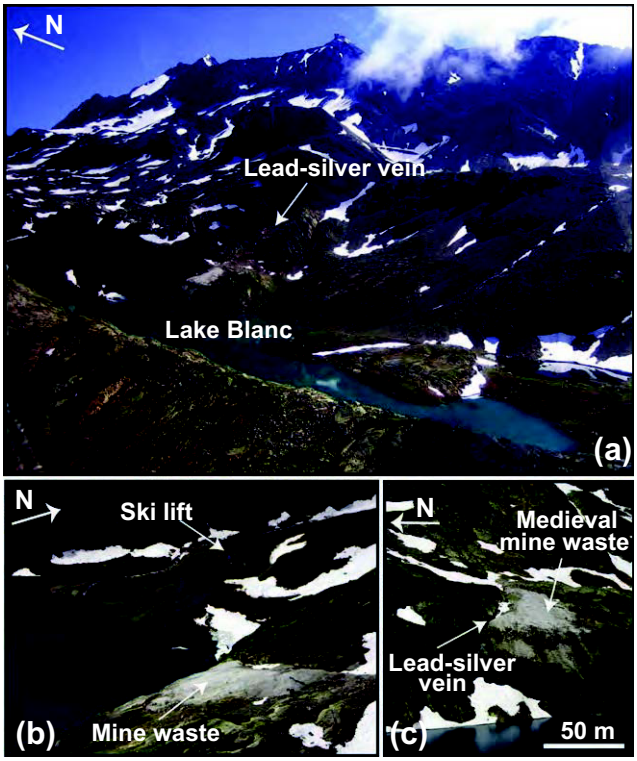

Fig. 2. Photographs of the Lake Blanc Huez area. (a) Aerial view of Lake Blanc Huez and its catchment area, (b) small Gilbert-type delta in the northern part of Lake Blanc Huez and (c) the Pb–Ag vein and the medieval mine waste (essentially barite and quartz) on the lakeshore of Lake Blanc Huez.

In addition to glacier fluctuations that cause significant erosion of the bedrock, the catchment area of Lake Blanc Huez has been affected by human activities. No trace of Roman mining activities has yet been discovered in the Grandes Rousses Massif (M.C. Bailly-Maitre pers. comm.; Legros and Legros, 1979), but archeological investigations have found clear relics of medieval mining in the catchment area (Bailly-Maitre and Bruno-Dupraz, 1994). From AD 1150–1200 to AD 1339, a Pb–Ag vein located a few meters from the eastern shore of Lake Blanc Huez (Figs. 1 and 2) was exploited along a 120-m long mineralized fault, and Ag ore was extracted using wood fires inside the mine to break the quartz–barite gangue. The Ag ore was separated from gangue on the lakeshore, next to the extraction trench using various techniques (mortar crushing, grindstone grinding, barite calcination and water washing). According to Bailly-Maitre and Bruno-Dupraz (1994), ore treatment and continuous circulation of water from the mine to the lake constitute two potential sources of pollution in Lake Blanc Huez during the period of mining. After closure of the mine in the middle of the XIV^{e} century and up to the XVIII^{e} century, several attempts were undertaken to rehabilitate the galleries but no mining is reported in historical texts (Bailly-Maitre and Bruno-Dupraz, 1994; Legros and Legros, 1979).

More recently, human activities restarted with the construction of the Alpe d'Huez ski resort. The first ski lifts were installed in the 1930s and subsequent activity has modified the geomorphology and the drainage of Lake Blanc Huez catchment area considerably (Chardon, 1986; Fig. 2). As described in more detail by Chapron et al. (2007), the development of the resort induced major environmental changes that should be recorded in recent sediments.

3. Sampling

The lake sediments analyzed in this study come from two long piston cores drilled in the deepest part of the lake (Figs. 1 and 3). Samples of the Pb–Ag vein were collected a few meters from the lakeshore (see location of the abandoned mine on Figs. 1 and 2).

The 80 cm long LBH-03 core was recovered in September 2003 using the ETH Zurich short gravity corer. It consists of proglacial sediments (Fig. 3) with intercalated angular drop stone levels that have been interpreted as erosive snow avalanche debris deposited on the frozen lake during winter (Chapron et al., 2007). The age range of the sedimentary sequence is poorly constrained because only the top few centimeters were dated using ^{210}Pb and ^{137}Cs. Detailed information about the sedimentary facies and age-depth models used to date the core LBH-03 can be found in Chapron et al. (2007). The samples analyzed in this study were selected to represent as much as possible the diversity of sedimentary facies identified in the core; their positions are indicated by arrows on Fig. 3.

The 7 m long LBH-06 core was recovered in March 2006 using a UWITEC piston corer from the frozen surface of the lake. A simplified description of its lithology, from Chapron et al. (2008) and Do Couto (2008), is presented on Fig. 3. The bottom of the core consists of black sandy silts with 3% of Total Organic C (TOC) interpreted as gyttja. It is overlain by a clastic sequence between 680 and 470 cm core depth interpreted as proglacial glacio-lacustrine materials. This sequence is made of gray sandy silts with TOC < 2% and includes a 90 cm thick deposit of coarse angular gravels mixed with light gray compacted sandy silts interpreted as a subaqueous moraine (Fig. 3). Lying on top of an erosive surface between 470 and 270 cm is another black colored gyttja unit (sandy silts with TOC values between 4% and 6%). A grayish, silty and finely laminated clastic sequence (TOC < 2%) between 270 and 30 cm is interpreted as proglacial lacustrine sediments. As in the core LBH-03, angular drop stone layers interpreted as erosive snow-avalanche debris are intercalated in the last two sequences (see Fig. 3). In contrast, the upper 30 cm of core LBH06 consists of contorted sandy layers and massive silts that are attributed to the subaqueous slide caused by the Corrençon earthquake in AD 1962. Correlations between subaqueous slides and local earthquakes were used to establish the LBH-06 recent chronology indicated on Fig. 3. The ages of older and deeper sediments in core LBH-06 were obtained by AMS ^{14}C dating (Table 1) at Poznan Radiocarbon Laboratory (Poland) on terrestrial macrofossils (two samples) and organic-rich bulk sediments (two samples). Arrows in Fig. 3 show the location of analyzed samples. As in the case of the core LBH-03, samples were taken of all the main sedimentary facies.

In addition to the two sediment cores, several samples were selected from the Pb–Ag vein (Fig. 1). Samples were isolated by hand-picking five different types of minerals that were characterized using an X-ray μ-fluorescence spectrometer (EDAX Eagle III μXRF). Galena (PbS), malachite ($Cu_2CO_3(OH)_2$) and bournonite ($CuPbSbS_3$) lie in a gangue of quartz and barite. Legros and Legros (1979) identified similar minerals in other Pb–Ag veins in the Grandes Rousses Massif.

4. Analytical procedure

Before analyses, all samples were lyophilized to remove interstitial water and ground by hand with an agate mortar to insure homogeneity of sample powders.

4.1. Trace elements

All trace element concentrations were measured using a Plasmaquad 2 + ICP-MS in Grenoble. To ensure complete dissolution, about 100 mg of lyophilized sediment powder were dissolved using a $HF–HNO_3–HClO_4$ mixture in Teflon containers placed in

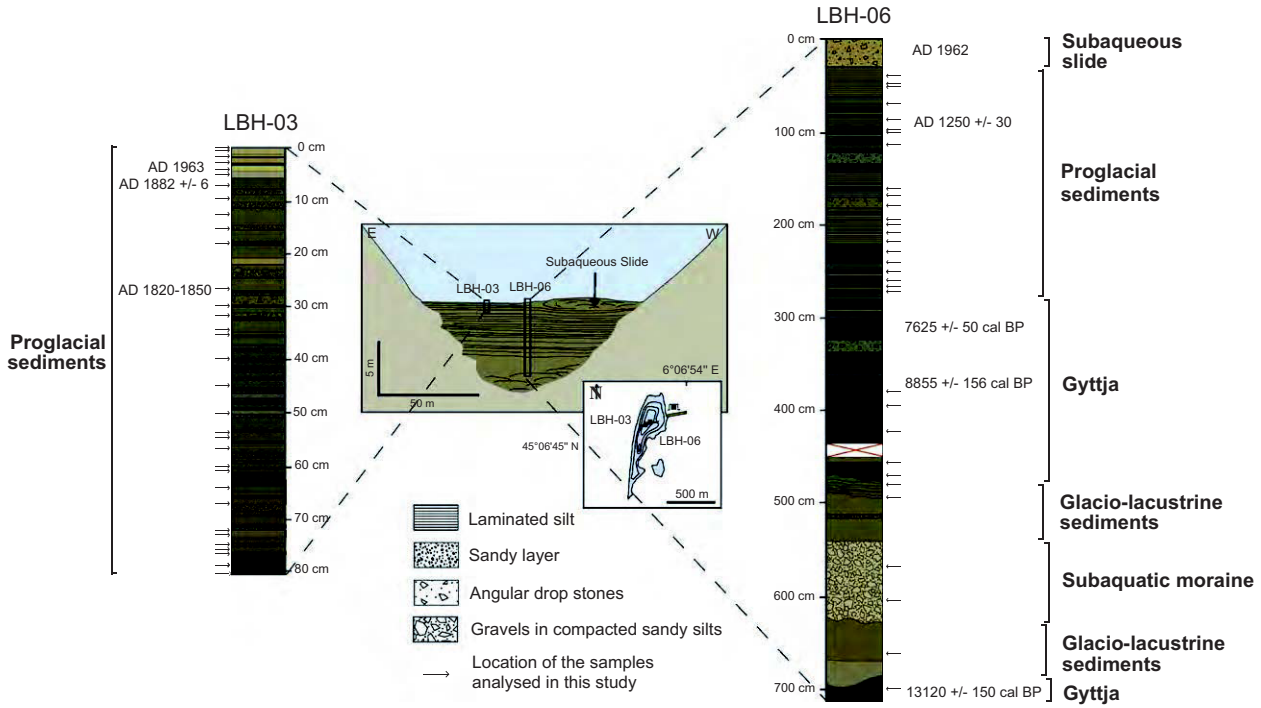

Fig. 3. Location of the two drill cores on a section of Lake Blanc Huez and lithologies of the cores LBH-03 and LBH-06. The figure showing the section of Lake Blanc Huez and its location in the lake was adapted from seismic profiles from Chapron et al. (2007, 2008). Major sedimentary units as well as ages are indicated for each core. Further details on the LBH-03 and LBH-06 sedimentary units can be found in Chapron et al. (2007, 2008). Locations of all samples analyzed in this study are shown by arrows for each core.

Table 1
Radiocarbon ages obtained for core LBH-06.

Depth (cm)	Laboratory	Radiocarbon age	Calibrated age ±1σ	Calibrated age ±2σ	Calibrated age ±2σ	Material
87	Poz-18873	774 ± 50 BP	1238–1271 cal AD	1216–1280 cal AD	702 ± 30 cal years BP	Wood debris
312	Poz-18874	6770 ± 40 BP	5707–5683 cal BC	5726–5625 cal BC	7625 ± 50 cal years BP	Bulk sediment
372	Poz-18875	8000 ± 50 BP	7048–6982 cal BC	7062–6749 cal BC	8855 ± 156 cal years BP	Wood debris
703	Poz-18877	11240 ± 80 BP	11271–11124 cal BC	11316–11013 cal BC	13,120 ± 150 cal years BP	Bulk sediment

Radiocardon ages have been calibrated using Calib.5 (Stuiver et al., 1998).

Parr steel bombs for 7 days at 150 °C. High-precision measurements on ICP-MS were obtained by diluting samples in 2% HNO_3 with traces of HF at a dilution factor of about 2000. ICP-MS analytical drift was corrected for by adding an internal standard (multispike of Be, As, In, Tm, Bi) in all samples. Concentrations were calculated using an external calibration based on the composition of BHVO-2 or BR standards (see footnote of the Supplementary Table) after correction for drift and oxide interferences on the heavy REE. Silver concentrations were measured using rock standards doped with single element solutions and As concentrations were calculated and calibrated using the MESS-2 standard composition after subtraction of the As added by the multispike internal standard. Repeated analyses of international rock standards BHVO-1, BEN and MESS-2 measured as unknown samples are provided in the Supplementary Table together with more details on the analytical procedure.

4.2. Pb isotopic compositions

For all sediments, about 100 mg of powder were digested in a mixture of pure concentrated HF, $HClO_4$ and HNO_3. In contrast, the minerals from the Pb–Ag vein were dissolved without grinding in a mixture of pure concentrated HF, $HClO_4$ and HCl. Dissolution was improved with the alternate use of an ultrasonic bath and heating to 120 °C. Following the classical anion exchange technique described by Marsh et al. (1978) and Manhès et al. (1984), isolation of Pb was carried out with anion AG1-X8 resin and dilute HBr followed by 6 N HCl. During the course of the analyses, the total procedural blank was always less than 120 pg and thus considered as negligible relative to the amount of Pb present in the samples. Lead isotopic ratios were measured on a Nu Plasma MC-ICP-MS at ENS Lyon. As described by White et al. (2000), mass fractionation was corrected using a Th spike and the classical standard bracketing technique. Analytical drift was monitored and corrected by measuring the NBS 981 standard every 2 or 3 samples. The NBS 981 Pb isotopic ratios used for the standard bracketing are those given by Galer and Abouchami (1998). During the analyses, this Pb standard was measured 52 times with a reproducibility (2σ) of 200 ppm for $^{208}Pb/^{204}Pb$, 170 ppm for $^{207}Pb/^{204}Pb$ and 180 ppm for $^{206}Pb/^{204}Pb$. The reproducibility (2σ) of the total analytical procedure estimated using four complete duplicate analyses is better than 130 ppm for $^{208}Pb/^{204}Pb$, 50 ppm for $^{207}Pb/^{204}Pb$ and 290 ppm for $^{206}Pb/^{204}Pb$.

5. Results

5.1. Chronology of core LBH-06

The chronology of core LBH-06 is poorly defined and the age-depth model was established based on the few constraints that

are listed below. The first is the landslide deposit in the upper 30 cm of the core that is correlated with the AD 1962 Corrençon earthquake. This deposit corresponds to the distal facies of a larger slide identified both on seismic reflection profiles and in a short core along the eastern slope of the main basin, close to the medieval mining site (Chapron et al., 2007). Below the slide deposit, the chronology is fixed by a 1250 ± 30 cal a BP age of wood debris in proglacial sediments in a flood layer at a depth of 87 cm (Table 1). Two other ages in the upper gyttja sequence are late Holocene: bulk sediment at 312 cm is dated at 7625 ± 50 cal a BP and wood debris at 372 cm is dated at 8855 ± 156 cal a BP. Organic-rich sediment at 703 cm at the base of core LBH-06 is dated at 13120 ± 150 cal a BP suggesting that the subaquatic moraine in overlying glacio-lacustrine sediment in core LBH-06 was deposited during the Lateglacial–Holocene transition.

Because radiocarbon ages obtained on bulk sediments are not always reliable due to uncertain C provenance (Grimm et al., 2009), it is recognized that additional high-quality dates are needed to improve the core chronology and to calculate the accumulation rates for the elements. In the discussion below, care is taken on overinterpretation of the chronology. This is why it was chosen to discuss only the large and significant variations in concentrations.

5.2. Trace elements in LBH-06 and LBH-03 core samples

Trace-element concentrations measured in sediments are given in Supplementary Table and variations of Ag, Pb, U and As concentrations as a function of depth are shown in Fig. 4. The trace-element concentrations in the upper samples of core LBH-06 are similar to those of samples from core LBH-03. This confirms that the sedimentation rates between 80 and 40 cm depth are similar at the two coring sites, i.e. the age of sediments at a given depth between 80 and 40 cm can be considered the same at the two coring sites.

Except for Ag, Pb, As and U, most elements display relatively small variations in their concentrations over the sedimentary record, relative standard deviations are less than 20%. Barium and Sr contents are moderately variable with relative standard deviations around 50%. In contrast, Ag and Pb concentrations display large fluctuations: Ag ranges from 0.612 to 16.6 ppm and Pb from 45.0 to 750 ppm. The highest Ag and Pb contents occur at the same depths (at 480, 410, 190, 100 and 30 cm, as shown in Fig. 4). Uranium and As concentrations are also variable and range from 4.29 to 59.9 ppm for U and from 27.6 to 453 ppm for As. The highest U and As concentrations are found in the two gyttja units in the lower half of the core LBH-06 (480, 410 and 390 cm). The lowest U and Pb contents are found into the moraine unit in core LBH-06 (604 and 569 cm).

Compared to the upper continental crust (UCC) composition of McLennan (2001), all analyzed samples show strong enrichment of Li, As, Ag, Cs, Ba, Tl, Pb and U. Concentrations of Li, Cs and Tl are 3 to 6 times higher than the UCC values while Ag, Ba, Pb, As and U concentrations are more variable with enrichment factors of 12–332 for Ag, 2–10 for Ba, 3–44 for Pb, 18–302 for As and 2–21 for U. The concentrations are much higher than normally observed in sediments with average Ag, Ba, Pb, As and U contents of 2.25, 1920, 304, 124 and 13.1 ppm whereas lake sediment standards LKSD-1, LKSD-2, LKSD-3, LKSD-4, GSS-9 and JLk-1 have average concentrations of only 0.8, 550, 53, 21.7 and 9.8 ppm (Govindaraju, 1994; Imai et al., 1996; Lynch, 1999; Wang et al., 2001).

5.3. Pb isotopic compositions

5.3.1. LBH-06 and LBH-03 core samples

Lead isotopic ratios measured in cores LBH-03 and LBH-06 are presented in Table 2 and variations with depth of $^{208}Pb/^{204}Pb$ are shown in Fig. 4. The Pb isotopic ratios in samples from the top of core LBH-06 are similar to those measured in samples from core LBH-03.

All through the sedimentary pile, $^{206}Pb/^{204}Pb$ ranges between 18.546 and 18.768, $^{207}Pb/^{204}Pb$ between 15.653 and 15.664 and $^{208}Pb/^{204}Pb$ between 38.648 and 38.814. These variations are small but significantly larger than the errors on measurements and can, therefore, be considered significant. The highest ratios are in the moraine unit at about 6 m depth while the lowest values are in

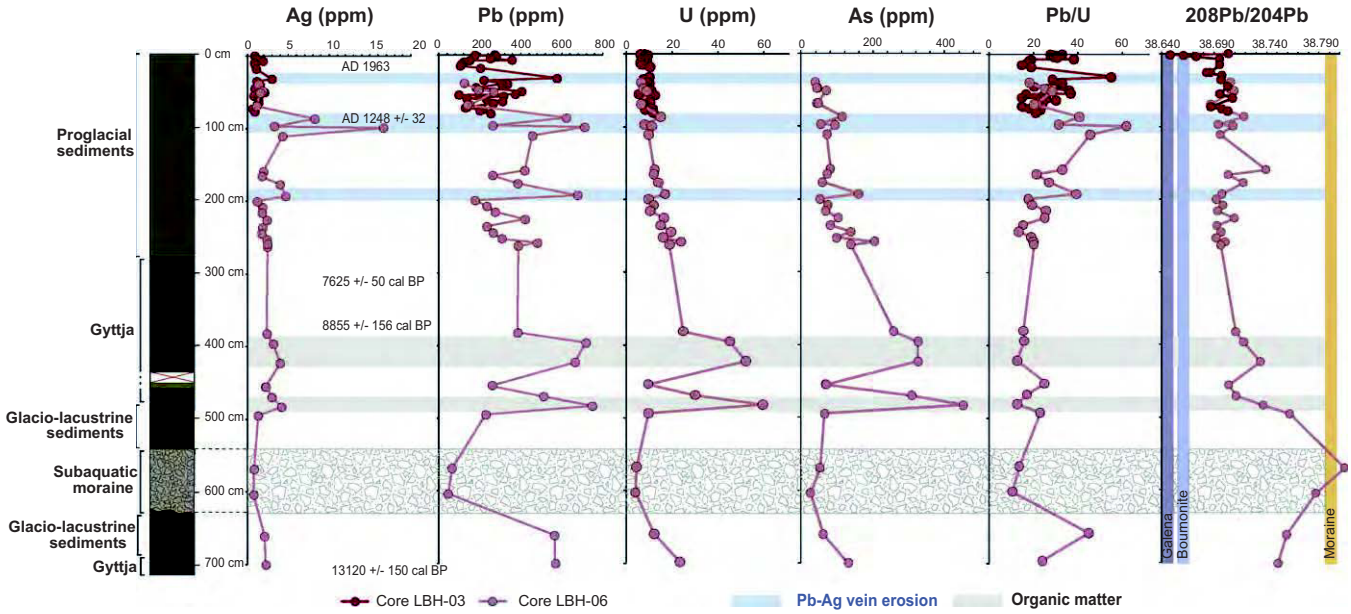

Fig. 4. Variations of Ag, Pb, U and As concentrations, Pb/U ratios and $^{208}Pb/^{204}Pb$ isotopic ratios with depth. The main units identified in the sedimentary pile are represented on the left. Chronology established along the sedimentary pile is also indicated. On the $^{208}Pb/^{204}Pb$ depth profile, Pb isotopic signatures of the subaqueous moraine, galena and bournonite are shown by colored vertical bars. Analytical errors for $^{208}Pb/^{204}Pb$ isotopic ratios and Ag, Pb, U and As concentrations are smaller than the symbol size.

Table 2
Pb isotopic compositions measured in cores LBH-03 and LBH-06 and in the lead–silver vein.

Core LBH-03	Depth (cm)	$^{206}Pb/^{204}Pb$	±2σ	$^{207}Pb/^{204}Pb$	±2σ	$^{208}Pb/^{204}Pb$	±2σ
LB1 0	0	18.6011	±2	15.6594	±2	38.7038	±11
LB1 1.5	1.8	18.5457	±3	15.6558	±3	38.6484	±2
LB1 2.5	3	18.5593	±3	15.6533	±2	38.6613	±17
LB1 4	4.3	18.5595	±2	15.6563	±2	38.6733	±14
LB1 7	7	18.5789	±3	15.6569	±2	38.6956	±18
LB1 15	15	18.5757	±3	15.6593	±2	38.6956	±12
LB1 26	26	18.5601	±4	15.6638	±3	38.6867	±22
LB1 26 Dup	26	18.5564	±2	15.6631	±2	38.6833	±13
LB1 30	30	18.5852	±1	15.6566	±1	38.6976	±12
LB1 36	36	18.5807	±2	15.6602	±2	38.6968	±14
LB1 45	45	18.5817	±3	15.6610	±2	38.7030	±11
LB1 55	55	18.5488	±2	15.6631	±2	38.6957	±15
LB1 61	61	18.5896	±2	15.6574	±2	38.7079	±13
LB1 73	73	18.5857	±2	15.6575	±2	38.6872	±13
LB1 76	76	18.5871	±2	15.6605	±2	38.6978	±14
LB1 79	79	18.5955	±2	15.6585	±2	38.7034	±15
Core LBH-06	Depth (cm)	$^{206}Pb/^{204}Pb$	±2σ	$^{207}Pb/^{204}Pb$	±2σ	$^{208}Pb/^{204}Pb$	±2σ
1A	39	18.6181	±2	15.6616	±2	38.7059	±15
2A	48	18.6005	±4	15.6615	±2	38.7053	±20
2A Dup	48	18.6029	±3	15.6607	±2	38.7059	±13
3A	51	18.6153	±3	15.6590	±2	38.7094	±12
4A	69	18.5849	±2	15.6599	±2	38.6868	±12
4A Dup	69	18.5818	±2	15.6600	±2	38.6852	±12
8A	86.5	18.6244	±2	15.6568	±2	38.7185	±9
6A	97	18.5815	±3	15.6612	±2	38.6942	±13
5A	99	18.5943	±2	15.6607	±2	38.7081	±12
7A	111	18.5900	±2	15.6561	±1	38.6960	±10
9A	159	18.6346	±2	15.6604	±1	38.7396	±10
10A	166	18.5982	±2	15.6588	±2	38.7037	±12
11A	177	18.6159	±3	15.6586	±2	38.7181	±13
12A	193	18.5943	±2	15.6552	±2	38.6975	±10
13A	200	18.5824	±2	15.6609	±1	38.6921	±10
14A	208	18.6030	±2	15.6588	±2	38.6988	±14
15A	216	18.5938	±3	15.6577	±2	38.6936	±13
16A	226	18.6015	±3	15.6603	±2	38.7096	±14
17A	236	18.5829	±3	15.6619	±3	38.6928	±18
18A	245	18.6075	±3	15.6580	±2	38.6968	±22
19A	253	18.5899	±3	15.6613	±2	38.6921	±15
32A	258.5	18.6070	±4	15.6560	±3	38.7009	±15
20A	263	18.6042	±4	15.6589	±3	38.6964	±17
21A	382	18.6117	±3	15.6589	±3	38.7108	±18
22A	396	18.6290	±4	15.6578	±3	38.7183	±16
23A	423	18.6479	±3	15.6563	±2	38.7343	±10
24A	455	18.6001	±2	15.6590	±2	38.7041	±12
26A	470	18.6079	±2	15.6592	±2	38.7109	±12
27A	483	18.6478	±2	15.6569	±1	38.7369	±12
25A	495	18.6817	±2	15.6579	±2	38.7621	±13
28A	569	18.7683	±2	15.6631	±2	38.8141	±16
29A	604	18.7427	±2	15.6637	±2	38.7867	±11
30A	661	18.6742	±2	15.6530	±1	38.7592	±13
31A	700	18.6638	±2	15.6554	±2	38.7510	±13
Vein samples	Minerals	$^{206}Pb/^{204}Pb$	±2σ	$^{207}Pb/^{204}Pb$	±2σ	$^{208}Pb/^{204}Pb$	±2σ
LBV 1	Bournonite and	18.5312	±3	15.6542	±2	38.6447	±16
LBV 2	Malachite	18.5237	±2	15.6517	±2	38.6275	±12
LBV 3	Galena	18.5165	±2	15.6618	±2	38.6588	±13
LBV 4	Quartz and Malachite	18.5390	±2	15.6614	±2	38.6661	±13
LBV 5	Barite	18.5376	±2	15.6599	±1	38.6628	±11
LBV 7	Barite	18.5186	±2	15.6613	±2	38.6548	±13
LBV 7 Dup	Barite	18.5200	±3	15.6616	±1	38.6563	±14
LBV 8	Quartz	18.5336	±8	15.6607	±7	38.6613	±44
LBV 9	Quartz	18.5351	±2	15.6608	±2	38.6607	±11

Uncertainties (±2σ) indicated in the Table are in-run errors for each Pb isotope ratio. Pb isotope ratios are relative to NBS 981 values given by Galer and Abouchami (1998). NBS 981 was measured with a reproducibility (2σ) of 200 ppm for $^{208}Pb/^{204}Pb$, 170 ppm for $^{207}Pb/^{204}Pb$ and 180 ppm for $^{206}Pb/^{204}Pb$ (total of 52 measurements). The reproducibility (2σ) calculated for reruns of the same sample solutions (not given in the Table) is better than calculated for standards.

samples located just below the surface. The variations of Pb isotopic ratios correlate neither with lithology nor Pb concentration.

5.3.2. Lead–silver vein samples

The Pb isotopic ratios of the Pb–Ag vein minerals are given in Table 2. The $^{206}Pb/^{204}Pb$ ratios are systematically lower than those of the lake sediments and the samples form two separate groups in Pb isotopic spaces (see Fig. 5): the bournonite–malachite mixture has lower $^{207}Pb/^{204}Pb$ and $^{208}Pb/^{204}Pb$ (at about 15.653 and 38.630, respectively) than the galena, quartz and barite assemblages but their $^{206}Pb/^{204}Pb$ ratios are indistinguishable. The Pb–Ag vein is, therefore, characterized by Pb isotopic signatures that

are similar but resolvable within analytical uncertainties. They correspond to the two Pb-bearing minerals identified in the vein, galena and bournonite.

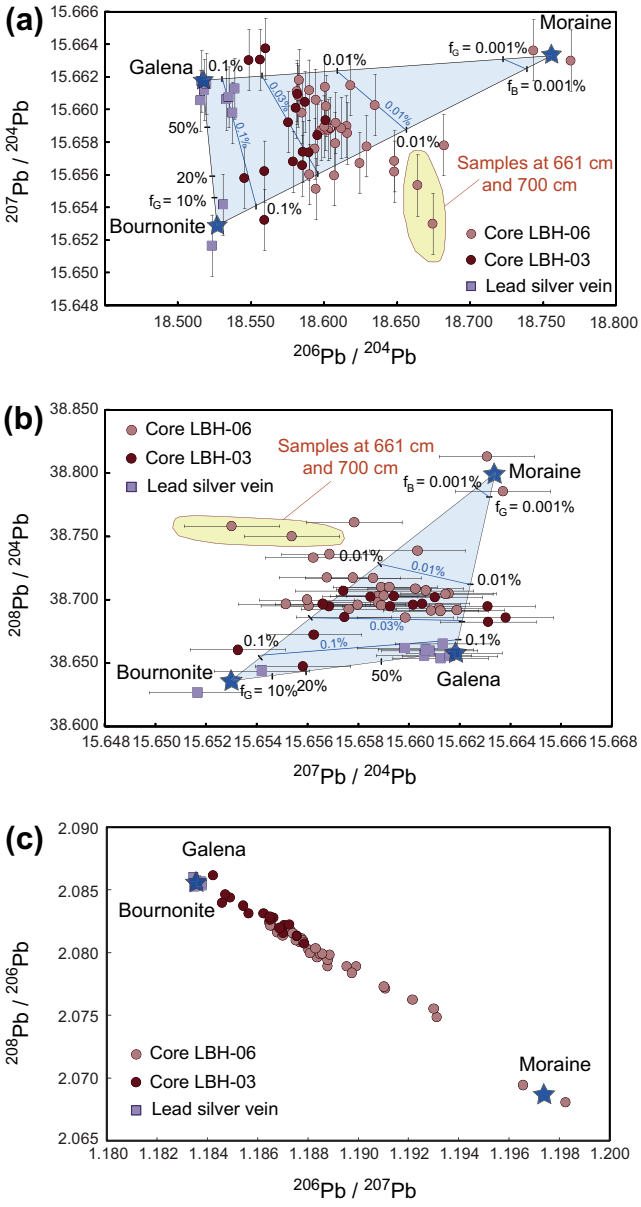

6. Discussion

6.1. Sources of sediments

The subaquatic moraine unit, which is located at 6 m depth in core LBH-06, consists of an accumulation of unconsolidated debris that was eroded from the bedrock as glaciers advanced. From the geomorphology of the Grandes Rousses Massif and glacier flow directions (Fig. 1), the lake debris must originate from the catchment area. Following Zdenek (1971), it is accepted that the composition of the moraine reflects the average lithology and geochemistry of the catchment area. This hypothesis is consistent with the trace element concentrations measured in the two moraine samples from core LBH-06. Fig. 6 shows the trace element enrichment factor of the two moraine samples normalized to the average upper continental crust values of McLennan (2001). Except for Li, As, Ag, Cs, Ba, Tl and Pb, the trace-element concentrations of the moraine strongly resemble those of upper continental crust (enrichment factors between 0.8 and 2.3). The Lake Blanc Huez catchment area consists of metamorphic Permian flysch-type sediments derived from continental materials. Considering that redistribution of chemical elements is limited during metamorphism (Krauskopf and Bird, 1995), this material is likely to retain a chemical composition comparable to average continental crust. The enrichments in Li, As, Cs, Ba, Ag, Tl and Pb (see Fig. 6) must, therefore, derive from peculiar materials in the catchment area or to processes occurring during the formation of the moraine itself. Lithium and Cs are highly mobile in fluid phases and it is possible that they were leached out of the rock material located under the glaciers during glacial abrasion and re-concentrated in the lake sediment. On the other hand, the Pb–Ag vein is the obvious source of As, Ba, Ag, Tl and Pb.

Assuming that the moraine has the average geochemical composition of the catchment area, the trace element concentrations measured in cores LBH-03 and LBH-06 were normalized to the mean of the two moraine samples (see Fig. 7) to highlight the changes in sediment composition as a function of depth or lithology. The concentrations of most trace elements are very similar to the moraine values and the enrichment factors are always <2.5 (see Fig. 7). They do not show systematic variation as a function of depth or lithology. The exceptions are As, Ag, Pb and U, which show positive and variably large anomalies in all the analyzed samples. The concentrations of these elements are greater in the sediment than in the moraine and the positive anomalies of As, Ag and Pb (but not Ba) are magnified in the sediment. In addition, a positive U anomaly is present in the sediment but not in the moraine. These selective enrichments relative to the starting composition of the catchment area, as recorded by the moraine samples, can be explained either by changes in sediment sources or by processes occurring during sediment formation and/or after their deposition.

To get a more general view of the trace-element data on the entire sample set and to investigate if processes other than those described above occurred, a Principal Component Analysis (PCA) was performed on the LBH-06 data set after normalization of each concentration to its standard deviation and propagation of uncertainties (see Table 3 for details). Calculations show that seven significant principal components (PCs) are required to account for 94% of the total variance (Table 3). However, for almost all elements, the percentage of variance related to each component (loading factors) is less than 10%, suggesting that their variability cannot be explained by one particular principal component. Few exceptions exist and include Ag, Ba and some other elements (Table 3). Such dispersion makes the interpretation of the PCA results very difficult and unreliable (DelValls et al., 1998; Reid and

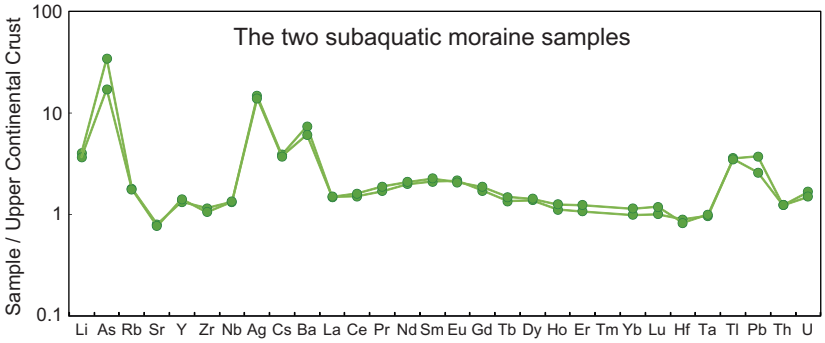

Fig. 6. Trace element patterns of the subaquatic moraine samples from the core LBH-06 normalized to the average upper continental crust composition given by McLennan (2001).

Spencer, 2009). Because almost all the principal components are strongly influenced by extreme samples such as the moraines or the Ag–Pb–U–As-rich samples, an attempt was made to improve the treatment using two different methods: (1) the moraine samples were removed to keep only sediments, and (2) the dataset were normalized to one immobile element (Th) prior to the PCA analysis to minimize the dilution effect (Reid and Spencer, 2009). In both cases, no significant change in the loading factors occurs. The only interesting observation coming out of the PCA analysis is that Sr, Ba, Tl, Ag, As, U and Pb are all negatively correlated along the first component while all other elements lie on the positive side. This suggests that the first group of elements is controlled by processes different from those controlling all the other elements: it could be source changes, processes occurring during sediment formation or diagenetic processes for example. This observation is thus entirely consistent with the interpretation suggested above using the variation of trace element contents.

In Fig. 5, the Pb isotopic ratios measured in Pb–Ag vein minerals and in cores LBH-03 and LBH-06 are plotted as $^{207}Pb/^{204}Pb$ vs. $^{206}Pb/^{204}Pb$ and $^{208}Pb/^{204}Pb$ vs. $^{207}Pb/^{204}Pb$. As ^{204}Pb is relatively difficult to measure because of its low abundance (about 1.4% of total Pb), many environmental studies use the $^{206}Pb/^{207}Pb$ vs. $^{208}Pb/^{206}Pb$ diagram to represent and interpret their data. Thus the current data were also plotted in this manner (Fig. 5c) to allow comparison between the results and those obtained in other studies. Except for the deepest sediments (samples located at 661 and 700 cm in core LBH-06), all sediments plot within uncertainty in a triangle in the $^{207}Pb/^{204}Pb$ vs. $^{206}Pb/^{204}Pb$ and $^{208}Pb/^{204}Pb$ vs. $^{207}Pb/^{204}Pb$ diagrams (see Fig. 5). This relationship suggests mixing of three Pb sources that remained distinct and identical since at least the end of the Lateglacial and through the entire Holocene lake sedimentation. The variations of Pb isotopic ratios in the sediments can thus be explained by mixing between Pb from the subaquatic moraine and Pb from galena and bournonite in the Pb–Ag vein. As can be seen in Fig. 5c, all sediments, including the deepest ones, define a linear array in $^{208}Pb/^{206}Pb$ vs. $^{206}Pb/^{207}Pb$ space indicating mixing between two Pb sources, the subaquatic moraine and the ore bearing minerals. In this isotopic space, part of the complexity of the mixing processes is lost because changes in the proportions of ^{206}Pb, ^{207}Pb and ^{208}Pb relative to ^{204}Pb are not taken into account. The authors would thus encourage future studies to report data for the four Pb isotopes to achieve a better understanding of the source of Pb in the studied material.

Using the Pb isotopic compositions of the three endmembers and the equations of Faure (1977), the proportion of Pb supplied by each source can be calculated. Three binary mixing series are assumed: the first between galena and bournonite, the second between galena and the subaquatic moraine and the third between bournonite and the subaquatic moraine. The calculated proportions depend greatly on the Pb concentrations of the three endmembers and here the following parameters were chosen: for the moraine, the average Pb content of the two subaquatic moraine samples from core LBH-06 was used; for the two Pb-bearing minerals, the theoretical concentrations of 870,000 ppm for the galena and 420,000 ppm for the bournonite were used, values that correspond to the mass percentage of Pb in pure galena and bournonite. The calculated proportions along each binary mixing line are shown by ticks in Fig. 5a and b. To better constrain the contribution of Pb from the Pb–Ag vein, the proportions of Pb supplied by galena and bournonite are indicated with blue lines in the mixing triangles of Fig. 5a and b. Because Pb concentrations in galena and bournonite are four orders of magnitude higher than those of the moraines, the results indicate that a contribution of less than 0.05% Pb–Ag vein material in the final sediment is enough to overwhelm the isotopic compositions of almost all sediments.

The two samples located at the bottom of the LBH-06 core differ from the others in that they do not fall in the mixing triangle (Fig. 5a and b). This feature suggests that the Pb sources in the oldest sediments are different from those of the rest of the sedimentary pile. The position of these samples in the isotope plots suggests that the average $^{207}Pb/^{204}Pb$ in the catchment area was lower during the earliest stages of lake sedimentation, before deposition of the Lateglacial moraine. This feature is not fully understood but may result from a change in dominating sediment source within the catchment area; for example, a particular rock type could have been eroded away during glaciation and is now insignificant or even no longer existent in the catchment area. In addition, the last glaciation could have changed the drainage morphology and the shape of the catchment area.

6.2. Origin of the Ag, Pb, As and U enrichments in sediments

As mentioned above, Ag, Pb, As and U peaks occur at various depths in the lake sediments but these enrichments are not synchronous in all cases (see Fig. 7 and blue and gray bands in Fig. 4). The Ag and Pb enrichments are partly coupled and occur at different depths in all lithologies. There is one obvious peak around 100 cm and some smaller peaks around 30, 190, 410 and 480 cm. In contrast, U and As enrichments occur only in the deeper layers. They are coupled with the deepest Ag and Pb enrichments located around 410 and 480 cm, suggesting that the processes that caused these enrichments may be different from those causing the enrichments at shallower depths. In fact, the very high U and As contents are restricted to the gyttja units (mixture of organic and fine mineralogical materials) where enrichment factors relative to sediment background concentrations are >2.5 for As and >3.5 for U (Fig. 8 and gray bands in Fig. 4). Several studies (Welch and Lico, 1998; El Bilali et al., 2002; Dowdall et al., 2005; Eusterhues

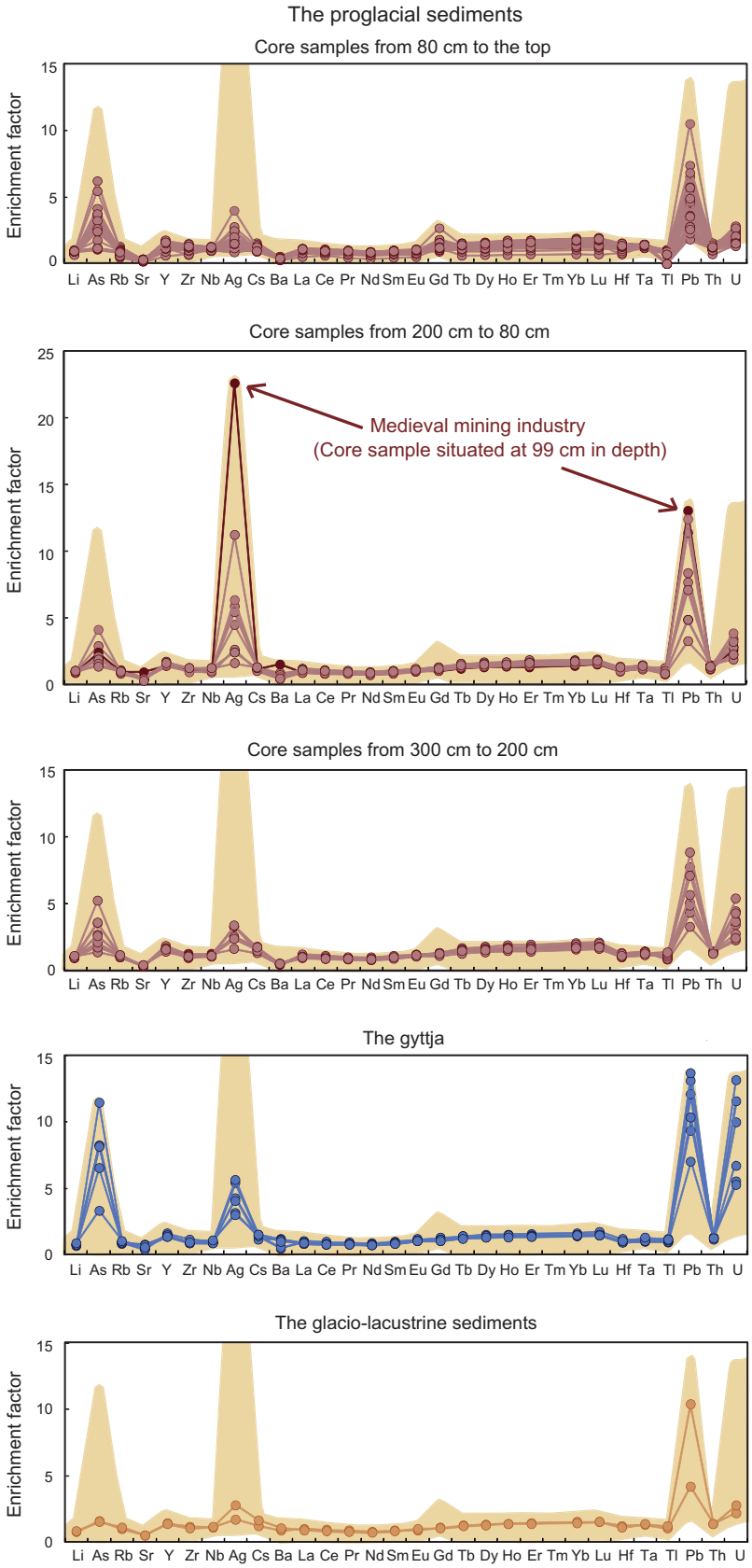

Fig. 7. Trace element patterns of Lake Blanc Huez sediments normalized to the average composition of the moraine from core LBH-06. Patterns are grouped by core lithologies and separated as a function of depth for proglacial sediments. In each graph, the maximal variability of enrichment factors for the entire sedimentary pile is indicated by the colored fields. The Pb and Ag peaks corresponding to the medieval mining activities are also shown.

Table 3
Results of the PCA performed on the LBH-06 trace element concentrations normalized to their standard deviations.

Principal component (PC)	% of total variance	Loading factors >10%
PC1	49.1	
PC2	18.2	
PC3	9.0	Sm (11.5%), Eu (17.7%)
PC4	6.8	Rb (43.3%), Tl (24.0%)
PC5	5.0	Ag (41.4%), Ba (16.7%)
PC6	3.1	Li (11.0%), Ag (15.0%), Cs (30.0%)
PC7	2.9	Cs (49.9%)
Total	94.1	

The uncertainties on measurement (±2σ = 5%) were propagated using a Monte-Carlo method and they were used to determine which principal component was statistically significant.

et al., 2005; Sachs et al., 2007; Schmidt et al., 2008; Wang and Mulligan, 2009) have demonstrated that organic matter plays a key role in the enrichment of U, Pb and As in lake sediments because these elements are strongly complexed by humic acids. In addition, redox-sensitive elements such as As and U tend to be trapped in gyttja due to its reducing conditions. Guyard et al. (2007) also measured high Pb concentrations in organic sediments from Lake Bramant, which is located only few kilometers away from Lake Blanc Huez. It is suggested, therefore, that the enrichments at depth are related to organic matter in the sediment and that gyttja may act as a sink for metal(loid)s weathered from catchment rocks. Considering the geology of the catchment area, the Ag and Pb enrichments at shallower depths, at 30, 100, 180–190 cm, are probably related to changes of source proportions; or, more specifically, to periods of enhanced erosion of the Pb–Ag vein (see Fig. 8).

The correlations in Fig. 9 between the concentrations of U and As, Pb or Ag clearly support the interpretation. In Fig. 9a, U and As are well correlated and show a simple trend to the highest concentrations in the gyttja samples. In contrast, two distinct trends can be identified when Pb or Ag concentrations are plotted as a function of U (see Fig. 9b and c). The first trend, which includes the Ag–Pb-rich samples corresponding to the medieval mining exploitation of the Pb–Ag vein (see following section), as well as the moraine, glacio-lacustrine and proglacial sediments, is characterized by high Pb and Ag contents at relatively low U contents (blue bands in Fig. 9b and c). This trend most probably corresponds to fluctuations of the erosion intensity next to the lake, fluctuations that led to changing contributions from the Pb–Ag vein. The second trend, shown by the gray bands in Fig. 9b and c, is characterized by very high U contents and includes the organic-rich samples (gyttja samples) that preferentially adsorbed U, As, Pb and Ag. As shown by the two trends, the high Ag and Pb concentrations in some sediments can either be explained by a change in the source input i.e. increased erosion of the Pb–Ag vein (blue trend) or by a sedimentary process i.e. enhanced adsorption of these elements on organic matter (gray trend).

Because no U-rich material such as U-rich granite or U mineralization has been reported in the catchment area, it is believed that Pb/U can be used as a proxy to distinguish between the two major processes that caused Ag and Pb enrichments in the lake sediments. The combination of high Pb/U and high Ag and Pb concentrations indicates an increased contribution from the Pb–Ag vein whereas low Pb/U and high U and As concentrations are associated with the presence of organic matter preserving reducing conditions in the sediment.

Note that the very high Ag, Pb, U and As contents found in the sediments from Lake Blanc Huez are quite unusual and may be toxic for some forms of aquatic life if the elements are released into the water column or in the sediment pore water. In this study, lake water was not analyzed but such analysis would certainly be helpful to evaluate the impact of the very high concentrations in the sediments.

6.3. Impact of human activities

In numerous studies, analyses of Pb isotopic compositions of lake sediments record a contribution of Pb from distant and local industrial activities (Kober et al., 1999; Monna et al., 1999; Eades et al., 2002; Renberg et al., 2002; Arnaud et al., 2004). Lead-rich particles from a variety of human activities are transported in the atmosphere and deposited far from their sources (Monna et al., 1997; Sangster et al., 2000; Geraldes et al., 2006). Some of these particles have distinctive Pb isotopic compositions (Monna et al., 1997; Hansmann and Koppel, 2000) that trace the source of pollution.

In Fig. 10, the Pb isotopic ratios measured in Lake Blanc Huez sediments are compared to values reported for various types of anthropogenic Pb (e.g. leaded gasoline, airborne particulate matter measured in several big cities and urban incinerators) to evaluate the potential impact of human activities, including the construction work related to the Alpe d'Huez ski resort development since the 1930s. As can be seen in all isotopic spaces, Lake Blanc Huez Pb isotopic ratios differ clearly from values reported for industrial Pb sources but they completely overlap with the composition of European Pb ore deposits. This is not surprising in view of the proximity of the Pb–Ag vein located a few meters from the lake and the extremely high Pb content of this facies. Even if anthropogenic Pb is present in the recent sediments, its isotopic signature is overwhelmed by the Pb from the Pb–Ag vein. The Lake Blanc Huez sediments thus clearly are an inappropriate target to assess Pb pollution due to recent human activities. Because Pb veins are

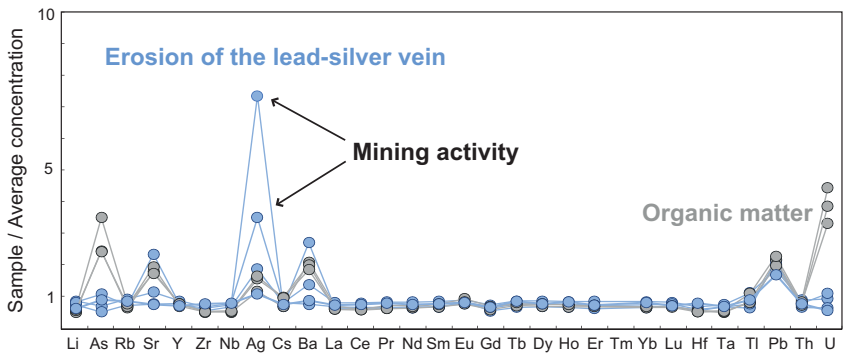

Fig. 8. Trace element patterns of the Pb–Ag rich samples normalized to the average composition of Lake Blanc Huez sediments. Samples represented in this figure are those highlighted in blue and gray in Fig. 4 (samples located at 483, 423, 396, 99 and 86.5 cm depth in core LBH-06 and at 32 cm in core LBH-03).

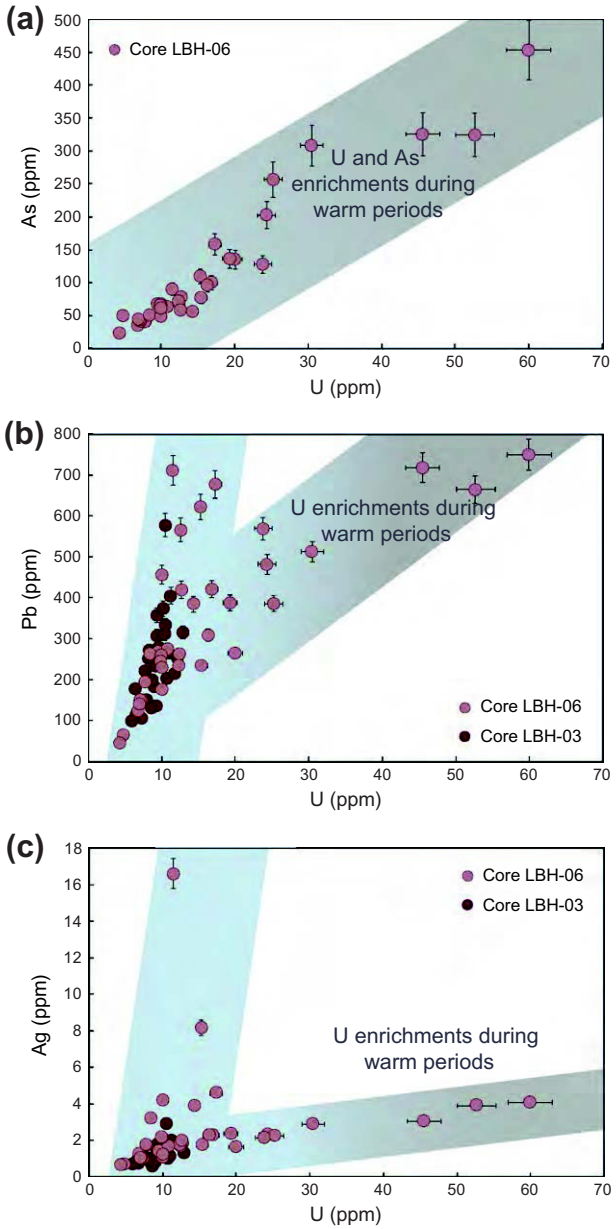

Fig. 9. Variations of As, Pb and Ag concentrations as a function of U concentrations in Lake Blanc Huez sediments. The catchment rock trend is indicated by a blue field and the U enrichment trend in organic-rich sediments is indicated by a gray field. Analytical errors for As, Pb, Ag and U concentrations are indicated by bars.

common in the Alps and in the other mountain ranges, it is believed that Lake Blanc Huez sediments are not an isolated case. Studies aiming to assess recent pollution using Pb isotopic ratios in lake sediment should, therefore, systematically and carefully examine the geology of the catchment area to ensure that no Pb-rich materials would overwhelm the isotopic composition of the studied sediments.

In contrast to the very recent sediments, Ag and Pb display concomitant and very high concentrations at 99 cm and 86.5 cm depth in core LBH-06, that is to say during the medieval period, around AD 1250 ± 30 according to the available chronology (see Fig. 4). Compared to the average composition of the Lake Blanc Huez sediments, these samples also have the highest Ag concentrations and high Pb/U ratios (see Figs. 4 and 8). These enrichments thus probably result from intense erosion of the Pb–Ag vein. Based on archeological techniques, Bailly-Maitre and Bruno-Dupraz (1994) have suggested that the Pb–Ag vein was mined for Ag from AD 1150–1200 to AD 1339. The very high Ag and Pb contents at 99 cm and 86.5 cm thus agree with this interpretation. This result constitutes the first geochemical evidence that confirms the existence of medieval mining industries on the shore of Lake Blanc Huez. Surprisingly, this activity does not seem to have had a significant impact on the Pb isotopic compositions of the sediments since the Pb isotope ratios of samples at 99 cm and 86.5 cm are not significantly displaced towards the galena and bournonite values (see Fig. 4). However, when quantitative mixing calculations are made, the absence of a systematic shift in Pb isotopic composition is not surprising. For example, when the proportion of Pb from the Pb–Ag vein is tripled from 0.01% to 0.03%, the calculated Pb concentrations are doubled but $^{206}Pb/^{204}Pb$, $^{207}Pb/^{204}Pb$ and $^{208}Pb/^{204}Pb$ ratios stay within the background noise (see Fig. 5a and b). Thus, an increased input of Pb from the Pb–Ag vein does not systematically lead to significant variation in the Pb isotope ratios of the lake sediments. Surprisingly, a possible trace of medieval mining is found in the top centimeters of core LBH-03, where Pb isotopic ratios are significantly lower than values obtained for the other sediments. Between 1 and 5 cm depth, the Pb isotopic compositions are almost identical to those of the Pb–Ag vein (Fig. 4) suggesting a larger contribution of Pb from galena and bournonite. The presence of reworked sediments including sand layers, at the top of core LBH-06, has been reported by Chapron et al. (2007) who interpreted it as being due to a subaqueous slide triggered by the AD 1962 Corrençon earthquake (see Fig. 3). It is proposed that this subaqueous slide could have remobilized medieval mine waste (essentially barite and quartz) and re-deposited it in the part of the lake where core LBH-03 was drilled. Remnants of medieval mine waste dumps are still visible on the lakeshore near the Pb–Ag vein (Fig. 2). An alternative explanation is that construction related to the ski resort led to enhanced erosion and re-deposition of the mine waste.

6.4. Record of climate changes

Over the 13 ka of sedimentation in the lake, climate conditions have changed (Davis et al., 2003; Mayewski et al., 2004) and several glacier fluctuations have been recorded in the Alps (Ivy-Ochs et al., 2009, and references therein). A period of cooler climate and high glacier activity has been identified during the Younger Dryas towards the beginning of the Holocene (Joerin et al., 2006, 2008). The climate then became significantly warmer until the Mid-Holocene. Periods of glacial recession were generally long and glaciers were often smaller than today (Leemann and Niessen, 1994; Haas et al., 1998; Hormes et al., 2001; Joerin et al., 2006, 2008). During the second half of the Holocene, climatic conditions were cooler allowing glaciers to advance to lower altitudes, closer to those currently observed in the Alps (Hormes et al., 2001; Deline and Orombelli, 2005; Joerin et al., 2006; Guyard et al., 2007). Many alpine glaciers reached their maximum Holocene extent during the Little Ice Age although a lot of shorter climate fluctuations have been recorded at different times all over the Alps during the last 1 ka (Holzhauser et al., 2005; Joerin et al., 2006; Chapron et al., 2007; Guyard et al., 2007).

Lake Blanc Huez is characterized by glacial meltwater-induced sedimentation and these past Holocene climate changes should be recorded in the sedimentary pile (Dhal et al., 2003). Indeed, in proglacial sites, warmer periods associated with glacial retreat can readily be correlated to periods with greater vegetation cover or higher rates of within-lake primary production resulting in higher concentrations of organic matter in the lake sediment (Dhal et al., 2003). As mentioned earlier, from a geochemical point of view, these periods can be recognized by elevated U and As contents associated with low Pb/U ratios. Such characteristics exist

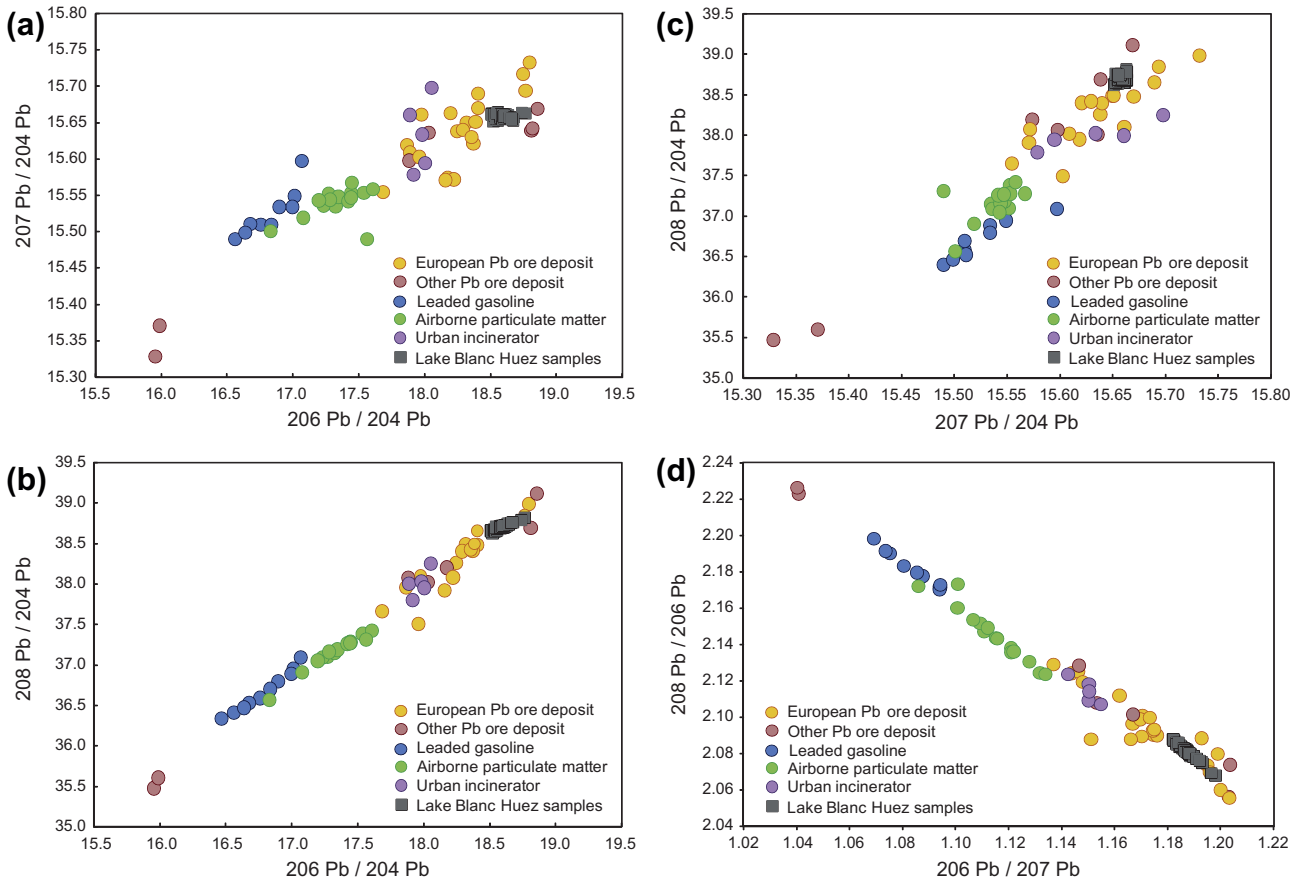

Fig. 10. Pb isotopic compositions of Lake Blanc Huez samples compared to Pb ore deposits and various pollutants. Data for Pb ore deposits were selected from data compiled by Sangster et al. (2000) and only values with low uncertainties were selected. Data for leaded gasoline, airborne particulate matter and urban incinerators are those published by Monna et al. (1997) and Hansmann and Kopel (2000). It is worth noting that the large variations of $^{207}Pb/^{204}Pb$ at a given $^{206}Pb/^{204}Pb$ or $^{208}Pb/^{204}Pb$ for the literature data probably do not reflect the variability of the analyzed materials, but are most probably due to large analytical errors arising from non-accurate mass fractionation correction during analyses.

in the organic-rich gyttja around 410 cm and 480 cm in core LBH-06. These enrichments occurred after the deposition of the moraine and before 7625 cal. BP according to available chronology (see Fig. 4). They, therefore, correlate with the warmer period identified at many Alpine high-altitude sites during the first half of the Holocene. During colder and wetter periods, glaciers covered larger areas and abrasion of the bedrock produces abundant fine rock and mineral fragments (Leemann and Niessen, 1994; Dhal et al., 2003). The Pb–Ag vein next to Lake Blanc Huez is within a long mineralized fault that crosses the catchment area (see Figs. 1 and 2) and it would have been efficiently eroded during periods of glacial advance. An input of Ag–Pb-rich material can, therefore, be used as an on/off signal of glacial advance in the catchment area. In the sediments, the two layers with high Pb and Ag concentrations associated with high Pb/U, the signature of enhanced erosion of the Pb–Ag vein, could register periods of colder climate.

The Pb–Ag enrichment in core LBH-03 at about 30 cm (Fig. 4) coincides with a drop stone level consisting of erosive snow avalanche debris (see Fig. 3). This level is located just under a facies transition that Chapron et al. (2007) attributed to the last advance of glaciers during the Little Ice Age at AD 1820–1850. Moreover, the moraine belts of the Little Ice Age mapped by Flusin et al. (1909) and Chardon (1991) at an altitude of 2600 m on the western side of the massif show that glaciers advanced very close to Lake Blanc Huez (2543 m) at that time. These observations provide strong support for the hypothesis that the Ag and Pb enrichments observed at about 30 cm depth in core LBH-03 are directly linked to enhanced erosion of the Pb–Ag vein during the Little Ice Age.

Similarly, the Ag–Pb enrichments around 190 cm in core LBH-06 are found in proglacial sediments containing several angular drop stones and flood deposits that indicate significant glacier fluctuations in the catchment area. These enrichments are attributed to significant glacier advances during the second half of the Holocene. At this depth, the chronology of the sedimentary pile is poorly constrained but this event could be related to the glacial activity recorded between 3600 and 3300 cal. BP in the sediments of Lake Bramant in the Grandes Rousses Massif (Guyard et al., 2007).

7. Conclusions

Trace-element concentrations and Pb isotope compositions measured in Lake Blanc Huez sediments show that the Pb–Ag vein located a few meters from the lake dominates the overall geochemistry of the sediments. Lead and Ag background concentrations are vastly above concentrations usually measured in lake sediments and variations of Pb isotopes suggest that the Pb found in Holocene lake sediments is a mixture of Pb from the catchment area rocks and Pb from galena and bournonite in the Pb–Ag vein. Less than 0.05% of Pb-bearing material from the vein is enough to dominate the isotopic signature of the sediments. As a consequence, the Pb isotopic signature due recent human activities is totally obscured.

The medieval mining activities in the catchment area are well recorded in the sedimentary pile by strong Ag enrichments in the

lake sediments. The study shows that major climate changes can be identified using the geochemistry of sediments. The first part of the Holocene was characterized by significant glacier retreats and warmer climatic conditions that favor the sedimentation of organic-rich materials with high U and As contents associated with low Pb/U ratios. Using the Pb–Ag vein as an indicator of increased erosion next to the lake, two significant glacier advances can be identified by concomitant Ag and Pb enrichments and high Pb/U ratios in sediments. According to the available core chronologies, higher glacial activity may have occurred during the 3600–3300 cal. BP colder event and during the more recent Little Ice Age.

Lead isotopes cannot be used to trace pollution because of the overwhelming effect of the nearby Pb–Ag vein. However, they still remain a valuable tool to trace local sources. Since Pb-rich veins are quite common in orogenic belts, it is suspected that they could also dominate Pb isotopic compositions in several other high-mountain lake sediments. Trace element concentrations could, therefore, be used as an alternative tool to decipher the environmental changes. More specifically, the presence of Pb-rich materials in the catchment area of a proglacial lake constitutes a potential indicator of erosion rates.

Acknowledgments

We would like to thank P. Telouk (ENS, Lyon) for assistance during Pb isotopic measurements in Lyon, Thierry Dumont (LGCA, Grenoble) for his help in designing the 3D map, Eric Lewin (LGCA, Grenoble) for his PCA expertise, and Jérome Nomade (LGCA, Grenoble) and Nicholas Arndt (LGCA, Grenoble) for constructive discussions that helped to improve the content of this paper. We also thank Flavio Anselmetti (EAWAG, Dubendorf, Switzerland), Thierry Winiarski and David Goutaland (ENTPE, Lyon), Maxime Debret (ISTO, Orléans), Fabien Arnaud (EDYTEM, Chambéry) and the staff from the SATA (Alpe d'Huez) for their contribution to the coring expeditions and logistical support. Very constructive reviews by the associate editor Rich Wanty and an anonymous reviewer helped improve the final version of this manuscript. Financial support for this study was provided by the Observatoire des Sciences de l'Univers de Grenoble (OSUG), by the French Mountain Institute (Chambéry) and by the GDR JURALP 2992 of the French CNRS for radiocarbon dating.

Appendix A. Supplementary material

Supplementary data associated with this article can be found, in the online version, at doi:10.1016/j.apgeochem.2011.12.010.

References

Arnaud, F., Revel-Rolland, M., Bosh, D., Winiarski, T., Desmet, M., Tribovillard, N., Givelet, N., 2004. A 300 years history of lead contamination in northern French Alps reconstructed from distant lake sediment records. J. Environ. Monitor. 6, 448–456.

Bailly-Maitre, M.C., Bruno-Dupraz, J., 1994. Brandes en Oisans: La mine des dauphins (XII–XIV e s.) Isère. Documents d'Archéologie en Rhône-Alpes, vol. 9, p. 172.

Barbier, R., Barfety, J.C., Bordet, P., Bulard, P.F., Debelmas, J., Fabre, J., Feys, R., Grèber, C., Gillot-Barbiéri, C., Lacombe, J.C., Vialon, P., Fort, P.L., Mouterde, M., Pécher, A., PetiteVille, J., Rivoirard, R., Tissot, B., 1976. Carte Géol. France (1/50,000), feuille La Grave. BRGM: Notice explicative par R. Barbier, J-C. Barfety, A. Bocquet, P. Bordet, P. Le Fort, J. Meloux, R. Mouterde, A. Pécher et M. Petiteville (1973).

Battarbee, R.W., Grytnes, J.-A., Thompson, R., Appleby, P.G., Catalan, J., Korhola, A., Birks, H.J.B., Heegaard, E., Lami, A., 2002. Comparing palaeolimnological and instrumental evidence of climate change for remote mountain lakes over the last 200 years. J. Paleolimnol. 28, 161–179.

Beniston, M., Diaz, H.F., Bradley, R.S., 1997. Climatic change at high elevation sites: an overview. Climatic Change 36, 233–251.

Brown, S., Bierman, P., Lini, A., Davis, P.T., Southon, J., 2002. Reconstructing lake and drainage basin history using terrestrial sediment layers: analysis of cores from a post-glacial lake in New England, USA. J. Paleolimnol. 28, 219–236.

Camarero, L., Masqué, P., Devos, W., Ani-Ralgota, I., Catalan, J., Moor, M.C., Pla, S., Sanchez-Cabeza, J.A., 1998. Historical variations in lead fluxes in the Pyrénées (northeast Spain) from a dated lake sediment core. Water Air Soil Pollut. 105, 439–449.

Chapron, E., Faïn, X., Magand, O., Charlet, L., Debret, M., Mélières, M.A., 2007. Reconstructing recent environmental changes from proglacial Lake sediments in the Western Alps (Lake Blanc Huez, 2543 m a.s.l., Grandes Rousses Massif, France). Palaeogeogr. Palaeoclimatol. Palaeoecol. 252, 586–600.

Chapron, E., Bailly-Maitre, M.-C., Anselmetti, F., Guyard, H., Saint-Onge, G., Desmet, M., Chauvel, C., Winiarski, T., Magand, O., Arnaud, F., Charlet, L., Deline, P., Magny, M., Mélières, M.-A., 2008. Impacts des fluctuations glaciaires et des anciennes activités minières d'altitude sur la sédimentation lacustre proglaciaire au cours du Tardiglaciaire et de l'Holocène dans le massif des Grandes Rousses, Alpes Occidentales, France. Collection EDYTEM-no. 6-Cahiers de Paléoenvironnement, pp. 39–50.

Chardon, M., 1986. Transformations économiques et mutations des paysages en Oisans: le cas de l'Alpe d'Huez. Revue de Géographie Alpine, vol. 74, pp. 177–187.

Chardon, M., 1991. L'évolution tardiglaciaire et holocène des glaciers et de la vegetation autour de l'Alpe d'Huez (Oisans, Alpes Françaises). Revue de Géographie Alpine, vol. 79, pp. 39–53.

Davis, B.A.S., Brewer, S., Stevenson, A.C., Guiot, J., 2003. The temperature of Europe during the Holocene reconstructed from pollen data. Quatern. Sci. Rev. 22, 1701–1716.

Deline, P., Orombelli, G., 2005. Glacier fluctuations in the western Alps during the Neoglacial, as indicated by the Miage morainic amphitheatre (Mont Blanc massif, Italy). Boreas 34, 456–467.

DelValls, T.Á., Forja, J.M., González-Mazo, E., Gómez-Parra, A., Blasco, J., 1998. Determining contamination sources in marine sediments using multivariate analysis. Trends Anal. Chem. 17 (4), 181–192.

Dhal, S.O., Bakke, J., Lie, O., Nesje, A., 2003. Reconstruction of former glacier equilibrium line altitudes based on progacial sites: an evaluation of approaches and selection of sites. Quatern. Sci. Rev. 22, 275–287.

Do Couto, D., 2008. Reconstitution paléoenvironnementale au sein du massif des Grandes Rousses (Alpes Occidentales françaises) à partir de l'étude des sédiments organiques du lac Blanc Huez. Unpublished Master Thesis, Université d'Orléans.

Dowdall, M., Gwynn, J.P., Moran, C., Davids, C., Dea, J.O., Lind, B., 2005. Organic soil as a radionuclide sink in a High Arctic environment. J. Radioanal. Nucl. Chem. 266, 217–223.

Eades, L.J., Farmer, J.G., MacKenzie, A.B., Kirika, A., Bailey-Watts, A.E., 2002. Stable lead isotopic characterisation of the historical record of environmental lead contamination in dated freshwater lake sediment cores from northern and central Scotland. Sci. Total Environ. 292, 55–67.

Eggermont, H., Russell, J.M., Schettler, G., Damme, K.V., Bessems, I., Verschuren, D., 2007. Physical and chemical limnology of alpine lakes and pools in the Rwenzori Mountains (Uganda–DR Congo). Hydrobiologia 592, 151–173.

El Bilali, L., Rasmussen, P.E., Hall, G.E.M., Fortin, D., 2002. Role of sediment composition in trace metal distribution in lake sediments. Appl. Geochem. 17, 1171–1181.

Eusterhues, K., Heinrichs, H., Schneider, J.D., 2005. Geochemical response on redox fluctuations in Holocene lake sediments, Lake Steisslingen, Southern Germany. Chem. Geol. 222, 1–22.

Faure, G., 1977. Principles of Isotope Geology. Wiley, New York.

Flusin, G., Jacob, C., Offner, J., 1909. Etudes glaciaires, géographiques et botaniques dans le massif des Grandes Rousses. Etudes glaciologiques. Ministère de l'Agriculture, Paris, pp. 107–112.

Galer, S.J.G., Abouchami, W., 1998. Practical application of lead triple spiking for correction of instrumental mass discrimination. Mineral. Mag. 62A, 491–492.

Geraldes, M.C., Paula, A.H., Godoy, J.M., Valeriano, C.M., 2006. Pb isotope signatures of sediments from Guanabara Bay, SE Brazil: evidence for multiples anthropogenic sources. J. Geochem. Explor. 88, 384–388.

Govindaraju, K., 1994. 1994 Compilation of working values and sample description for 383 geostandards. Geostand. Newslett. 18, 1–158.

Grimm, E.C., Maher, L.J., Nelson, D.M., 2009. The magnitude of error in conventional bulk-sediment radiocarbon dates from central North America. Quatern. Res. 72, 301–308.

Guyard, H., Chapron, E., St-Onge, G., Anselmetti, F.S., Arnaud, F., Magand, O., Francus, P., Mélières, M.A., 2007. High-altitude varve records of abrupt environmental changes and mining activity over the last 4000 years in the Western French Alps (Lake Bramant, Grandes Rousses Massif). Quatern. Sci. Rev. 26, 2644–2660.

Haas, J.N., Richoz, I., Tinner, W., Wick, L., 1998. Synchronous Holocene climatic oscillations recorded on the Swiss Plateau and at timberline in the Alps. Holocene 8, 301–309.

Hansmann, W., Koppel, V., 2000. Lead-isotopes as tracers of pollutants in soils. Chem. Geol. 171, 123–144.

Holzhauser, H., Magny, M., Zumbühl, H.J., 2005. Glacier and lake-level variations in west-central Europe over the last 3500 years. Holocene 15, 789–801.

Hormes, A., Müller, B.U., Schlüchter, C., 2001. The Alps with little ice: evidence for eight Holocene phases of reduced glacier extent in the Central Swiss Alps. Holocene 11, 255–265.

Imai, N., Terashima, S., Itoh, S., Ando, A., 1996. 1996 Compilation of analytical data on nine GSJ geochemical reference samples, "Sedimentary rock series". Geostand. Newslett. 20, 165–216.

Ivy-Ochs, S., Kerschner, H., Maisch, M., Christl, M., Kubik, P.W., Schlüchter, C., 2009. Latest Pleistocene and Holocene glacier variations in the European Alps. Quatern. Sci. Rev. 28, 2137–2149.
Joerin, U.E., Stocker, T.F., Schlüchter, C., 2006. Multicentury glacier fluctuations in the Swiss Alps during the Holocene. Holocene 16, 697–704.
Joerin, U.E., Nicolussi, K., Fischer, A., Stocker, T.F., Schlüchter, C., 2008. Holocene optimum events inferred from subglacial sediments at Tschierva Glacier, Eastern Swiss Alps. Quatern. Sci. Rev. 27, 337–350.
Kober, B., Wessels, M., Bollhöfer, A., Mangini, A., 1999. Pb isotopes in sediments of Lake Constance, Central Europe constrain the heavy metal pathways and the pollution history of the catchment, the lake and the regional atmosphere. Geochim. Cosmochim. Acta 63, 1293–1303.
Koinig, K.A., Schmidt, R., Sommaruga-Wögrath, S., Tessadri, R., Psenner, R., 1998. Climate change as the primary cause for pH shifts in a high Alpine lake. Water Air Soil Pollut. 104, 167–180.
Koinig, K.A., Shotyk, W., Lotter, A.F., Ohlendorf, C., Sturm, M., 2003. 9000 years of geochemical evolution of lithogenic major and trace elements in the sediment of an alpine lake – the role of climate, vegetation, and land-use history. J. Paleolimnol. 30, 307–320.
Krauskopf, K.B., Bird, D.K., 1995. Introduction to Geochemistry. McGraw-Hill, New York.
Lavilla, I., Filgueiras, A.V., Valverde, F., Millos, J., Palanca, A., Bendicho, C., 2006. Depth profile of trace elements in a sediment core of a high-altitude lake deposit at the Pyrénées, Spain. Water Air Soil Pollut. 172, 273–293.
Leemann, A., Niessen, F., 1994. Holocene glacial activity and climatic variations in the Swiss Alps: reconstructing a continuous record from proglacial lake sediments. Holocene 4, 259–268.
Legros, A., Legros, M., 1979. Histoire des Anciennes Mines et Gites de l'Oisans. Presses Midi, Pyrenees.
Lynch, J., 1999. Additional provisional elemental values for LKSD-1, LKSD-2, LKSD-3, LKSD-4, STSD-1, STSD-2, STSD-3 and STSD-4. Geostand. Newslett. 23, 251–260.
Manhès, G., Allegre, C.J., Provost, A., 1984. U–Th–Pb sytematics of the eucrite "Juvinas": precise age determination and evidence for exotic lead. Geochim. Cosmochim. Acta 48, 2247–2264.
Marsh, S.F., Alarid, J.E., Hammond, C.F., McLeod, M.J., Roensch, F.R., Rein, J.E., 1978. Anion Exchange of 58 Elements in Hydrobromic Acid and Hydroiodic Acid, Los Alamos Scientific Laboratory report LA-7084. Available from National Technical Information Service US Department of Commerce. Sprigfield, USA.
Mayewski, P.A., Rohling, E.E., Curt Stager, J., Karlén, W., Maasch, K.A., David Meeker, L., Meyerson, E.A., Gasse, F., van Kreveld, S., Holmgren, K., Lee-Thorp, J., Rosqvist, G., Rack, F., Staubwasser, M., Schneider, R.R., Steig, E.J., 2004. Holocene climate variability. Quatern. Res. 62, 243–255.
McLennan, S.M., 2001. Relationships between the trace element composition of sedimentary rocks and upper continental crust. Geochem. Geophys. Geosyst. 2, 1021. doi:10.1029/2000GC000109.
Monna, F., Lancelot, J., Croudace, I.W., Cundy, A.B., Lewis, J.T., 1997. Pb isotopic composition of airborne particulate material from France and the Southern United Kingdom: implications for Pb pollution. Environ. Sci. Technol. 31, 2277–2286.
Monna, F., Dominik, J., Loizeau, J.L., Pardos, M., Arpagaus, P., 1999. Origin and Evolution of Pb in Sediments of Lake Geneva (Switzerland–France). Establishing a Stable Pb Recor. Environ. Sci. Technol. 33, 2850–2857.
Monna, F., Hamer, K., Lévêque, J., Sauer, M., 2000. Pb isotopes as a reliable marker of early mining and smelting in the Northern Harz province (Lower Saxony, Germany). J. Geochem. Explor. 68, 201–210.
Mosello, R., Lami, A., Marchetto, A., Rogora, M., Wathne, B., Lien, L., Catalan, J., Camarero, L., Ventura, M., Psenner, R., Koinig, K., Thies, H., Sommaruga-Wögrath, S., Nickus, U., Tait, D., Thaler, B., Barbieri, A., Harriman, R., 2002. Trends in the water chemistry of high altitude lakes in Europe. Water Air Soil Pollut. Focus 2, 75–89.
Ohlendorf, C., Sturm, M., Hausmann, S., 2003. Natural environmental changes and human impact reflected in sediments of a high alpine lake in Switzerland. J. Paleolimnol. 30, 297–306.
Piotrowski, J.A., 2006. Groundwater under ice sheets and glaciers. In: Knight, P.G. (Ed.), Glacier Science and Environmental Change. Blackwell, pp. 50–60.
Reid, M.K., Spencer, K.L., 2009. Use of principal components analysis (PCA) on estuarine sediment datasets: the effect of data pre-treatment. Environ. Pollut. 157, 2275–2281.
Renberg, I., Brännvall, M.L., Bindler, R., Emteryd, O., 2002. Stable lead isotopes and lake sediments – a useful combination for the study of atmospheric lead pollution history. Sci. Total Environ. 292, 45–54.
Sachs, S., Brendler, V., Geipel, G., 2007. Uranium(VI) complexation by humic acid under neutral pH conditions studied by laser-induced fluorescence spectroscopy. Radiochim. Acta 95, 103–110.
Sangster, D.F., Outridge, P.M., Davis, W.J., 2000. Stable lead isotope characteristics of lead ore deposits of environmental significance. Environ. Rev. 8, 115–147.
Schmidt, R., Kamenik, C., Tessadri, R., Koinig, K.A., 2006. Climatic changes from 12,000 to 4000 years ago in the Austrian Central Alps tracked by sedimentological and biological proxies of a lake sediment core. J. Paleolimnol. 35, 491–505.
Schmidt, R., Roth, M., Tessadri, R., Weckström, K., 2008. Disentangling late-Holocene climate and land-use impacts on an Austrian alpine lake using seasonal temperature anomalies, ice-cover, sedimentology, and pollen tracers. J. Paleolimnol. 40, 453–459.
Sommaruga-Wögrath, S., Koinig, K.A., Schmidt, R., Sommaruga, R., Tessadri, R., Psenner, R., 1997. Temperatures effects on the acidity of remote alpine lakes. Nature 387, 64–67.
Stuiver, M., Reimer, P., Bard, E., Beck, J., Burr, G., Hughen, K., Kromer, B., McCormac, G., Van der Plicht, J., Spurk, M., 1998. INTCAL98 radiocarbon age calibration, 24,000–0 cal BP. Radiocarbon 40, 1041–1083.
Swift, D.A., 2006. Haut Glacier d'Arolla, Switzerland: hydrological controls on basal sediment evacuation and glacial erosion. In: Knight, P.G. (Ed.), Glacier Science and Environmental Change. Blackwell, pp. 23–25.
Torinesi, O., Letreguilly, A., Valla, F., 2002. A century reconstruction of mass-balance of Glacier de Sarennes, French Alps. J. Glaciol. 48, 142–148.
Tranter, M., 2006. Glacial chemical weathering, runoff composition and solute fluxes. In: Knight, P.G. (Ed.), Glacier Science and Environmental Change. Blackwell, pp. 70–75.
Valla, F., 1993. Sarennes. Un glacier sous haute surveillance. Massif de l'Oisans, France. Revue de Géographie Alpine, vol. 81, pp. 33–49.
Vincent, C., 2002. Influence of climate change over the 20th Century on four French glacier mass balances. J. Geophys. Res. 107, 4375. doi:10.1029/2001JD000832.
Wang, S., Mulligan, C.N., 2009. Effect of natural organic matter on arsenic mobilization from mine tailings. J. Hazard. Mater. 168, 721–726.
Wang, C., Gu, T., Chi, Q., Yan, W., Yan, M., 2001. New series of rock and sediment geochemical reference materials. Geostand. Newslett. 25, 145–152.
Welch, A.H., Lico, M.S., 1998. Factors controlling As and U in shallow ground water, southern Carson Desert, Nevada. Appl. Geochem. 13, 521–539.
White, W.M., Albarède, F., Télouk, P., 2000. High-precision analysis of Pb isotope ratios by multi-collector ICP-MS. Chem. Geol. 167, 257–270.
Zdenek, K., 1971. Geology of Recent Sediments. Academic Press Inc., London.